FLUX REVERSAL IN FERROMAGNETIC THIN FILMS

Thesis by

Mark Howard Kryder

In Partial Fulfillment of the Requirements

For the Degree of

Doctor of Philosophy

California Institute of Technology

Pasadena, California

1970

(Submitted September 24, 1969)

Acknowledgements

The efforts of a large number of individuals and organizations have made this study possible. The author gratefully acknowledges F. B. Humphrey and C. H. Wilts for providing the opportunity to perform this research and for their many stimulating questions and suggestions throughout the research and the writing of this report. H. Hoffmann provided the original concept of "locking" as described in this report and through many long discussions and equally long correspondence contributed much to the explanations of the observed phenomena. Discussions with K. J. Harte also provided many useful concepts. T. Suzuki, C. Bajorek, G. Johnson, E. Evans, and L. Brownlow are also acknowledged for helpful and enjoyable discussions. The help of J. E. Guisinger in the design and construction of much of the electronic apparatus is gratefully acknowledged.

Financial support for this research was provided by the National Aeronautics and Space Administration under contract NAS 7-100. During this research the author gratefully received three teaching assistantships and various summer research assistantships from the Institute, two fellowships from the National Science Foundation, one from the Ford Foundation, one from Fairchild Camera and Instrument Corporation, and two from the Tektronix Foundation. Tektronix Incorporated contributed several pieces of electronic equipment and L. C. Hedrick was instrumental in these contributions.

The secretarial services of C. Elsbree, N. M. Kosowicz, R. A. Stratton, and C. M. Teeter were essential to the preparation of the final manuscript of this dissertation.

Finally, the author thanks his wife, Sandy, for understanding and support during his stay at the Institute.

ABSTRACT

Flux reversal in Ni-Fe thin films has been studied with the use of 10 nsec exposure time Kerr magneto-optic photographs which depict the dynamic magnetization configuration with 10 μ resolution during the reversal process. The photographs show that at least five mechanisms are involved in the reversal of thin films: (1) domain wall motion, (2) coherent rotation, (3) diffuse boundary propagation, (4) nucleation and subsequent reversal of partially reversed regions, and (5) non-coherent rotation. The present investigation has been concerned mainly with the latter three mechanisms as they have either been previously unreported or poorly understood.

Non-coherent rotation is a complex rotational reversal process wherein the rate of the magnetization rotation varies over the surface of the magnetic film. It occurs only when transverse fields are applied. The Kerr magneto-optic photographs show that initially there is a fast relaxation of the ripple and a coherent rotation of the magnetization during the risetime of the pulse field, followed by a breakup of the magnetization into a striped configuration after the field exceeds the Stoner-Wohlfarth threshold. With fields just exceeding the Stoner-Wohlfarth threshold, after the stripes form, regions of reversed magnetization nucleate throughout the stripes and complete the reversal process. With larger applied fields, the reversal is completed by the slow (as compared to coherent rotation) rotation of the magnetization which is accompanied by a gradual decrease in amplitude of the stripes. The angle at which the stripes form is dependent on the applied field and varies from film to film, but indicates that the magnetization

rotates coherently to angles significantly greater (5° to 20°) than the critical angle for reversal. The previously proposed fast relaxation models of Stein and Harte both predict that the coherent rotation should cease before the critical angle and therefore do not agree with the data. A model, based on ripple theory, has been constructed to show that after the magnetization rotates past the critical angle, an instability should occur in the ripple and cause a striped configuration at the observed angles.

The nucleation and subsequent reversal of partially reversed regions is a reversal process occuring predominantly with zero or small transverse fields. During this process the magnetization reverses in small (0.01 mm^2) regions of the film sequentially in time. With zero transverse field, the nucleation occurs with longitudinal fields exceeding a well defined nucleation threshold ($>H_k$) to fields greater than $2H_k$. Anisotropy dispersion and magnetostatic stray fields are believed to be important in the nucleation process.

Diffuse boundary propagation involves a poorly defined, jagged, and diffuse boundary separating regions of anti-parallel magnetization. With zero transverse field the boundary lies transverse to the easy axis and propagates in the longitudinal direction -- just the opposite of domain wall motion. When a transverse field is applied, the boundary propagates rapidly from diffuse tips pointing in the direction of the stripes which are observed during non-coherent rotation. The boundary velocity varies roughly as the fifth power of the field and ranges from 0.033 cm/μsec at fields near H_c to 1.25 cm/μsec at 1.3 H_k which is one to three order of magnitude faster than domain wall motion. The high

velocity is in part attributed to the large width of the boundary which widens from 0.2 mm to 2 mm as the field is increased.

Photographs taken when the drive field is terminated before saturation of the magnetic film show that the magnetization configuration continues to change for more than 200 nsec in the absence of an applied field. The diffuse boundaries become more sharply defined, though still quite jagged, and are found to change structure and propagate more slowly during subsequent pulses. Many of the partially reversed nucleated regions revert to the non-reversed state when the field is terminated. The striped partially rotated magnetization of the non-coherent rotation process, depending on the direction of the magnetization and the magnitude of the magnetostatic fields arising from the stripes, either relaxes to the non-reversed state or continues to reverse. Usually the static state shows no evidence of the stripes, and those which are observed are broken up by nucleated regions and frequently lie at different angles than the dynamic stripes. The large changes which occur after the field is terminated show that it is misleading to try to infer the dynamic state from the final static state as has been previously done. The long relaxation time is attributed to the sequential nature of the relaxation process.

Photographic materials on pages 27, 31, 52, 65, 68, 72, 96, 97, 101, 102, 103, 105, 106, 107, 108, 109, 111, 113, 115, 117, 122, 127, 130, 134, 135, 142, 143, 147, 151, 152, 155, 165, 166, 168, 169, 170, 177, 179, 180, 181, 189, 191, 195, 197, 198, 199, 200, 201, 202, 206, 209 and 211 are essential and will not reproduce clearly on Xerox copies. Photographic copies should be ordered.

TABLE OF CONTENTS

Chapter 1

Introduction

The magnetization in ferromagnetic thin films with no applied field is stable only when it lies parallel or antiparallel to an induced easy axis of magnetization. The dynamic processes by which the magnetization goes from one stable state to another when a magnetic field pulse is applied have been the subject of study by numerous investigators for the past fourteen years. This interest has been stimulated largely by the potential use of the films as computer memory elements where the stable states of the films are binary memory states. As a result of these investigations, the very low speed quasi-static reversal by movement of walls separating domains of antiparallel magnetization has been identified and a phenomenological model has been found to describe it reasonably well. The very high speed process of coherent rotation has also been identified, although the important damping methanisms are not yet known. The intermediate speed reversal processes have been investigated, but they have remained poorly understood largely because of the lack of a suitable means of investigation. This report describes an exploratory study of the intermediate speed processes, made with the use of a recently constructed Kerr magneto-optic camera equipped with a 10 nsec Kerr electro-optic shutter. The photographs obtained show the dynamic magnetization configuration in a 1 cm diameter magnetic thin film with 10 μ resolution.

The approach used in this investigation was to photograph the reversal processes with various applied fields and to identify and investigate the distinct reversal mechanisms. The mechanisms involved

with and without a transverse field were found to be different, and they are therefore treated in separate chapters of this report. Diffuse boundary propagation and non-coherent rotation, in addition to domain wall motion and coherent rotation mentioned above, were found to be important in the transverse field case. Domain wall motion, diffuse boundary propagation, and the nucleation and subsequent reversal of partially reversed regions were found to be the mechanisms of zero transverse field flux reversal.

Relaxation processes occuring when the drive field is terminated before saturation of the magnetic film have also been investigated. The observed relaxation has revealed important differences between the static and dynamic magnetization configurations, and has proven the importance of observing the dynamic configurations for an understanding of the reversal process.

Chapter 2

Magnetic Thin Films--Background

2.1 Preparation and Quasistatic Characteristics

M. S. Blois (1955) first observed uniaxial anisotropy in ferromagnetic thin films and reported on film properties and methods for their preparation. The uniaxial anisotropy and the fact that the magnetization could reverse in direction in times of the order of 1 nsec upon application of a magnetic field made thin films potentially suitable as memory elements in computers. Hence there has been great interest in the properties of ferromagnetic thin films.

Ferromagnetic thin films have been made by evaporation, electroplating, sputtering and chemical deposition. For the purposes of this investigation, evaporation was used exclusively. This technique permits reasonable control of the materials that are put into the thin films and facilitates a mirror-like surface on the film which is necessary for the observation of these thin films with a Kerr magneto-optic apparatus.

The film samples used were evaporated onto glass substrates from a Ni-Fe melt contained in an Alundum crucible and heated by induction heating in a moderate vacuum of 10^{-6} Torr. The temperature of the substrates, composition of the melt, and rate of evaporation were controlled in order to produce films of the desired characteristics. The shape of the films was determined by masking. During the evaporation a uniform magnetic field of 63 oe was maintained in the plane of the glass substrate in order to determine the direction of the unaxial anisotropy.

After the films were evaporated and cooled to room temperature, before removing them from the vacuum, a 330 Å thick layer of SiO was evaporated onto their surfaces. This layer is necessary to enhance the Kerr magneto-optic effect used to observe the magnetization configuration in the films. The 330 Å thickness was experimentally determined to be optimum for this purpose. This SiO coating and the Kerr magneto-optic effect is discussed later in Chapter 6.

The films made in this manner exhibited a uniaxial anisotropy of the form

$$\epsilon_u = K_u \sin^2 \varphi_o \tag{2.1}$$

where ϵ_u is the uniaxial anisotropy energy density, K_u is the uniaxial anisotropy constant and φ_o is the angle of the magnetization with respect to the preferred direction of magnetization or easy axis. The axis at which ϵ_u is a maximum is referred to as the hard axis. The torque per unit volume which this uniaxial anisotropy exerts on the magnetization is

$$T = - \frac{d\epsilon_u}{d\varphi_o} = - K_u \sin 2\varphi_o \ , \tag{2.2}$$

and the anisotropy field, H_k, defined as the restoring field for a virtual displacement $\delta\varphi_o$ of the magnetization from the easy axis is found from

$$\delta T|_{\varphi_o = 0} = \frac{dT}{d\varphi_o} \delta\varphi_o|_{\varphi_o = 0} = - M_s H_k \delta\varphi_o \tag{2.3}$$

$$\delta T|_{\varphi_o = 0} = - 2 K_u \tag{2.4}$$

or

$$H_k = \frac{2K_u}{M_s} \tag{2.5}$$

Typical values are:

$H_k \approx 4.0$ oe

$K_u \approx 1600$ erg/cm^3

$M_s \approx 800$ emu

If a magnetic field, H, is applied in the plane of the film at an angle α (see Fig. 2-1) to the easy axis, the total energy density of the film is given by

$$\epsilon = K_u \sin^2 \varphi_o - M_s H \cos (\alpha - \varphi_o). \tag{2.6}$$

where in a uniformly magnetized film at static equilibrium $\theta_o = \pi/2$, $\vec{M}(\vec{r},t) = \vec{M}_o(t)$. Equilibrium is determined by the disappearance of the first derivative of ϵ with respect to φ_o or equivalently by the vanishing of the torque density $T = -d\epsilon/d\varphi_o$:

$$T = -\frac{d\epsilon}{d\varphi_o} = M_s H \sin (\alpha - \varphi_o) - K_u \sin 2\varphi_o = 0. \tag{2.7}$$

In order that (2.7) describe a stable equilibrium, it is necessary that the second derivative of the energy be positive, or again equivalently that the field which the magnetization observes after a virtual displacement, $\delta\varphi_o$, be positive. This field may be calculated from:

$$\delta T = \frac{dT}{d\varphi_o} \delta\varphi_o = -(2K_u \cos 2\varphi_o + H M_s \cos (\alpha - \varphi_o)) \delta\varphi_o \quad . \tag{2.8}$$

$$\delta T = -H(\alpha) M_s \delta\varphi_o \tag{2.9}$$

or

$$h(\alpha) = \frac{H(\alpha)}{H_k} = h \cos (\alpha - \varphi_o) + \cos 2\varphi_o, \tag{2.10}$$

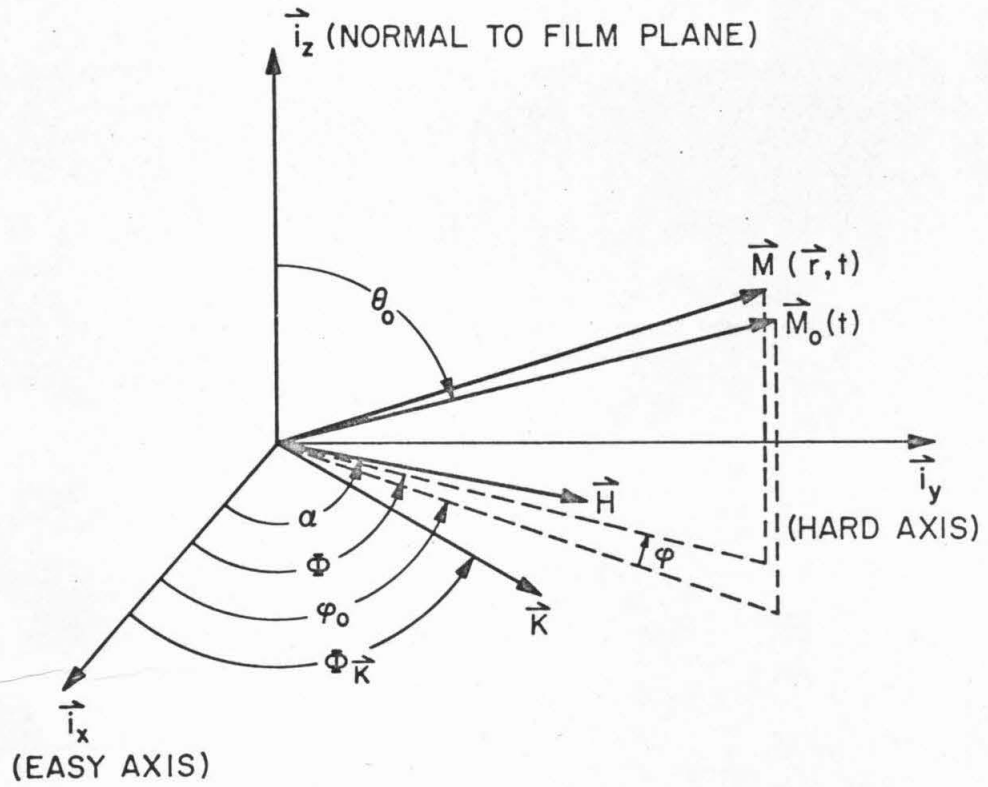

Fig. 2-1. The coordinate system of a thin film.

where $h = H/H_k$. For stable equilibrium to occur, $h(\alpha)$ must be positive. Therefore a switching threshold may be defined by (2.7) and

$$h(\alpha) = h \cos(\alpha-\varphi_o) + \cos 2\varphi_o = 0 \tag{2.11}$$

By solving (2.7) and (2.11) for $h_x = h \cos\alpha$ and $h_y = h \sin\alpha$, one obtains:

$$h_x = -\cos^3\varphi_o \tag{2.12a}$$

$$h_y = \sin^3\varphi_o. \tag{2.12b}$$

This result may be plotted as in Fig. 2-2. This curve is commonly referred to as the Stoner-Wohlfarth threshold after the two workers who first made this calculation (Stoner-Wohlfarth (1948)). The significance of the curve is that if a magnetic film uniformly magnetized along the +x axis is subjected to a magnetic field which is gradually increased at an angle α (defined from the +x axis) such that $90^\circ < \alpha < 270^\circ$, then φ_o, the angle which the magnetization makes with the easy axis, will increase in magnitude remaining in stable equilibrium with the magnetic field (defined by equation (2.7)) until the field reaches the threshold curve. When the field reaches the threshold, φ_o will make a discontinuous jump to a new stable position in either the second or third quadrant (depending upon α). It can be shown that at stable equilibrium $h(\alpha)$ is the distance from the tip of the field vector in Fig. 2-2 to a tangent on the Stoner-Wohlfarth threshold as shown.

The single domain field, $h(\alpha)$, may be thought of as the "stiffness" of φ_o. That is, for large positive $h(\alpha)$, the restoring torque for a

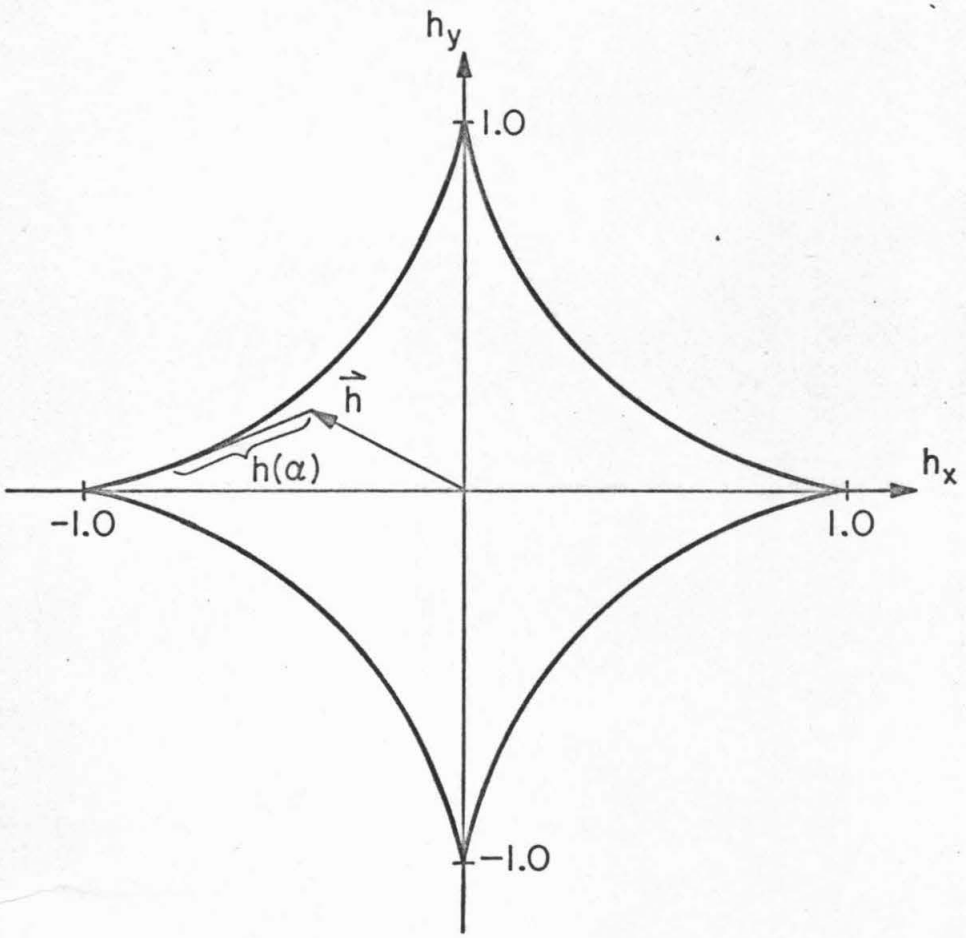

Fig. 2-2. The Stoner-Wohlfarth threshold curves. The single domain field $h(\alpha)$ is the distance from the tip of the field vector $\vec{h}$ to the tangent on the threshold curve as shown.

virtual displacement, $\delta\varphi_o$, of the magnetization is large. As $h(\alpha)$ decreases, the restoring torque decreases until at $h(\alpha) = 0$, there is no longer a restoring torque and φ_o may make a discontinuous jump to a new stable position. When the magnetization in a film makes such a discontinuous jump, the film is said to have switched.

It is easily verified with use of equation (2.7) and the stability criterion, $h(\alpha) > 0$, that if a magnetic film with a uniaxial anisotropy given by equation (2.1) could be made to remain in a single domain form it would exhibit low frequency hysteresis loops in the easy and hard directions like those diagrammed in Fig. 2-3. The easy axis coercive force, H_c, would be equal to H_k, the anisotropy field. In reality magnetic thin films do not exhibit these ideal characteristics. Seldom is the coercive force equal to the anisotropy field. In some films $H_c < H_k$ because domains do form and domain wall motion does occur. In other films $H_c > H_k$ because of reaction torques from ripple which will be discussed later. Furthermore, the ideal hard axis loop shown in Fig. 2-3 is not always obtained. One of the causes of this is anisotropy dispersion or variations in the easy axis direction (angular dispersion) or magnitude of the anisotropy field (amplitude dispersion) as a function of position in the film. Fig. 2-4 shows the easy and hard axis hysteresis loops of a typical permalloy thin film in which $H_c = 1.8$ oe and $H_k = 3.6$ oe. By properly calibrating the hysteresis loop tracer for each composition of the film, it is possible to determine the thickness of a film by the magnitude of the hysteresis loop. This was done for the loop tracer used to observe the hysteresis loops of films used in this study.

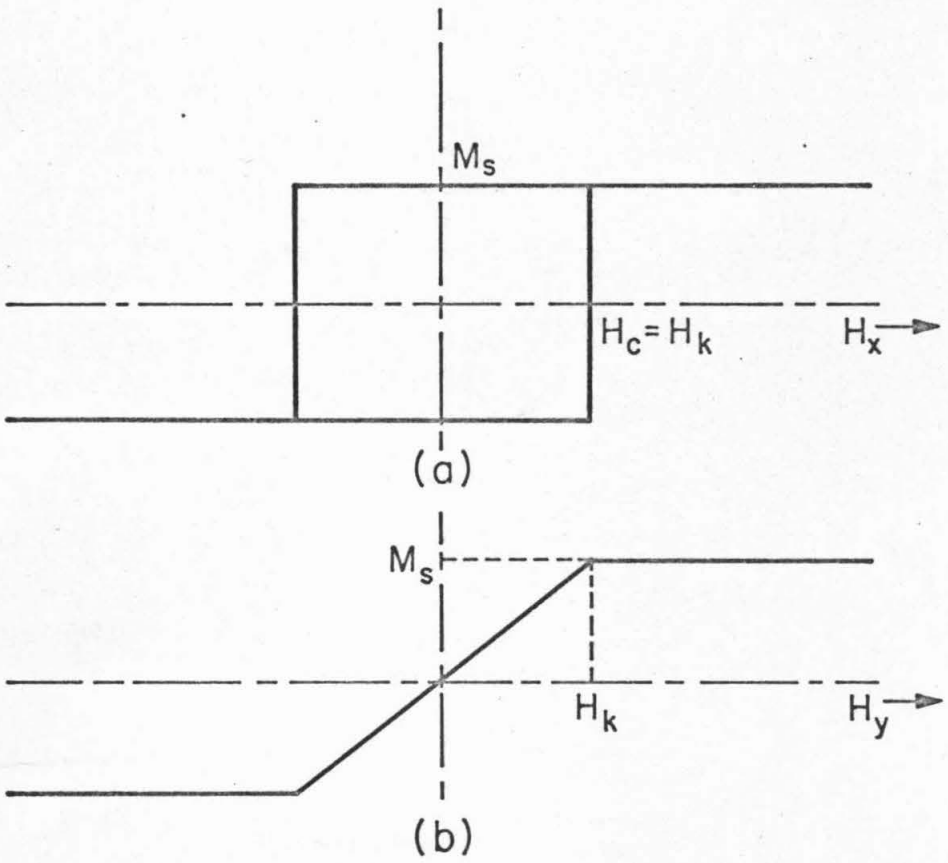

Fig. 2-3. (a) An idealized easy axis hysteresis loop for a film with anisotropy field equal to H_k. (b) An idealized hard axis hysteresis loop for a film with anisotropy field equal to H_k.

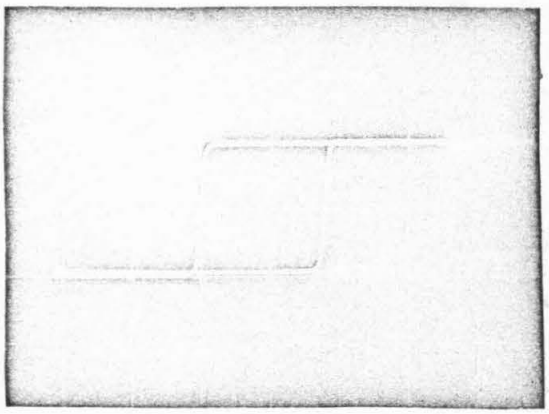

(a)

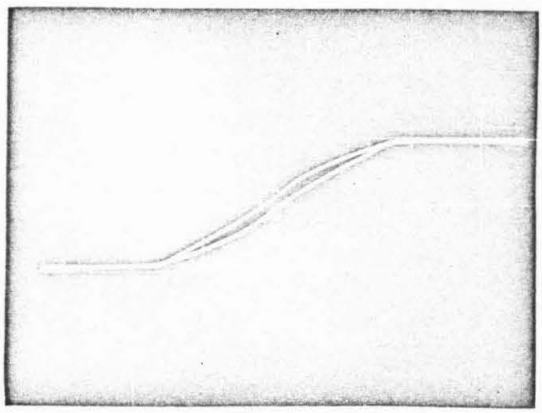

(b)

Vertical: relative.
Horizontal: 2 oe/div.

Fig. 2-4. (a) A typical easy axis hysteresis loop. (b) A typical hard axis hysteresis loop.

(For a description of the loop tracer see Humphrey (1967)). The calibration was done by determining the composition of films by X-ray fluorescence and the thickness by Tolansky multiple beam interferometry (Tolansky(1948)).

The torquemeter provides a means of measuring H_k in films at high fields where the effects of dispersion are reduced. Humphrey and Johnston (1963) have previously described the torquemeter used in this study and also gave a summary of the measurements which could be made with it. In this study the torquemeter was used to determine the relative values of K_u and M_s; from these $H_k = 2K_u/M_s$ was determined. The method used to determine the relative value of K_u was to apply a field in the plane of the film and to measure the resultant torque on the film. The torque on the film is given by

$$\vec{T}_f = V\vec{M} \times \vec{H} = \hat{i}_z VM_s H \sin(\alpha-\varphi_o), \tag{2.13}$$

where V is the volume of the film. It is known from (2.7) that at equilibrium $M_s H \sin(\alpha-\varphi_o) = K_u \sin 2\varphi_o$ so that

$$\vec{T}_f = \hat{i}_z VK_u \sin 2\varphi_o \ . \tag{2.14}$$

If the applied field is greater than H_k and is rotated about the film, the magnetization will also rotate. At some time during the rotation φ_o will be equal to 45^o and the torque will be at its maximum value T_m. Then K_u may be determined from

$$K_u = T_m/V. \tag{2.15}$$

In practice this torque measurement is usually done at several different values of field much greater than H_k. A plot of T_m vs. $1/H$ is then extrapolated to $H = \infty$ to determine the value of T_m to be used for a determination of K_u. In the films used in this study T_m was constant from 50 oe to 400 oe.

To measure M_s with a torquemeter a field is applied at some angle ω to the plane of the magnetic film. With the easy axis perpendicular to the torsion axis there will then be a torque parallel to the plane of the film. So long as the applied field is much less than the demagnetizing field, $4\pi M_s \approx 10^4$ gauss, the magnetization will remain approximately in the plane of the substrate. The torque on the film from the applied field will then be given by

$$T_\omega = - M_s HV \sin \omega \tag{2.16}$$

so that the saturation magnetization may be determined by

$$M_s = - \frac{T_\omega}{HV \sin \omega} \quad . \tag{2.17}$$

Using (2.15) and (2.17) , $H_k = 2K_u/M_s$ may be determined independently of the calibration of the torque meter.

Many methods of measuring anisotropy dispersion in magnetic films have been used. Crowther (1959) proposed a method of measuring angular anisotropy dispersion. Basically his method was to switch a magnetic film from one hard axis to another and to observe the voltage induced in a pickup loop oriented to measure the longitudinal (easy axis direction) flux. If the mean hard axis were correctly aligned with the pulse

field then the voltage induced would be zero as half the magnetization in the film would rotate in one direction and half in the other. If the hard axis of the film is rotated by an angle β from the switching field direction then more magnetization will rotate in one direction than another and a signal will be induced in the pickup loop. A distribution function describing the percentage of magnetization rotating in one direction versus β can be deduced from the induced voltage versus β data. As a simplification, the angles α_{90} and α_{50} can be measured at which the voltage is 90% and 50%, respectively, of its peak value. Although α_{90} and α_{50} measured in this way do give a measure of the anisotropy dispersion, it is not clear that that is all one is measuring when he uses this technique. Exchange and magnetostatic coupling between regions of high and low angular dispersion, for example, can and probably does effect the measured values. Hoffmann (1964) in his ripple theory did calculate expressions to relate the values α_{90} and α_{50} to the r.m.s. anisotropy dispersion (both angular and amplitude), however his calculation does not take into account macroscopic anisotropy dispersion in which large fractions of the film have different uniaxial anisotropy. Rather, his calculation includes only microscopic anisotropy dispersion such as crystalline anisotropy which varies over regions much smaller than the dimensions over which one can expect exchange and magnetostatic coupling. Many films do exhibit macroscopic anisotropy dispersion and therefore Hoffmann's calculation is frequently not applicable. In spite of the poor present understanding of α_{90} and α_{50} they do give a qualitative description of

anisotropy dispersion in magnetic films. Because they are commonly used to characterize magnetic films, they will be given for each of the films investigated in this study.

Table 2-I lists the films used in this study and their characteristics. They were all evaporated at a rate of roughly 1000 Å per minute. The compositions of the melt and of the film differ because the iron evaporates more quickly than the nickel. The coercive force, H_c, and thickness, d, of the films were determined with a hysteresis loop tracer; the anisotropy field, H_k, with the torque magnetometer; the saturation magnetization, M_s, from the values given by Bozorth (1951) for bulk materials; the anisotropy constant, K_u, from the relation $K_u = 1/2\ H_k M_s$; and the quantities α_{50} and α_{90} were measured by the method of Crowther (1959). Also listed in the table is the temperature of the glass substrate at the time of deposition.

2.2 Flux Reversal in an Ideal Single Domain Film

The gyromagnetic equation for describing the motion of the magnetization, $\vec{M}(\vec{r},t)$, is

$$\frac{d\vec{M}}{dt} = -\gamma \vec{M} \times \vec{H}^* + (\text{damping term}), \tag{2.18}$$

where γ is the absolute value of the gyromagnetic ratio and $\vec{H}^*$ is the total effective magnetic field. For the idealized model in which $\vec{M}(\vec{r},t) = \vec{M}_o(t)$, not a function of position, $\vec{H}^*$ is the sum of the external applied fields; the effective uniaxial anisotropy field; and the demagnetizing field, $-4\pi\vec{M}_o(t)\cdot\vec{i}_z\ \vec{i}_z$, where $\vec{i}_z$ is a unit vector normal to the plane of the film.

Table 2-I

FILM PROPERTIES

Film	81-4-6	81-4-12	81-10-4	84-8-7	88-14-3	88-14-3a*
Composition of Melt (Ni-Fe)	83-17	83-17	75-25	83-17	83-17	83-17
Composition of Film (Ni-Fe)	81-19	81-19	68-32	81-19	81-19	81-19
Temp. of Substrate (^{o}C)	200	200	200	27	50	300*
d (A°)	930	960	1225	900	525	525
H_c (oe)	1.7	1.7	2.5	3.0	4.7	4.2
H_k (oe)	3.6	3.6	7.7	5.1	6.5	4.5
M_s (emu)	780	780	990	780	780	780
K_u (ergs/cm^3)	1400	1400	3900	2000	2540	1760
α_{50} (deg)	0.5	0.4	0.9	0.75	0.6	1.5
α_{90} (deg)	2.1	1.7	2.2	2.1	2.3	3.9

*Film 88-14-3 was annealed for 18 hours at 300^{o}C in a vacuum with a 30 oe field applied parallel to the easy axis, after evaporation onto a substrate at 50^{o}C. The annealed film is referred to as 88-14-3a.

The precise damping term is unknown. Various phenomenological damping terms have been proposed, but no adequate description of the actual damping mechanism has been found. Indeed, one of the purposes of the research described in this thesis is to find explanations for the observed damping. However, since we do not know the damping that exists but still would like to examine what type of effect damping might have, we shall consider a damping term proposed by Landau and Lifschitz (1935). They proposed the term

$$- \frac{\alpha_d \gamma}{M_s} \vec{M} \times (\vec{M} \times \vec{H}^*), \tag{2.19}$$

where α_d is the so-called damping parameter and $|\vec{M}| = M_s$.

Assume the coordinate system shown in Fig. 2-1 in which the $\vec{i}_x$ direction is the easy direction of anisotropy nearest to $\vec{M}_o(0)$. If $\epsilon_o(\theta_o,\varphi_o)$ is the energy density of $\vec{M}_o(t)$ in the applied, demagnetizing, and anisotropy fields, then the effective field is

$$\vec{H}^* = - \nabla_{\vec{M}_o} \epsilon_o \tag{2.20}$$

Using (2.18) with (2.19) and (2.20):

$$\frac{d\theta_o}{dt} = \frac{-\gamma}{M_s} \frac{\partial \epsilon_o}{\partial \varphi_o} - \frac{\alpha_d \gamma}{M_s} \frac{\partial \epsilon_o}{\partial \theta_o} \tag{2.21a}$$

and

$$\sin \theta_o \frac{d\varphi_o}{dt} = \frac{\gamma}{M_s} \frac{\partial \epsilon_o}{d\theta_o} - \frac{\alpha_d \gamma}{M_s} \frac{\partial \epsilon_o}{\partial \varphi_o} . \tag{2.21b}$$

Assuming uniaxial anisotropy perpindicular to the plane of the film equal to that in the plane,

$$\epsilon_o = - M_s H \sin \theta_o \cos (\varphi_o-\alpha)+2\pi M_s^2 \cos^2\theta_o -K_u(1-\sin^2\theta_o\cos^2\varphi_o). \quad (2.22)$$

Then, let $\psi_o = \theta_o - \frac{\pi}{2}$ and assume

$$|\psi_o| \ll 1 \quad (2.23)$$

which should be well satisfied if

$$4\pi M_s \gg H . \quad (2.24)$$

Furthermore if

$$4\pi M_s \gg H_k \quad (2.25)$$

which is almost always true in practice, by substituting (2.22) into (2.21a,b) one obtains:

$$\frac{d\psi_o}{dt} = \gamma H \sin (\varphi_o-\alpha) + \frac{\gamma}{2} H_k \sin 2\varphi_o - \alpha_d\gamma 4\pi M_s \psi_o \quad (2.26a)$$

$$\frac{d\varphi_o}{dt} = \gamma 4\pi M_s \psi_o + \alpha_d\gamma H \sin (\varphi_o-\alpha) + \frac{\alpha_d\gamma}{2} H_k \sin 2\varphi_o . \quad (2.26b)$$

Now consider the case usually used in thin film flux reversal in which a pulse field H_p is applied at an angle α_p in the presence of a static bias field H_b applied at an angle α_b. By introducing the dimensionless variables

$$\tau = \sqrt{4\pi M_s H_p}\ \gamma t \quad (2.27a)$$

$$\sigma_o = \sqrt{\frac{4\pi M_s}{H_p}}\ \psi_o \quad (2.27b)$$

into (2.26a,b) and again using (2.24), two coupled equations describing

the flux reversal process are obtained:

$$\dot{\sigma}_o = \frac{T(\varphi_o)}{M_s H_p} - \alpha_d \sqrt{\frac{4\pi M_s}{H_p}}\ \sigma_o \qquad (2.28a)$$

$$\dot{\varphi}_o = \sigma_o \ . \qquad (2.28b)$$

where $T(\varphi_o)$ is given as in (2.7), but is not zero when the magnetization is not at equilibrium.

The equations (2.28a,b) describe thin film flux reversal by uniform rotation. They demonstrate that there is a primary precession about the applied and anisotropy field followed by a secondary precession about the demagnetizing field. Except for a small term which was neglected in obtaining (2.28b), it is seen that the primary precession about the demagnetizing field is all that is damped.

In general (2.28a,b) cannot be solved analytically for an anisotropic film with an arbitrary value of α_d; instead, numerical methods must be used. In the few cases which can be solved analytically and in those solved numerically, using typical values of $\alpha_d \approx .01$ found from ferromagnetic resonance, the reversal time is found to be field dependent and to be on the order of a nanosecond when fields on the order of one oersted over the Stoner-Wohlfarth threshold are applied.

2.3 Flux Reversal-Experimental Background.

2.3.1 General. It was suggested by Humphrey and Gyorgy (1959) that three different mechanisms were involved in the reversal process. They based this proposal on the fact that a plot of the reciprocal of the time for flux reversal versus applied longitudinal field for constant

transverse bias field, could be divided into two linear and one nonlinear region. The low speed nonlinear region was ascribed to domain wall motion and nucleation processes. The facts that supported this conclusion were that no current was induced in a transverse sense loop around the film and that low speed quasistatic reversal was observed to be by domain wall motion with the Kerr magneto-optic effect and Bitter techniques. The process believed to be involved in the high speed region was uniform rotation. Olson and Pohm (1958) showed that for reversal in this region, the slope of the curves predicted values of α_d, the damping parameter in the Landau-Lifschitz equation, to be within a factor of 2 or 3 of that obtained by ferromagnetic resonance in thin films. However, as Humphrey and Gyorgy (1959) pointed out, the threshold for this high speed region did not correspond to the Stoner-Wohlfarth threshold as it should if the uniform rotation model was truly correct. In fact, it was found that the intermediate speed region extrapolated roughly to the Stoner-Wohlfarth threshold. Yet, the flux reversal times in the intermediate speed region were much too slow for uniform rotation. Humphrey and Gyorgy (1959) suggested that in this intermediate region, the magnetization rotated coherently at first and then broke up into "noncoherent rotation" whereby the phase of the precession varied with position in the film. They based this proposal on the observed signals induced in longitudinal and transverse pickup loops around a film.

Typical examples of flux reversal curves are shown in Figs. 2-5 and 2-6 where the reciprocal of the reversal time is plotted against

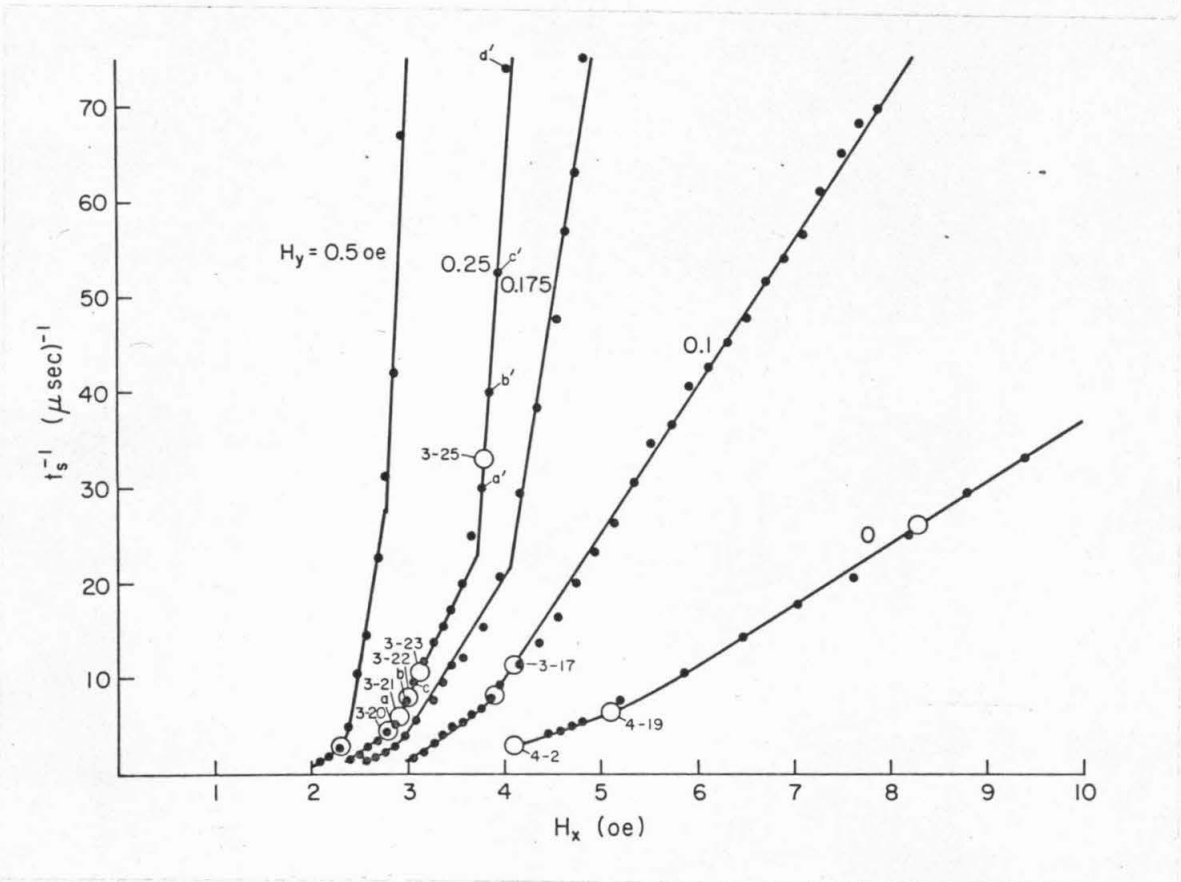

Fig. 2-5. Plots of the reciprocal of the switching time, t_s, versus applied longitudinal pulse field, H_x, with transverse bias field, H_y, (given in oersteds) as a parameter for film 81-4-6. Data indicated by ° were taken using inductive sense loops. The symbols O represent the values of field at which the reversal process has been photographed. Figure numbers are indicated.

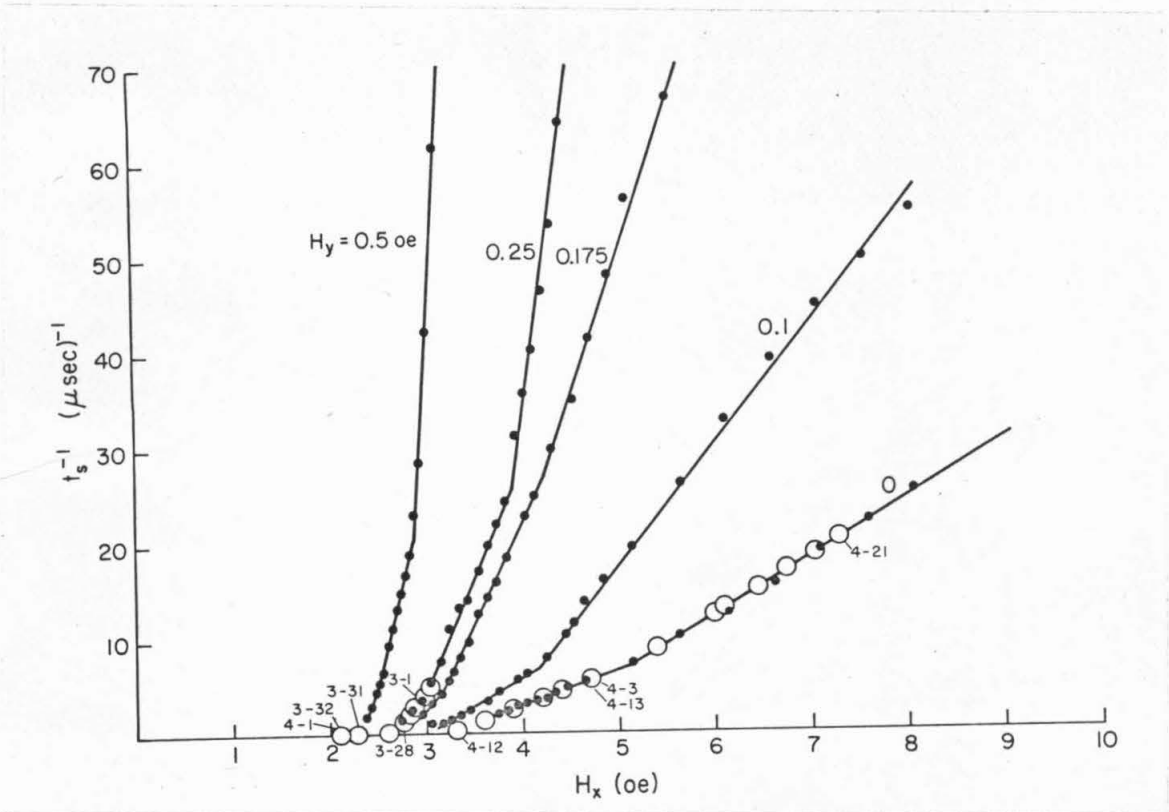

Fig. 2-6. Plots of the reciprocal of the switching time, t_s, versus applied longitudinal pulse field, H_x, with transverse bias field, H_y, (given in oersteds) as a parameter for film 81-4-12. Data indicated by • were taken using inductive sense loops. The symbols O represent the values of field at which the reversal process has been photographed. The figure numbers are indicated.

longitudinal pulse field with the transverse bias field as a parameter for films 81-4-6 and 81-4-12. The data represented by · were taken by observing the integrated signal induced in a single turn loop oriented so as to pickup the easy axis flux change in the magnetic film. The 10% - 90% risetime of the observed signal was defined as the reversal time, t_s. The apparatus with which this data were taken is similar to that described by Humphrey (1967). It is seen that the curves taken with a transverse field may indeed be fitted by two linear and one nonlinear curve, as Humphrey and Gyorgy (1959) suggested. The nonlinear portion is only slightly visible on these curves and corresponds to very low speed switching. The intermediate linear region is fairly well defined and extends up to $t_s^{-1} \approx 20\ \mu sec^{-1}$ for transverse fields of 0.175, 0.25, and 0.5 oe. The high speed linear portion extends up from the intermediate linear region.

Also shown in Figs. 2-5 and 2-6 are some of the values of applied fields at which the flux reversal process has been photographed with the Kerr magneto-optic camera described in Chapter 6. The figures in which the reversal process is shown is indicated. The symbols, 0, are not true data points as the reversal time determined from the Kerr photographs is frequently different from that determined with the inductive sense loops because bandwidth limitations of the inductive sense loop apparatus prevent some of the reversal process from being sensed. These bandwidth limitations will be discussed in more detail later in Section 3.2.6.

The photographs obtained from the Kerr magneto-optic camera have

made it possible to observe the detailed dynamic flux reversal processes occurring in magnetic thin films. The reversal processes have been found to be extremely complex. Due to the complexity, they are most easily described with reference to Kerr photographs which show the dynamic magnetization configuration. Many of these photographs will be shown in subsequent chapters. From these photographs it has been found that rather than three mechanisms of flux reversal there are at least five. All of these mechanisms are quite distinct. They are (1) domain wall motion, (2) diffuse boundary propagation, (3) non-coherent rotation, (4) coherent rotation, and (5) nucleation and subsequent reversal of partially reversed regions. Non-coherent rotation and coherent rotation occur only during flux reversal with a transverse field, while all of the other mechanisms occur during flux reversal either with or without a transverse field. Each of these mechanisms will be discussed in some detail later. It should be stressed that the classification was made on the basis of the observed magnetization configuration rather than on the basis of the flux-reversal curves. Previously the term "non-coherent rotation" has been used to describe whatever processes were occurring during the intermediate linear portion of the flux-reversal curve obtained with a transverse field and also during the linear portion of the zero transverse field curve.

2.3.2 Domain Wall Motion. Domain wall motion is a relatively well known phenomenon occuring in the flux reversal of most ferromagnetic materials. In thin films possessing a uniaxial anisotropy, when no transverse fields are applied, the magnetization is normally along the

easy axis so that the 180° domain wall is the expected configuration. Magnetostatic fields created by the change in the component of $\vec{M}$ perpendicular to the wall cause the wall to lie parallel to the easy axis. When an easy axis field greater than the coercive force is applied, the wall moves in the hard axis direction causing the domain whose magnetization lies parallel to the applied field to grow at the expense of the other. The velocity of the wall is field dependent and goes to zero near the coercive force of the film. Typically the velocity versus field plot has a constant slope or mobility.

Landau and Lifshitz (1935) first calculated expected velocities of a wall separating reverse domains in bulk material by considering losses in a phenomenological manner. Their analysis was based on the previously mentioned Landau-Lifshitz equation. Galt (1952) advanced their phenomenological treatment to obtain the domain wall velocity of walls with arbitrary magnetization distribution. Eddy current losses in bulk material were considered by Williams, Schockley, and Kittel (1950) who approximated the wall by a transition region of zero width. Ford (1960) adapted the calculation of eddy current losses to thin films, but retained the assumption of a zero-width wall. Subsequently Patton, McGill, and Wilts (1966) calculated eddy current losses for a wall of finite width and found them to be not significantly different from the zero-width prediction.

Experimentally Menyuk (1955) observed the thickness dependence of the reversal time of permalloy tape cores and concluded that eddy current losses were negligible for tape thinner than 3×10^4 Å. Ford

(1960), on the other hand, found domain wall velocities in films 700-4000 Å thick that were in agreement with his predictions of eddy current losses. However, more recent wall motion measurements by Copeland and Humphrey (1963), Il'icheva and Kolotov (1965), Patton and Humphrey (1966), and Middelhoek (1966) do not agree with Ford's data and indicate that eddy-current losses are negligible in thin films.

The most complete and recent study is that of Patton and Humphrey (1966). Their data clearly indicate that eddy current losses are negligible in thin films. They found that a phenomenological treatment of losses based on the Landau-Lifshitz equation and calculated static wall shapes did fit the data for films in the 300-800 Å range. However, for thicker films the data did not agree with this treatment, and they suggested that the calculated static wall shapes may be in error for the thicker films. This view is supported by Suzuki, Wilts, and Patton (1968) who found large differences between calculated wall shapes and wall shapes experimentally observed by Lorentz microscopy for films thicker than 800 Å.

Although a detailed study of domain wall motion has not been made with the use of the Kerr magneto-optic camera described in Chapter 6, for purposes of comparison with other processes some photographs showing domain wall motion are displayed in Fig. 2-7. This figure shows static domains on film 81-4-6 during interrupted-pulse flux reversal with zero transverse field and a 1.9 oe longitudinal pulse field. The 1 cm diameter thin film appears as an ellipse because the camera is oriented at 60° to the normal of the film. In these photographs, like

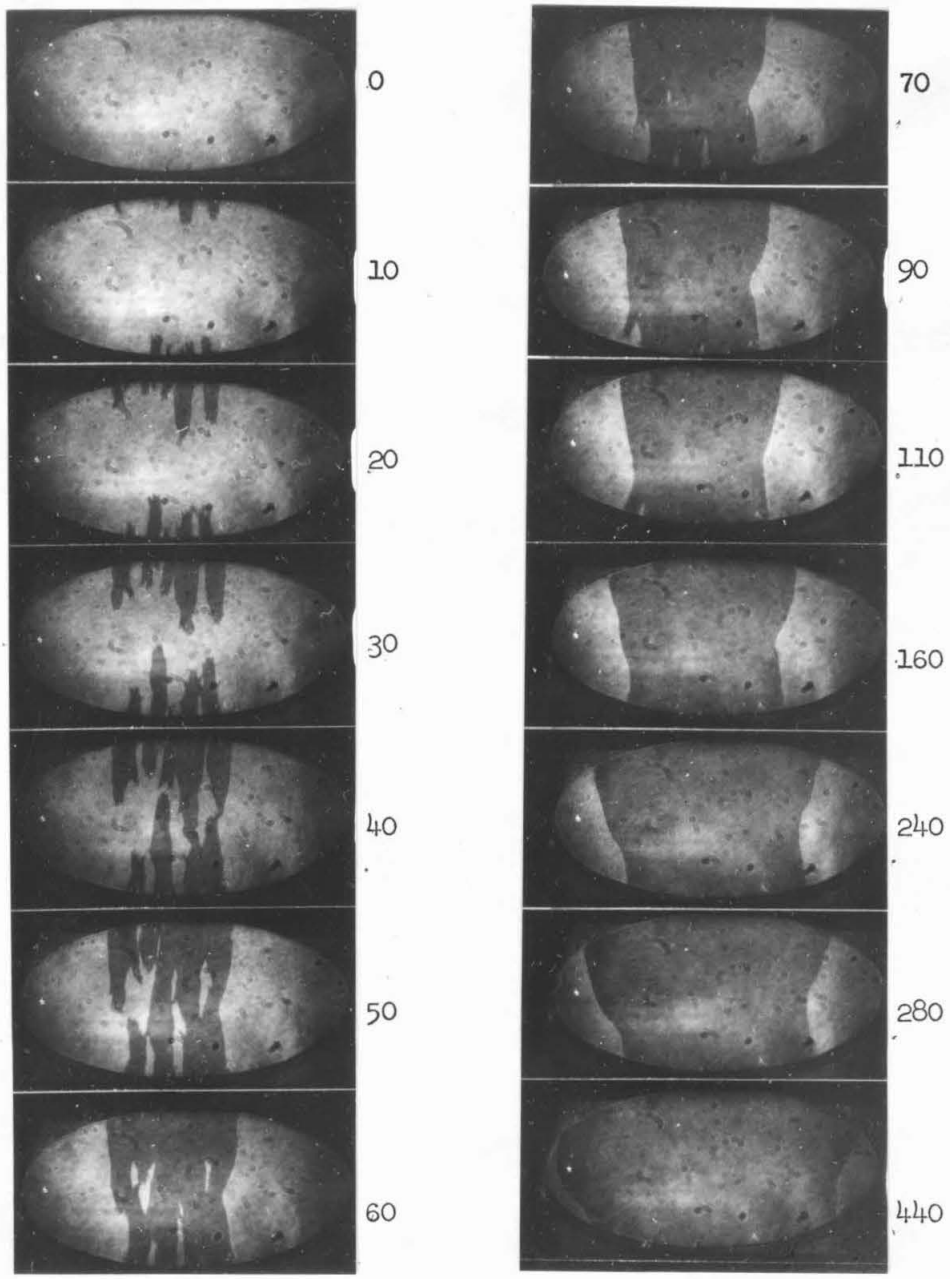

Fig. 2-7. Film 81-4-6 in the process of quasi-static domain wall motion with a 1.9 oe longitudinal pulse field. The total time duration in microseconds of the applied field (applied in 10 μsec long pulses) before the taking of each photograph is indicated.

all others in this thesis, the easy axis corresponds to the minor axis of the ellipse (vertical in the photographs shown here). In the lighter regions on the photographs, the direction of the magnetization is toward the top of the photograph. In the darker regions the magnetization is directed toward the bottom which is the direction of the applied pulse field.

It should be emphasized that these are photographs of static, not dynamic, domain configurations. These photographs were not taken during the actual reversal process like others which will be shown later, but rather were taken some time after the application of 10 μsec long pulses. The total duration in microseconds of the 1.9 oe magnetic field pulses applied before the taking of each photograph is indicated by the number at the right of each photograph.

In the 0 μsec photograph no reverse domains are visible because no pulse field has yet been applied. After a single 10 μsec pulse, reverse domains are visible as dark areas at the upper and lower edges of the magnetic film. With subsequent 10 μsec pulses these reverse domains grow in the easy axis direction, until at roughly 60 μsec the domains from the upper and lower edges join. After 60 μsec domain wall motion occurs. It is seen in the 70 μsec photograph that the walls are sharply defined and lie approximately parallel to the easy axis. With subsequent pulses after 70 μsec the domain walls move in the hard axis direction, sweeping out the unswitched portion of the film. There are clear differences between the reversal process occuring before and after 60 μsec. In this study and in that made by Patton (1967) only

the process after 60 μsec is called domain wall motion. The velocity of propagation occuring before 60 μsec in the easy axis direction is on the order of 0.01 cm/μsec while the velocity of domain wall motion occuring after 60 μsec is on the order of .00075 cm/μsec. Furthermore the propagation before 60 μsec involves diffuse tips rather than well defined domain walls.

The practice of observing flux reversal processes by interrupting the drive field and observing the resultant static domain pattern must be used with extreme care. It will be shown in Chapter 5 that if a pulse field is interrupted during high speed flux reversal processes, considerable change occurs in the magnetization configuration before static equilibrium is obtained. Interrupted pulse techniques were used in obtaining the photographs of Fig. 2-7 for two reasons. First of all, the Kerr magneto-optic camera is presently equipped with a pulser which allows no longer than 10 μsec pulses to be applied. Secondly, there is evidence that the interrupted pulse technique is valid if used with care during domain wall motion processes. Patton (1967) showed that the measured velocity of a domain wall was independent of pulse length from 1 μsec to 50 μsec indicating that any changes from the static to dynamic configuration occured in much less than 1 μsec and therefore that so long as pulses longer than 1 μsec were used that the technique should be valid.

2.4 Ripple Theory.

Fuller and Hale (1960) used a defocused electron microscope to observe the Lorentz deflection of electrons by the magnetic induction

$\vec{B} = 4\pi\vec{M}(\vec{r})$ in a thin magnetic film. They observed not only the expected discontinuities of domain walls, but also a wave-like magnetic structure which they called ripple. Subsequently Fuchs (1961) and Suzuki and Wilts (1968) have confirmed this discovery. Fig. 2-8 is a Lorentz micrograph taken by Takao Suzuki which shows ripple structure. Both longitudinal and transverse ripple with wave vector parallel and perpendicular, respectively, to the mean magnetization are assumed to exist in a thin film. The two types are diagrammed in Fig. 2-9. Since the volume divergence of the magnetization is large for the transverse ripple and small for the longitudinal ripple, while the exchange and anisotropy energies are equal, the longitudinal component is the dominant type of ripple existing in static equilibrium. Hence the mean magnetization is perpendicular to the observed fine structure lines. Suzuki (1969) has shown that the mean wave length is dependent upon the applied field and that it varies from about 1μ to 7μ for fields applied along the easy axis in the range $-H_k < H < 3H_k$.

The cause of ripple is not entirely clear. Suzuki (1969) and Suzuki and Wilts (1968) indicate that, at least for films which have been removed from their substrates, the random crystalline anisotropy produced by the random orientation of the crystallites in the magnetic film is a major factor. It is probable that other sources of local anisotropy such as magnetostrictive effects also contribute to ripple in films still attached to a substrate.

Hoffmann (1968) and Harte (1968) have both treated the origin of ripple theoretically. Using different viewpoints, they arrived at results which differ only by numerical factors. Hoffmann (1968)

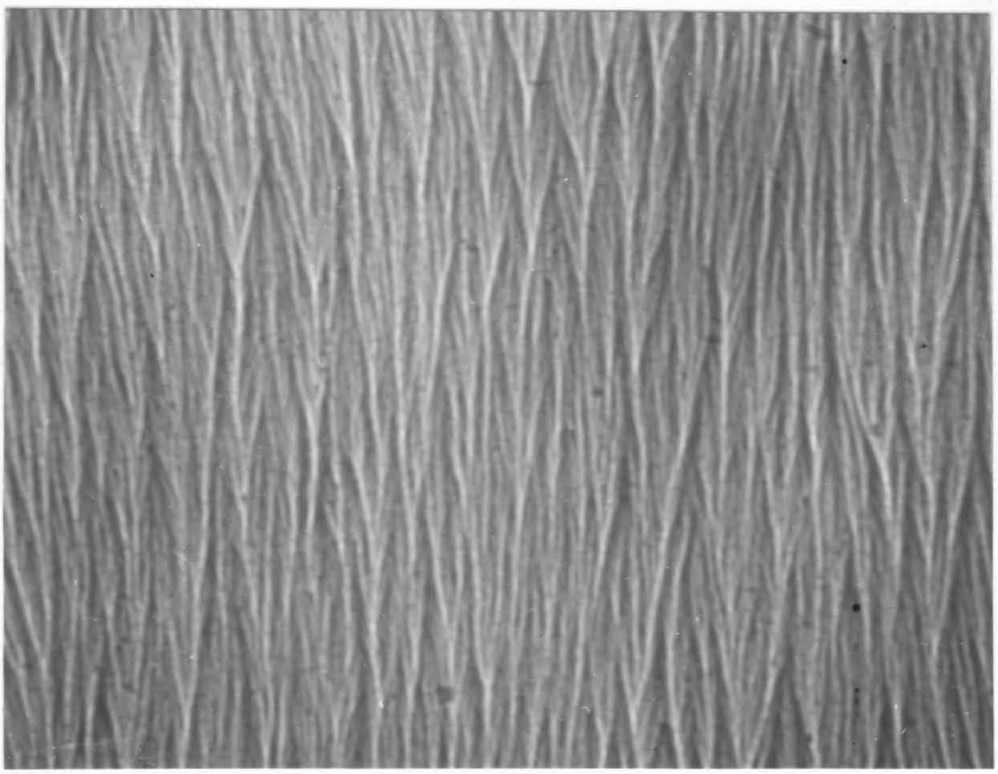

Fig. 2-8. A Lorentz micrograph of ripple structure in a magnetic film--taken by T. Suzuki.

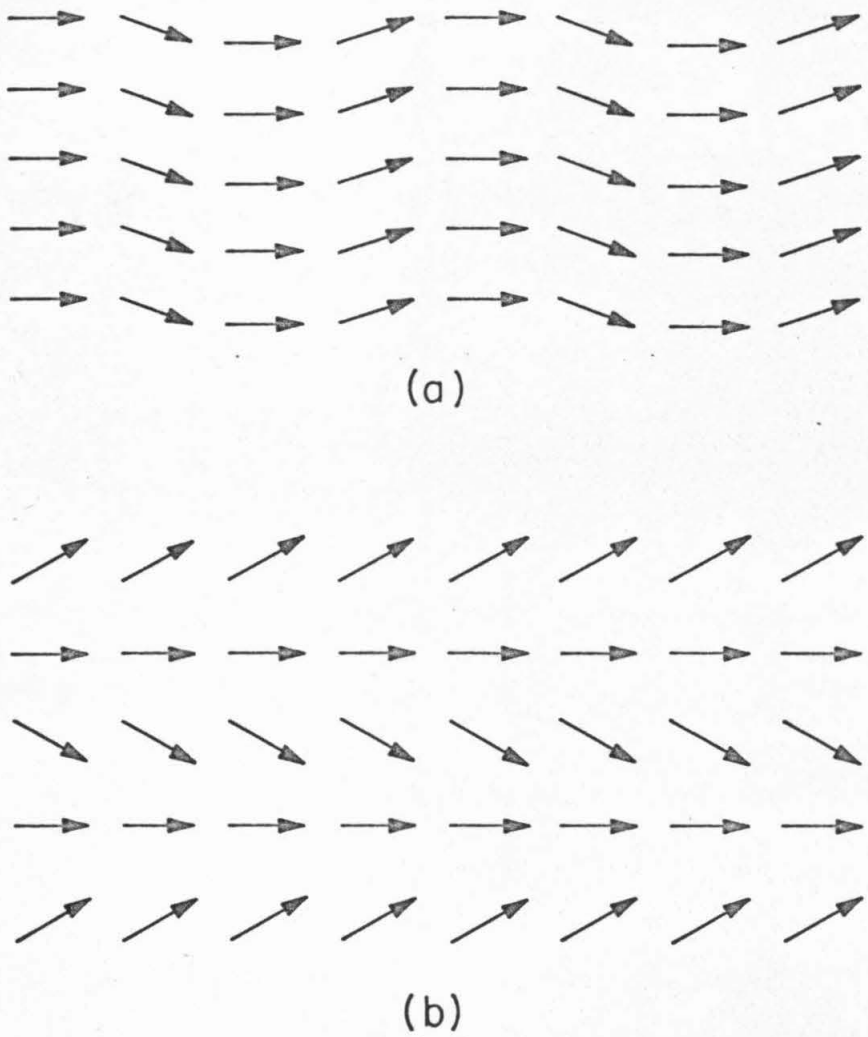

Fig. 2-9. (a) Longitudinal ripple. (b) Transverse ripple.

approached the problem by considering the spatial dependences of the various components of fields and magnetization. In order to do this he used a Taylor series expansion for the magnetostatic energy keeping only the low order terms. Harte (1968), on the other hand, made a Fourier analysis of the ripple. By doing this he was able to include the magnetostatic energies without a Taylor series expansion and therefore, as Brown (1969) pointed out, made a more rigorous treatment in that respect. Because Hoffmann included the spatial dependences of the fields and magnetization, local effective fields may be computed by his method, while with Harte's method only average effective fields may be computed. Harte's method is useful because time dependences of the various Fourier components can easily be investigated. Since both local fields and time dependences are important in the flux reversal problem, it is necessary to combine their analyses, being consistent in choice of numerical factors. Because of the general agreement among their results, and because both models are reasonably well established by experiment, such an approach is justified.

Both authors considered contributions to the total energy or alternatively the torque on the magnetization, from exchange, uniaxial anisotropy, applied fields, magnetostatic fields, and local anisotropy. A central result of their calculations is the root-mean-square amplitude of the ripple, or the magnetization dispersion,

$$\sqrt{\overline{\varphi^2}} = 0.243 \frac{\left(\frac{K_s D \sigma_1}{\sqrt{n}}\right)}{(AK_u)^{3/8}(M_s\sqrt{d})^{1/2}(\overline{h_{eff}(\alpha)})^{3/8}} , \qquad (2.29)$$

where:

K_s = r.m.s. value of the local anisotropy constant.

D = mean crystallite diameter.

σ_1 = standard deviation of the angular function describing the local anisotropy.

n = number of crystallites through the film thickness with different preferred directions of local anisotropy.

A = exchange constant.

K_u = uniaxial anisotropy constant.

M_s = saturation magnetization.

and

d = film thickness.

The term $\overline{h_{eff}}(\alpha)$ is a mean effective field defined by:

$$\overline{h_{eff}}(\alpha) = h(\alpha) + \overline{h_d}(\alpha) + \overline{h_{k3}}(\alpha) + \overline{h_{u3}}(\alpha) + \ldots \qquad (2.30)$$

where $h(\alpha)$ is the single domain field given by (2.10), $\overline{h_d}(\alpha)$ is a mean effective field caused by the nonlinear magnetostatic stray fields of the longitudinal ripple, $\overline{h_{k3}}(\alpha)$ is a nonlinear mean effective field caused by the random anisotropy variations, and $\overline{h_{u3}}(\alpha)$ is the nonlinear mean effective field caused by uniaxial anisotropy and applied fields. The derivation of each of these terms will be discussed later.

The notation used above is that of Hoffmann (1968). Harte (1968) treated only the case in which $\sigma_1 = 1/\sqrt{2}$ and $n = 1$. The numerical factor of 0.243 was chosen in a manner thought to reconcile the theories. Because Harte (1968) did not approximate the magnetostatic energy while

Hoffmann (1968) did it is believed that Harte's results are more accurate. On the other hand in real films local anisotropy variations with other than sinusoidal energy dependences surely occur and therefore Hoffmann's theory is slightly more general in that it allows for angular fluctuations for which the standard deviation, σ_1, is other than $1/\sqrt{2}$. In order to retain the accuracy of Harte's (1968) calculations and also the more general form of Hoffmann (1968), Hoffmann's notation with the numerical factor of Harte (1968) was used but multiplied by $\sqrt{2}$ to account for the more general case in which $\sigma_1 \neq 1/\sqrt{2}, n \neq 1$. Numerical factors throughout all the calculations in this study were chosen to be consistent with this method.

Suzuki (1969) has pointed out that because of wave optical limitations, Lorentz microscopy cannot be used to measure ripple amplitude. Nevertheless, Fuchs (1961), Baltz (1964), and Suzuki (1969) did show that ripple vanished at the composition at which magnetocrystalline anisotropy goes to zero. This is in agreement with (2.29) and shows that for films which have been removed from substrates, magnetostrictive effects do not add significantly to ripple.

Both Harte and Hoffmann's analyses may be used to calculate the Fourier components of the ripple. The expressions obtained indicate how exchange and transverse magnetostatic fields affect the ripple and also can be used to determine the wavelength of ripple expected to be seen with an electron microscope, thereby providing an important contact with experiment. Furthermore, the Fourier expressions illustrate the nature of Hoffmann's magnetostatic field approximation.

Hoffmann's approach leads to

$$\varphi_{\vec{k}} = \frac{-K_s}{2K_u \overline{h}_{eff}} \frac{f_{1\vec{k}}}{1 + r_e^2 k^2 + r_m' d k^2 \sin^2(\varphi_o - \Phi_{\vec{k}})} \tag{2.31}$$

where

$$r_e^2 = \frac{A}{K_u \overline{h}_{eff}} \tag{2.32a}$$

$$r_m' = \frac{C_y M_s^2}{d2K_u \overline{h}_{eff}} \quad . \tag{2.32b}$$

The quantity $\Phi_{\vec{k}}$ is the angle which the wave vector $\vec{k}$ makes with the easy axis, and $f_{1\vec{k}}$ is a Fourier component of a random function describing the local anisotropy. The parameter, C_y, which Hoffmann evaluated by a self consistency argument is

$$C_y = 16\, d \sqrt{\frac{A}{K_u \overline{h}_{eff}}} \quad . \tag{2.33}$$

Harte (1968) on the other hand calculates $\varphi_{\vec{k}}$ to be:

$$\varphi_{\vec{k}} = \frac{-K_s}{2K_u \overline{h}_{eff}} \frac{f_{1\vec{k}}}{1 + r_e^2 k^2 + \frac{2r_m}{d} \tilde{\chi}_{\vec{k}} \sin^2(\varphi_o - \Phi_{\vec{k}})} \tag{2.34}$$

where

$$r_m = \frac{\pi M_s^2 d}{K_u \overline{h}_{eff}(\alpha)} \tag{2.35a}$$

and

$$\tilde{\chi}\left(\frac{kd}{2}\right) = 1 - \left(\frac{kd}{2}\right)^{-1} e^{\frac{-kd}{2}} \sinh\left(\frac{kd}{2}\right) . \tag{2.35b}$$

For long wave length ripple ($\frac{kd}{2} \ll 1$), $\tilde{\chi}$ may be approximated by

$$\tilde{\chi}\left(\frac{kd}{2}\right) = \frac{kd}{2} - \frac{2}{3}\left(\frac{kd}{2}\right)^2 + \ldots , \qquad (2.36a)$$

while for short wave length ripple it may be approximated by

$$\tilde{\chi}\left(\frac{kd}{2}\right) = 1 - \frac{1}{2\left(\frac{kd}{2}\right)} + \ldots \quad . \qquad (2.36b)$$

The only difference in equations (2.31) and (2.34) for the Fourier components of the ripple is in the terms involving $\sin^2(\varphi_o - \Phi_{\vec{k}})$. These terms come from the magnetostatic fields produced by transverse components of the ripple. Harte's result which was calculated without a Taylor series expansion of the magnetostatic field, varies as k for ripple with wave-length long compared to the film thickness and is independent of k for wave-lengths short compared to the film thickness. On the other hand, Hoffmann's result varies as k^2 at all times. Hence Hoffmann's approximation underestimates the long wave-length magnetostatic interaction and overestimates the short wave-length magnetostatic interaction. In obtaining the r.m.s. ripple amplitude he effectively averages over both long and short wave-length components and the result is that his approximation is good.

Harte's expression for $\varphi_{\vec{k}}$ (2.34) characterizes the ripple. Because of the term $r_e^2 k^2$, ripple with wave-length less than $2\pi r_e$ is attenuated. For a film with no applied field, a typical value is $2\pi r_e \approx 1.5 \times 10^{-4}$ cm. Furthermore, transverse ripple (for which $\varphi_o - \Phi_{\vec{k}} = \frac{\pi}{2}$) with wave lengths less than $2\pi r_m$ is also strongly suppressed. Typically $2\pi r_m \approx 8 \times 10^{-2}$ cm. Hence, it is seen that indeed components of transverse ripple are very strongly suppressed, and as expected the ripple is mainly longitudinal.

Both Hoffmann (1968) and Harte (1968) calculated the dimensions of a coupling region within which the magnetization was strongly coupled by magnetostatic and exchange forces. Hoffmann's region is elliptical in shape with the minor axis parallel to the mean magnetization in the film, while Harte's is diamond shaped with a similar arrangement of axes. The minor axis of Harte's region is

$$d_{\parallel} = 2\pi r_e = 2\pi \sqrt{\frac{A}{K_u \overline{h_{eff}}(\alpha)}} \tag{2.37a}$$

and the major axis is

$$d_{\perp} = 2\pi r_m^{1/2} r_e^{1/2} = \frac{2\pi^{3/2} M_s d^{1/2} A^{1/4}}{K_u^{3/4} (\overline{h_{eff}})^{3/4}} \quad . \tag{2.37b}$$

Hoffmann's value for $d_{\perp}$ is 1.6 times Harte's while both values for $d_{\parallel}$ are the same. For a typical saturated film with no applied field so that $\overline{h_{eff}} \approx 1$, $d_{\parallel} \approx 1.5 \times 10^{-4}$ cm and $d_{\perp} \approx 3.5 \times 10^{-3}$ cm.

Also, from both Harte and Hoffmann's expressions for $\varphi_{\vec{k}}$, it is possible to calculate the dominant ripple wave length which one expects to see in an electron microscope. Fuller and Hale (1960) showed that the variation in intensity of the electron beam in the electron microscope due to the $\vec{k}^{th}$ component of ripple varied as $k|\varphi_{\vec{k}}|$. Hence, the most intense periodic variations in intensity seen with the electron microscope should be those with a wave length such that $k|\varphi_{\vec{k}}|$ is a maximum. Using either (2.31) or (2.34) the wave length λ, expected to be observed is

$$\lambda = 2\pi \sqrt{A/(K_u \overline{h_{eff}})} \quad . \tag{2.38}$$

Note that this is equal to $d_{\|}$, the longitudinal dimension of the coupling region which was calculated above to be 1.5μ. This is roughly the wavelength observed with zero applied field by Fuller and Hale (1960). Furthermore, Suzuki (1969) has examined the field dependence of the wavelength observed in thin films and found a dependence like that indicated by (2.38).

The average effective field, $\overline{h_{eff}}$, was calculated by both Harte (1968) and Hoffmann (1968). Hoffmann, however, in addition to calculating $\overline{h_{eff}}$ calculated the local effective field, h_{eff}, which includes the spatial variations in the effective field which are lost when one averages to obtain $\overline{h_{eff}}$. Since local effective fields are important in the flux reversal process, it is necessary to follow Hoffmann's calculation and compare the values of $\overline{h_{eff}}$ which he obtains with those of Harte (1968). For this calculation the coordinate system shown in Fig. 2-1 will be used. Since this calculation is based on static energy considerations only, $\theta_o = \frac{\pi}{2}$.

In order to calculate h_{eff} Hoffmann (1968) began with an equation for the total energy density, ε. This total energy density included energy from applied fields, uniaxial anisotropy, exchange, magnetostatic fields and local anisotropy. In order to find the equilibrium condition Hoffmann took the first variation of the energy density integral and set it equal to zero:

$$\delta \int \epsilon d\tau = 0 \quad . \tag{2.39}$$

This was used to calculate Euler's equation. Hoffmann (1968) then obtained Jacobi's differential equation by variation of Euler's equation. Such an analysis leads to

$$h_{eff}(\alpha) = h(\alpha) + h_{k2} + h_{k3} + h_{u2} + h_{u3} + h_d \tag{2.40}$$

where

$$h_{k2} = \frac{K_s}{2K_u} f_2 \tag{2.41a}$$

$$h_{k3} = \frac{K_s}{2K_u} \varphi f_3 \tag{2.41b}$$

$$h_{u2} = \varphi [h \sin (\alpha - \varphi_o) - 2 \sin 2 \varphi_o] \tag{2.41c}$$

$$h_{u3} = \frac{-\varphi^2}{2} [h \cos (\alpha - \varphi_o) + 4 \cos 2 \varphi_o] \tag{2.41d}$$

$$h_d = \frac{-M_s{}^2 C_x}{K_u} [2\varphi \frac{\partial^2 \varphi}{dx^2} + (\frac{\partial \varphi}{\partial x})^2] \tag{2.41e}$$

and $h(\alpha)$ is given by (2.10). The functions f_1, f_2, and f_3 are defined by

$$f_1 = \frac{dF_s}{d\Phi} (\varphi_o, \vec{r}) \tag{2.42a}$$

$$f_2 = \frac{d^2F_s}{d\Phi^2} (\varphi_o, \vec{r}) \tag{2.42b}$$

$$f_3 = \frac{d^3F_s}{d\Phi^3} (\varphi_o, \vec{r}) \tag{2.42c}$$

where $\Phi = \varphi_o + \varphi$ and where $F_s (\Phi, \vec{r})$ is the local anisotropy energy density. The terms h_{k3} and h_{u3} were neglected by Hoffmann, but are included for completeness here. As in calculating C_y for the transverse magnetostatic fields, Hoffmann evaluates C_x from a self-consistency

argument,

$$C_x = 4d \sqrt{\frac{A}{K_u h(\alpha)}} \quad . \tag{2.43}$$

The mean effective field, $\overline{h_{eff}}(\alpha)$ may be found by averaging $h_{eff}(\alpha)$:

$$\overline{h_{eff}}(\alpha) = h(\alpha) + \overline{h_d} + \overline{h_{u3}} + \overline{h_{k3}} \tag{2.44}$$

and $\overline{h_{k2}} = \overline{h_{u2}} = 0$. Each of the terms in (2.44) calculated by Hoffmann's method may be compared to Harte's corresponding terms. The results for $\overline{h_d}$ and $\overline{h_{u3}}$ show all the same dependences on film parameters, but they do differ by numerical factors. Using Hoffmann's (1968) notation and Harte's (1968) numerical factors generalized to account for cases in which $\sigma_1 \neq 1/\sqrt{2}$, $n \neq 1$, it is found that

$$\overline{h_d} = 0.41 \frac{M_s \sqrt{d}\, S^2}{(AK_u)^{5/4} (\overline{h_{eff}})^{1/4}} \tag{2.45a}$$

$$\overline{h_{u3}} = - 0.03 \frac{S^2}{M_s \sqrt{d} (AK_u)^{3/4}} \frac{[h(\alpha) + 3 \cos 2\varphi_o]}{(\overline{h_{eff}})^{3/4}} \tag{2.45b}$$

where the structure factor, S, has been defined as $S = (K_s D \sigma_1 / \sqrt{n})$. In the calculation of $\overline{h_{k3}}$, Harte and Hoffmann's methods lead to different dependences on the applied field and film parameters. As was done in arriving at (2.45a,b), the result obtained with Harte's analysis is used but with Hoffmann's notation and suitably corrected for cases in which $\sigma_1 \neq 1/\sqrt{2}$, $n \neq 1$:

$$\overline{h_{k3}} = \frac{S^2}{4\sqrt{2\pi}\, M_s\, K_u \sqrt{A}\, D} \quad . \tag{2.45c}$$

Therefore, $\overline{h_{k3}}$ is independent of $\overline{\overline{h_{eff}}}$, unlike $\overline{h_d}$ or $\overline{h_{u3}}$.

Blocking is caused by a local instability in the magnetization. Before blocking occurs the ripple is in equilibrium with the magnetization and

$$h_{eff}(\alpha) \approx h(\alpha) + h_d \quad . \tag{2.46}$$

That is, the local effective field, h_{eff}, mainly consists of $h(\alpha)$, the single domain field, and of h_d, the magnetostatic stray fields produced by the divergence in the magnetostatic ripple. All other fields are sufficiently small that they can be neglected. The local effective field, h_{eff}, is the normalized effective field acting to produce the local torque

$$\delta T = - M_s H_k \delta\varphi \; h_{eff} \tag{2.47}$$

which arises with a virtual displacement, $\delta\varphi$, of the local magnetization. So long as $h_{eff} > 0$, the torque, δT, acts to restore the magnetization to equilibrium. However if $h_{eff} \leq 0$, δT acts to increase φ. Hence the condition for stability of the magnetization is $h_{eff} > 0$. Now from (2.41e) it can be seen that in the vicinity of $\varphi = 0$, h_d becomes

$$h_{d_2} = - \frac{M_s^2 \, C_x}{K_u} \left(\frac{\partial\varphi}{\partial x}\right)^2 \quad . \tag{2.48}$$

When fields are applied that approach the Stoner-Wohlfarth threshold with angle, α, such that $90^\circ < \alpha < 270^\circ$, the single domain field, $h(\alpha)$, is decreased. This is most easily seen from Fig. 2-2 where $h(\alpha)$ is the

length of the line segment connecting the tip of the field vector to the point of tangency on the Stoner-Wohlfarth threshold. Before the Stoner-Wohlfarth threshold is reached ($h(\alpha) = 0$), however, the condition $h_{eff}(\varphi = 0) = 0$ is obtained. When this occurs the direction $\varphi = 0$ is no longer a stable direction for the magnetization. Yet, large values of both positive and negative φ are still stable positions as in those regions $h_d > 0$. Thus the theory implies that when blocking occurs, the only stable states are those for which $|\varphi|$ is greater than some φ_{min}, and it might be expected that a discontinuity occurs in the ripple such that the local magnetization jumps from some $\varphi = +\varphi_{min}$ to $\varphi = -\varphi_{min}$. In reality, of course, a delta function discontinuity cannot occur as the magnetostatic and exchange energies would become infinite at such a discontinuity. The failure of the theory to account for the infinity lies in the fact that even though nonlinear terms were included in the analysis, the theory is based on the linear calculation. The linear calculation predicts a smoothly varying ripple with a dominant wave length given by (2.38). The effects of the nonlinear terms were calculated by assuming that a solution of the form obtained from the linear analysis is valid even when nonlinear terms become important. In reality it is expected that the ripple changes in form so that the predicted delta function discontinuity does not occur.

It can be shown that one of the magnetostatic effective fields, fourth order in φ, varies as $(\partial\varphi/\partial x_1)^4$ and is positive. For a delta function discontinuity this term would be larger than the term h_{d_2} (see equation (2.48)) which varies as $(\partial\varphi/\partial x_1)^2$ and is responsible for the

blocking. In general, however, the coefficients of these fourth order effective fields are much smaller than the coefficients of the second order effective fields. Hence they only become significant when $\partial\varphi/\partial x_1$ becomes large. Therefore, for stability to occur after the blocking threshold, there must be a fairly sharp discontinuity in the ripple near $\varphi = 0$ in order that these higher order terms become sufficiently large to cancel the effect of h_{d_2}. Unfortunately, no method has been found to calculate the actual blocked ripple configuration. Hoffmann (1966) suggested that the ripple formed walls near $\varphi = 0$ when blocking occurred. This idea is consistent with the view given above that the ripple must form fairly sharp discontinuities near $\varphi = 0$ in order that stability be maintained.

Hoffman's ripple theory predicts the value of $h(\alpha)$ at which blocking should occur. For this prediction it is necessary to calculate the average value of h_{d_2} at $\varphi = 0$. Hoffmann (1966) found that blocking occurred when $h(\alpha) = h_a$ where:

$$h_a = B \frac{(M_s \sqrt{d})^{4/5} S^{8/5}}{A K_u} \tag{2.49}$$

and where B is a numerical factor which can be calculated from Hoffmann's theory. In this study Harte's numerical factors generalized for the case $\sigma_1 \neq 1/\sqrt{2}$ are being used. In Hoffmann's (1966) calculation, B is equal to $(1/4\pi\sqrt{2})^{4/5}$ which is the numerical factor of $\overline{h_d}$ (found by Hoffmann) raised to the 4/5 power. In order to be consistent, in this study B is chosen to be $(0.41)^{4/5} = 0.49$, where 0.41 comes from (2.45a). As Hoffmann (1966) showed, the equations $h(\alpha) = h_a$ and (2.7) may be

combined to define the blocking curve which can then be plotted in the same manner as the Stoner-Wohlfarth threshold. This blocking curve is shown in Fig. 2-10 for $h_a = 0.5$. For vector fields which result in values of $h(\alpha) > h_a$, as for example h' in the figure, the film is in a free ripple state with $h_{eff} > 0$ throughout the film. For fields just reaching the blocking curve (for example h") $h_{eff} = 0$ in regions where $\varphi = 0$ and blocking occurs. With vector fields which exceed the blocking curve, (for example h‴) ripple theory as developed thus far cannot be used without further assumptions to describe the ripple state. The blocking curve is only valid for transitions from the free to the blocked ripple state and does not predict the transition from the blocked to the free ripple state. After blocking occurs it is necessary to resaturate a film with large fields in order to return it to a free state.

Hoffmann (1964a) explained that domain splitting occurs after blocking, and has calculated values of α_{90} and α_{50}, etc. using this formulation. In the domain splitting experiments the film is saturated in the hard axis by a large ($\gg H_k$) field. This field is then decreased to zero, allowing the magnetic film to break up into long slender domains which lie parallel to the easy axis. Hoffmann's explanation is that, when the decreasing field reaches the blocking curve at $H = H_k(1 + h_a)$, (see Fig. 2-10) small angle walls form in the ripple. Upon subsequent decreasing of the field, the ripple splits along these walls, forming the long slender domains. From Fig. 2-10 it is seen that saturating fields may be applied at a small angle to the hard

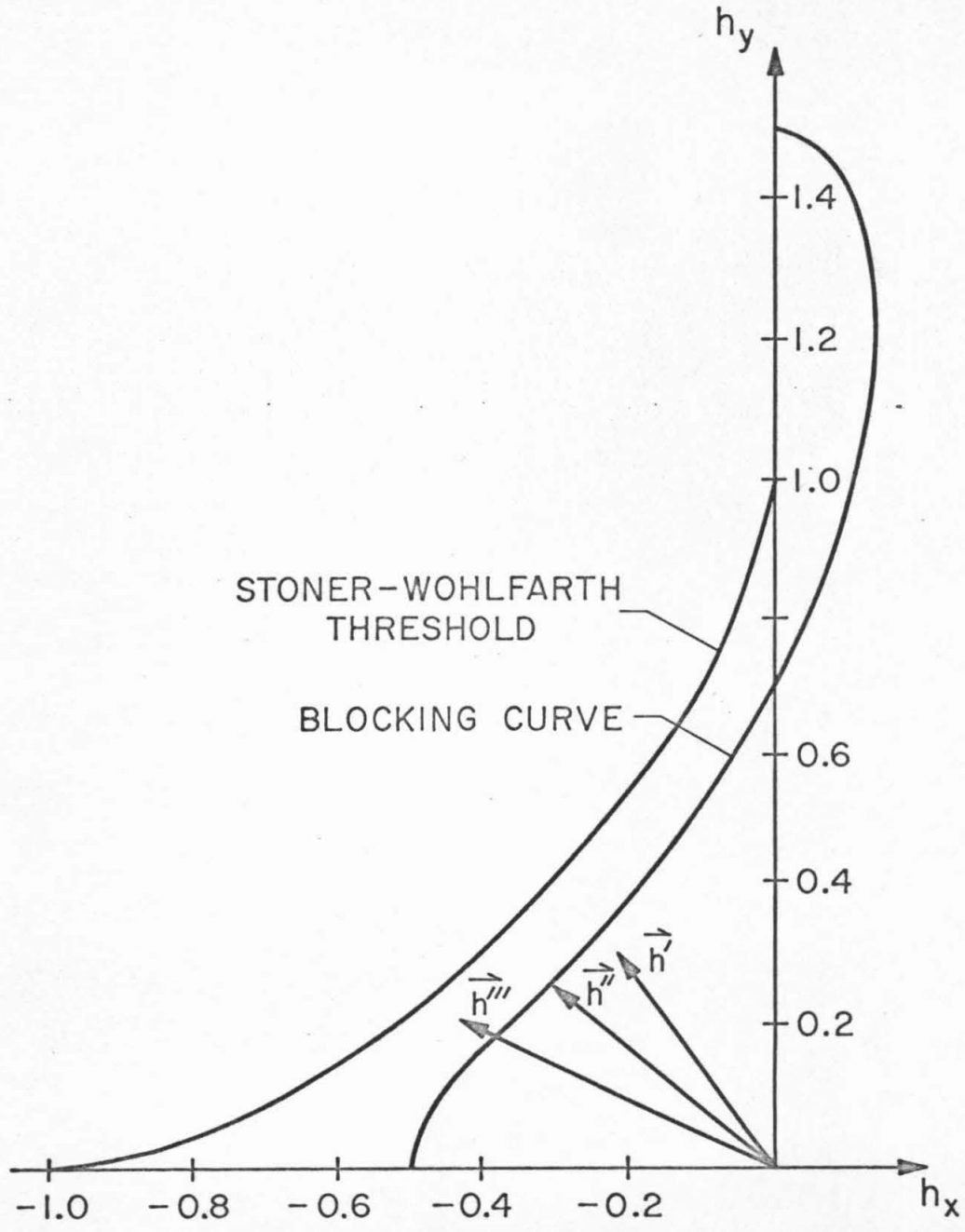

Fig. 2-10. The threshold curve for blocking with $h_a = 0.5$.

axis and still cross the blocking curve as they are decreased to zero. Hence, there is a certain angular region near the hard axis in which the magnetization will tend to split and fall to the easy axis with some of the magnetization rotating in one direction and the remainder in the other. The percentage which rotates in either direction depends on the direction of the magnetization in the blocked domains at the time of blocking which can be calculated using Hoffmann's theory.

Hoffmann (1969) has recently reported an experimental verification of the shape of the blocking curve. He found that when fields were applied that crossed the blocking curve a large rotational hysteresis was observed. This he explained was caused by the blocked walls in the ripple which acted to retard the rotation of the mean magnetization. By investigating at what values of applied field this large hysteresis effect began to occur he determined the position of the blocking curve. His experimental data agree quite well with the blocking curve which he calculated for the same film.

In summary, it has been shown that magnetization ripple is experimentally observed and that local anisotropy variations are an important cause of ripple. A model has been used that leads to expressions predicting the ripple wave length and amplitude as functions of film parameters. Two effective fields, $\overline{h_{eff}}(\alpha)$ and $h_{eff}(\alpha)$ can be used to predict macroscopic and microscopic instabilities, respectively, in the magnetization configuration. Within the limits of the theory, $\overline{h_{eff}}(\alpha)$ can never go to zero and hence the mean magnetization is always stable. On the other hand local instabilities are possible.

One form of local instability was blocking, and in later chapters the effects of blocking and other local instabilities on flux reversal will be discussed.

Chapter 3

Flux Reversal with a Transverse Field

3.1 Introduction.

Ever since Humphrey and Gyorgy (1959) and Olson and Pohm (1958) pointed out that data on the flux reversal process did not fit the uniform rotation model, there has been speculation about the mechanisms involved in the flux reversal process. There have been numerous models suggested to describe the magnetization configuration in a magnetic film as a function of time and position, and there has been much experimental data obtained in attempts to establish whether any of the proposed models are correct. Yet flux reversal in magnetic films is not understood.

To clearly show the dynamic magnetization configuration during flux reversal, the Kerr magneto-optic camera described in Chapter 6 was constructed. The photographs obtained from the camera give a detailed visual picture of the dynamic magnetization configuration during flux reversal. The Kerr photographs obtained with the camera show not only the change in the average magnetization as a function of time to compare to the signals induced in pickup loops about a film, but also the direction of the local magnetization as a function of both time and position in the film. Furthermore, unlike previous Kerr cameras this camera permits photographs to be taken of the dynamic magnetization configuration while the reversing field is still applied rather than the static configuration resulting when the drive field is terminated. The apparatus employs a Q-spoiled ruby laser and a Kerr electro-optic shutter to provide a 10 nsec exposure time. The time at which the

photograph is taken relative to the initial application of the pulse field is variable from -100 nsec to +10 μsec with a relative time stability at any setting of ±3 nsec. To obtain a sequence of photographs depicting a flux reversal process, it is necessary to rely on the experimentally verified fact that the reversal processes are reproducible and take photographs at different delay times during successive reversals. For flux reversal with a transverse field, photographs of (1) domain wall motion, (2) diffuse boundary propagation, and (3) non-coherent rotation have been taken. Domain wall motion was briefly discussed in Section 2.3.2. Diffuse boundary propagation will be discussed in this chapter after the discussion of non-coherent rotation since an understanding of the locking mechanism involved in non-coherent rotation is necessary. Coherent rotation will be briefly discussed; however, the camera does not have a short enough exposure time to verify its existence. Some photographs of the nucleation of partially reversed regions are shown in this chapter but the process is mainly discussed in Chapter 4 because it occurs predominantly when zero or very small transverse bias fields are applied.

3.2 Non-Coherent Rotation.

3.2.1 General. Non-coherent rotation is a moderate speed process that has been one of the least understood and most discussed mechanisms of flux reversal. Previous workers have referred to non-coherent rotation as the complete flux reversal process occurring during the intermediate linear region of the reversal curve. In this study non-coherent rotation will be used more specifically to refer to a particular mechanism of flux reversal which first begins to occur at the beginning of

the intermediate linear region of the reversal curves, but, as will be shown later, is not the only mechanism occurring in this part of the curve. Because of the complexity of this mechanism, it is best described qualitatively with reference to Kerr photographs which depict the dynamic magnetization configuration, concentrating on a quantitative description of some of the features of the reversal process. Because the process is so complex, no attempt is made to explain all features of the process in detail. Ripple strongly influences non-coherent rotation. As was mentioned in Section 2.4, instabilities in the magnetization ripple can and do occur. Blocking, which was one form of instability, is found to have at most minor effects in the non-coherent rotation process. However, a different instability called locking is found to cause the ripple to grow very large in amplitude forming a striped magnetization configuration. Magnetostatic fields, which become large when the striped configuration occurs, cause a rotational reversal process which is much slower than the predicted uniform rotation.

The striped configuration appears in the Kerr photographs of Fig. 3-1 which shows film 81-4-12 in the process of flux reversal. In this case, the transverse field is 0.25 oe, directed to the left and the pulse field is 2.98oe directed downward. As is the case with all pictures shown in this thesis, the 1 cm diameter circular thin film appears as an ellipse because the camera is oriented at 60^{o} to the normal of the film. The easy axis of the film corresponds to the minor axis of the ellipse (vertical in the photographs shown here). The time in nanoseconds, relative to the initial application of the pulse field, at which each photograph was taken is indicated to the right of each

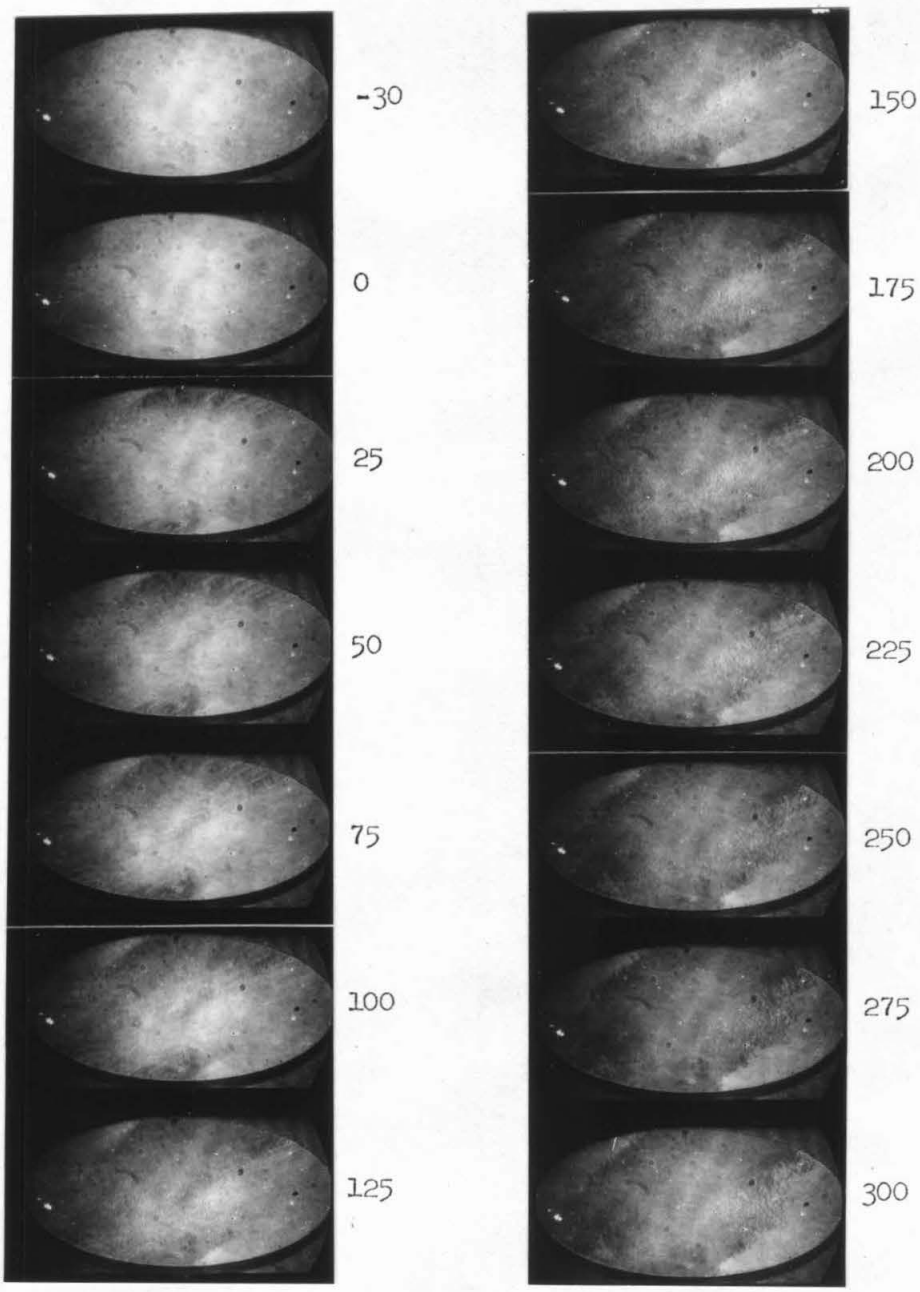

Fig. 3-1. Film 81-4-12 in the process of flux reversal in the presence of a 0.25 oe transverse bias field directed to the left and a 2.98 oe longitudinal pulse field directed downward. Time in nanoseconds relative to initial application of pulse field is indicated.

photograph. A picture was taken 30 nsec before the field was applied to show the film in the saturated state, with its magnetization directed upward along the easy axis in the photograph. This photograph shows the non-uniformity of illumination and the imperfections in the optics and surface of the film which can be expected to remain relatively constant throughout the sequence. At 0 nsec there has been no significant change, however, by 25 nsec, near the upper and lower edges, the photograph has darkened considerably indicating that the magnetization has rotated from its original saturated state. Note that the contrast is not uniformly dark as it was in the domains shown in Fig. 2-7. The degree of darkness indicates the amount by which the magnetization has rotated. The striped pattern is already beginning to occur in the partially rotated regions of the 25 nsec photograph. By 50 nsec, more of the film has darkened indicating that the magnetization has continued to rotate. The striped pattern has become more evident and can now be seen faintly in the center of the film. The 75 and 100 nsec photographs show the film continuing to become darker while the stripes remain visible. By 125 nsec a large portion of the film near the upper edge has totally reversed, and the striped pattern in the center of the film is beginning to disappear, as small regions of partially reversed magnetization nucleate in the striped region. These small regions continue to appear and reverse as time continues, until at 300 nsec all except the extreme right and left-hand edges of the film have reversed. Although it is not shown in this series of photographs, the reversal process is completed by a slower propagational process which will be discussed later.

The film reverses by basically a rotational process with the

exception of the extreme right and left-hand edges; however, the rotation takes place more quickly in some areas of the film than in others. This spatial non-uniformity in position must be caused by anisotropy dispersion, both microscopic (the source of ripple) and macroscopic, and by non-uniform demagnetizing fields located mostly at the film edges.

Macroscopic anisotropy dispersion is responsible for the reversal of large areas of film before others as shown in Fig. 3-1. Since the applied field is uniform any local variations in the anisotropy constant (amplitude dispersion) produce local variations in the uniform torque on the local magnetization. In general, the regions with low values of local anisotropy will switch more quickly than those with high anisotropy. Variations in the local easy axis direction (angular dispersion) will cause the magnetization direction to vary throughout the film, producing variations in the torque from the pulse field. The regions with large angular dispersion, such that the local magnetization lies far from the mean easy axis and closer to the direction of the transverse field, will switch the fastest.

Edge demagnetizing fields also alter the speed at which the magnetization will reverse. It is possible to calculate these demagnetizing fields by approximating the divergence at the edge by an effective line charge. Figure 3-2 is a diagram of a film showing the effective charge per unit length $M_s d \cos\beta$ existing at the edge ($r = a$). The mean magnetization is at angle φ_o to the easy axis because of the hard axis bias field, $\vec{H}_y$. The demagnetizing field in the plane of the film may be evaluated using the Green's function expansion in spherical harmonics given by Jackson (1965) and assuming that the film lies in the plane,

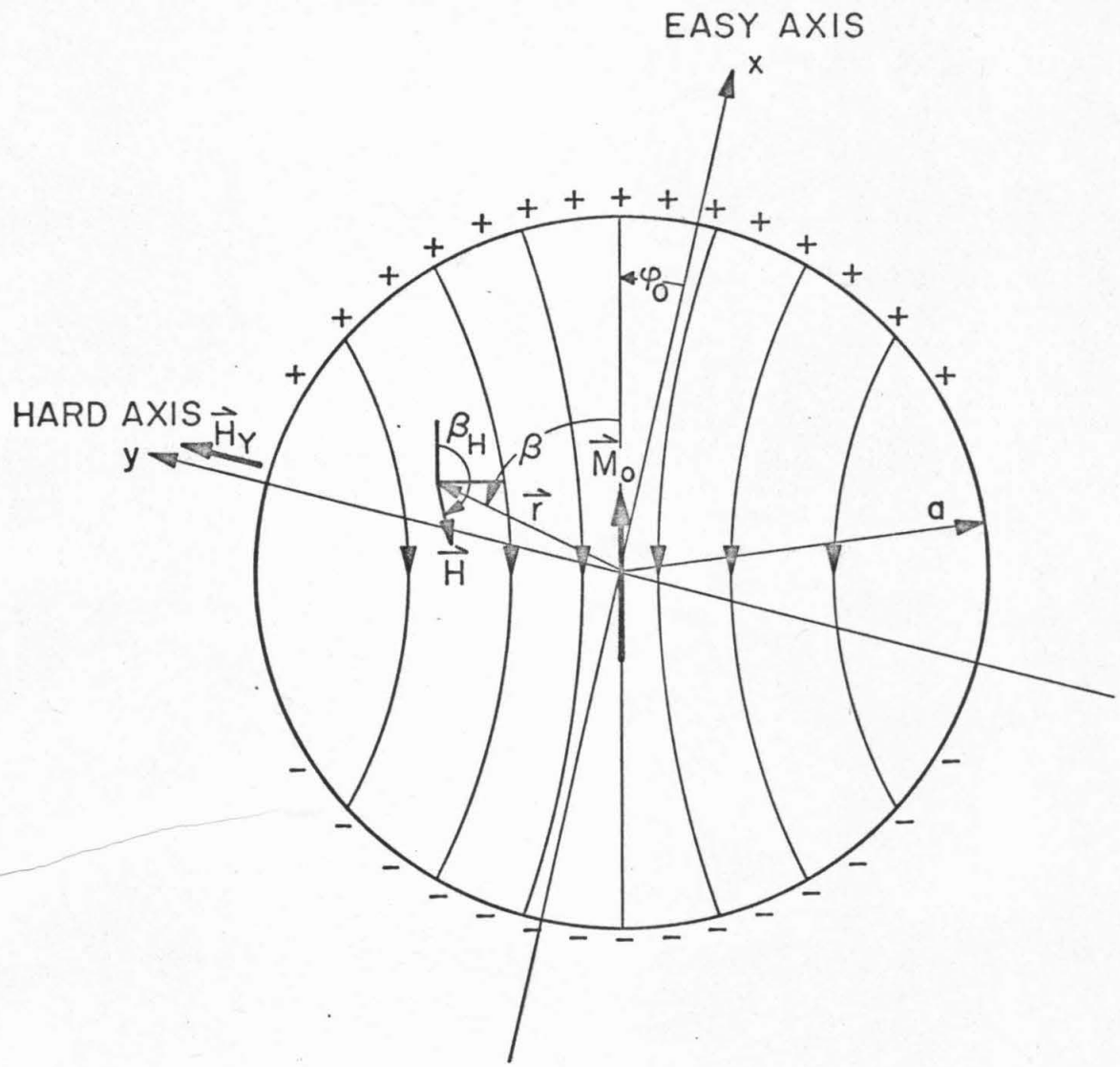

Fig. 3-2. A diagram of a thin film showing the effective charge and the direction of the stray field from the divergence of the magnetization at the edge.

$\theta = \pi/2$, where θ is the polar angle. At a point $(r,\theta,\beta) = (r',\pi/2,\beta')$, where $r' < a$, the field is given by the components

$$H_r = \frac{2\pi M_s d}{a} \cos\beta' \sum_{\ell=o}^{\infty} \ell \left(\frac{r'}{a}\right)^{\ell-1} P_\ell^1(o) P_\ell^{-1}(o) \tag{3.1a}$$

$$H_\beta = \frac{-2\pi M_s d}{a} \sin\beta' \sum_{\ell=o}^{\infty} \left(\frac{r'}{a}\right)^{\ell-1} P_\ell^1(o) P_\ell^{-1}(o) \tag{3.1b}$$

At points with $r' \leq a/2$, these series converge rapidly and the sums are readily evaluated by the first few terms. At $(a/2,\pi/2,-\pi/4)$ for a typical film with $M_s = 800$ emu, $d = 1000$ Å, $a = 0.5$ cm, the field is found to be 0.063 oe and to be directed at an angle $\beta_H \simeq 186.2^o$. Thus, at $(a/2,\pi/2,-\pi/4)$ the demagnetizing field tends to increase the angle, Φ, of the magnetization near that point. By symmetry it can be seen that it also tends to increase Φ at $(a/2,\pi/2,3\pi/4)$ and to decrease Φ at $(a/2,\pi/2,\pi/4)$ and $(a/2,\pi/2,-3\pi/4)$. Furthermore, the magnitude of the field (0.063 oe) is significant in comparison to the 0.25 oe transverse bias field, H_y, and can be expected to produce significant effects when fields only a few tenths of an oersted over the Stoner-Wohlfarth threshold are applied as they were in Fig. 3-1 and in many other figures seen in this chapter.

For points near to the edge, the series in (3.1a,b) do not converge rapidly and other solutions for the field must be found. For points sufficiently close to the edge, it is reasonable to approximately calculate the demagnetizing field by assuming an infinite line charge of $M_s d \cos\beta'$ exists a distance $(a - r')$ from the point $(r',\pi/2,\beta')$ at which the field is being calculated. This yields the result that the field is $(2M_s d \cos\beta')/(a - r')$. Using the same parameters as above the field at

$(0.9a, \pi/2, -\pi/4)$ is calculated to be 0.226 oe. The infinite line charge approximation suggests that the angle β_H at this point would be $\beta_H = 5\pi/4$, however, because the charge is greater at $\beta = 0$ than at $\beta = \pi/2$, the field actually curves qualitatively as shown in Fig. 3-2 so that $\beta_H \leq 5\pi/4$. Hence, 0.5 mm from the edge of the film at $\beta = -\pi/4$, the demagnetizing field is approximately equal in magnitude to the transverse bias field, H_y, and is directed so as to aid $\vec{H}_y$ in increasing the angle Φ of the magnetization near that point. Thus, closer to the edge the demagnetizing fields are expected to have even a larger effect than they do at $r' = a/2$.

The effects of the demagnetizing fields are qualitatively like the above calculations of the demagnetizing field would suggest. In Fig. 3-1 the upper right ($\beta \approx -\pi/4$) and lower left ($\beta \approx 3\pi/4$) regions of the film reverse quite rapidly while the regions at the upper left ($\beta \approx \pi/4$) and lower right ($\beta \approx -3\pi/4$) are the slowest to reverse.

The formation of stripes in the magnetization configuration during flux reversal in permalloy thin films is characteristic of the non-coherent rotation process. Such stripes are observed during flux reversal which occurs in times as short as 25 nsec, at which point the temporal resolution of the Kerr magneto-optic camera is significantly affecting the photographs. In later sections, it will be shown that the stripes occur when an instability in the ripple causes the magnetization in regions where $\varphi > 0$ to become unstable and switch, producing magnetostatic fields that lock the magnetization into a striped configuration and cause a reaction torque opposite in sign to the torque produced by the applied field. If this reaction torque grows as large as the uniform

torque from applied field and uniaxial anisotropy, the mean magnetization will stop rotating until some rearrangement of the stripes occurs which reduces the reaction torque. In Fig. 3-1 this rearrangment consisted of the nucleation of many partially reversed regions. In other cases, the reaction torque does not become as large as the uniform torque, but does slow the rotation of the magnetization, and in such cases nucleation does not occur - rather, after they form, the stripes are observed to decrease in amplitude until they can no longer be seen.

3.2.2 Slow Versus Fast Ripple Relaxation. Harte (1964) was one of the first to propose that ripple was responsible for the fact that films did not reverse by coherent rotation when fields slightly in excess of the Stoner-Wohlfarth threshold were applied. He proposed that the initial ripple existing in the film before the pulse field was applied could relax to a new stable position with respect to $\vec{M}_o$ only in times which were very long compared to the time required for the mean magnetization to rotate coherently to a new stable position in a film. Hence, the initial ripple was assumed to remain in the film even though $\vec{M}_o$ rotated away from $\vec{k}$, the wavevector of the mean ripple. Figures 3-3a,b illustrate what would occur if $\vec{M}_o$ did rotate away from $\vec{k}$. In Fig. 3-3a, $\vec{M}_o$ is still parallel to $\vec{k}$ so that the ripple is longitudinal, $\nabla\cdot\vec{M}$ is small, and there is no reaction torque from the ripple on $\vec{M}_o$. In Fig. 3-3b, $\vec{M}_o$ has rotated slightly away from $\vec{k}$, hence, the ripple has acquired a transverse component. Divergences in the magnetization create fields h_{str_1} and h_{str_2} which result in an effective torque to restore $\vec{M}_o$ so it is once again parallel to $\vec{k}$.

Harte calculated the reaction torque of the initial ripple on $\vec{M}_o$

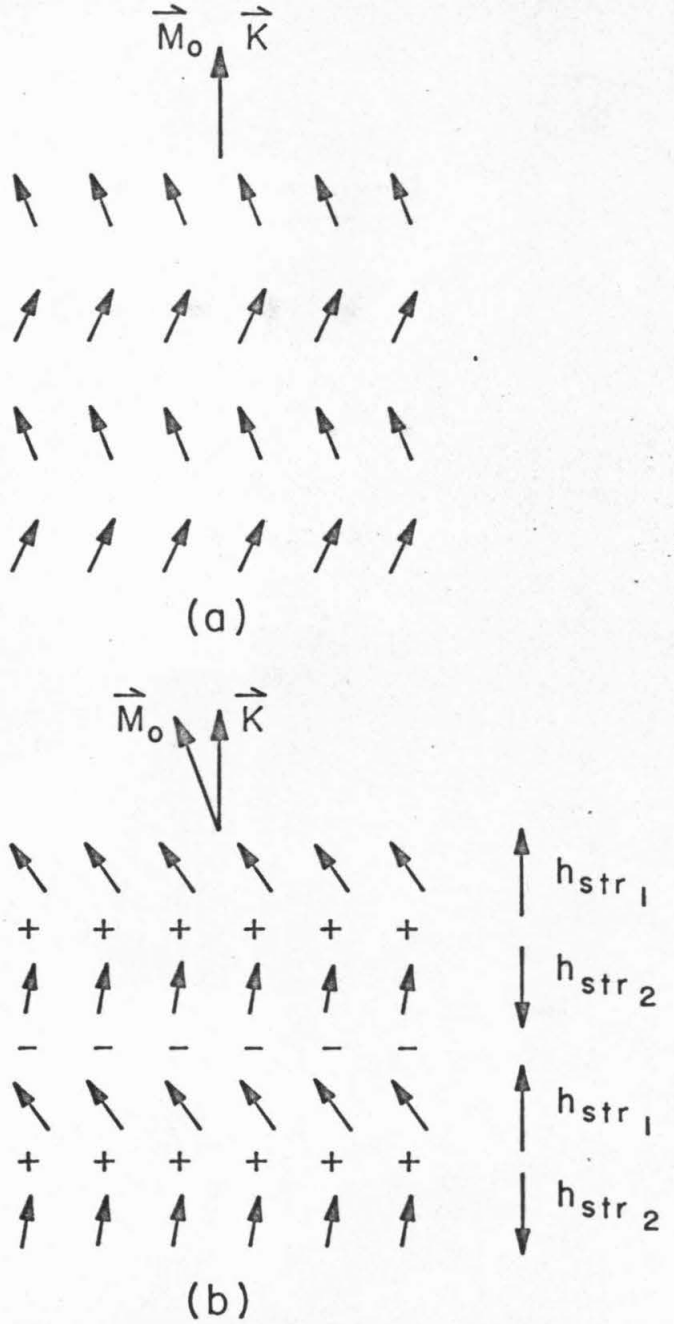

Fig. 3-3. (a) A diagram of longitudinal ripple. (b) A diagram showing the ripple with $\vec{M}_o$ rotated away from $\vec{K}$.

by solving the equations of motion for each Fourier component of the ripple as $\vec{M}_o$ rotated away from $\vec{k}$, assuming that no ripple relaxation occurred. He then calculated the average reaction torque which the sum of the ripple Fourier components had on the mean magnetization and found that the effect of the initial ripple was to retard the rotation of $\vec{M}_o$ in the first 90^o and to speed the rotation of $\vec{M}_o$ in the second 90^o. Since most of the switching time was involved in the first 90^o, the effect of the reaction torque was to slow the rotation process. Furthermore, it was found that for fields less than a certain threshold but greater than the Stoner-Wohlfarth threshold that the reaction torque of the ripple in the first 90^o of rotation would become equal to the driving torque of the applied and uniaxial anisotropy fields. When this occurred there would be no net torque to rotate the magnetization and hence switching would stop until the ripple could relax sufficiently to allow $\vec{M}_o$ to begin rotating again.

Harte's (1964) model rests heavily upon the assumption that the initial ripple does not relax with the mean magnetization. Hoper (1968) was the first to suggest that ripple relaxation could be calculated in a phenomenological manner using either the Gilbert (1955) or Landau-Lifshitz (1935) phenomenological damping. Using either damping term, it is possible to arrive at the equation of motion of a ripple component:

$$\frac{\partial^2 \varphi_{\vec{k}}}{\partial \tau^2} + \alpha_d \sqrt{\frac{4\pi M_s}{H_p}} \frac{\partial \varphi_{\vec{k}}}{\partial \tau} + \frac{\chi_{\vec{k}} H_k \overline{h_{eff}}(\alpha)}{H_p} \left[1 + r_e^2 k^2 + 2 r_m \tilde{\chi}_k \sin^2 (\varphi_o - \Phi_{\vec{k}}) \right] \varphi_{\vec{k}} = \frac{\chi_k f_{1\vec{k}}}{M_o H_p} \qquad (3.2)$$

where τ is the normalized time variable, $\tau = \gamma\sqrt{4\pi M_s H_p}\, t$, used earlier in Chapter 2. From this equation it is seen that if $\vec{M}_o$ is instantaneously rotated from one position $\varphi_o(\tau_1)$ to $\varphi_o(\tau)$, that the ripple amplitude will go through damped oscillations until the final state of equilibrium is attained at which $\ddot{\varphi}_{\vec{k}} = \dot{\varphi}_{\vec{k}} = 0$, and $\varphi_{\vec{k}}$ has the value (2.34) as would be expected. It is readily observed that the decay time of the oscillations in $\varphi_{\vec{k}}$ is

$$t_r = (2\pi M_s \gamma \alpha_d)^{-1} \tag{3.3}$$

as Hoper (1968) first reported. The value of t_r calculated using typical values of $\alpha_d \approx 0.01$ (determined from ferromagnetic resonance) and (3.3) is $t_r \approx 1$ nsec.

Hoper (1968) determined experimentally that the ripple relaxation time is of the order of 1 nsec by observing the fallback of the magnetization in a thin film when a 0.25 nsec risetime pulse field sufficient to rotate $\vec{M}_o$ by 7^o was applied and then terminated. By varying the pulse field magnitude he was able to vary the time it took $\vec{M}_o$ to rotate by 7^o from 0.6 nsec to 9 nsec. He found that if $\vec{M}_o$ rotated through 7^o in less than 1 nsec that there was a significant reaction torque from the ripple which acted to speed the fallback of $\vec{M}_o$ upon termination of the field, but if the time of rotation were much longer than 1 nsec then the effect was insignificant.

Depending upon the magnitude of the applied field, the relaxation time of the ripple could be either shorter or longer than the switching

time of $\vec{M}_o$. In most experimental situations the risetime of the magnetic field is not sufficiently fast that the applied field appears as a true step function. The risetime of the pulse magnetic field in the apparatus used in this study is 10 nsec, long compared to switching times by coherent rotation and compared to ripple relaxation times. The pulse field is not a step function then, but a slowly rising field and it can be assumed that the magnetization remains in quasi-static equilibrium with the field as it rises. In order for such a quasi-static analysis to be made it is necessary that the rotation of the magnetization be critically or nearly critically damped.

The condition for critical damping may be derived from (2.28a,b). Harte (1964) calculated the condition for critical damping to be that α_d obtain the value

$$\alpha_{d_c} = 2\sqrt{\frac{H_k h_f(\alpha)}{4\pi M_s}} \tag{3.4}$$

where $h_f(\alpha)$ is the value which $h(\alpha)$ obtains when the magnetization comes to rest. Critical or over-damping can therefore be expected during a slowly rising magnetic field so long as

$$h(\alpha) \leq \frac{\alpha_d^2 \pi M_s}{H_k} , \tag{3.5}$$

which for a typical permalloy film with $\alpha_d \approx .01$, $M_s \approx 800$ emu and $H_k \approx 3$ oe gives $h(\alpha) \leq 0.1$. This implies that although critical damping may not be achieved early in the risetime of the pulse field (with $h = 0$, $h(\alpha) = 1$), as the Stoner-Wohlfarth threshold is approached, critical

damping is obtained because right at the Stoner-Wohlfarth threshold, $h(\alpha) = 0$. Hence, during a 10 nsec risetime pulse field, quasi-static equilibrium is expected to be approximately achieved for fields roughly equal to the Stoner-Wohlfarth threshold. For reversal times long compared to the 10 nsec risetime then, the initial condition of the magnetization should not be important in determining the reversal process.

The fast ripple relaxation time has been independently verified using the Kerr magneto-optic camera. Consider the pulse sequence shown in Fig. 3-4a. Film 81-10-4, reset with a longitudinal field equal to 15 oe ($\approx 2\ H_k$), initially is subjected to a steady transverse bias field equal to 2.75 oe ($0.358\ H_k$). From equation (2.7) φ_o, the angle which $\vec{M}_o$ makes with the easy axis, can be calculated to be 21^o. A 10 nsec risetime pulse longitudinal field of 2.8 oe ($0.364\ H_k$) is then applied to the thin film, and photographs are taken during the flux reversal process both at 75 and 200 nsec after application of the pulse field. The film is then subjected to the pulse sequence in Fig. 3-4b. It is initially reset as before in the presence of a 2.75 oe ($0.358\ H_k$) transverse field. An additional longitudinal field equal to 6.0 oe ($0.78\ H_k$) is applied in the reset direction so that the initial angle of $\vec{M}_o$ is only $\varphi_o \approx 12^o$. A 10 nsec risetime pulse field equal to 8.8 oe ($1.144\ H_k$) is then applied and photographs are taken at the same times as during the previous reversal. Note that the total field applied to the film is the same whichever pulse sequence is used, but that the initial condition is very different for each pulse sequence. Figures 3-5a,b show photographs of film 81-10-4 obtained with such pulse sequences. The pictures are essentially identical even though the initial

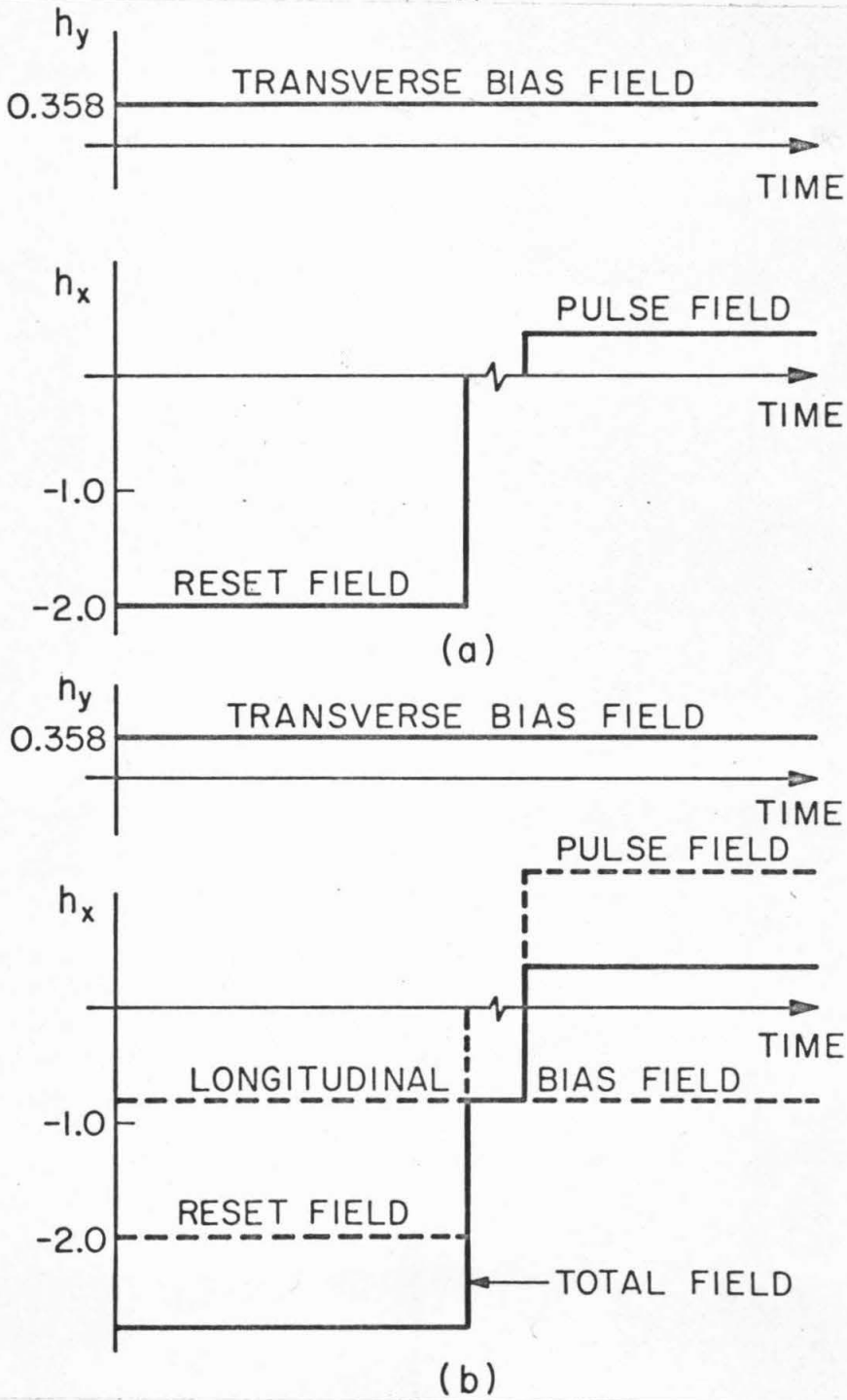

Fig. 3-4. (a,b) Alternative pulse sequences used to verify that the initial condition of the magnetization does not affect the flux reversal process.

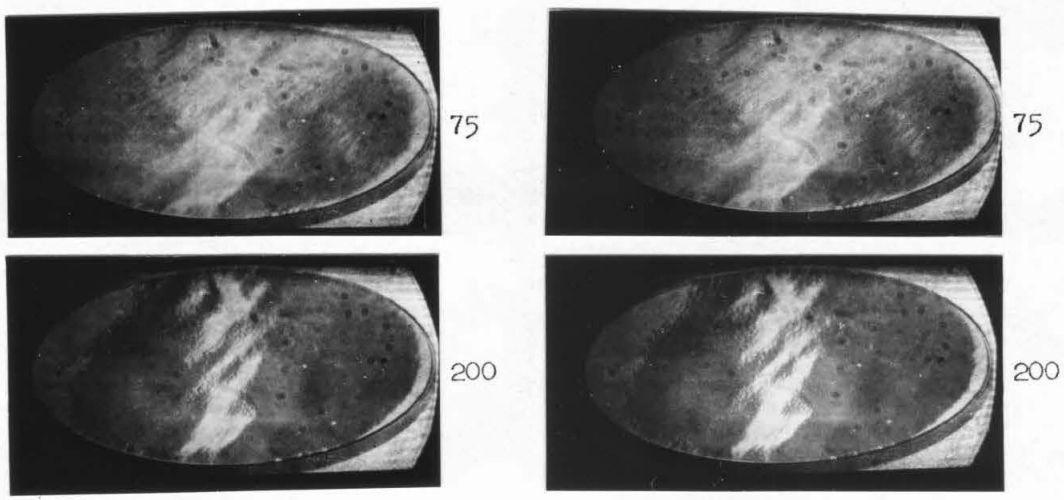

Fig. 3-5. (a) Photographs taken 75 and 200 nsec after application of a 2.8 oe longitudinal pulse field directed downward to film 81-10-4 in the presence of a 2.75 oe transverse bias field. (b) Photographs taken 75 and 200 nsec after application of an 8.8 oe longitudinal pulse field to film 81-10-4 in the presence of a 2.75 oe transverse bias field and a 6.0 oe longitudinal bias field in the reset direction.

direction of the magnetization was different by 9^{o}. This shows that the initial ripple must not have a significant effect on the observed reversal process. Therefore, it must be concluded that ripple relaxation is fast compared to the magnetization rotation during the 10 nsec risetime of the pulse field.

It is possible to demonstrate with another experiment that the magnetization rotates coherently prior to the formation of the stripes. Figure 3-6 shows the pulse sequence used for this experiment. First a steady transverse bias field of 5.75 oe (0.746 H_k) was applied to film 81-10-4. A reset field of 15 oe (≈ 2 H_k) was then applied in addition to a longitudinal bias field in the reset direction of 6.0 oe (0.78 H_k). Figure 3-7 is a series of photographs taken during the flux reversal process using a longitudinal pulse field of 6.9 oe (0.896 H_k). The -30 nsec photograph shows the film with the reset field removed and with its magnetization at equilibrium at an angle of 23^{o} to the easy axis. The shutter for the zero nanosecond photograph is open during the entire 10 nsec risetime of the field, so that the darkness of this photograph is representative of the average of the direction of magnetization during the risetime. The 0 nsec photograph is clearly darker than the -30 nsec photograph. Furthermore, the photograph is uniformly darker, indicating that the magnetization is rotating coherently during the risetime of the pulse field. The photograph taken at 25 nsec is darker than the 0 nsec photograph and also shows structure in the magnetization configuration just beginning to appear. By 50 nsec the structure is clearly evident. There are faint stripes which are oriented at 75^{o} to the hard axis throughout the center section of the film which is lighter than the

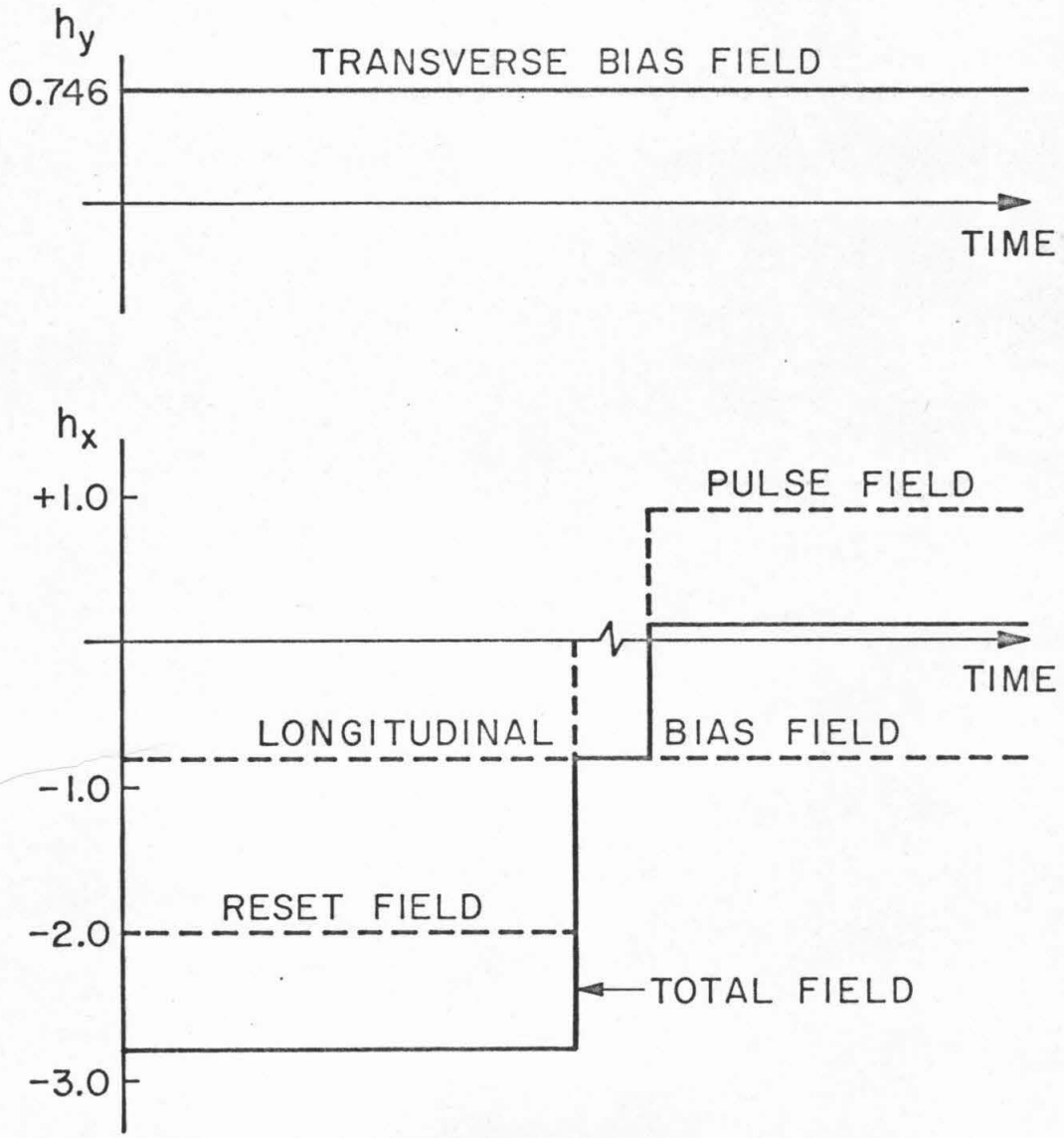

Fig. 3-6. The pulse sequence used to obtain the series of photographs shown in Fig. 3-7.

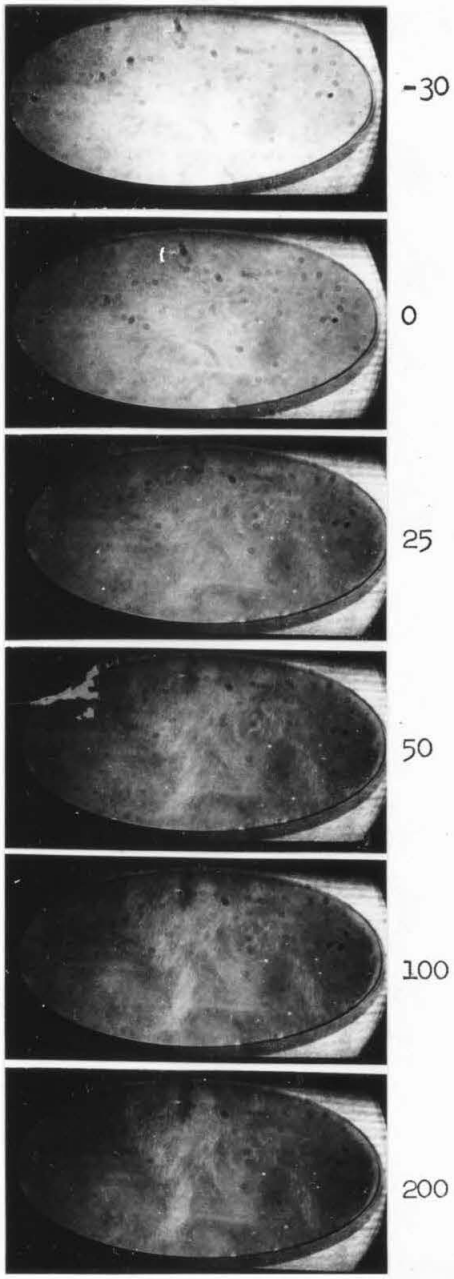

Fig. 3-7. Film 81-10-4 in the process of flux reversal after the application of a 6.9 oe longitudinal pulse field directed downward with a transverse bias field of 5.75 oe directed to the left and a longitudinal bias field of 6.0 oe directed upward. Time in nanoseconds relative to initial application of pulse field is indicated.

sides. This area is roughly the same darkness as the 0 nsec photograph indicating that, at least within this area, the magnetization has not rotated significantly beyond that rotation which occurred during the risetime of the pulse field. The pictures at 100 and 200 nsec show the film continuing to reverse. This series of photographs was repeated many times in order to be certain that the laser intensity was constant throughout the series.

The interpretation of this series is that during the 10 nsec risetime of the pulse field, the magnetization rotates coherently with the ripple in equilibrium with it. After the field exceeds the Stoner-Wohlfarth threshold and the mean magnetization has rotated to 75^{o} (perpendicular to the stripes) the ripple grows in amplitude forming the striped pattern. After the stripes first appear the reversal process is slowed considerably. Whereas the magnetization rotated from 23^{o} to 75^{o} during the risetime of the pulse field, the contrast indicates that at least within the central portion of the film the rotation to the final equilibrium angle of 140^{o} is not complete in even 200 nsec. The reason that the edges of the film switch more quickly is thought to be due to macroscopic anisotropy dispersion (either angular or amplitude dispersion) which lowers the threshold for reversal in these areas. It should be pointed out that the conjecture that the magnetization rotates coherently at first and then breaks up into domains is in agreement with the early work done by Humphrey (1958) and Sakurai et al. (1966) on non-coherent rotation. They based their conclusions on the shape of the longitudinal and transverse switching signals induced in inductive pick-up loops about the film.

It is clear then, that ripple relaxation occurring in times of the order of 1 nsec is observed and that slow relaxation models are not appropriate. The initial condition of the magnetization does not significantly affect the reversal process. Furthermore, the magnetization in a film rotates coherently during the risetime of the pulse field (when this risetime is several nanoseconds) until some instability occurs to prevent further coherent rotation.

3.2.3 The Fast Relaxation Model of Harte. Harte (1967) proposed a fast relaxation model for flux reversal. It is based on Hoffmann's (1966) proposed blocking threshold which was briefly discussed in Chapter 2 and assumes that the ripple is able to relax rapidly with the mean magnetization until blocking occurs. At that instant he assumes the ripple can no longer relax with the mean magnetization. Blocking was visualized as producing fairly sharp discontinuities or low angle "walls" in the ripple in regions where $\varphi = 0$; hence, any reorientation of the ripple must involve the rearrangement of these walls. Since domain wall motion is a sequential process and relatively slow, it is easy to imagine that the presence of the "walls" would slow the ripple relaxation.

This fast relaxation model fails to explain the experimentally observed stripes. The stripes cannot be the blocked ripple as the angles which the stripes make with the easy axis do not correspond to that expected if the stripes formed as soon as blocking occurred, assuming, of course, that the direction of the mean magnetization at blocking is perpendicular to the stripes. In several films, the angle of the stripes was investigated as a function of transverse field with longitudinal

pulse fields just sufficient to exceed the Stoner-Wohlfarth threshold and cause the stripes. In all cases the angle of the stripes indicated that when the stripes formed the magnetization had already rotated past φ_{SW}, the angle of the magnetization as predicted by the Stoner-Wohlfarth model for a threshold field. Since the blocking curve lies inside the Stoner-Wohlfarth threshold, the stripes could not have formed when the ripple blocked.

An example of the photographs from which the angles were measured is shown in Fig. 3-8. In the figure film 81-4-6 is seen in the process of flux reversal with a 1.5 oe transverse bias field directed to the right and a 1.1 oe longitudinal pulse field directed downward. The striped pattern in this figure illustrates that the angle at which the stripes form is strongly field dependent. Not only are the stripes at a very different angle than those in Fig. 3-1, but because the transverse field is in the opposite direction, the stripes lie in a different quadrant from those in Fig. 3-1. It is readily seen from the 150 and 200 nsec photographs in Fig. 3-8 that the angle which the stripes make can be measured accurately. In this case, it was determined that the stripes make an angle of about 60° with the hard axis (horizontal in the photographs) of the film while $\varphi_{SW} \approx 48^{\circ}$. In making this measurement, it is necessary to take into account the fact that the camera is oriented at 60° to the normal of the film resulting in a 2:1 correction of distances measured in the vertical direction. The angle which the stripes makes with the hard axis, φ_{ℓ}, is consistently greater than φ_{SW}, as can be seen in Fig. 3-9 showing data on three different films. These data are plotted as a function of the normalized transverse bias field,

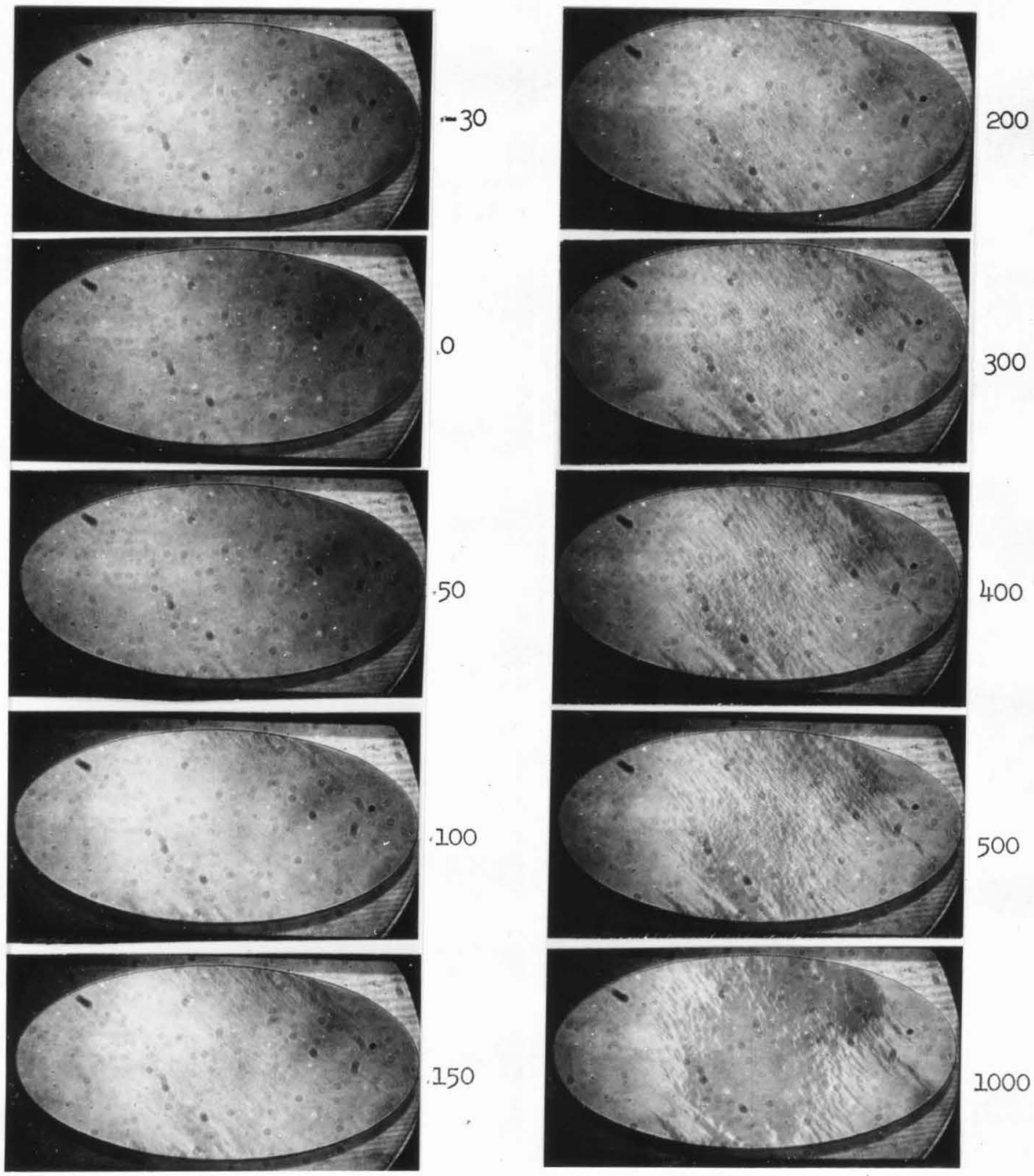

Fig. 3-8. Film 81-4-6 in the process of flux reversal with a 1.5 oe transverse bias field directed to the right and a 1.1 oe longitudinal pulse field directed downward. Time in nanoseconds relative to initial application of pulse field is indicated.

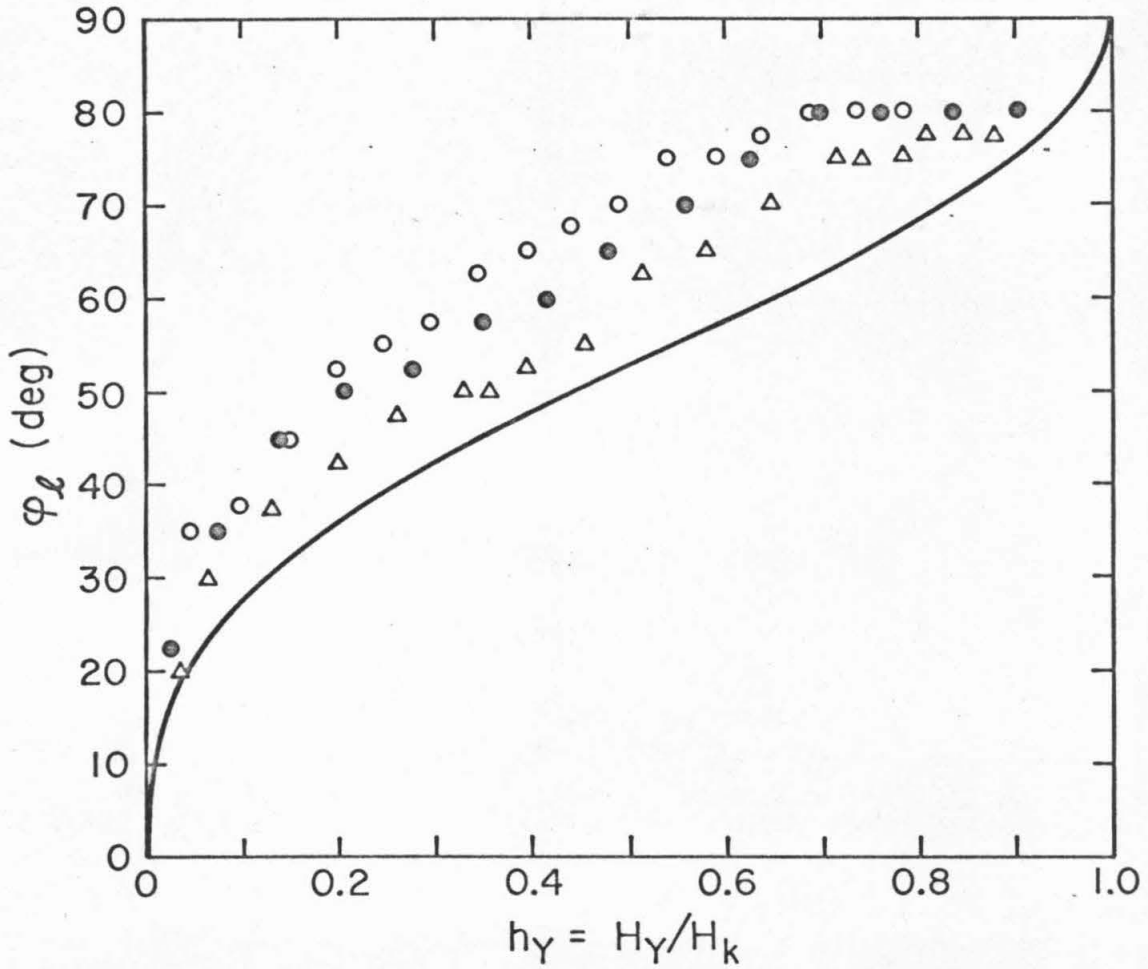

Fig. 3-9. A plot of φ_ℓ as a function of transverse bias field for films 81-4-6 = •; 81-10-4 = Δ; and 84-8-7 = o. The solid line is a plot of φ_{SW} versus transverse bias field.

$h_y = H_y/H_k$. The longitudinal pulse field was, in each case, just sufficient to exceed the Stoner-Wohlfarth threshold. Also shown in the plot is φ_{SW} as a function of transverse bias field. Clearly $\varphi_\ell > \varphi_{SW}$ in all cases.

Other characteristics of blocked ripple as predicted by Harte's (1967) model are inconsistent with the concept that the stripes are blocked ripple. The calculation predicts that each component of ripple will oscillate as $\vec{M}_o$ rotates away from $\vec{k}$, the wavevector of the ripple. For the width of stripes observed in the Kerr photographs (50-100 μ), the oscillation would occur at a frequency of roughly 10^9 cps or at a rate which is more than an order of magnitude faster than the camera could resolve. Hence, the camera should not be able to resolve the blocked ripple in Harte's (1967) theory. Furthermore, as may be observed in Fig. 3-8, the stripes maintain the same phase relationship (dark stripes remain dark and light stripes remain light) over times longer than 100 nsec. Therefore, they certainly are not oscillating at even 10^6 cps. In addition, the blocked ripple in Harte's (1967) model should decrease in amplitude as time proceeds rather than becoming very large in amplitude as it does in Fig. 3-8. The contrast between stripes in Fig. 3-8 suggests that the observed amplitude is at least 20^o instead of the 2^o theoretically predicted.

It was thought that the possibility that an additional field might add into the expression $h_{eff}\big|_{\varphi = 0} = h(\alpha) + h_{d2}\big|_{\varphi = 0}$ from which the blocking threshold was calculated should be explored. This field would shift the blocking threshold and if it were sufficiently large could even make blocking occur after φ_{SW}. The field $\overline{h_{u3}}$ can be dismissed

because, depending on φ_o, it may be either positive or negative and hence would tend to shift the blocking differently for different applied fields. Furthermore, it is too small by an order of magnitude to explain the observed shift. The local anisotropy field $\overline{h_{k3}}$ on the other hand can and probably does shift the blocking curve, however, by roughly an order of magnitude too little to account for the observed shift. The fields h_{u2} and h_{k2} can be dismissed because they are local fields and have no average values ($\overline{h_{u2}} = 0 = \overline{h_{k2}}$).

In summary it can be seen that neither Harte's slow (1964) nor fast (1967) model is adequate to explain the observed stripes which form during the non-coherent rotation process. This is not meant to imply that blocking has no effect on the reversal process nor that Harte's models do not have a region of application. In fact it will be shown later that ripple reaction torques do slow the rate at which $\vec{M}_o$ rotates before the stripes form. Furthermore, it is expected that with sufficiently large amplitude pulse fields of very fast risetime that Harte's approximation of a slow ripple relaxation time will be valid.

3.2.4 The Fast Relaxation Model of Stein. Stein (1965a, 1965b, 1966) also proposed a model for non-coherent rotation in which the longitudinal ripple should increase in amplitude at or immediately after the minimum in the torque curve. If the ripple grew sufficiently large, it would appear as a striped configuration when observed with the Kerr effect. In his model he assumed that the ripple initially relaxed with $\vec{M}_o$, the mean magnetization; hence, it is a fast relaxation model as is required by the experimental evidence. To understand why the ripple was expected to grow in amplitude shortly after the minimum in the torque

consider the curve plotted in Fig. 3-10. If the mean magnetization is at φ_o and there are local magnetization components from the ripple at $\varphi_o \pm \varphi$, then while $0 < \varphi_o < \varphi_{o_{min}}$ (where $\varphi_{o_{min}}$ is the angle at which the torque is a minimum), there is more torque on the magnetization at $\varphi_o - \varphi$ than on $\vec{M}_o$ and there is less torque on the magnetization at $\varphi_o + \varphi$ than on $\vec{M}_o$. The uniform torque acts, then, to suppress the ripple by accelerating the magnetization which trails $\vec{M}_o$ more than it accelerates the magnetization which leads $\vec{M}_o$. On the other hand, if the pulse field is sufficient to exceed the Stoner-Wohlfarth threshold, then the torque curve does not go to zero until the magnetization has reversed, so that $\vec{M}_o$ will rotate to and beyond $\varphi_{o_{min}}$. For φ_o at or slightly past $\varphi_{o_{min}}$, there is more torque on the magnetization at $\varphi_o + \varphi$ than on $\vec{M}_o$ while there is less torque on the magnetization at $\varphi_o - \varphi$ than on $\vec{M}_o$. Therefore, now the uniform torque tends to increase the ripple amplitude by accelerating the magnetization which leads the mean magnetization by more than it accelerates the magnetization which trails the mean magnetization. Stein therefore suggested that the ripple would grow large in amplitude when φ_o reached $\varphi_{o_{min}}$ forming a striped magnetization configuration which would slow the reversal process. Now $\varphi_{o_{min}}$ may be calculated by setting $\partial T/\partial \varphi_o = 0$, and this simply yields the result

$$h(\alpha) = h \cos(\alpha - \varphi_{o_{min}}) + \cos 2\varphi_{o_{min}} = 0 \ . \qquad (3.6)$$

The prediction that a large amplitude ripple would appear when $\varphi_o = \varphi_{o_{min}}$ was checked by replotting the data of Fig. 3-9 in Figs. 3-11a, b,c which show $h \cos(\alpha - \varphi_\ell)$ as a function of $(-\cos 2\varphi_\ell)$. The experimental data are shown by error bars representative of the experimentally

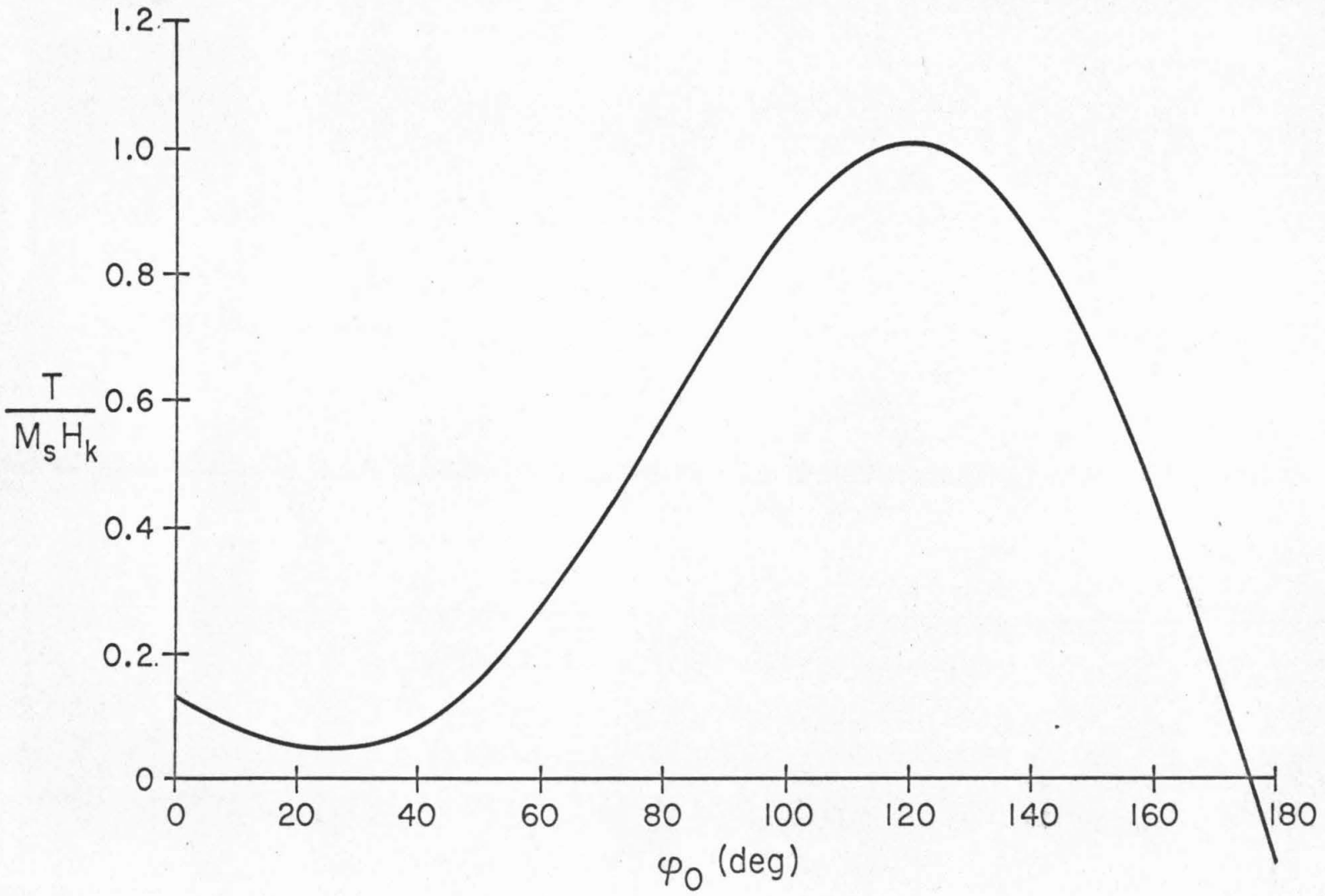

Fig. 3-10. A theoretical plot of the driving torque from applied fields and uniaxial anisotropy as a function of φ_o for h = 0.75, $\alpha = 170^o$.

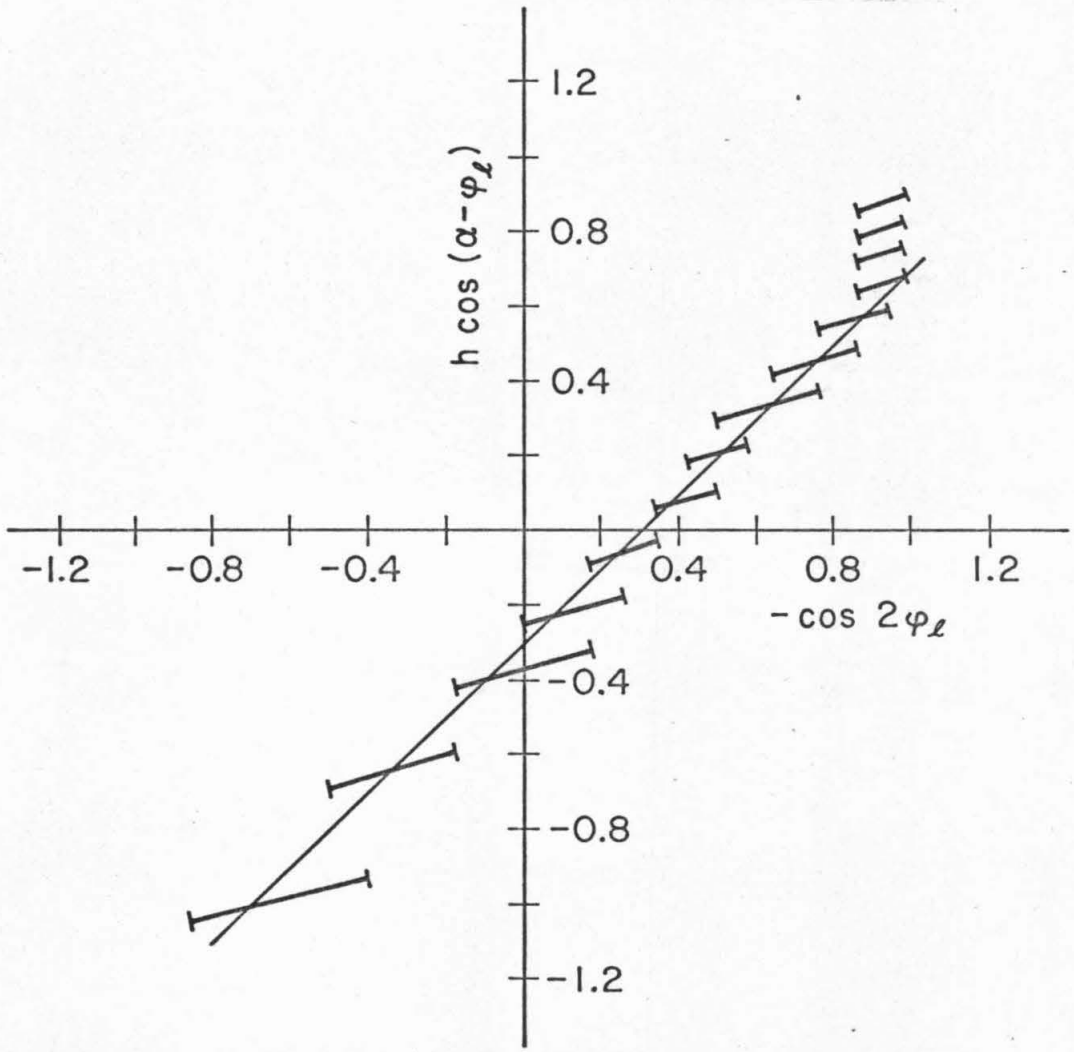

Fig. 3-11. (a) A plot of h $\cos(\alpha - \varphi_\ell)$ against $(-\cos 2\varphi_\ell)$ for film 81-4-6. Bars represent range of values observed.

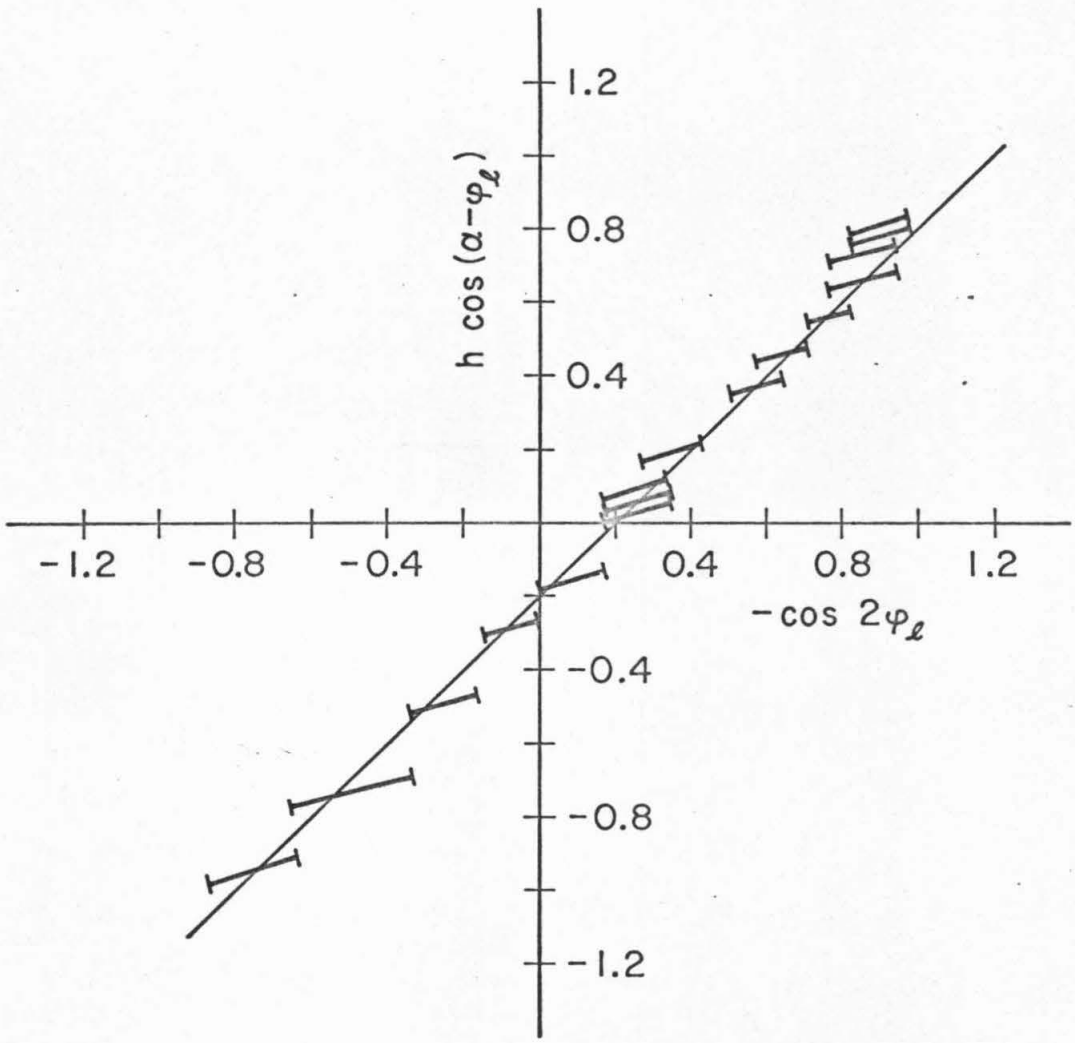

Fig. 3-11. (b) A plot of h $\cos(\alpha - \varphi_\ell)$ against $(-\cos 2\varphi_\ell)$ for film 81-10-4. Bars represent range of values observed.

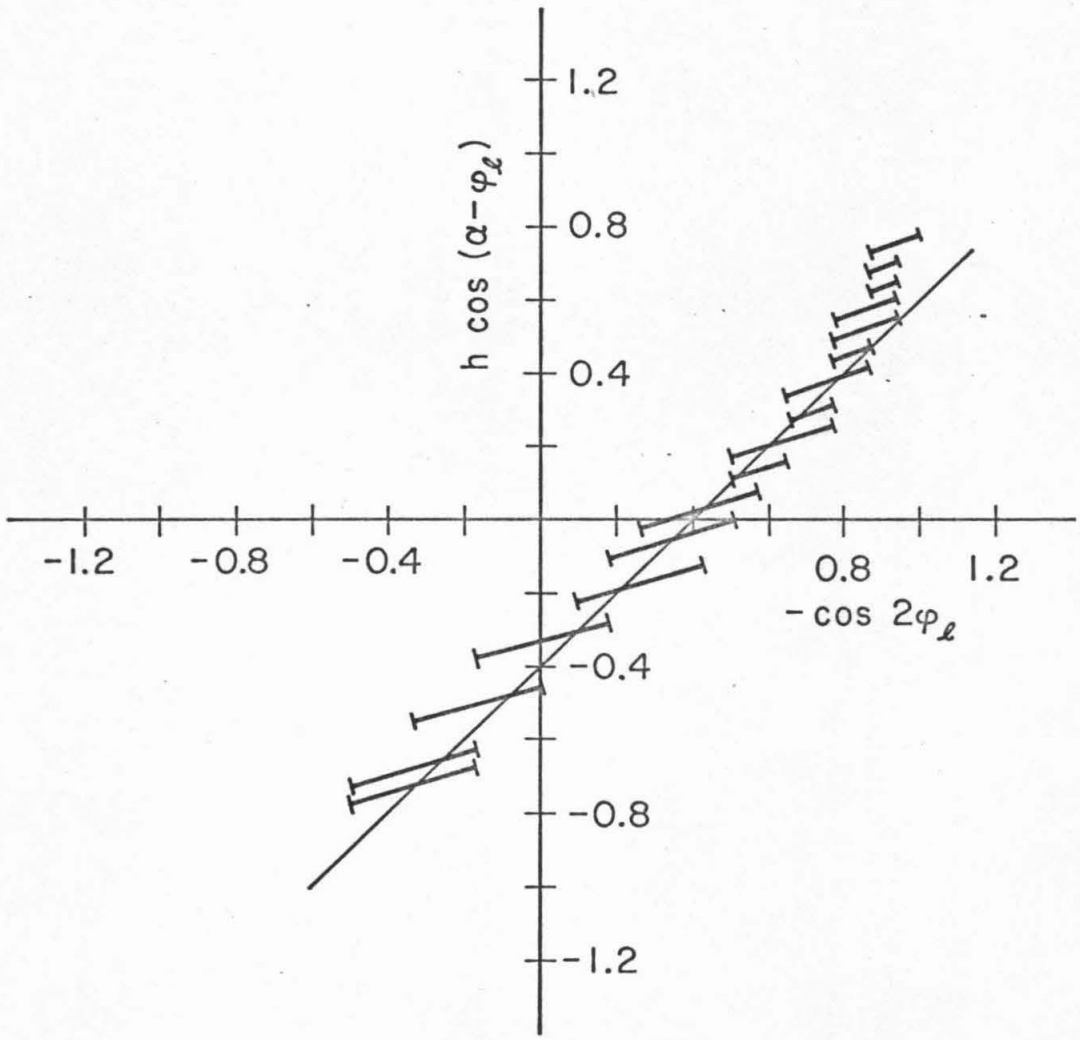

Fig. 3-11. (c) A plot of h $\cos(\alpha - \varphi_\ell)$ against $(-\cos 2\varphi_\ell)$ for film 84-8-7. Bars represent range of values observed.

observed spread in φ_ℓ. Typically this is about $\pm 5^o$ and is attributed largely to macroscopic anisotropy dispersion and edge effects. Stein's predicted result (3.6) would be a straight line of unit slope through the origin. It is clear that the data forms a straight line of unit slope, but it is shifted by various amounts from the origin for the three different films. The experimental data fit curves of the form

$$h(\alpha) = h \cos(\alpha - \varphi_\ell) + \cos 2\varphi_\ell = -h_\ell \qquad (3.7)$$

where h_ℓ is a constant positive parameter characteristic of each film. Hence, the experimental results are similar to what Stein suggests, but an explanation for the shift by h_ℓ must be found.

3.2.5 Magnetization Locking. A theoretical framework which attempts to provide an explanation for the observed striped configuration can now be presented. It is proposed that a local instability in the ripple occurs to produce the stripes. This instability is caused by a non-linear local effective field arising from applied fields and uniaxial anisotropy. This local effective field grows sufficiently negative to overcome the non-linear magnetostatic field, $\overline{h_d}$, in regions where $\varphi > 0$. At this time the magnetization in regions where $\varphi > 0$ will switch, producing magnetostatic fields that prevent the regions where $\varphi < 0$ from reversing and thereby locking a striped domain pattern into the film. A quasi-static analysis based on the theory derived for free ripple in Chapter 2 can be justified with low applied fields. The effects of blocking can be included later by the addition of reaction torque terms. For the films investigated, the additional terms are

minor in significance and in any case are not necessary for an understanding of how the stripes form. Under conditions in which this analysis is valid, the model accurately predicts the experimentally observed angular dependence of the stripes on applied field except when fields are applied very near to the Stoner-Wohlfarth threshold (Fig. 2-2) in the region of high transverse field.

The effective field responsible for the locking is h_{u2} (see (2.41c)), the non-linear field which arises from the uniaxial anisotropy and applied field. This field is effectively a correction to $h(\alpha)$, the linear effective field arising from the same source. To obtain an intuitive feeling for the meaning of h_{u2}, consider Fig. 3-12 which shows, for comparison, the uniform torque from applied fields and uniaxial anisotropy, T; the linear uniform field, $h(\alpha)$; and the non-linear uniform field, h_{u2} plotted as functions of φ_o, for $h = 0.6$ and $\alpha = 170^o$. In a Taylor series expansion of the uniform torque about an equilibrium position, it is seen that T is contained in the zero order term, $h(\alpha)$ in the first order term, and h_{u2} in the second order term:

$$\begin{aligned} T_u/M_s H_k = {} & h \sin(\alpha-\varphi_o) - \tfrac{1}{2} \sin 2\varphi_o \\ & + \varphi[-h \cos(\alpha-\varphi_o) - \cos 2\varphi_o] \\ & + (\varphi^2/2)[-h \sin(\alpha-\varphi_o) + 2 \sin 2\varphi_o] \\ & + \cdots \end{aligned} \qquad (3.8a)$$

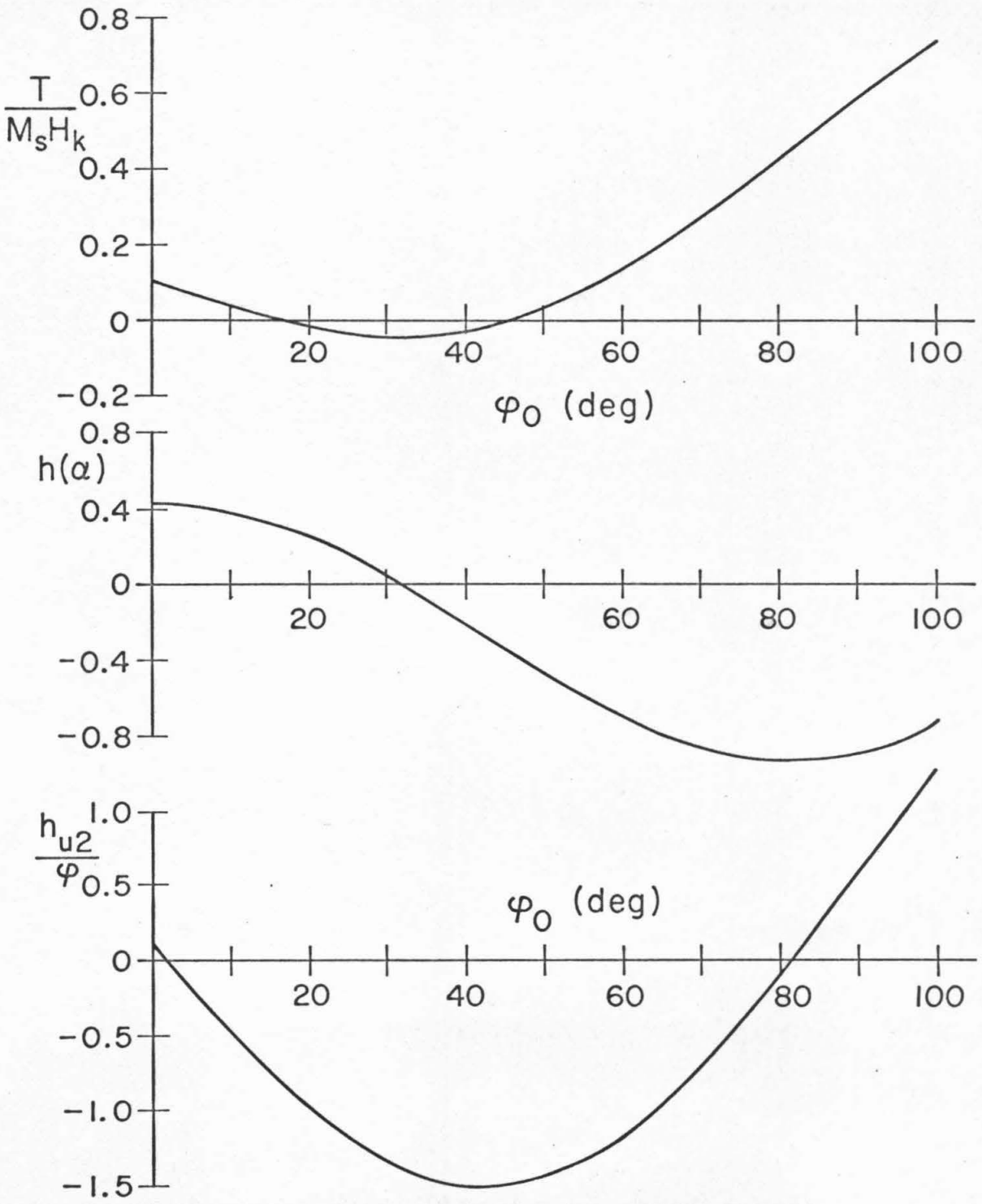

Fig. 3-12. Plots of T, $h(\alpha)$, and h_{u2}/φ as functions of φ_o for $h = 0.6$ and $\alpha = 170^{\circ}$.

$$T_u/M_sH_k = T/M_sH_k - \varphi h(\alpha) - (\varphi/2)h_{u2} + \ldots \qquad (3.8b)$$

With the mean magnetization at $\varphi_o \approx 16.5^o$, which corresponds to static equilibrium (T=0), it is seen that $-\varphi h(\alpha)$ is the linear restoring torque from applied fields and uniaxial anisotropy seen by magnetization at an angle $\varphi_o+\varphi$. So long as φ is not very large, $h(\alpha) > 0$ and the resultant torque, $-\varphi h(\alpha)$, tends to restore the magnetization to equilibrium. The second order torque is $-\varphi^2/2[h \sin(\alpha-\varphi_o)-2 \sin 2\varphi_o]$ or $-(\varphi/2)h_{u2}$. So long as φ is small, this torque is positive regardless of whether φ is greater than or less than zero. Hence, this second order torque restores magnetization where $\varphi < 0$, but tends to push the magnetization away from equilibrium for $\varphi > 0$. Of course, for the magnetization near static equilibrium (T=0), φ is small and the first order torque is much greater than the second order torque. Therefore, the total torque is a restoring torque.

When the field is increased beyond the Stoner-Wohlfarth threshold, the uniform torque does not become negative until the magnetization in the film has reversed. In this case, T, $h(\alpha)$, and h_{u2}/φ depend on φ_o as shown in Fig. 3-13. These curves were drawn for h=0.70, $\alpha = 170^o$. If for example the mean magnetization is during an instant of time at $\varphi_o = 40^o$, the first order torque, $-\varphi h(\alpha)$, is positive for $\varphi > 0$ and negative for $\varphi < 0$. Hence, the first order torque causes the ripple to grow. However, the mean demagnetizing field, $\overline{h_d}$, acts to suppress the ripple amplitude and since $\overline{h_d} \propto (\overline{h_{eff}})^{-1/4}$, $\overline{h_d}$, always cancels the effect of $h(\alpha)$ so that no instability of the mean magnetization can occur. A local instability can occur, however, and the second order uniform torque, $-(\varphi^2/2)[h \sin(\alpha - \varphi_o) - 2 \sin 2\varphi_o]$ is the cause of it. This non-

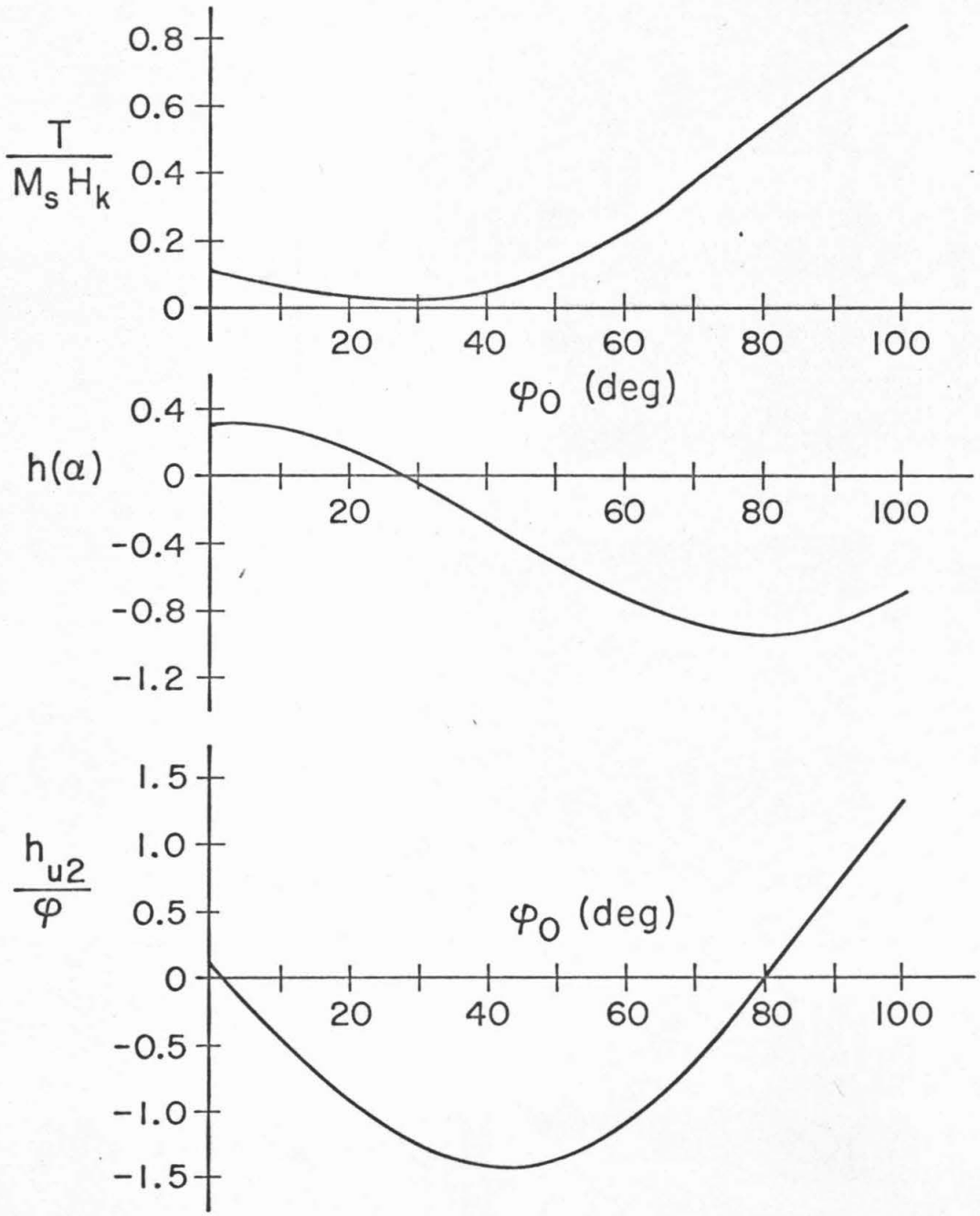

Fig. 3-13. Plots of T, $h(\alpha)$, and h_{u2}/φ as functions of φ_o for $h = 0.7$ and $\alpha = 170^o$.

linear torque in the vicinity of $\varphi_o = 40^o$ is large and positive whether φ is positive or negative. Therefore, it causes the magnetization trailing $\vec{M}_o$ to catch up, but it causes the magnetization leading $\vec{M}_o$ to increase its angle. This may also easily be seen from the expression for h_{u2}:

$$h_{u2} = \varphi[h \sin(\alpha-\varphi_o) - 2 \sin 2\varphi_o] , \tag{2.41c}$$

which shows that at $h = 0.7$, $\alpha = 170^o$, $\varphi_o = 40^o$ that for $\varphi > 0$, $h_{u2} < 0$. Of course, because h_{u2} is proportional to φ, it averages to zero, but locally in regions where $\varphi > 0$ it may cause h_{eff} to go to zero, allowing the magnetization in these regions to switch.

In calculating when h_{u2} becomes sufficiently negative that $h_{eff} = 0$ for $\varphi > 0$, the fields h_{u3}, h_{k2}, and h_{k3} are all negligible in comparison to h_d and h_{u2}. Then, for locking,

$$h_{eff}(\varphi > 0) = h(\alpha) + h_d + h_{u2}(\varphi > 0) = 0. \tag{3.9}$$

For h_d, its average value, $\overline{h_d}$, is used, and for φ in h_{u2}, its r.m.s. value, $\sqrt{\overline{\varphi^2}}$, is used. Then, since $\overline{h_d} \gg \overline{h_{u3}}, \overline{h_{k3}}$, at locking,

$$\overline{h_{eff}} \approx h(\alpha) + \overline{h_d} \approx -h_{u2}(\varphi > 0). \tag{3.10}$$

Because $\overline{h_d} \gg h_{u2}(\varphi > 0)$, at locking,

$$h(\alpha) \approx -\overline{h_d}\,(\overline{h_{eff}} = -h_{u2}(\varphi > 0)) = -h_\ell \tag{3.11}$$

$$h_\ell = 0.53 \frac{(M_s\sqrt{d})^{\frac{12}{11}}}{(AK_u)^{\frac{13}{11}}} \frac{S^{\frac{20}{11}}}{\left[-h \sin(\alpha-\varphi_\ell)+2 \sin 2\varphi_\ell\right]^{\frac{2}{11}}}, \qquad (3.12)$$

where φ_o(at locking) = φ_ℓ . Hence, the condition for locking is $h(\alpha) = -h_\ell$.

Although h_ℓ is not totally independent of h, α, and φ_ℓ, for the experimentally observed case, with fields near the Stoner-Wohlfarth threshold, $[-h \sin(\alpha-\varphi_\ell) + 2 \sin 2\varphi_\ell]^{\frac{2}{11}} \approx 1\pm0.25$. Hence, h_ℓ is nearly constant and as was already pointed out, the data shown in Fig. 3-11a-c approximately fit such a relation. In Fig. 3-14a-c the data of Fig. 3-11a-c are plotted again, but this time including the fact that h_ℓ is weakly dependent on h, α, and φ_ℓ. The experimental data fit the model very well with the exception of data taken with $H_y \geq 0.7\ H_k$ which shows a deviation from the straight line. At low to moderate transverse fields, the slope of the data agrees with the predicted slope of one to better than 10%.

The value of S from equation (3.12) can be calculated using h_ℓ from the data (0.3 for 81-4-6, 0.2 for 81-10-4, and 0.4 for 84-8-7), and using $A = 10^{-6}$ erg cm^{-1} and the values of M_s, d, and K_u listed in Table 2-I. The values $S = 6.1 \times 10^{-3}$, 9.6×10^{-3}, and 9.1×10^{-3} erg cm^{-2} were obtained for films 81-4-6, 81-10-4, and 84-8-7, respectively. If a numerical correction of 2.9 is applied to the values in order that they may be made consistent with Hoffmann's theory, they are typical of values found by Kempter (1969) in films of similar composition and evaporation conditions, although no direct comparison with values

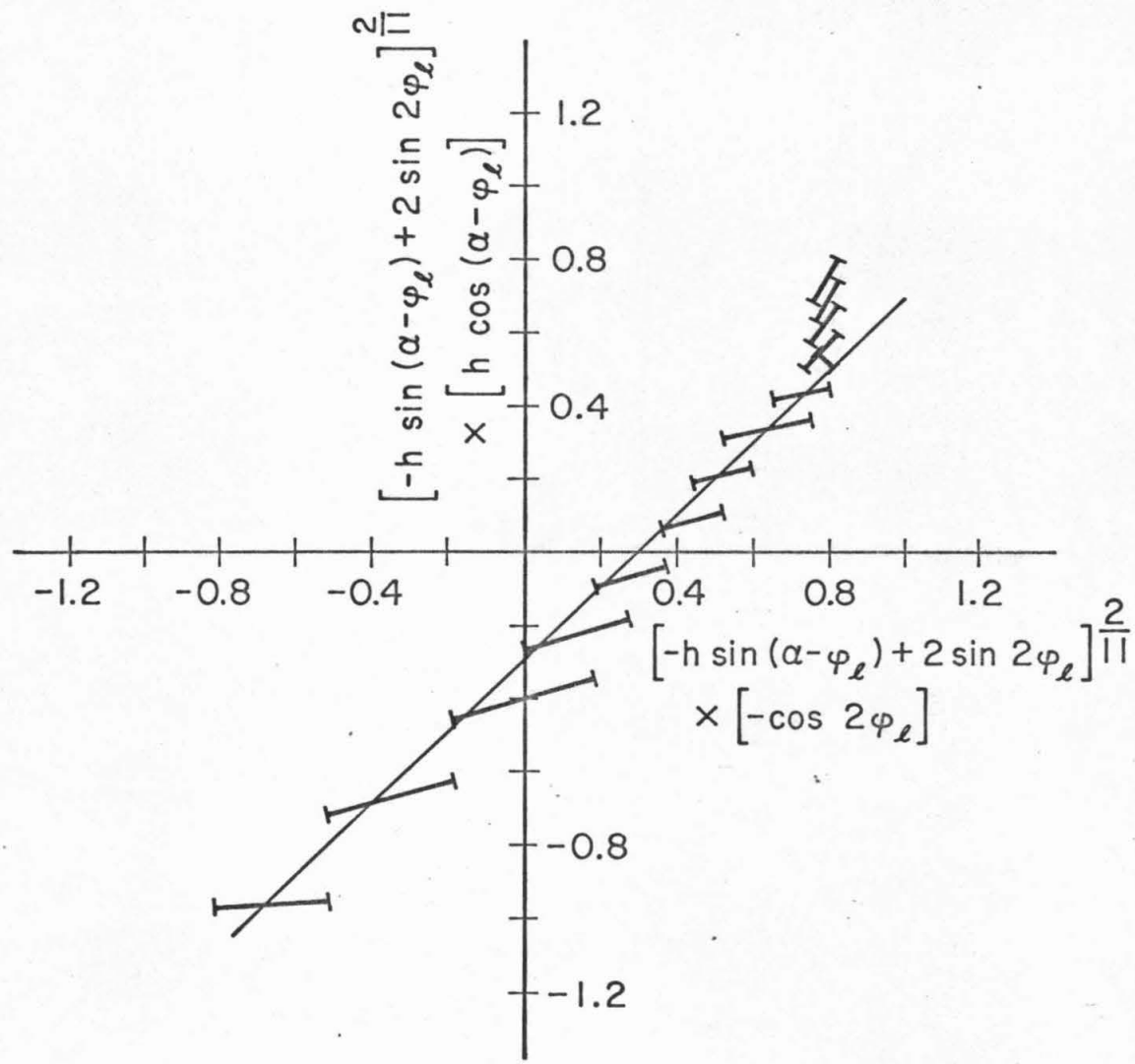

Fig. 3-14 (a) A plot showing how the data fit the relation $h(\alpha) = h_\ell$ for film 81-4-6. Bars represent range of values observed.

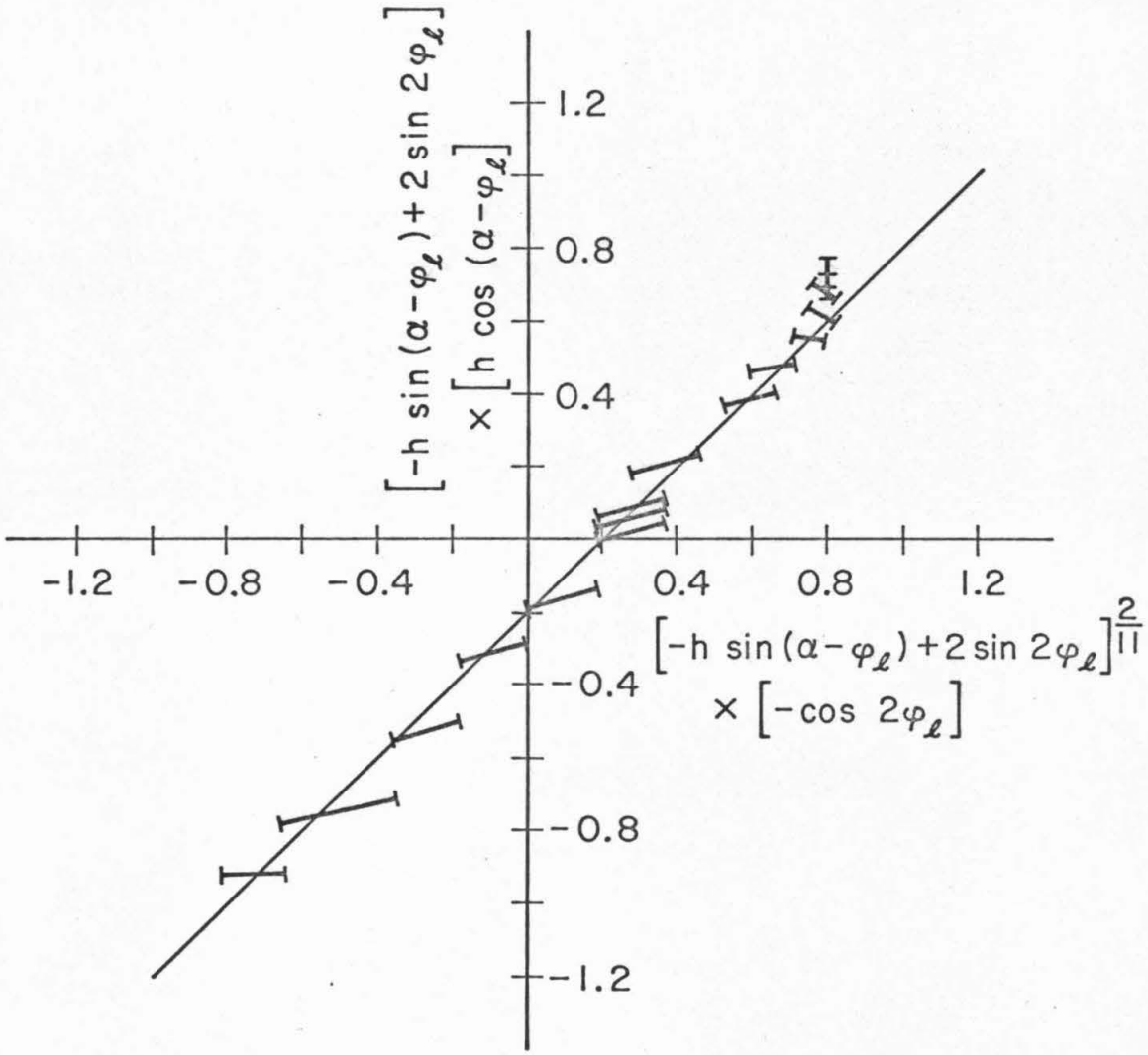

Fig. 3-14 (b) A plot showing how the data fit the relation $h(\alpha) = h_\ell$ for film 81-10-4. Bars represent the range of values observed.

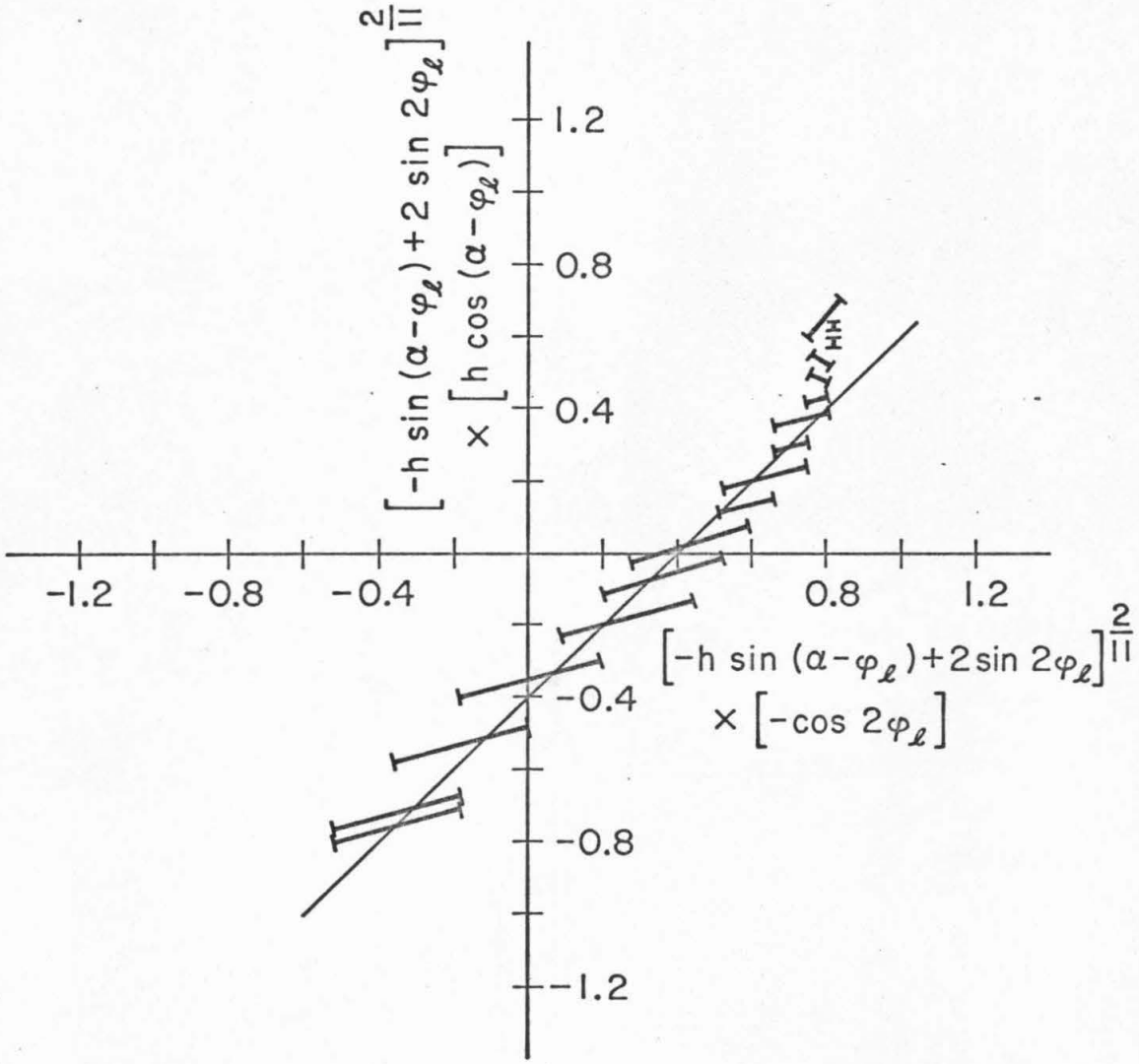

Fig. 3-14 (c) A plot showing how the data fit the relation $h(\alpha) = h_\ell$ for film 84-8-7. Bars represent range of values observed.

determined by other methods, e.g., by susceptibility measurements as Kempter (1969) has done, has been made. At high transverse fields the observed φ_ℓ tends to constant values such that $[-h \sin(\alpha-\varphi_\ell)+2\sin 2\varphi_\ell]^{\frac{2}{11}}$ $(-\cos 2\varphi_\ell) \simeq 0.8$. This behavior is not predicted by the locking model. The data in the high transverse field region suggest that the explanation for the unpredicted behavior may be that ripple relaxation stops at some angle $\varphi_{\ell_{max}}$. As was seen in Fig. 3-9 which showed φ_ℓ plotted as a function of h_y with h_x sufficient to reach the Stoner-Wohlfarth threshold, φ_ℓ tends to a constant value when $H_y > 0.7\, H_k$. If ripple relaxation does stop, then as $\vec{M}_o$ continues to rotate $h(\alpha)$ will decrease and because the ripple is in a blocked state ($h(\alpha) < h_a$) domain splitting like that predicted by Hoffmann (1964a) and discussed briefly in Section 2.4 should occur. This domain splitting would also appear as a striped configuration.

An alternative method of obtaining a transverse component of applied field is simply to apply a pulse field at an angle to the easy axis. All of the data plotted in Fig. 3-14a-c were obtained by applying an easy axis pulse field to a film which had a static hard axis bias field applied. In order to show that either method led to the same results, the data in Fig. 3-15 were obtained by varying the direction of the pulse field. It can be seen that the data indicate $h_\ell = 0.3$ for film 81-4-6 as did the data obtained using static transverse bias fields and longitudinal pulse fields.

Basically, the blocked ripple and the fact that the magnetization is rotating so that ripple relaxation must occur have some of the same possible effects. Because of the blocking and the finite ripple

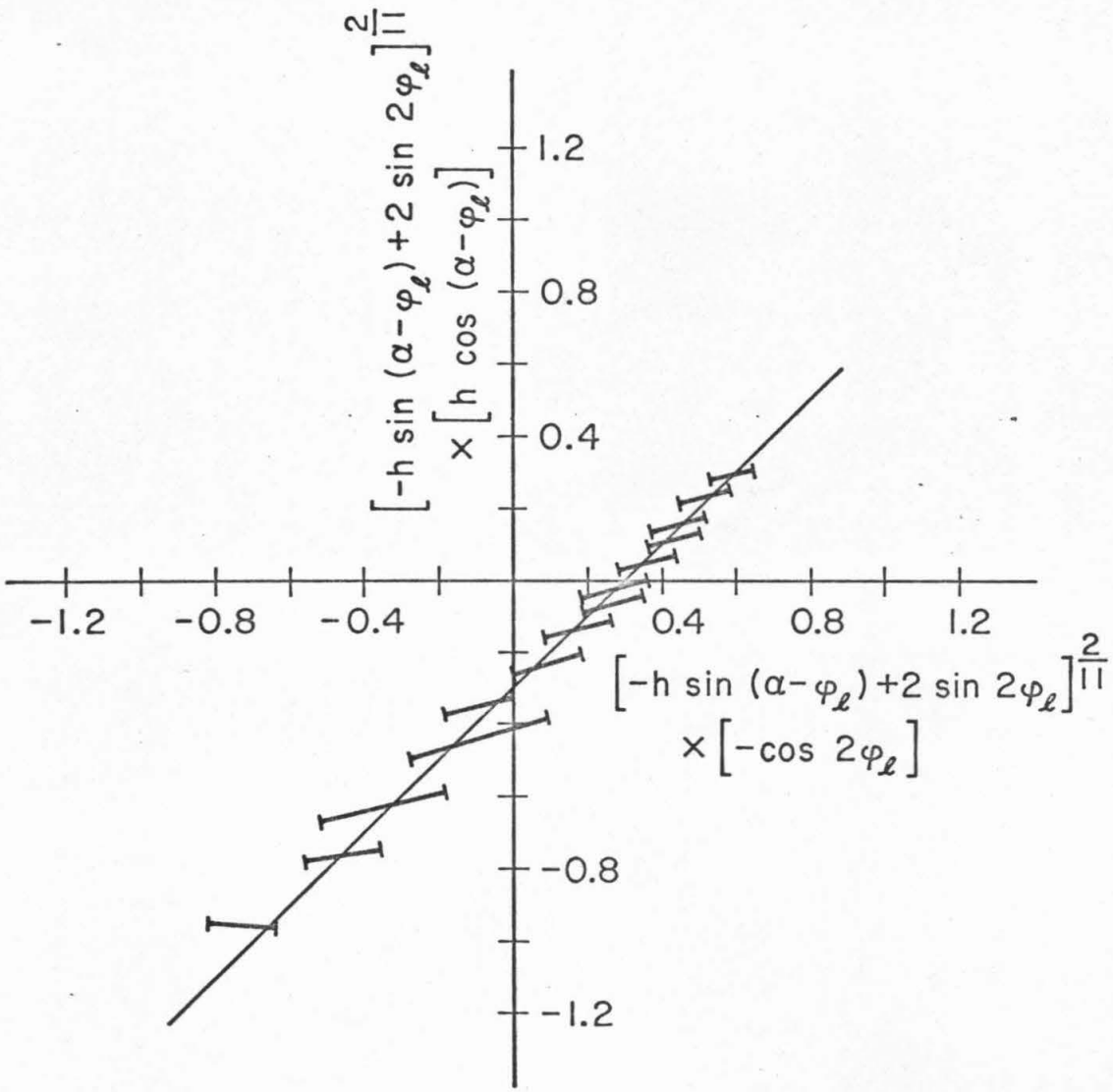

Fig. 3-15. A plot showing how the data fit the relation $h(\alpha) = h_\ell$ for film 81-4-6 when the pulse field is applied at various angles to the easy axis of the film.

relaxation time, it can be expected that $\overline{\Phi_{\vec{k}}} < \varphi_o$, where $\overline{\Phi_{\vec{k}}}$ is the angle of the wavevector for the mean ripple components. Therefore, the ripple is expected to exert a reaction torque, via magnetostatic fields, on $\vec{M}_o$. To discover whether the angle $\eta = \varphi_o - \overline{\Phi_{\vec{k}}}$ is large enough to produce a significant reaction torque, comparisons will be made between the time for the magnetization to rotate and the speed of ripple relaxation. For the former a solution to (2.28a,b) valid for an anisotropic film is needed. Combining (2.28a) with (2.28b):

$$\ddot{\varphi}_o + \alpha_d \sqrt{\frac{4\pi M_s}{H_p}}\, \dot{\varphi}_o = \frac{T(\varphi_o)}{M_s H_p} \,. \tag{3.13}$$

Now, over small intervals of time such that $\varphi_o(\tau) - \varphi_o(\tau_1) \ll 1$, $T(\varphi_o(\tau))$ may be approximated by the value $T(\varphi_o(\tau_1))$. Making such a substitution, a solution is obtained:

$$\varphi_o(t) = \left[\frac{T(\varphi_o(t_1))}{4\pi M_s^2 \alpha_d^2} - \frac{1}{\alpha_d \gamma 4\pi M_s}\frac{\partial \varphi}{\partial t_1}\right]\left[e^{-\alpha_d \gamma 4\pi M_s (t-t_1)} - 1\right] + \frac{T(\varphi_o(t_1))}{M_s \alpha_d}\gamma(t-t_1) + \varphi_o(t_1) \,. \tag{3.14}$$

Although it is not difficult to obtain a computer solution for $\varphi_o(t)$, equation (3.14) can be used to obtain quite accurate values for $\varphi_o(t)$ if a number of consecutive short time intervals are used.

It was pointed out in Section 3.2.2 that since the risetime of the pulse field is 10 nsec, up until the time at which the Stoner-Wohlfarth threshold is reached, the mean magnetization should maintain quasi-static equilibrium with the rising field because times for coherent

rotation of the magnetization are short compared to 10 nsec. By using (3.14) repeatedly with 0.2 nsec time intervals and assuming for example a step function pulse field of 0.7 H_k applied at 170^o (for which T is plotted in Fig. 3-13), it is found that the time required for rotation from $\varphi_o = 0$ to $\varphi_o = \varphi_{SW} = 29^o$ is about 2 nsec, indicating that indeed $\vec{M}_o$ should be in quasi-static equilibrium with the 10 nsec risetime pulse field. Furthermore, the ripple must be able to follow the 29^o rotation of $\vec{M}_o$ in 10 nsec as Hoper (1968) found that the ripple was able to follow $\vec{M}_o$ rotating at 7^o per nanosecond. Therefore, the assumption that both $\vec{M}_o$ and the ripple maintain quasi-static equilibrium with the field up until the Stoner-Wohlfarth threshold is reached is certainly valid. However, as the mean magnetization rotates past the torque minimum of the Stoner-Wohlfarth threshold, it begins to rotate more quickly because of the increasing torque. In film 81-4-6, locking occurs at $h(\alpha) \approx -0.3$ which, as may be seen from Fig. 3-13, is obtained at $\varphi_o \approx 40^o$. By using equation (3.14) repeatedly as before with (0.2 nsec) intervals and assuming $\alpha_d \approx .01$, it is found that at $\varphi_o = 40^o$, the magnetization is rotating at a rate of roughly 14^o/nsec. Hence, the assumption that the ripple maintains quasi-static equilibrium with $\vec{M}_o$ is not really justified, though it might be guessed that η is only a few degrees. The reaction torque from the ripple will slow the rotation of $\vec{M}_o$ thereby improving the assumption of quasi-static equilibrium.

To calculate the static reaction torque exerted by the ripple on $\vec{M}_o$, lying at angle φ_o to the easy axis, the ripple configuration was assumed to be that obtained when ripple came to equilibrium with $\vec{M}_o$ at angle $\varphi_o - \eta$. For η small, this should be a reasonable approximation. The

calculation is done in Appendix A in detail. The resultant reaction torque, $\vec{T}_r$, is given by

$$\vec{T}_r = \vec{i}_z M_s H_k \overline{h_d} \frac{\sin 2\eta}{2} \qquad (A.9)$$

To have the reaction torque a function of sin 2η is intuitively satisfying because it implies that the torque changes sign when η does and also that it changes sign at $\eta = 90^o$ as is expected.

The reaction torque, T_r, should be compared with the uniform driving torque, T. At locking, $\overline{h_d} = 0.3$ for film 81-4-6, as $h_\ell \simeq \overline{h_d}|_{\text{at locking}}$. Then assuming $\eta << 1$, $T_r \simeq -0.3\ \eta\ M_s H_k$. From Fig. 3-13 and the fact that $h_\ell = 0.30$, it is observed that $T = 0.045\ M_s H_k$ when locking occurs and a field of $0.7\ H_k$ is applied at 170^o to the easy axis. Now by substituting $T + T_r$ for T in equation (3.14), φ_o can be calculated as a function of time with the effects of the reaction torque included. It is found that if $T + T_r \simeq 0.02\ M_s H_k$, the magnetization rotates at approximately 7^o/nsec. This requires $\eta \simeq .07$ rad or 4^o. Thus, for fields only slightly in excess of the Stoner-Wohlfarth threshold the ripple is expected to lag $\vec{M}_o$ by less than 4^o, indicating the assumption that the ripple is able to maintain quasi-static equilibrium with $\vec{M}_o$ is quite good.

Another experimentally measurable quantity is the stripe width or alternatively the wavelength of the stripes. The photographs of Fig. 3-16a clearly show the locked ripple as it forms in film 81-4-6. Note the very short wavelength stripes which are forming as time proceeds. In Fig. 3-16b the area within the rectangle in the 200 nsec photograph

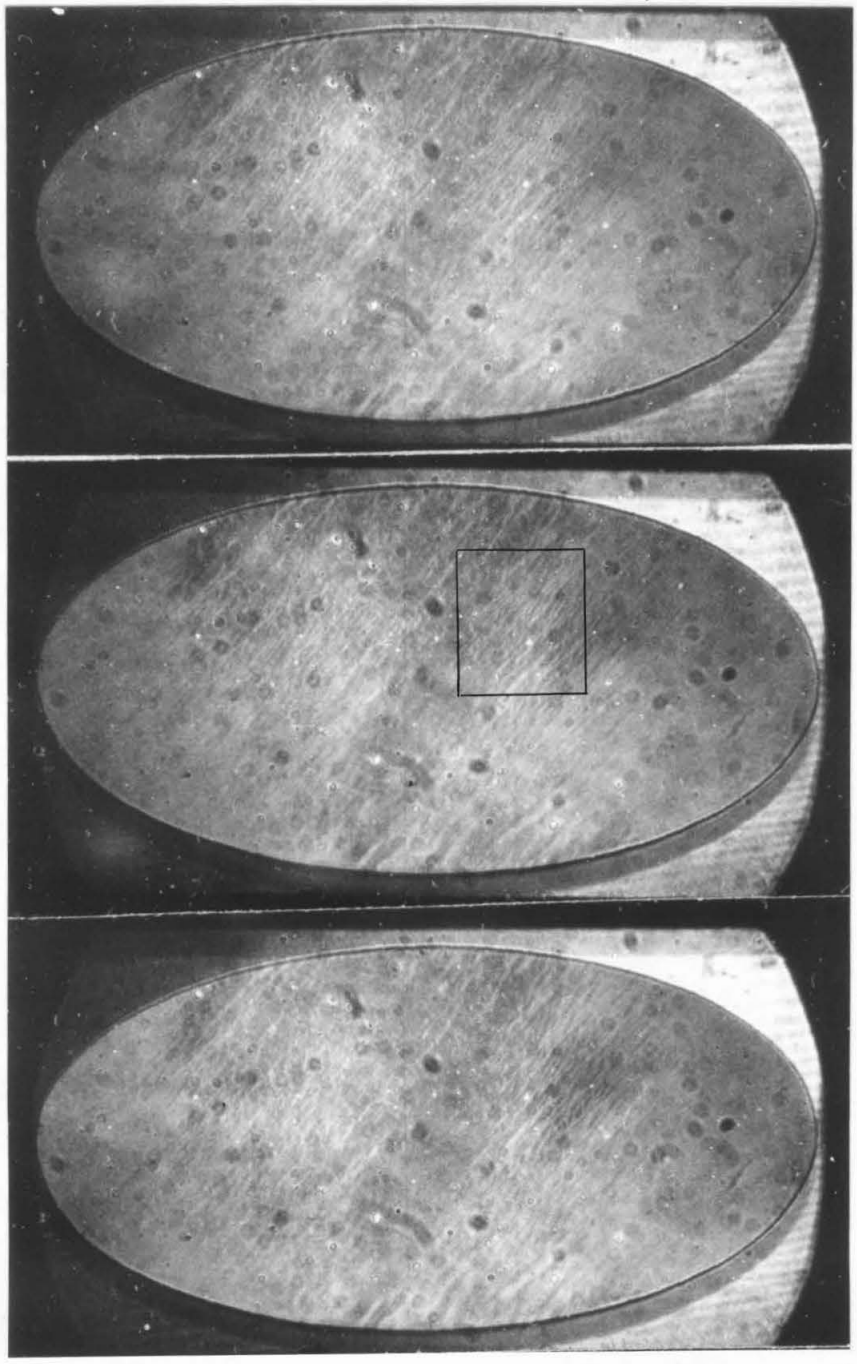

Fig. 3-16. (a) Film 81-4-6 in the process of flux reversal with a 1.75 oe transverse bias field directed to the left and a 0.88 oe longitudinal pulse field directed downward. Time in nanoseconds relative to initial application of pulse field is indicated.

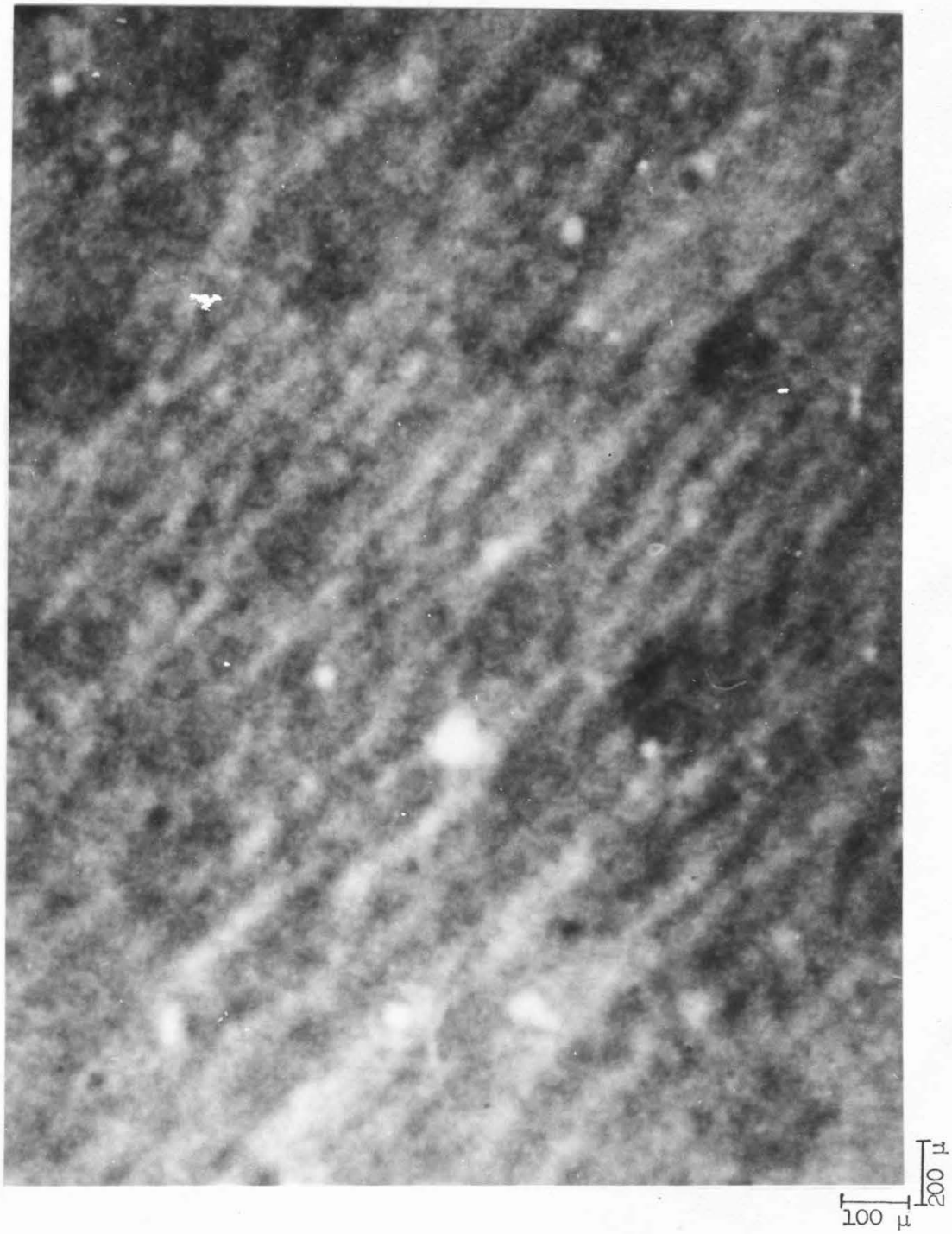

Fig. 3-16. (b) The rectangular section of the 200 nsec photograph of Fig. 3-16a.

of Fig. 3-16a is shown magnified. In Fig. 3-16b, 1 cm in the horizontal direction corresponds to 100 μ on the magnetic film, while 1 cm in the vertical direction corresponds to 200 μ on the magnetic film. Stripes with wavelengths in the 50 μ to 100 μ range are easily discernible, though the limited 10 μ resolution of the photographic film is seen to be affecting the visibility of the shorter wavelengths.

In contrast to the locked ripple, the wavelength of the most intense ripple in the electron micrograph of Fig. 2-8 was in the 1 μ to 2 μ range. Hence, there is considerable difference in wavelength between the locked ripple observed with the Kerr magneto-optic camera and the free ripple with no field applied observed with the electron microscope. As was pointed out in Chapter 2, Fuller and Hale (1960) showed that the magnitude of the change in intensity of the electron beam of an electron microscope due to the $\vec{k}^{th}$ component of ripple is proportional to $k|\varphi_{\vec{k}}|$; hence, the wavelength of the most intense periodic structure seen with an electron microscope is that which makes $k|\varphi_{\vec{k}}|$ a maximum

$$\lambda = 2\pi\sqrt{A/(K_u \overline{h_{eff}})} \quad . \tag{2.38}$$

At locking in film 81-4-6, $\overline{h_{eff}}$ may be calculated using the parameters given in Table 2-1 and the value $S = 6.1 \times 10^{-3}$ determined from Fig. 3-14a. From equation (3.10) is obtained $\overline{h_{eff}}|_{\text{at locking}} \tilde{\simeq} 0.039$, which gives $\lambda \tilde{\simeq} 10$ μ . On the other hand, the magnitude of the change in intensity of the light beam in the Kerr magneto-optic camera due to the

$\vec{k}^{th}$ component of ripple, is proportional only to $|\varphi_{\vec{k}}|$; consequently, the components of ripple most easily seen in the photographs obtained with the Kerr magneto-optic camera are those with the largest amplitude. It was shown in Chapter 2 that the Fourier ripple spectrum consisted of components given by (2.34). It is seen that, since $f_{1\vec{k}}$ is constant in the region of interest (Harte (1964)), there actually is a broad spectrum of ripple components which are not attenuated by exchange or transverse magnetostatic fields. In particular note that there is no long wavelength ($k \to 0$) attenuation from either the exchange or transverse magnetostatic fields. Therefore, long wavelength components of ripple with large amplitudes do exist in the free ripple spectrum before locking occurs. Of course, the density of longer wavelength components is less than that of the shorter wavelength components because the density is proportional to k, but this does not alter the fact that such long wavelength components do exist. Since the transverse magnetostatic fields which arise when the locking occurs are proportional to k, (for $\frac{kd}{2} \ll 1$), it is to be expected that only components of ripple with longer wavelengths will be able to obtain large amplitudes. Therefore, it is the longer wavelength components which one should expect to see with the Kerr magneto-optic camera.

In this section an explanation for the observed stripe formation process was given. It was suggested that the cause of the stripes was an instability in the ripple which occurred when the non-linear uniform field h_{u2} grew sufficiently large and negative in regions where $\varphi > 0$ to overcome the average effective field $\overline{h_{eff}}$ in that region. When this occurred, it was expected that the magnetization in regions where $\varphi > 0$

would switch and that the magnetization in regions where $\varphi < 0$ would not. Thus, stripes would form in the magnetization. Quantitative agreement between the theory and the experimental data was good, with the exception of data obtained with high transverse fields. Finally, the wavelength of the observed stripes was discussed, but no quantitative test of the theory could be made.

3.2.6 Flux Reversal after Locking. When locking occurs, locked ripple in the form of stripes grows in amplitude and without changing its orientation as seen in the photographs in Figs. 3-1, 3-8, and 3-16. For the applied fields used, reversal would be expected to take place in a few nanoseconds on the basis of equations (2.28a,b); however, it is clear that it takes much longer. There must be some torque caused by the locked ripple acting to slow the rotation of $\vec{M}_o$. Just as the free or blocked ripple with $\overline{\Phi}_k < \varphi_o$ was expected to exert a reaction torque on $\vec{M}_o$, we expect that the locked ripple does also. However, since a model valid for large φ^2 is not available, the total reaction torque cannot be calculated. If the reaction torque from the locked ripple is actually sufficient to prevent the rotation of $\vec{M}_o$, then a rearrangement of the ripple must take place before $\vec{M}_o$ can rotate. In Fig. 3-1 this rearrangment involved the nucleation of many small regions of partially reversed magnetization.

Nucleation of partially reversed regions can also be seen in Fig. 3-17 a,b,c where film 81-4-6 is reversing with only a 0.1 oe transverse bias field. In this case the angle of the stripes which form between 10 and 75 nsec indicates that $\varphi_\ell \simeq 25^o$. From 100 nsec on, nucleated regions appear throughout the striped area of the film. At

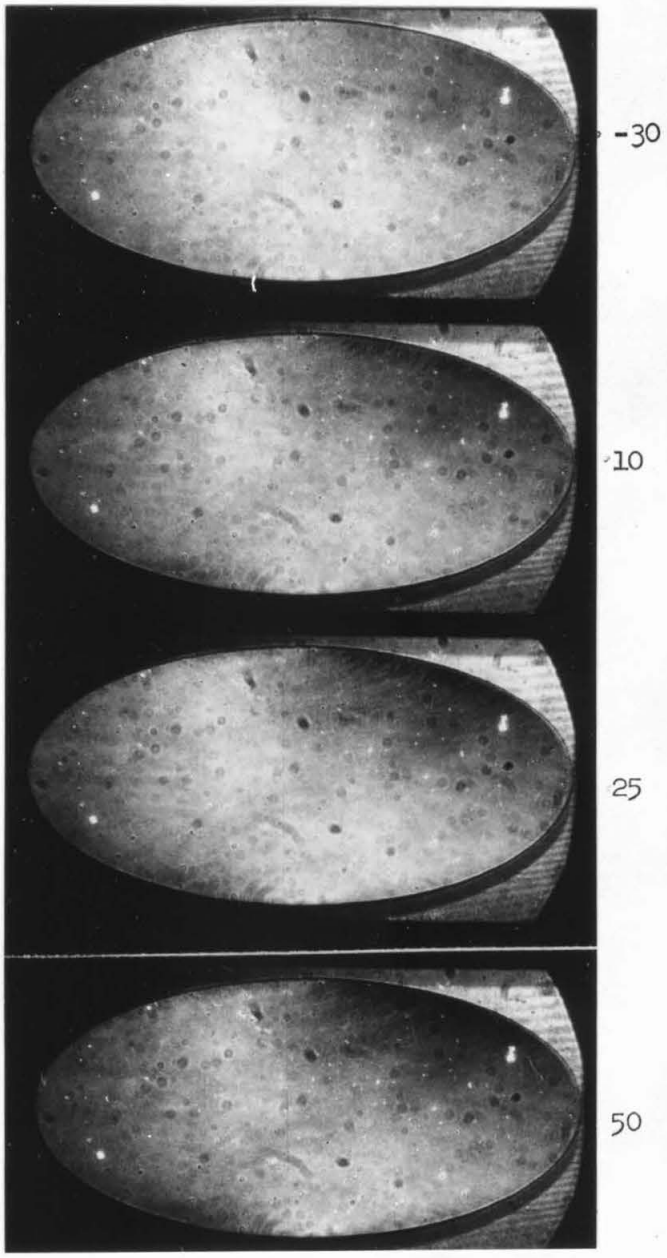

Fig. 3-17. (a) The film 81-4-6 in the process of flux reversal with a 0.1 oe transverse bias field directed to the left and a 4.1 oe longitudinal pulse field directed downward. Time in nanoseconds relative to initial application of pulse field is indicated.

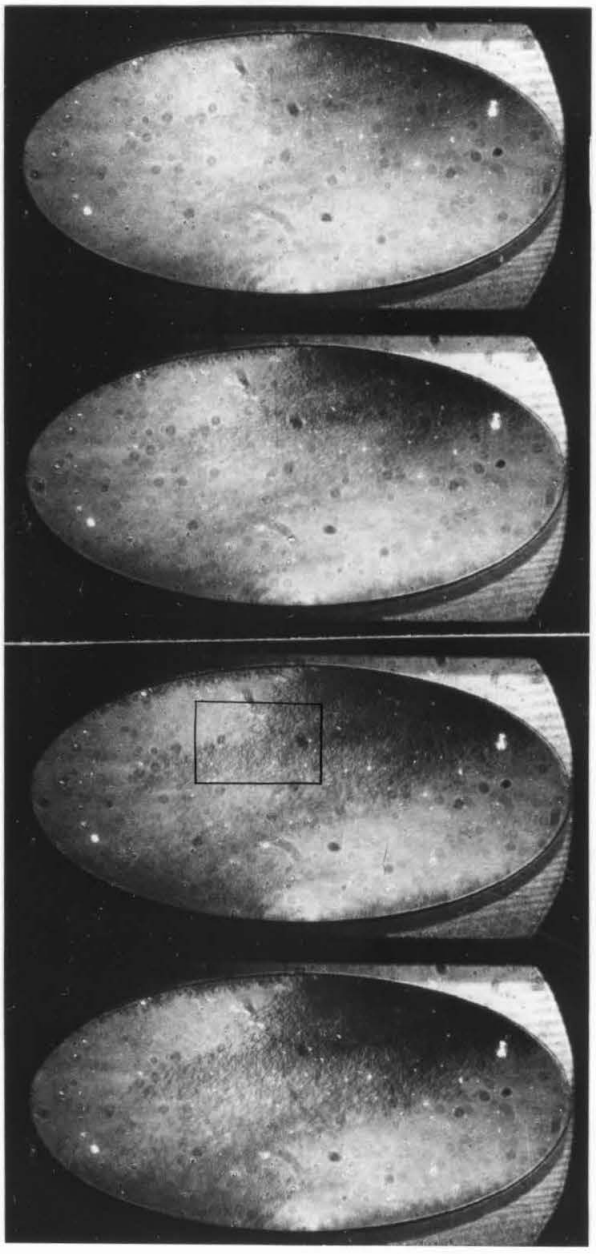

Fig. 3-17. (b) Film 81-4-6 in the process of flux reversal with a 0.1 oe transverse bias field directed to the left and a 4.1 oe longitudinal pulse field directed downward. Time in nanoseconds relative to initial application of pulse field is indicated.

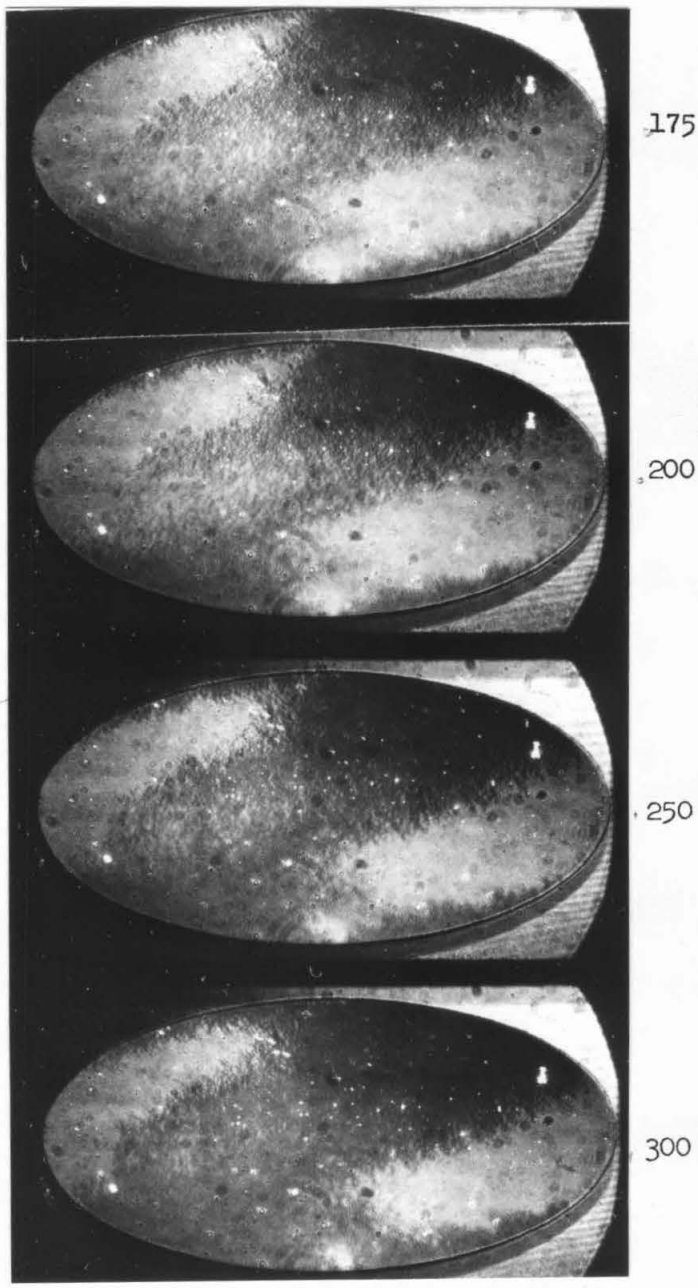

Fig. 3-17. (c) Film 81-4-6 in the process of flux reversal with a 0.1 oe transverse bias field directed to the left and a 4.1 oe longitudinal pulse field directed downward. Time in nanoseconds relative to initial application of pulse field is indicated.

25 nsec, the stripes with $\varphi_\ell \simeq 25^o$ are visible. There is a gradual darkening of the stripes until at 100 nsec nucleation begins to occur and as a result the stripes are obscured somewhat. The contrast of the nucleated regions indicates that the magnetization within them has not yet reversed, but rather that it has just begun to rotate. By 125 nsec, many nucleated regions have totally reversed as indicated by their sharp contrast. The poor depth of focus obscures some of the nucleated regions, but the regions within the in-focus area are quite clearly seen. The section of the 125 nsec photograph in the square is shown greatly magnified in Fig. 3-18. The nucleated regions are on the average elongated along the easy axis although the compression of the vertical scale by a factor of two caused by the 60^o angle at which the camera is oriented relative to the film plane must be considered. Qualitatively, this elongated shape is to be expected because of the demagnetizing fields in the reversed region. It is seen from the photograph of Fig. 3-18 that the nucleated regions have very complex shapes and do not form a simple pattern.

When the applied fields produce somewhat more torque on $\vec{M}_o$ than in Figs. 3-1 and 3-17, the nucleation processes do not occur. Rather, the stripes just slowly disappear as $\vec{M}_o$ reverses its direction. This is seen quite clearly in the photographs of Fig. 3-19, where film 81-4-6 is seen reversing with a 1.0 oe transverse bias field and a 1.65 oe longitudinal pulse field. At 25 nsec stripes have already begun to appear, hence, the magnetization is locked. By 75 nsec, the stripes have increased in contrast and are visible in a large region of the film. After 75 nsec, the entire striped region continues to become darker indicating that $\vec{M}_o$

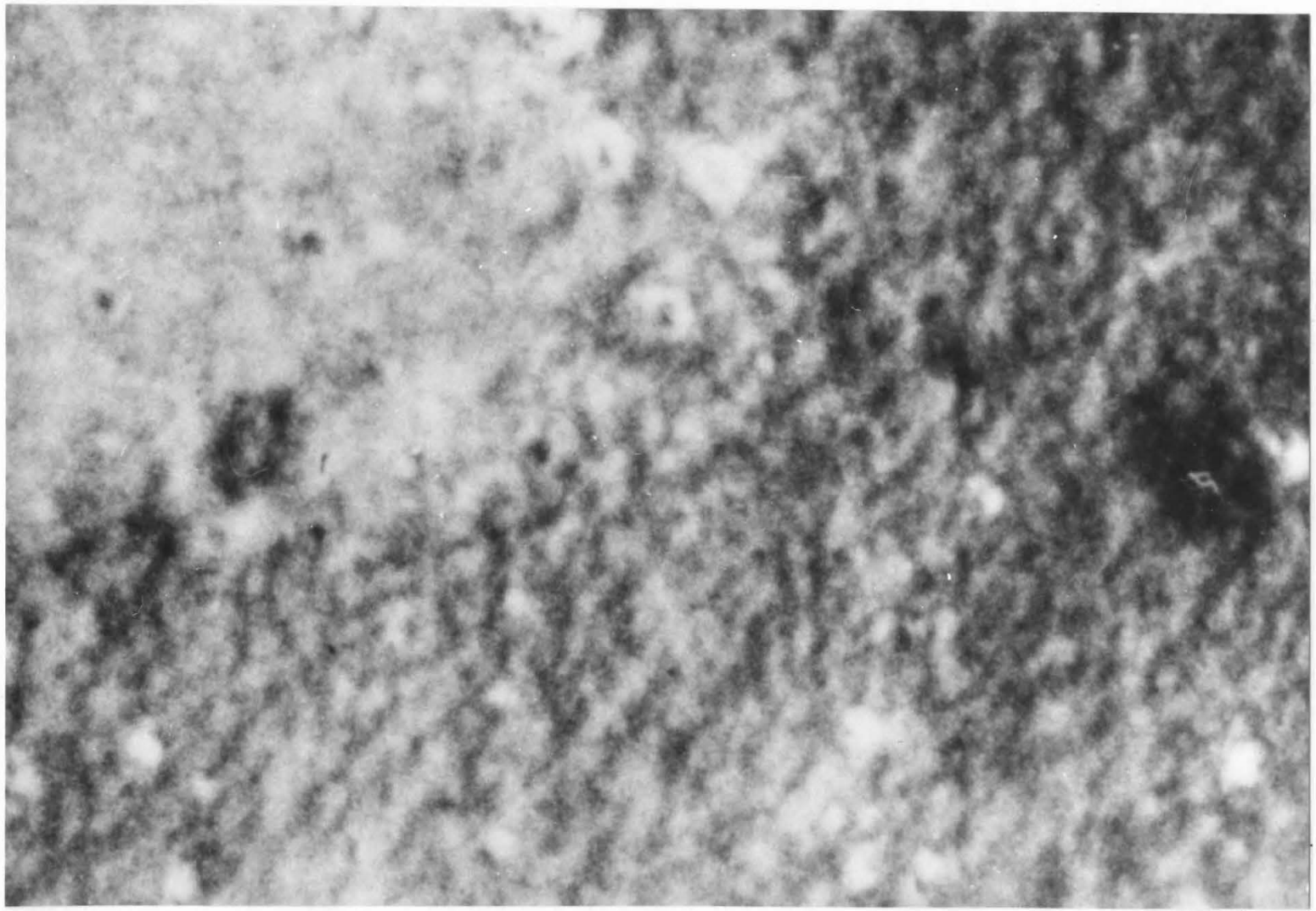

Fig. 3-18. Section of the 125 nsec photograph in Fig. 3-17b highly magnified.

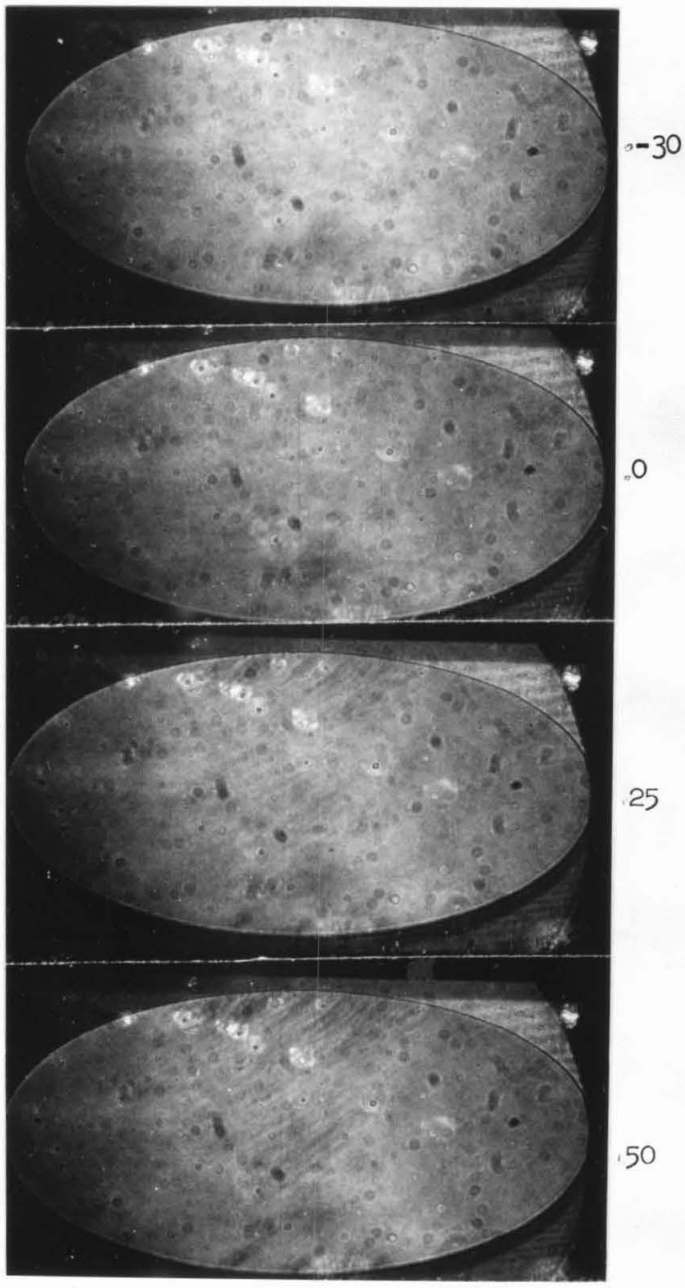

Fig. 3-19. (a) Film 81-4-6 in the process of flux reversal with a 1.0 oe transverse bias field directed to the left and a 1.65 oe longitudinal pulse field directed downward. Time in nanoseconds relative to initial application of pulse field is indicated.

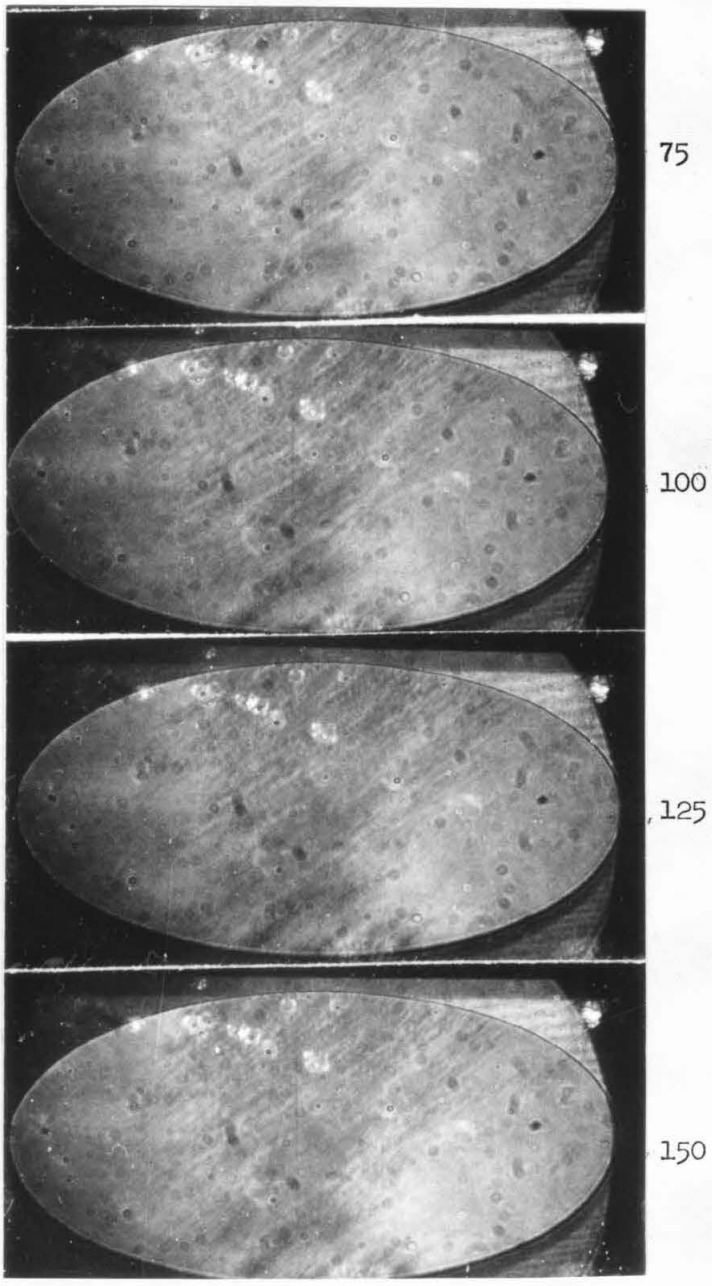

Fig. 3-19. (b) Film 81-4-6 in the process of flux reversal with a 1.0 oe transverse bias field directed to the left and a 1.65 oe longitudinal pulse field directed downward. Time in nanoseconds relative to initial application of pulse field is indicated.

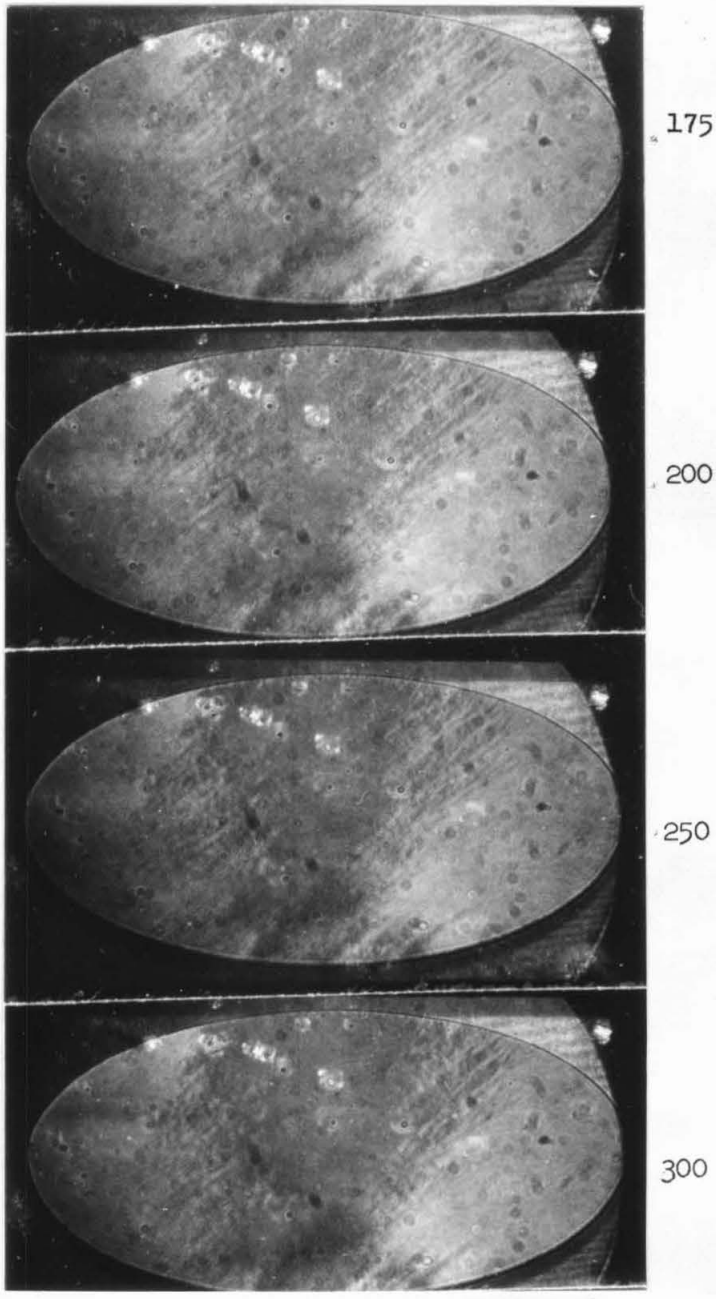

Fig. 3-19. (c) Film 81-4-6 in the process of flux reversal with a 1.0 oe transverse bias field directed to the left and a 1.65 oe longitudinal pulse field directed downward. Time in nanoseconds relative to initial application of pulse field is indicated.

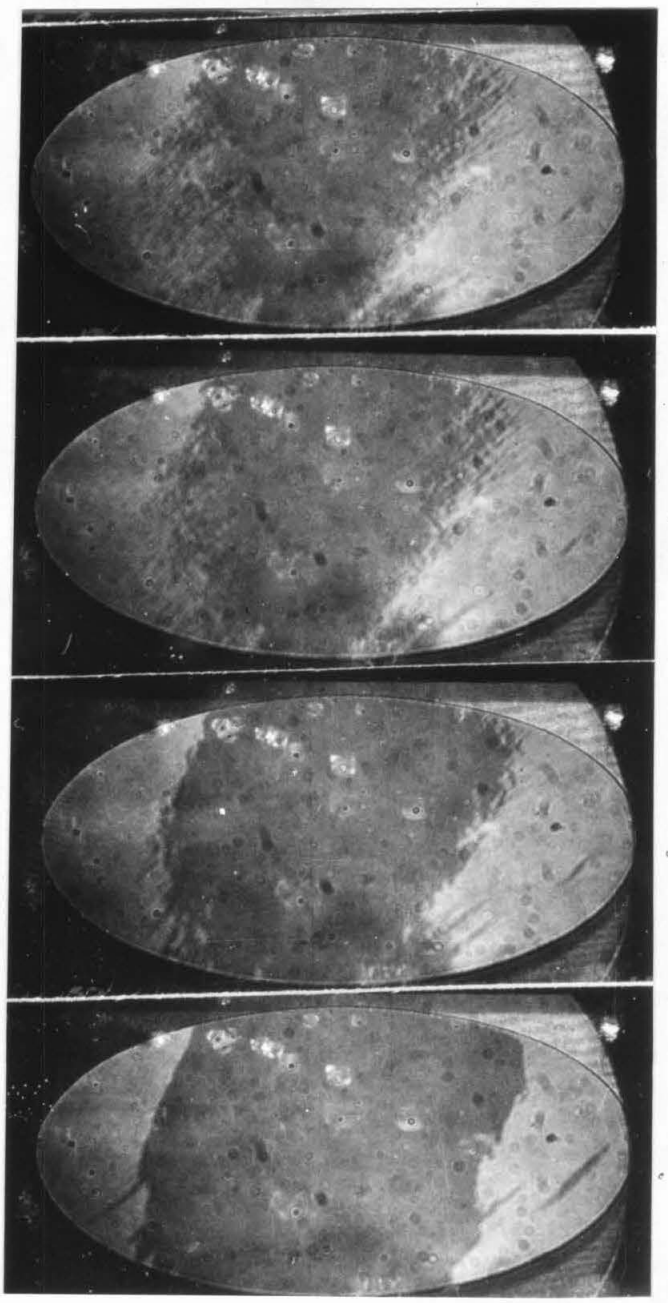

Fig. 3-19. (d) Film 81-4-6 in the process of flux reversal with a 1.0 oe transverse bias field directed to the left and a 1.65 oe longitudinal pulse field directed downward. Time in nanoseconds relative to initial application of pulse field is indicated.

is continuing to rotate. Nucleation like that in Fig. 3-17 does not occur, rather the stripes slowly fade away. By 200 nsec most of the stripes have vanished from the central portion of the film, and thereafter reversal is completed by slower propagational processes.

Qualitatively, it is reasonable that the stripes should decrease in amplitude after $\vec{M}_o$ rotates sufficiently far past φ_ℓ. We know that the transverse magnetostatic fields grow as the stripes become transverse. On the other hand, for sufficiently large φ_o , h_{u2} eventually decreases to zero and changes sign. Hence, as $\vec{M}_o$ rotates past φ_ℓ, the magnetostatic fields grow and the non-linear field which originally caused the instability in the ripple decreases. At some point the net result will be that the total effective field will act to suppress the amplitude of the locked ripple, and, when this occurs, the stripes should fade away. It is clear that the stripes vanish as their amplitude decreases rather than by Stein's (1965) proposed mechanism of wall motion. He proposed that after the stripes formed the reversal was completed by the movement of the "walls" between the light and dark stripes. From Fig. 3-19, it can be seen that many of the light stripes do not become narrow and eventually vanish as the wall motion concept would imply but rather that they slowly become darker and fade away.

To clearly show the effects of increasing the longitudinal pulse field while maintaining constant transverse bias field, four series of photographs were taken of film 81-4-6 reversing by non-coherent rotation with H_y = 0.25 oe and with different values of pulse field. In Fig. 3-20 the film is in the process of flux reversal with a 0.25 oe transverse bias field and a 2.80 oe longitudinal pulse field, which are

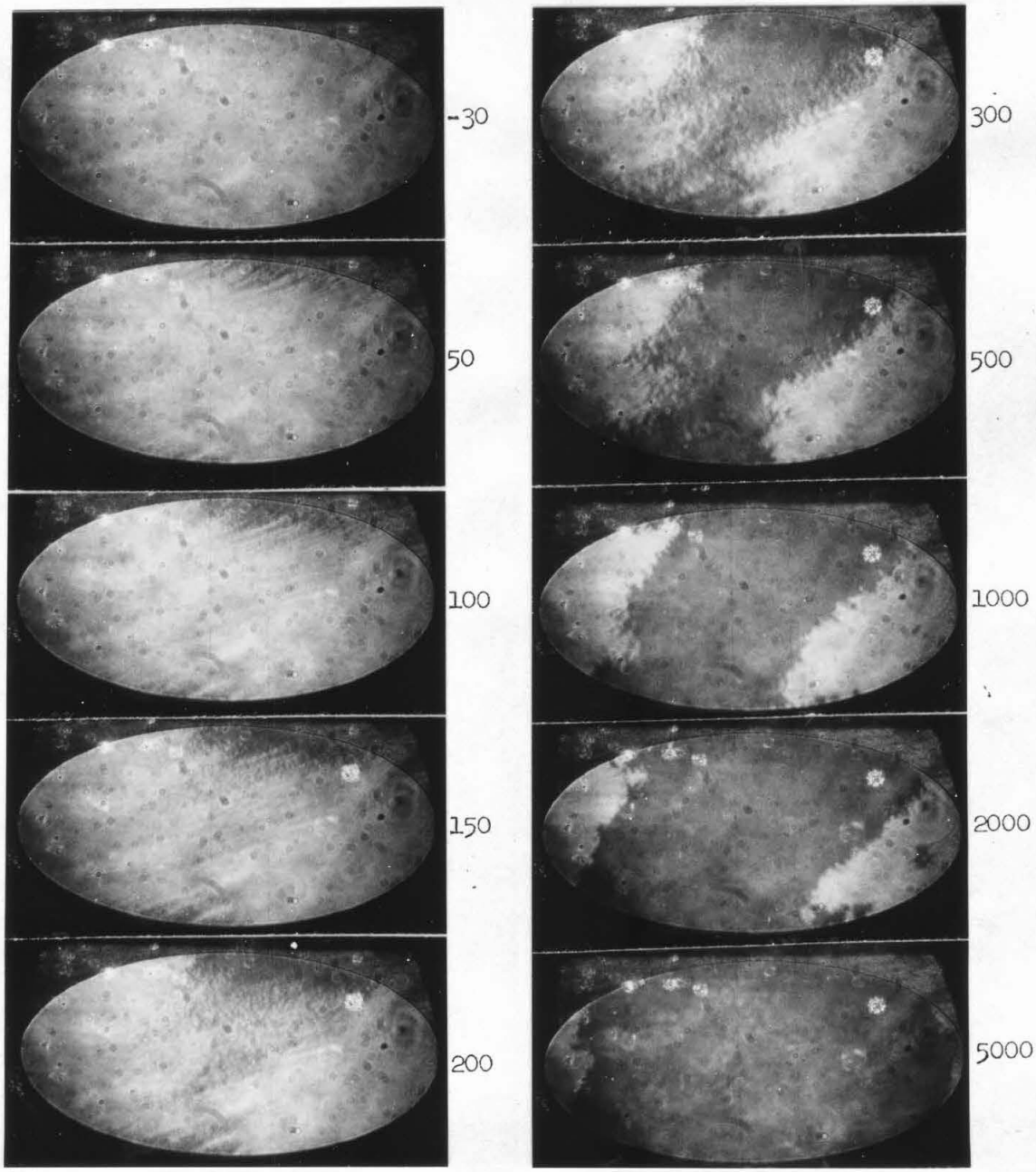

Fig. 3-20. Film 81-4-6 in the process of flux reversal with a 0.25 oe transverse bias field directed to the left and a 2.8 oe longitudinal pulse field directed downward. Time in nanoseconds relative to initial application of pulse field is indicated.

just sufficient to exceed the Stoner-Wohlfarth threshold and cause non-coherent rotation. In the 50 nsec photograph the striped configuration is just beginning to form near the upper edge of the film. Any locked ripple existing in the center of the film has not grown sufficiently in amplitude to be seen. By 100 nsec, the striped region has grown, and stripes are faintly visible in the central region of the film. By 150 nsec the stripes in the center of the film have increased in contrast, and the nucleation of partially reversed regions is occurring in the earlier formed stripes near the upper edge. At 200 nsec, the stripes throughout the film are being obscured by nucleation processes. At 300 nsec, a few stripes are still visible, but most of the magnetization in the central region has now reversed by the nucleation processes. By 500 nsec the reversed region has grown with the nucleation of more reversed areas and the propagation of a jagged and diffuse boundary. By 1000 nsec most of the nucleation processes are complete and the film is switching as a jagged and diffuse boundary propagates toward the extreme right and left-hand edges of the magnetic film. As time proceeds after 1000 nsec, the reversal is completed by the diffuse boundary propagation.

Figure 3-21 shows the same film is the process of flux reversal with the same 0.25 oe transverse bias field but with the longitudinal pulse field increased to 2.90 oe. A very small change in the drive field has produced a significant change in the reversal process. In the 25 nsec photograph $\vec{M}_o$ has already rotated through a large angle and the striped configuration indicative of the locked ripple is evident. Not much change occurs between 25 and 50 nsec, indicative of the effect of the large reaction torque exerted by the locked ripple on $\vec{M}_o$. Even at

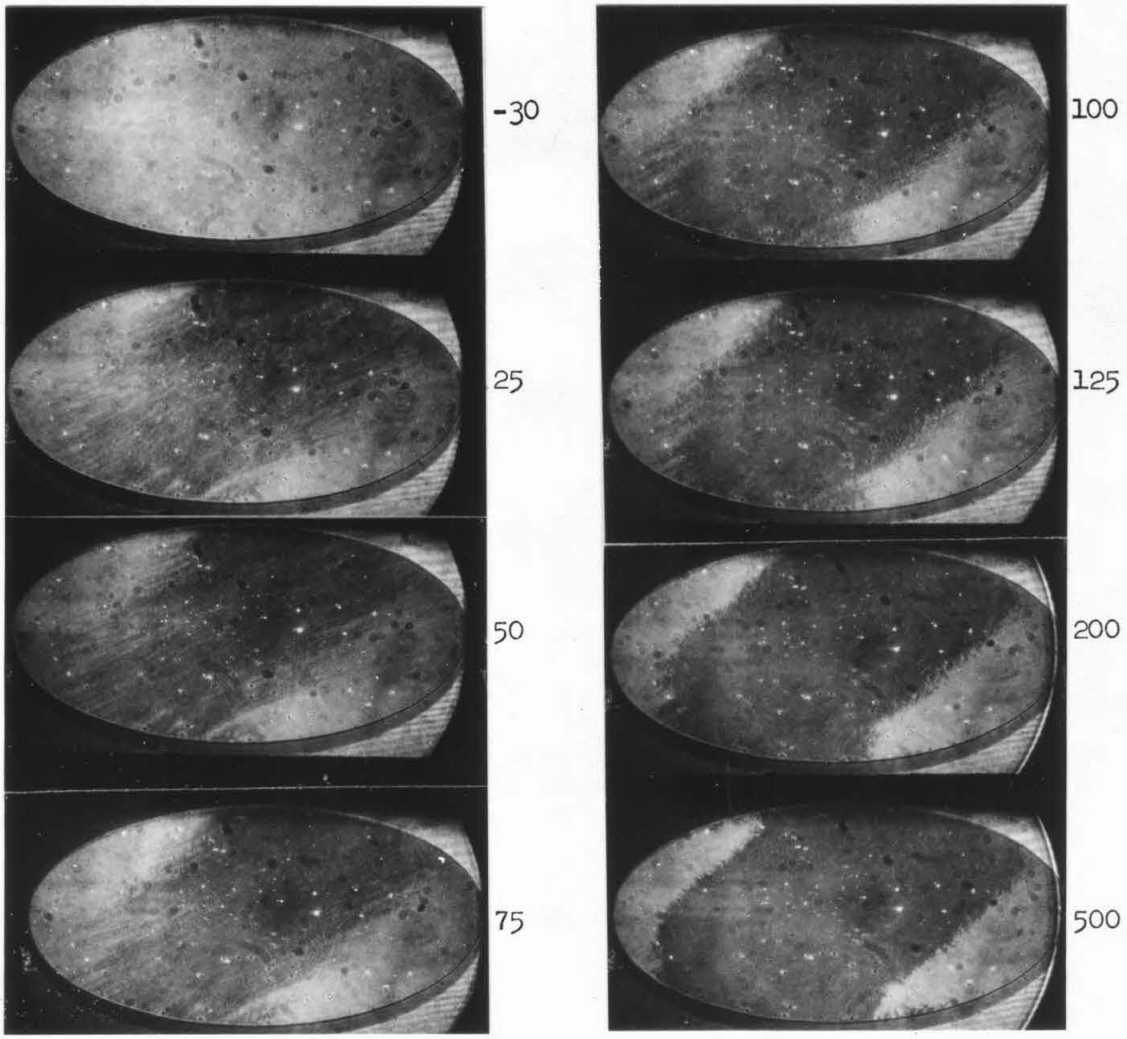

Fig. 3-21. Film 81-4-6 in the process of flux reversal with a 0.25 oe transverse bias field directed to the left and a 2.9 oe longitudinal pulse field directed downward. Time in nanoseconds relative to initial application of pulse field is indicated.

75 nsec large changes do not occur, though the stripes are beginning to fade away in the center of the film. By 100 nsec, most of the stripes disappear allowing $\vec{M}_o$ to rotate still further. By 200 nsec a diffuse boundary has formed, and after 200 nsec, the boundary propagates toward the extreme right and left-hand edges of the film. This propagation is very slow and although it is not shown in the photographs, flux reversal is not actually completed for several microseconds. It should be noted that unlike the reversal shown in Fig. 3-20 there was no significant nucleation in the reversal process shown in Fig. 3-21. In general, when fields are applied that barely exceed the Stoner-Wohlfarth Threshold or when there is zero or very small transverse bias fields, the nucleation of partially reversed regions occurs. However, with transverse fields applied and pulse fields exceeding the Stoner-Wohlfarth Threshold by more than 0.1 oe (in films with $H_k \simeq 3.5$ oe) nucleation is not observed, suggesting that the nucleation occurs only if the reaction torque from the locked ripple overcomes the uniform torque from applied fields and uniaxial anisotropy. In Fig. 3-21 the nucleation did not take place, presumably because the torque from applied fields was able to overcome the locked ripple reaction torque.

In Fig. 3-22 film 81-4-6 is shown reversing with a still larger pulse field of 3.0 oe. The reversal process is similar to that in Fig. 3-21, although it occurs in a somewhat shorter time interval. At 25 nsec the mean magnetization has rotated by a fairly large angle and the stripes, indicative of the locking, are present. By 50 nsec most of the stripes have vanished as $\vec{M}_o$ has rotated still further. By 100 nsec diffuse boundaries have begun to form separating the reversed from the

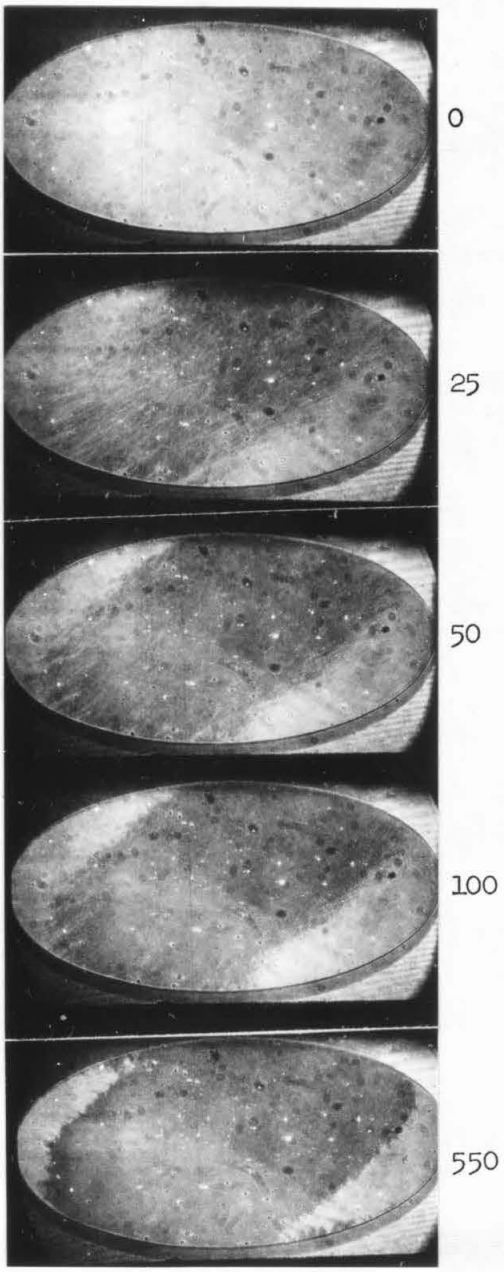

Fig. 3-22. Film 81-4-6 in the process of flux reversal with a 0.25 oe transverse bias field directed to the left and a 3.0 oe longitudinal pulse field directed downward. Time in nanoseconds relative to initial application of pulse field is indicated.

non-reversed regions. After 100 nsec these diffuse boundaries propagate toward the extreme right and left-hand edges of the film. Again, although it is not shown in the figure, the propagation is very slow and is not complete until several microseconds have passed.

In Fig. 3-23 the same film 81-4-6 is seen with a still higher pulse field of 3.15 oe. Unfortunately, the reversal process is now so fast that the time resolution of the camera is a handicap. The contrast in the 5 nsec picture indicates that $\vec{M}_o$ in the center of the film has already rotated by roughly 60^o. In the 25 nsec photographs a few stripes are visible near the edges of the reversed region lying at the same angle as those in Figs. 3-22, indicating that locking must still be occurring at least in a small portion of the film. As usual, a diffuse boundary forms to separate the reversed from non-reversed regions which then propagates to the extreme edge of the film.

The series of photographs in Figs. 3-20 through 3-23, when considered together, exhibit two remarkable characteristics. First, only minor changes occur in the non-coherent rotation process, with locking persisting to the fastest reversal that could be photographed and with no large changes occurring in φ_ℓ. Secondly, a small increase in pulse field produced a large change in reversal time in the center of the film (from about 300 nsec to less than 25 nsec). One fundamental change in the reversal process which did occur was the disappearance of nucleation processes when higher fields were applied.

Inductive sense loops have been used to observe flux reversal for some time, so it is instructive to relate the reversal processes observed here to the reversal curve plotted in Fig. 2-5. The four open

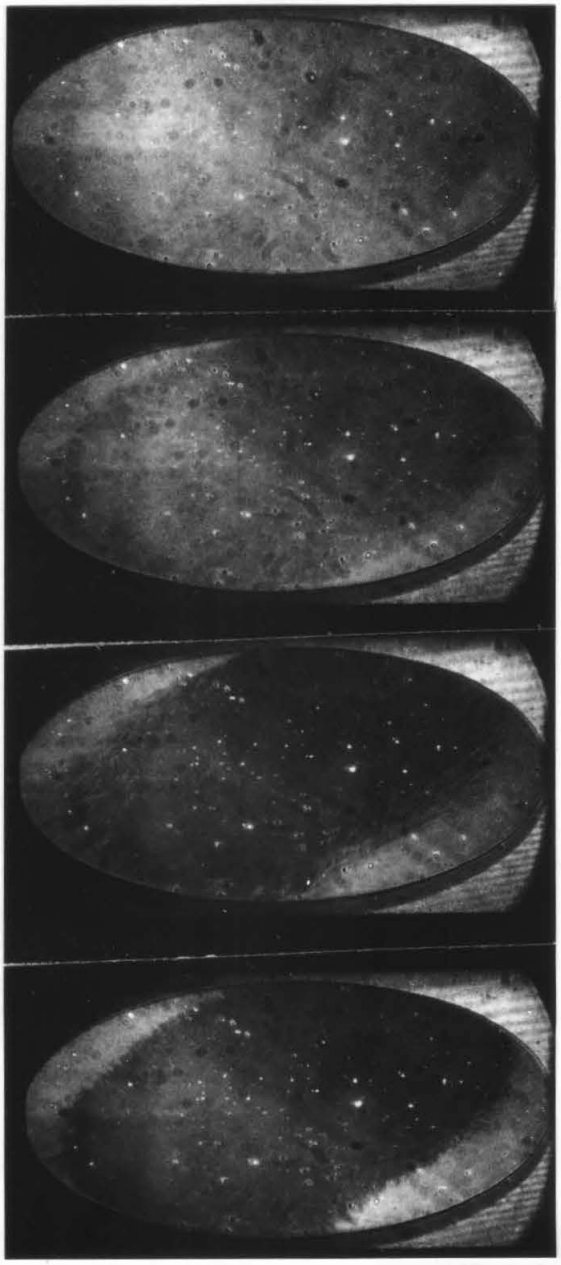

Fig. 3-23. Film 81-4-6 in the process of flux reversal with a 0.25 oe transverse bias field directed to the left and a 3.15 oe longitudinal pulse field directed downward. Time in nanoseconds relative to initial application of pulse field is indicated.

circles on the curve representing the data seen in Figs. 3-20 through 3-23 are indicated. As pointed out in Chapter 2, these circles are not data points but are placed to show where on the reversal curve the photographed process occurs. The photographs show that actually the reversal takes much longer than the data from the inductive sense loop apparatus indicates, which is because the inductive sense loop apparatus does not have a sufficiently broad bandwidth to detect all of the different processes occurring during the reversal. Because of the limited bandwidth the apparatus is not sensitive to both the fast non-coherent rotation occurring in less than 100 nsec and the slow propagation which takes place for several microseconds.

In Fig. 3-24a,b,c are shown the oscilloscope traces which yielded the inductive sense loop data points denoted by a,b,c, respectively, in Fig. 2-5. The 100% point on the vertical scale of the traces was determined by reversing the film with high fields (of the order of 5 to 6 oe) so that the edges of the film would switch completely in a short enough time interval to be measured on the oscilloscope trace. The reversal time, t_s, was defined as the time for the longitudinal flux to change from 10% to 90% its final value on the trace, the same definition used by Humphrey and Gyorgy (1959). The trace in Fig. 3-24a indicates that at 50, 100, and 200 nsec, the film was about 40%, 60%, and 75% switched, respectively. Between 200 and 450 nsec, the trace shows that the reversal is quite slow, and that even at 450 nsec, the film is only 85% reversed. This trace matches reasonably well the reversal process in Fig. 3-21 where, until roughly 100 nsec, the reversal is by non-coherent rotation and thereafter by slower propagation. The trace in

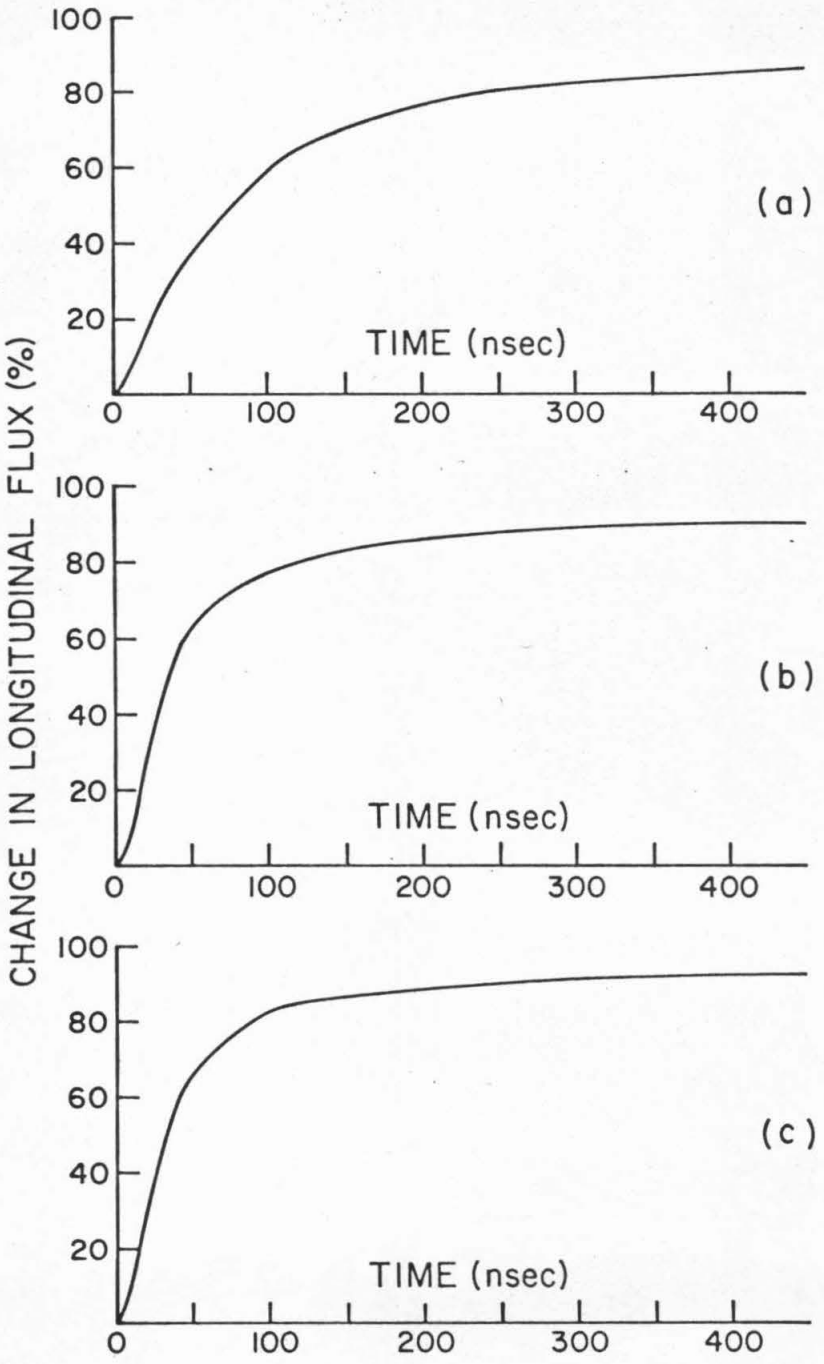

Fig. 3-24. The integrated signal induced in the longitudinal pickup loop around film 81-4-6 with a 0.25 oe transverse bias field and longitudinal pulse fields of (a) 2.86 oe, (b) 2.96 oe, and (c) 3.06 oe.

Fig. 3-24b matches the reversal of Fig. 3-22, indicating that at 25, 50, and 100 nsec the film is roughly 30%, 60%, and 75% reversed, respectively. Thereafter the reversal is quite slow which, as may be seen from Fig. 3-22, is because it is by propagation. The trace in Fig. 3-24c obviously matches a reversal which is somewhat faster than that of Fig. 3-22 and somewhat slower than that of Fig. 3-23 which was expected since the pulse field was 3.06 oe. The trace shows a reversal in which at 25, 50, and 100 nsec the film was 40%, 65%, and 80% reversed, respectively. The traces of Fig. 3-25 match the photographs of Figs. 3-20 through 3-23 quite well, then. Whatever deviations exist can certainly be explained by (1) the approximate 5% accuracy of calibration of the fields used to switch the film, (2) the 0.25^{o} (0.1^{o}) accuracy of alignment of the easy axis of the film in the inductive sense loop apparatus (Kerr apparatus), or (3) the difference in risetimes of the pulse fields (2 nsec in the inductive sense loop apparatus - 10 nsec in the Kerr apparatus).

The photographs of Figs. 3-20 through 3-23 provide an insight into the meaning of data obtained with inductive sense loops. In none of the traces does the longitudinal flux actually reach 100%, which is expected since the photographs show that by 450 nsec none of the reversals are complete. Since the reversal is not complete at the end of the trace, t_s must not be interpreted as a measure of the total reversal time, but rather as a measure of the reversal time by only the higher speed processes. Previously, t_s, as determined by inductive techniques, has not been interpreted in this manner.

The concept that a different mechanism is responsible for the

flux reversal in the intermediate linear region than in the lower speed non-linear region is clearly substantiated by the camera. Non-coherent rotation is first observed with the Kerr magneto-optic camera in film 81-4-6 with H_y = 0.25 oe at H_x = 2.8 oe (longitudinal pulse field). Similarly it is observed to first occur with H_y = 0.1 oe at H_x = 3.8 oe, and with H_y = 0.5 oe at H_x = 2.3 oe. All of these field values correspond to the start of the linear region of flux reversal curves of film 81-4-6. Similar agreement between the start of non-coherent rotation and the start of the intermediate linear region is obtained for film 81-4-12, also. Hence, it can be concluded that non-coherent rotation as it has been described in this chapter does first begin at the start of the intermediate linear region of the reversal curves.

As pointed out in Section 2.3.1, Humphrey and Gyorgy (1959) and Olson and Pohm (1958) suggested that in the high speed region of the reversal curve the reversal process was coherent rotation. Since that time, the third region of the reversal curves has often been referred to as the coherent rotation region. However, Stein (1965) reported that yet another break, this time to a region of smaller slope, occurred in the reversal curves in the vicinity of t_s = 2 nsec. He reported that the region prior to this final break was actually a transition region and was not coherent rotation.

In order to investigate the so-called coherent rotation region of Fig. 2-5 , photographs were taken of film 81-41-6 during flux reversal in the presence of a 0.25 oe transverse bias field and a 3.8 oe longitudinal pulse field. These photographs are shown in Fig. 3-25. The -30 nsec photograph shows the magnetic film in the reset condition. In the

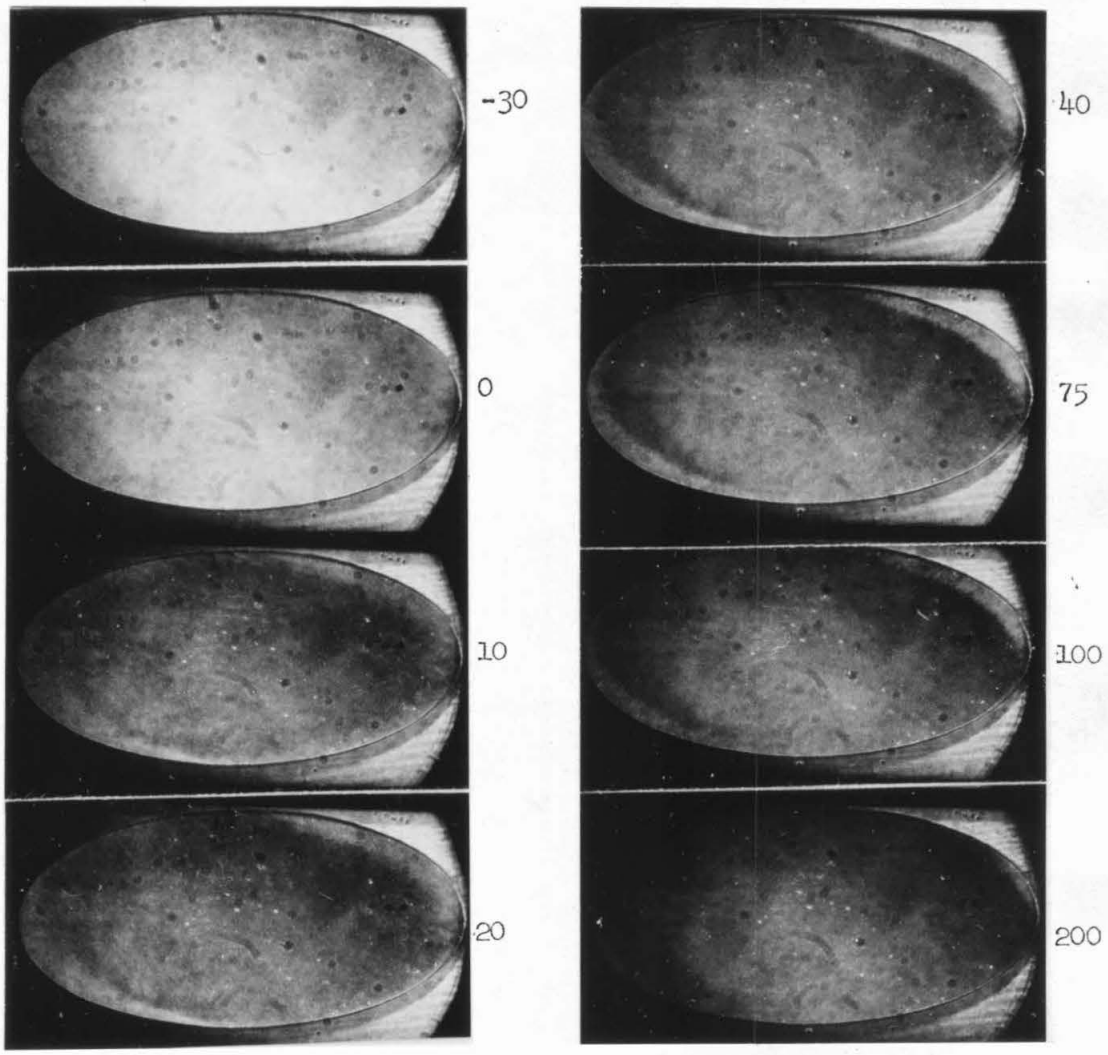

Fig. 3-25. Film 81-4-6 in the process of flux reversal with 0.25 oe transverse bias field directed to the right and a 3.8 oe longitudinal pulse field directed downward. Time in nanoseconds relative to initial application of pulse field is indicated.

0 nsec photograph which depicts the film during the risetime of the pulse field, there has been a slight darkening of the magnetic film indicating some rotation has taken place. By 10 nsec considerable rotation has occurred. The temporal resolution of the camera is not adequate for the photograph to depict any structure in the central portion of the film, and it is therefore unknown whether any exists. Clearly, however, at the edges of the film, there are non-reversed regions. These regions at the edges become more sharply defined in later photographs. It is seen that as time proceeds, the boundary defining the non-reversed regions propagates to the edges, thereby completing the reversal of the magnetic film. Whereas the propagation in Fig. 3-20 took several microseconds, in this series of photographs, it takes about 250 nsec.

The inductive sense loop apparatus is capable of detecting some of the faster propagation and in Fig. 3-26 the oscilloscope traces showing the integrated longitudinal flux change as a function of time are shown for points a', b', c', and d' of Fig. 2-5 . It is seen that in all cases there is a fast initial change in the longitudinal flux, followed by a long tail. A comparison of the traces taken for pulse fields of 3.76 oe and 3.85 oe with photographs of Fig. 3-25 shows that the long tail is caused by the propagation taking place at the edges of the film. The points at which the trace had reached 10% and 90% its final value are also shown. The time between these points was used as the reversal time, t_s, plotted in Fig. 2-5. The position of the 90% points illustrate how the steep slope in the reversal curve is created. As the field is increased, the 90% point moves rapidly down the tail of the

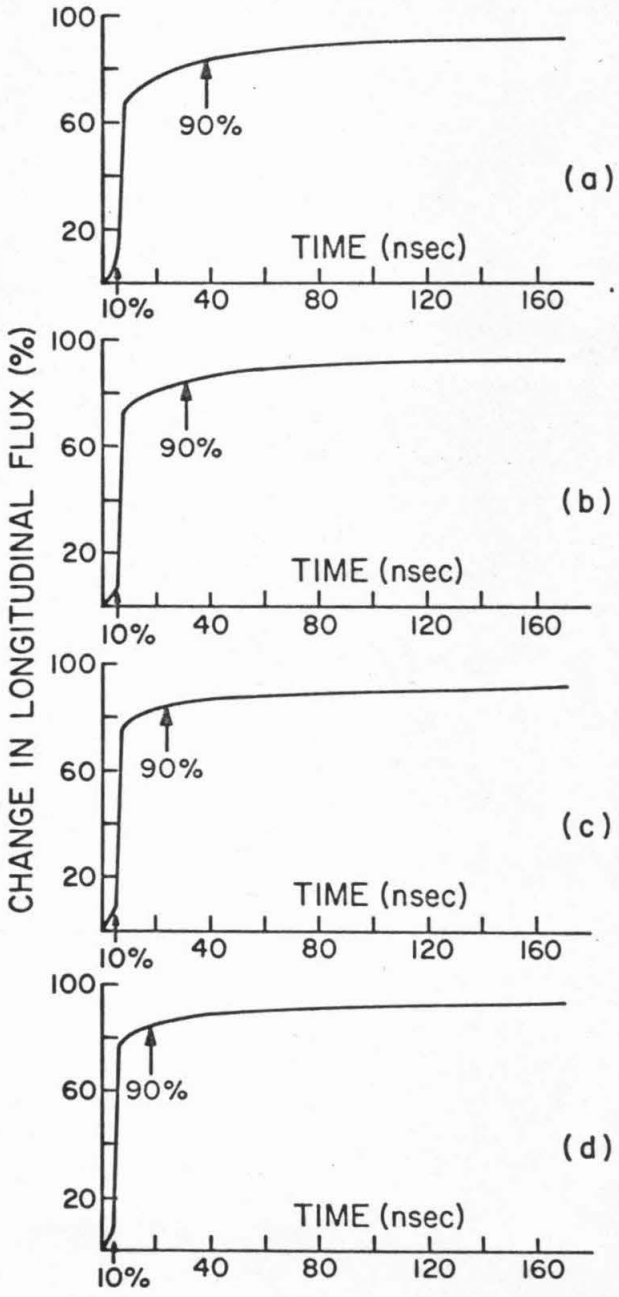

Fig. 3-26. Integrated signals induced in a longitudinal pickup loop around film 81-4-6 with a 0.25 oe transverse bias field and longitudinal pulse fields of (a) 3.76 oe, (b) 3.85 oe, (c) 3.95 oe, and (d) 4.05 oe. Points at which signal is 10% and 90% its final value are also indicated.

trace producing large changes in the measured reversal time. Clearly, however, the photographs in Fig. 3-25 show that coherent rotation of the whole film does not occur in the high speed region. Instead the high speed region of the reversal curve in Fig. 2-5 is actually a transition region which is caused by the disappearance of the slow propagational process occurring at the extreme edges of a film. Furthermore, using an inductive sense loop apparatus with a pulse field rise-time of 0.4 nsec and a response time of 0.25 nsec, it has been verified that another break in the reversal curves does occur as Stein suggested. In Fig. 3-27 data obtained from this high speed apparatus are plotted. Clearly a break does occur in the curves in the vicinity of $t_s \approx 3$ nsec. This break occurs when the 90% point seen in Fig. 3-26 reaches the leading edge of the signal. It is considered likely that coherent rotation is the reversal process in the region above the break at $t_s \approx 3$ nsec.

3.3 Diffuse Boundary Propagation with a Transverse Field.

Diffuse boundary propagation is the flux reversal mechanism which takes place with transverse bias fields and longitudinal pulse fields larger than required for domain wall motion, but smaller than required for non-coherent rotation. As the name suggests the mechanism involves a poorly defined, jagged and diffuse boundary which propagates through a film. The propagation occurs in a number of directions, but the velocity in one direction is much greater than in any other. This preferred direction of propagation corresponds to the direction of the stripes which form in the non-coherent rotation process.

Figure 3-28 shows film 81-4-12 in the process of flux reversal by diffuse boundary propagation. The transverse bias field is 0.25 oe and

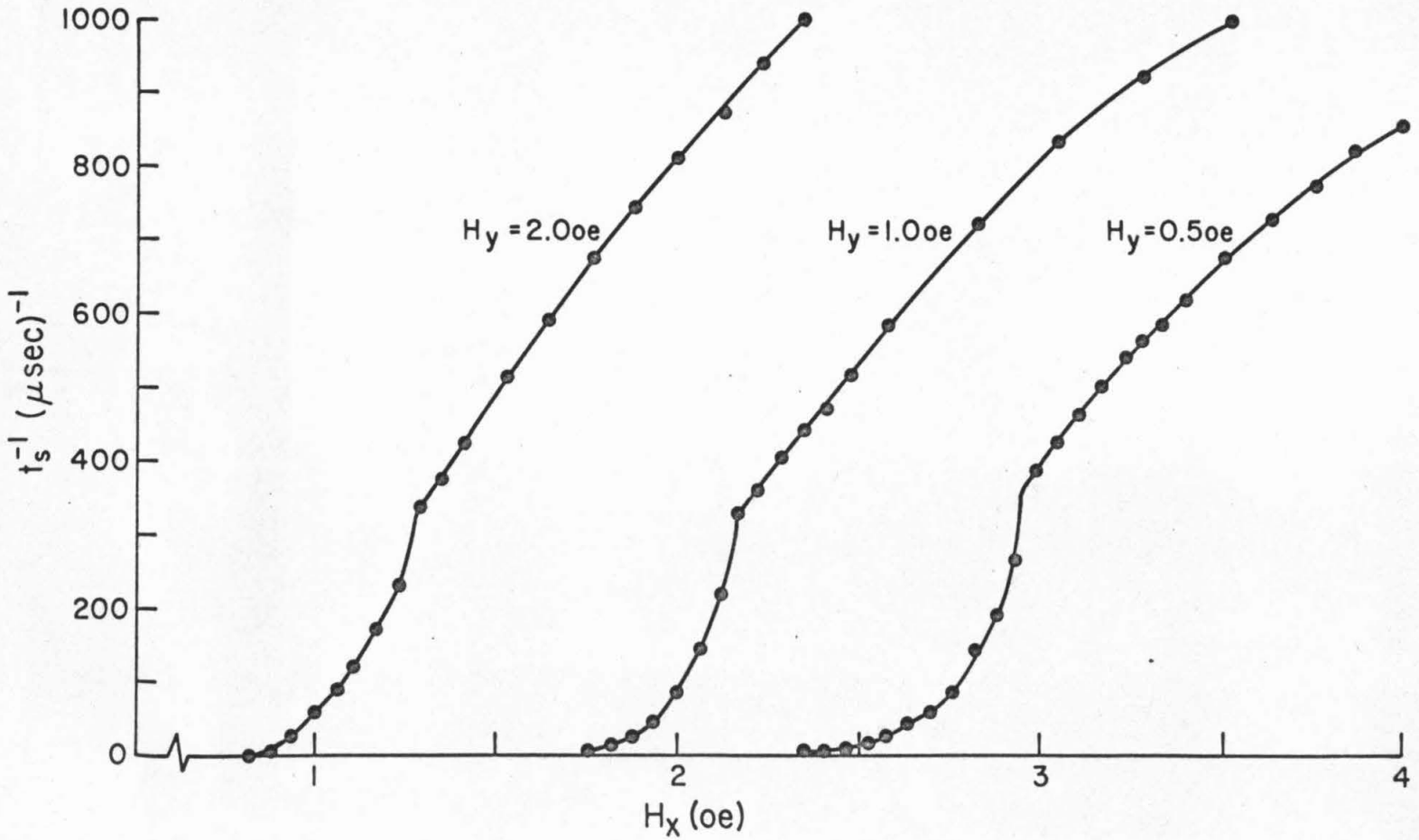

Fig. 3-27. High-speed reversal curves for film 81-4-6.

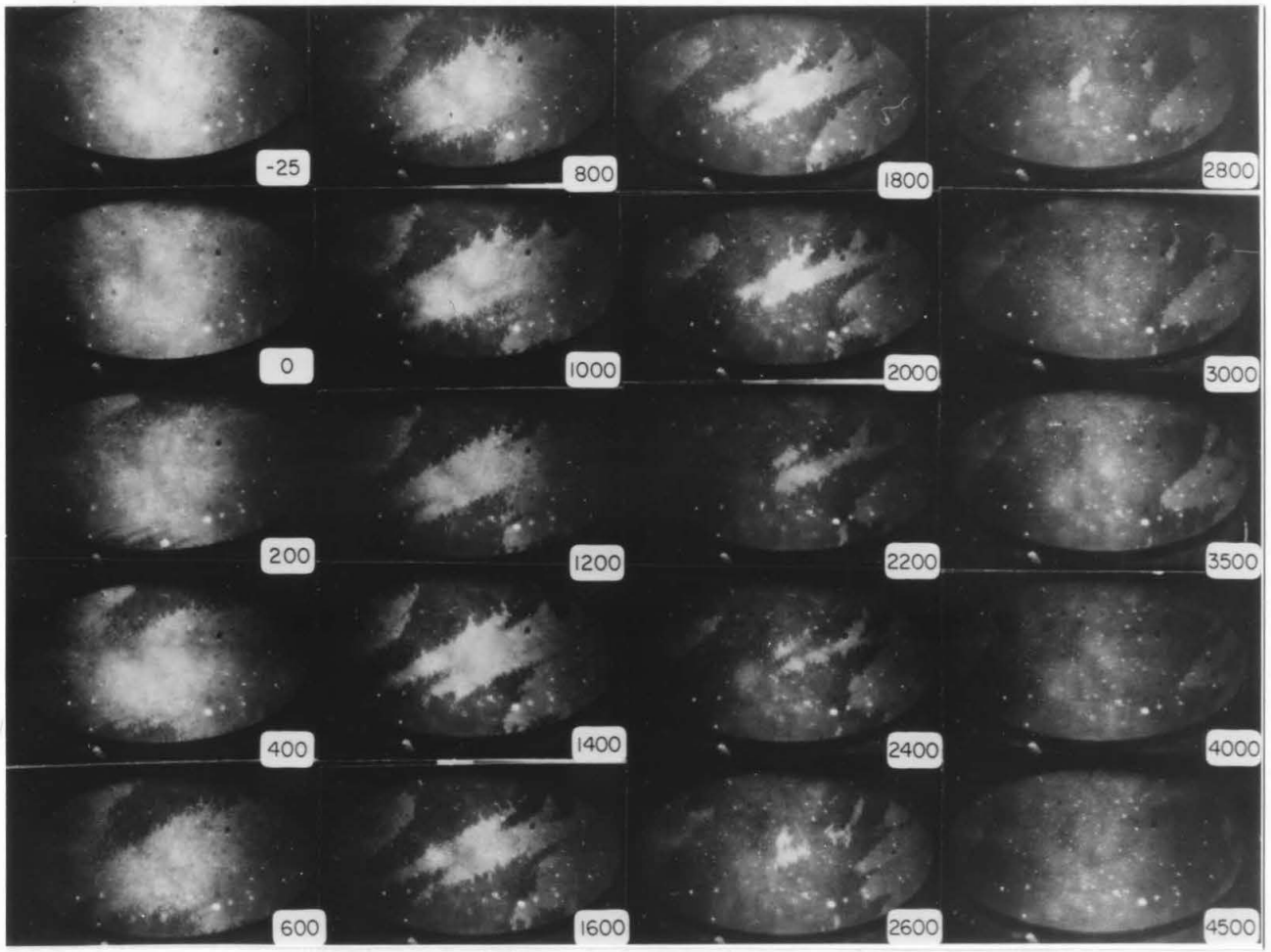

Fig. 3-28. Film 81-4-12 in the process of flux reversal with 0.25 oe transverse bias field directed to the left and a 2.76 oe longitudinal pulse field directed downward. Time in nanoseconds relative to initial application of pulse field is indicated.

the longitudinal pulse field is 2.76 oe, corresponding approximately to the Stoner-Wohlfarth threshold which is the upper limit for diffuse boundary propagation. At 200 and 400 nsec the striped pattern characteristic of the non-coherent rotation process is seen in the partially reversed regions at the upper and lower edges of the film. There has been considerable nucleation in the region near the upper edge. The reason these regions are able to reverse by non-coherent rotation is that the demagnetizing fields in these regions lower the rotational threshold as was discussed earlier in Section 3.2.1. After 400 nsec the propagation takes place. Note how jagged and diffuse the boundary separating the reversed and non-reversed regions is in contrast to the sharply defined domain walls observed in Fig. 2-7. It can be seen that the direction of fastest propagation is 35^{o} to 40^{o} to the hard axis, roughly the same angle at which the stripes formed in the same film with the same transverse bias field in Fig. 3-1. At roughly 1.8 μsec the boundaries that are propagating from the upper right and lower left-hand regions join, and by 3.0 μsec reversal is complete except for the extreme right and left-hand edges of the film. The reversal of the right-hand edge clearly illustrates the difference between diffuse boundary propagation and domain wall motion. The upper left-hand edge of the right-hand non-reversed region in the 3000 nsec photograph is a domain wall lying parallel to the easy axis. A diffuse boundary lies at the lower edge of the film and the non-reversed domain is seen reversing in the 3000 to 4500 nsec photographs as this diffuse boundary moves upward, while the domain wall remains approximately fixed in position. Clearly the diffuse boundary propagation has a much larger velocity than domain

wall motion.

A good example of the details of diffuse boundary propagation can be seen in Fig. 3-29 which shows the 1000, 1200, and 1400 nsec photographs from Fig. 3-28 at higher magnification. Remember that these photographs were taken on successive reversals and that, although each reversal is similar to the preceding one, they are not identical especially during lower speed propagational processes where the reproducibility becomes much worse than during the higher speed processes such as non-coherent rotation. Figure 3-29 shows how propagation occurs by the nucleation of long slender regions ahead of the tip. This is easily seen from the narrow regions of low contrast which extend ahead of the tips of the reversed regions and which are indicated by arrows in the photographs. These regions are roughly 1 mm in length (dimension on the magnetic film - about 1 cm on the photograph) indicating that the magnetization is partially rotated for relatively large distances in the tip. It can be seen that small regions ahead of the propagating tip lock into striped configurations much as the majority of the film does during the non-coherent rotation process discussed earlier. The angle of the stripes at the tip, in fact, matches that of the stripes observed during non-coherent rotation in the same film with the same transverse field (see Fig. 3-1).

To understand how the locking phenomenon occurs in the tip, consider Fig. 3-30 which shows a rough diagram of the magnetization configuration believed to be responsible for the observed patterns near the tip in the rectangle of the 1400 nsec photograph. In Fig. 3-30 the magnetization outside the tip is shown rotated away from the easy axis by the applied

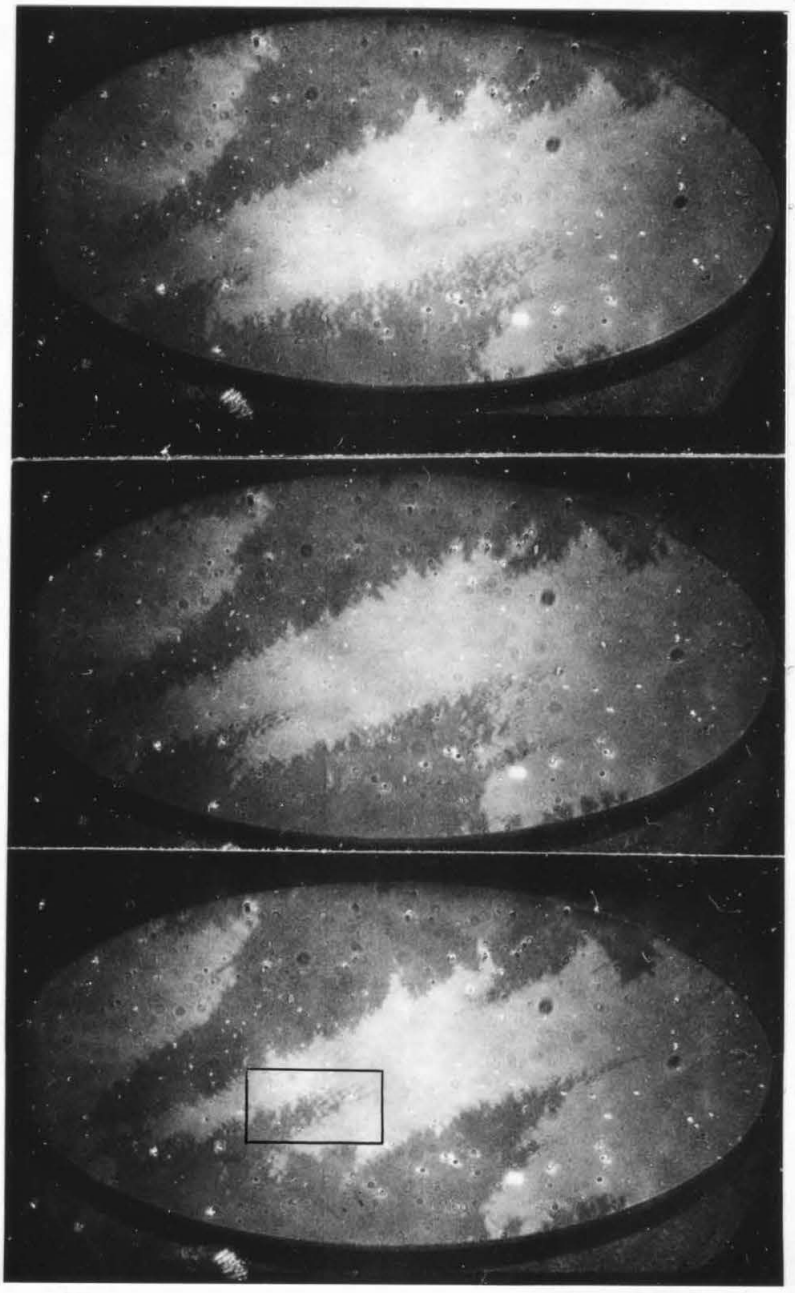

Fig. 3-29. Film 81-4-12 in the process of flux reversal with 0.25 oe transverse bias field directed to the left and a 2.76 oe longitudinal pulse field directed downward. Time in nanoseconds relative to initial application of pulse field is indicated.

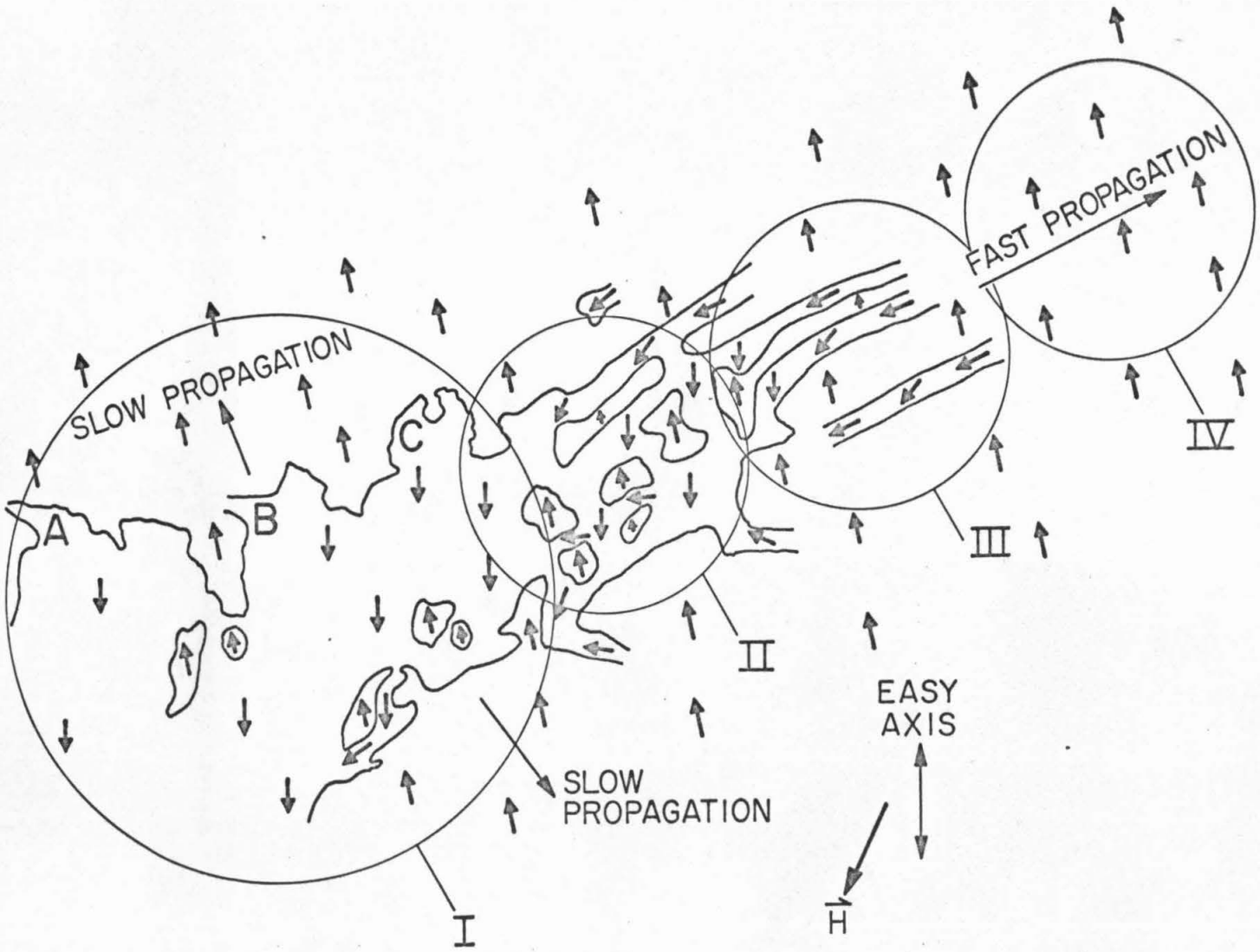

Fig. 3-30. A simplified diagram of the flux pattern near a diffuse tip.

fields, but not yet reversed, while the magnetization within the tip and in region I has reversed and therefore appears dark in the photograph. In region II of both the photograph and diagram there is a striped pattern which is broken up by nucleated regions connecting the stripes. The contrast in the photograph indicates that some of the stripes and nucleated regions are only partially reversed. In region III there are partially reversed stripes, but no nucleated regions have yet appeared, and in region IV reversal has not yet begun. The propagation from the tip is believed to take place as magnetostatic stray fields from the reversed or partially reversed magnetization in one region cause the magnetization within the next region to reverse. For example, the magnetostatic stray fields from the partially reversed magnetization of region II couple to the magnetization in region III causing it to rotate sufficiently for locking to occur. After locking in a small region, nucleation like that in region II occurs to complete the reversal. Since region III is now partially reversed, it can be expected to produce magnetostatic fields ahead in region IV. Thus, the propagation will continue. The poorly defined boundaries in region I propagate away from each other when the magnetization rotates in small areas extending from the reversed region, which has presumably just occurred in areas A,B,C.

The propagation from the tip is similar to the labyrinth propagation observed, during quasi-static reversals, by Smith and Harte (1962). They reported that films reverse when "long slender domains develop by extension from the tip, leaving behind regions of unswitched material and resulting in a labyrinth-like flux pattern." The directions of propagation which they observed showed dependence on applied fields like

the data in Fig. 3-9. It is therefore tempting to also apply the explanation of locking to labyrinth propagation, but the thickness dependence of h_ℓ does not indicate that the thickness dependence which Smith and Harte (1962) found should occur unless S depends implicitly on thickness in a manner which causes S to increase with decreasing thickness. At this time there are no grounds to warrant such an assumption.

The diffuse tip propagation becomes less pronounced than in Fig. 3-28 with lower pulse fields. For example, Fig. 3-31 shows film 81-4-12 with the same 0.25 oe transverse bias field as in Fig. 3-28, but with the pulse field decreased to 2.3 oe. Initially regions of reversed magnetization appear near the upper and lower edges of the film. At 500 nsec, for example, a small number of stripes is visible near the lower edge of the film. As time proceeds, these reversed regions grow, however, not so very rapidly from the tips. For example, at 5000 nsec, although tips pointing 35° to 40° to the hard axis are present, the propagation has not been limited to this direction. In fact, there has been considerable propagation in the easy axis direction by the diffuse boundaries which formed. At 7000 nsec, the diffuse boundaries join and thereafter the extreme right and left-hand edges of the magnetic film reverse by domain wall motion and diffuse boundary propagation.

At still lower fields the reversal process becomes even less like that in Fig. 3-28, but more like that in Fig. 2-7. Figure 3-32 shows film 81-4-12, again with the same 0.25 oe transverse bias field, but with a still lower pulse field of 2.1 oe. As usual regions of reversed magnetization first appear at the upper and lower edges of the film. In this case they grow predominantly in the easy axis direction and lean

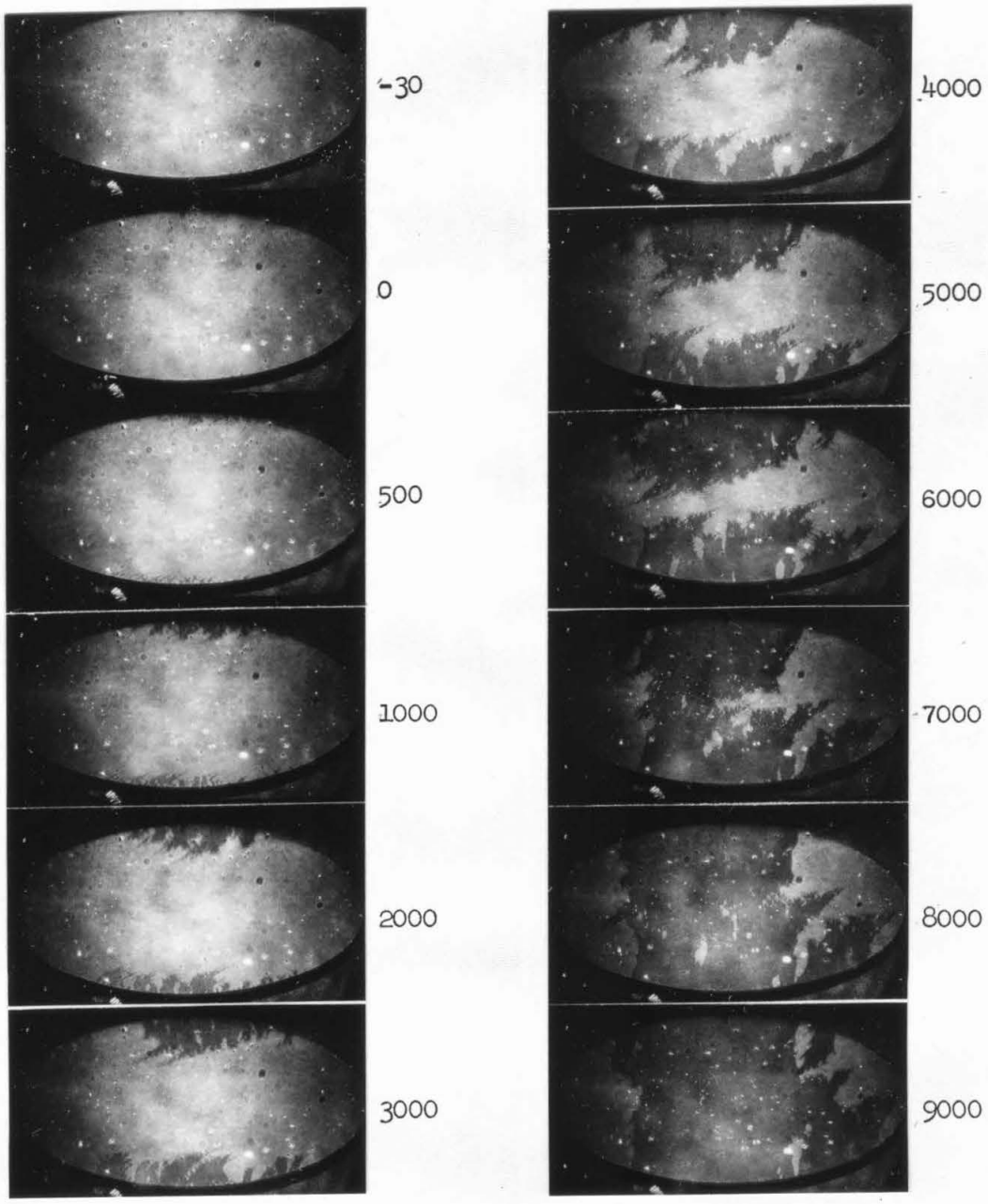

Fig. 3-31. Film 81-4-12 in the process of flux reversal with 0.25 oe transverse bias field directed to the left and a 2.3 oe longitudinal pulse field directed downward. Time in nanoseconds relative to initial application of pulse field is indicated.

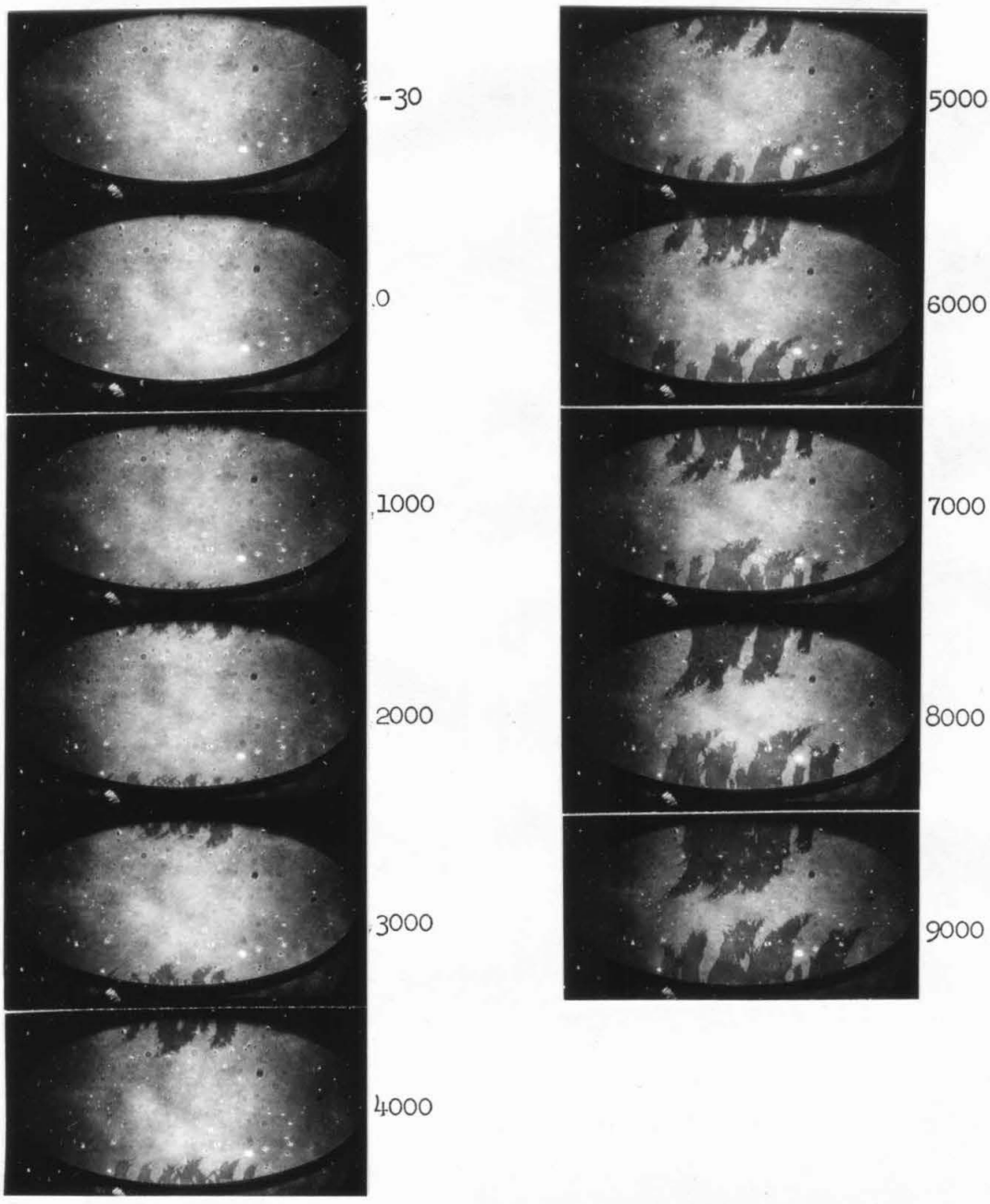

Fig. 3-32. Film 81-4-12 in the process of flux reversal with 0.25 oe transverse bias field directed to the left and a 2.1 oe longitudinal pulse field directed downward. Time in nanoseconds relative to initial application of pulse field is indicated.

only slightly in the direction of the diffuse tip propagation. With decreasing pulse fields, this growth in the longitudinal direction is becoming similar to that observed in Fig. 2-7 prior to the domain wall motion. Although field pulses longer than 10 μsec duration were not available, it is reasonable to expect that after the central band of the film in Fig. 3-32 is switched by the longitudinal growth of the domains that domain wall motion in the transverse direction occurs to reverse the edges of the film. In Chapter 4 when the zero transverse field diffuse boundary propagation is considered, the structure and propagation of the longitudinally propagating diffuse boundaries will be discussed in more detail.

To relate the diffuse boundary propagation process to the flux reversal curves note where the data points from the series of photographs seen in this section fall in Fig. 2-6 which shows the reversal curve for film 81-4-12. The large circles for H_y = 0.25 oe and H_x = 2.76, 2.3, and 2.1 oe were taken from the respective photographs of Figs. 3-28, 3-31, and 3-32. It can be seen that the diffuse boundary propagation is the dominant reversal process occurring when fields slightly below the intermediate linear portion of the reversal curve are applied. This diffuse boundary propagation occurs to a lesser extent, being replaced by normal domain wall motion, as the pulse field is decreased to below H_c. As in the case of non-coherent rotation discussed earlier, the reversal times determined from the inductive sense loop apparatus are much shorter than is observed in the photographs. This is because the low frequency limitations of the apparatus made it impossible to detect much of the diffuse boundary propagation, while the faster non-coherent

rotation observed, for example, for 400 nsec in Fig. 3-28 was detected. As a result the reversal times shown in Fig. 2-6 are representative of only the higher speed reversal processes occurring at the edges of the film.

3.4 Summary.

Non-coherent rotation and diffuse boundary propagation with a transverse field were shown in this chapter to involve a striped magnetization configuration. In the non-coherent rotation process, the striped pattern occurred after the magnetization uniformly rotated in a few nanoseconds through some angle. When the stripes appeared, the reversal process was completed either by the nucleation of partially reversed regions (when the applied field torque was very small) or by a rotational process taking on the order of 100 nsec. In diffuse boundary propagation, the stripes appeared in poorly defined tips of reversed magnetization which propagated across the film. The jagged and diffuse boundaries left behind these tips propagated to sweep out any remaining non-reversed regions in several microseconds.

Neither the slow nor fast relaxation models of Harte (1964,1967) nor the fast relaxation model of Stein (1965a,b,1966) could be used to explain the fact that the stripes appeared only after the mean magnetization rotated beyond the critical angle for reversal. A new model was proposed and shown to accurately predict the angular dependence of the stripes on applied field except in the high transverse field region. This model predicted that when the single domain field, $h(\alpha)$, reached a specific negative value an instability would occur in the ripple and lock the magnetization into a striped configuration.

Finally, the photographed reversal processes were related to the reversal curves taken with inductive sense loops. Comparison of the photographed reversal process with the oscilloscope traces depicting the change in longitudinal flux as a function of time showed that typically the inductive sense loop apparatus detected only the higher speed rotational processes but neglected low speed propagational processes. It was shown that the non-coherent rotation process, as described above, first occurs at the beginning of the intermediate linear portion of the reversal curve, and that diffuse boundary propagation occurs below this linear portion with domain wall motion becoming increasingly important at fields near H_c. Furthermore, it was shown that within the so-called "coherent rotation region" of the reversal curve, some slower speed propagational processes still occur.

Chapter 4

Flux Reversal with Zero Transverse Field

4.1 Introduction.

In an ideal single domain film in which the magnetization lies uniformly in the same direction, the Stoner-Wohlfarth model outlined in Chapter 2 predicts that if a field is applied approximately antiparallel to the magnetization, the magnetization direction will remain unchanged until the field becomes equal to H_k at which time a discontinuous reversal will occur. Of course, such a condition is not obtainable in practice because edge effects and anisotropy dispersion, microscopic and macroscopic, cause the magnetization direction to be a function of position in the film. With zero transverse field, not only the torque magnitude, but also the torque direction depends on how exactly antiparallel the field is applied to $\vec{M}$, and therefore the magnetization not only rotates at different speeds in different regions of the film, but in different directions. While blocking of the ripple was of minor significance when a transverse field was applied, here blocked ripple will be important in preventing films from reversing even though easy axis fields exceeding H_k are applied. Locking, on the other hand, does not occur without a transverse field.

Flux reversal processes with zero transverse field ($< \pm 0.002\ H_k$) in permalloy thin films have been investigated with the Kerr magneto-optic camera described in Chapter 6. Since typical low dispersion films have dispersion (α_{90}) of the order of 1^o, a maximum transverse field of $0.002\ H_k$ rotating the mean magnetization by 0.1^o was accepted as experimentally reasonable.

From Kerr magneto-optic photographs three distinct mechanisms of flux reversal have been identified. These three mechanisms are referred to as (1) domain wall motion, (2) longitudinal propagation of diffuse transverse boundaries, and (3) the nucleation and subsequent reversal of partially reversed regions. Domain wall motion was briefly discussed in Chapter 2 and shown to involve a well-defined domain wall lying parallel to the easy axis and propagating in the hard axis direction. On the other hand, diffuse boundary propagation with zero transverse field involves a poorly defined jagged and diffuse domain boundary lying parallel to the hard axis and propagating in the easy axis direction. The nucleation and subsequent reversal of partially reversed regions is a reversal process wherein the magnetization in small ($\sim$.01 mm^2) regions of the film reverses by rotation.

4.2 Diffuse Boundary Propagation

4.2.1 Introduction

The longitudinal propagation of diffuse transverse domain boundaries is a major mechanism involved in flux reversal with zero transverse field at least for times longer than about 500 nsec. In many respects the process is the direct opposite to domain wall motion. The diffuse boundary, although separating regions of opposite magnetization, is typically transverse to the easy axis and propagates in the longitudinal direction, whereas the normal domain wall lies parallel to the easy axis and propagates in the transverse direction. While the domain wall is typically a few thousand angstroms wide, the diffuse boundary ranges in width from a few hundred microns to several millimeters. Furthermore, the diffuse boundary propagates at velocities two

to three orders of magnitude greater than domain walls.

A series of photographs depicting film 81-4-12 in the process of flux reversal by diffuse boundary propagation is shown in Fig. 4-1. It can be seen that 1000 nsec after the application of the 2.1 oe longitudinal pulse field, reverse domains are visible as small dark spots at the upper and lower edges of the film. These domains grow in the longitudinal and transverse directions as time goes on, forming transverse diffuse boundaries. The transverse boundaries propagate in the longitudinal direction. After 10,000 nsec the unswitched portion of the film reverses by normal domain wall motion in the transverse directions.

Figure 4-2 shows the diffuse boundary during a higher pulse field (H = 4.1 oe). The boundary forms again near the upper and lower edges of the film. Note that in this case, however, the boundaries do not form from individual reverse domains at the edges, but instead form along the entire edge. Once formed, the boundaries propagate in the longitudinal direction. At 800 nsec there is a connection made between the upper left and lower right hand boundaries. This slight deviation from the perfect quadrantal symmetry is due to a $< 0.1^{o}$ misalignment of the easy axis with respect to the field. By 1.6 μsec the film is totally reversed.

In both Figs. 4-1 and 4-2 the diffuse boundaries formed at the upper and lower edges of the film and propagated in the easy axis direction. The observed boundaries are diffuse, jagged, and wide (on the order of 0.5 mm), in comparison to the domain walls seen in Fig. 2-7. Furthermore, the boundary velocity in either Fig. 4-1 or 4-2 is much greater than the velocity of the domain wall of Fig. 2-7.

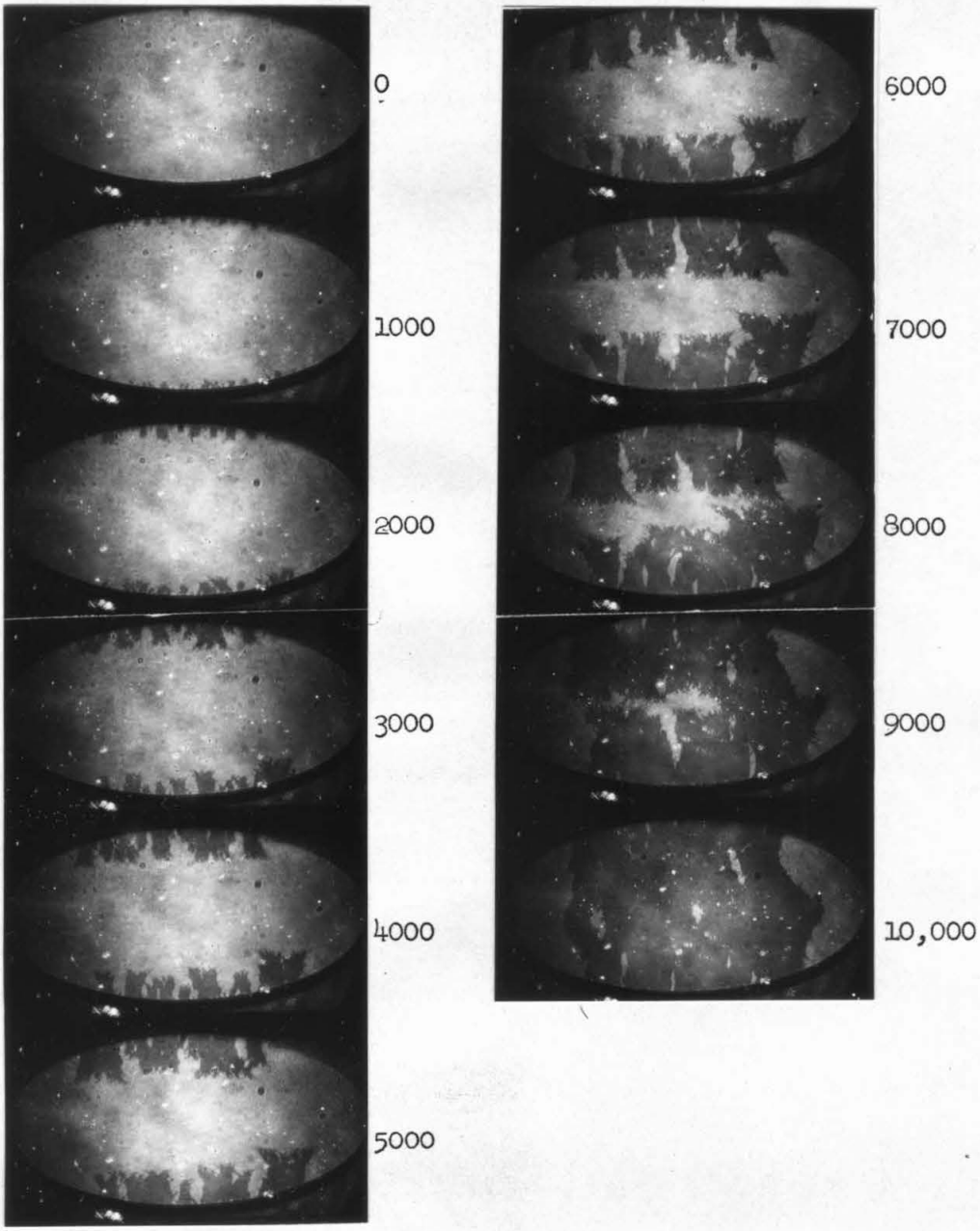

Fig. 4-1. Film 81-4-12 in the process of flux reversal with a 2.1 oe longitudinal pulse field. Time in nanoseconds relative to initial application of pulse field is indicated.

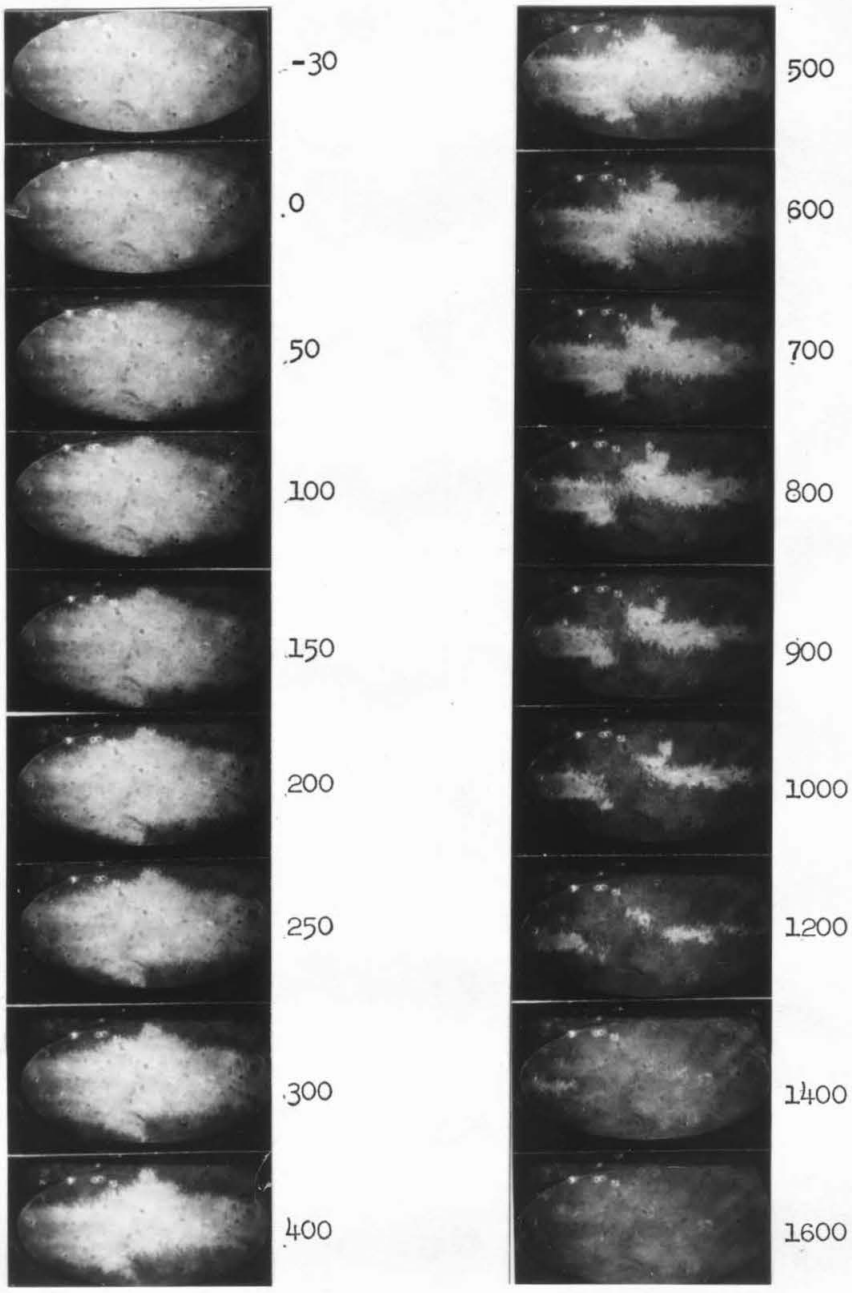

Fig. 4-2. Film 81-4-6 in the process of flux reversal with a 4.1 oe longitudinal pulse field. Time in nanoseconds relative to initial application of pulse field is indicated.

4.2.2 Blocking of the Coherent Rotation Process.

One question which must be answered in a discussion on the diffuse boundary propagation is why, when a field greater than H_k is applied to the film as it is in Fig. 4-2, does the magnetization not reverse by rotation. In an ideal single domain film the magnetization should reverse by rotation if the applied field exceeds the Stoner-Wohlfarth threshold, which for fields along the easy axis, corresponds to H_k, the anisotropy field. The film does not reverse by rotation, however, because of the magnetostatic stray fields caused by the blocked ripple. With zero transverse field, unlike when a transverse field is applied, there is so little torque on the mean magnetization from the applied field that the reaction torque from blocked ripple can be expected to prevent the rotation of $\vec{M}_o$. Increases in the torque from the applied field are expected to be canceled by increases in the reaction torque. Recall that the blocked ripple has "walls" separating regions where $\varphi > 0$ from regions where $\varphi < 0$. Increases in the applied field antiparallel to $\vec{M}_o$ will cause φ to increase; however, because the ripple is blocked and has walls, the wavelength is not free to adjust as it was before blocking occurred. Since the longitudinal magnetostatic field which is responsible for the reaction torque is proportional to the square of the ripple amplitude and inversely proportional to the wavelength, when the applied field is increased the reaction torque is expected to increase, thereby compensating for increases in the torque from the applied fields.

The reaction torque from blocked ripple, then, prevents the magnetization from reversing by coherent rotation, thereby giving

diffuse boundaries time to grow and propagate through the film. Of course, locking does not occur because the nonlinear uniform field that causes the locking

$$h_{u2} = \varphi[h \sin(\alpha - \varphi_o) - 2 \sin 2\varphi_o] \tag{2.41c}$$

is zero, since $\alpha \simeq \pi$, $\varphi_o \simeq 0$.

4.2.3 Boundary Formation

First appearance of the boundaries at the edges of the films suggests that edge demagnetizing fields are responsible for the boundary formation. In Fig. 4-1 the boundary is formed as small reverse domains appear at the extreme upper and lower edges of the film. When these reverse domains grow together a transverse boundary is created. In Fig. 4-2, on the other hand, no small reverse domains are seen. Instead the boundary forms when the magnetization near the upper and lower edges of the film rotates as evinced by the gradual change in contrast which takes place at the edges of the film. The major difference between these two cases is, of course, the magnitude of the pulse field, 0.584 H_k and 1.14 H_k , respectively. In Fig. 4-2 the applied field is sufficiently large that, when it is combined with the edge demagnetizing fields, it overcomes any blocking which may have occurred near the edge so that rotation of the magnetization may occur. In Fig. 4-1 with an applied field much less than H_k , however, there is no blocking but, of course, since the applied field is small, there also is very little rotation. Instead small reverse domains nucleate at the edge of the film where the demagnetizing fields are high.

A good example of how the boundary forms when a large field is applied is seen in Fig. 4-3 which shows film 81-4-12 during the initial stages of boundary formation. The longitudinal pulse field in this case is 1.31 H_k . The 25 nsec picture has slightly shaded regions near the lower right edge which extend roughly 1 mm into the film. The regions are darkest at the edges of the film and become lighter near the center of the film. This gradual change in contrast indicates that the transition from nonswitched to switched magnetization takes place over the entire shaded region. By 50 nsec the shaded regions have grown so that they extend up to 2 mm into the film, but still the transition from nonswitched to switched magnetization is gradual and smooth--the boundary is not yet jagged. By 75 nsec the shaded regions have grown still more, however now the boundary has begun to break up into slender domains so that it is no longer smooth but rather quite jagged.

These photographs suggest that at high fields the boundary is initially formed by coherent and unisensical rotation (rotation in one direction) of the magnetization in regions near the edges of the film. The magnetization within these regions is only partially rotated and if the field is quickly terminated, the magnetization configuration changes (see Section 5.2). Therefore, this partially rotated boundary is an unstable state. Furthermore, the fact that the boundary eventually becomes jagged indicates that the smooth boundary is not actually even a stable dynamic configuration. It appears, then, that the smooth transverse boundary is a configuration which can be temporarily created by a longitudinal pulse field, but cannot be maintained either

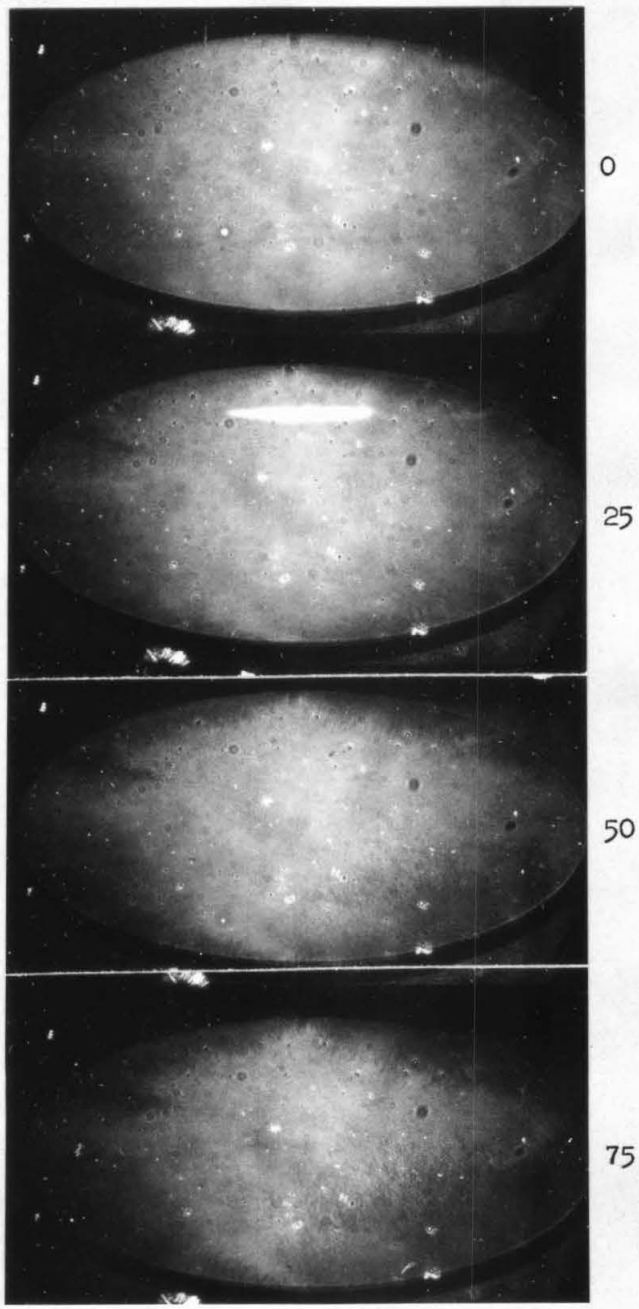

Fig. 4-3. Film 81-4-12 in the process of forming a diffuse boundary with a 4.7 oe longitudinal pulse field applied. Time in nanoseconds relative to initial application of pulse field is indicated.

statically or dynamically in time.

The demagnetizing fields in a saturated film were calculated in Section 3.2.1. From the direction of the fields, as shown in Fig.3-2, it can be seen that the magnetization near the edge of a film will be curled away from the easy axis qualitatively as indicated in Fig. 4-4. Reverse domains are shown at the top and bottom edges of the film because they are observed in those regions by Bitter techniques which will be discussed later. It was shown in Section 3.2.1 that 0.5 mm from the edge of a saturated film at the angle $\beta = -\pi/4$ the demagnetizing field was about 0.225 oe and directed at an angle $\beta_H \lesssim 5\pi/4$ (Fig. 3-2). In a film with $H_k = 3.6$ oe such a field would rotate the magnetization by roughly 2.5^o, which is the angle of the magnetization when an approximately 0.12 oe transverse bias field is applied. In Fig. 3-17 it was seen that when a 4.1 oe longitudinal pulse field was applied to such a film in the presence of a 0.1 oe transverse bias field, the reversal was by noncoherent rotation. Therefore, it should be expected that a larger pulse field of 4.7 oe used in Fig. 4-3 would cause the magnetization 0.5 mm from the edge of a film and at an initial angle of roughly 2.5^o to reverse by rotation in spite of any blocked ripple which may exist in that area.

For lower pulse fields significantly below H_k, as in Fig. 4-1, the fields are too small to cause the rotational process along the edge, and in this case the boundary is formed by the growth of many small reverse domains at the edge of the film. Static edge domains were observed with Bitter patterns (named for F. Bitter (1931), who first attempted to use the technique) in round films after a large

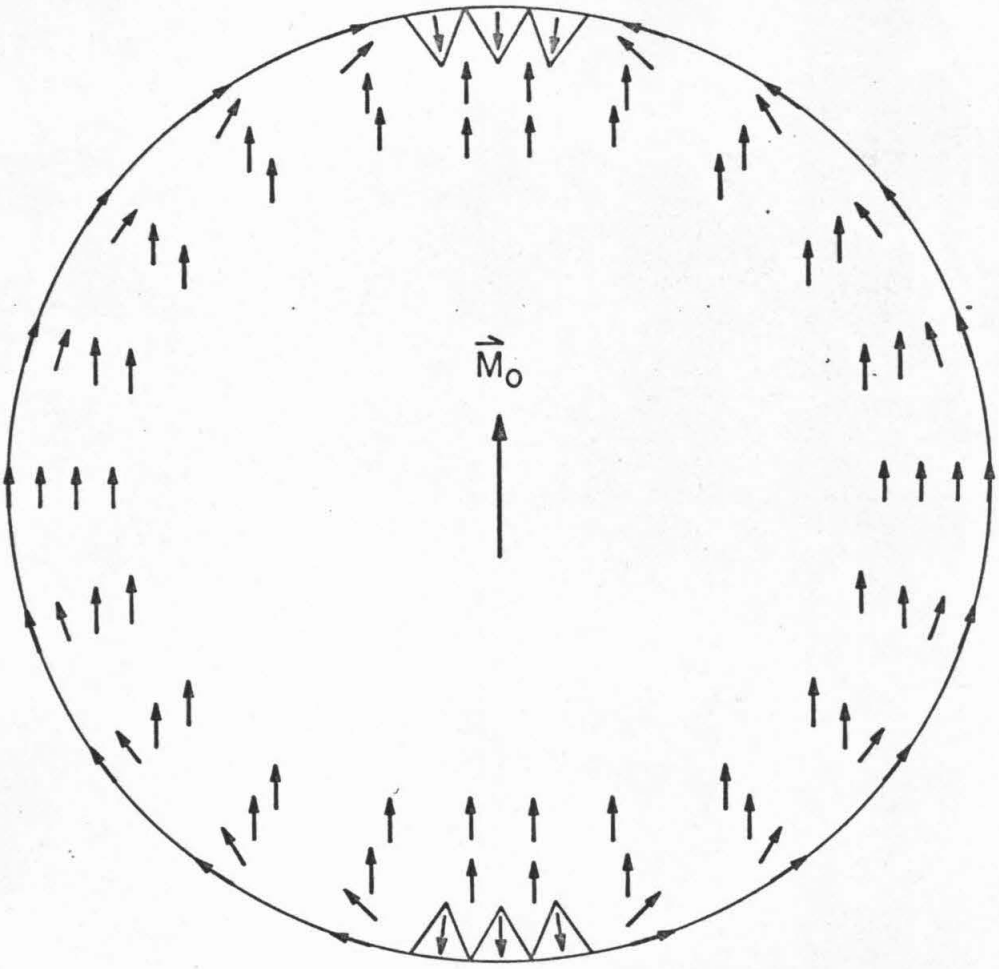

Fig. 4-4. Diagram showing in which direction the magnetization curls because of the demagnetizing fields near the edges of a film.

(>> H_k) easy axis field was terminated. Figure 4-5a is a photograph of the edge domains at the upper edge and Fig. 4-5b shows another portion of the edge where no domains exist. The domains are observed to extend about 100μ into the film. With zero applied field the edge domains were observed only along 1 mm segments of the edges which corresponded to the extreme upper and lower edges of the films in Figs. 4-1, 4-2, and 4-3. However, with increasing fields applied antiparallel to $\vec{M}_o$, the domains were observed to appear in wider segments of the edge. Therefore, when the pulse field is applied to the film in Fig. 4-1, there is both the growth of previously existing edge domains and the creation of additional edge domains. With increased pulse fields, the reverse domains appear farther out toward the extreme right and left-hand edges until at 3.3 oe (= 0.92 H_k) the boundary forms along almost all of the edge.

The effect of the edge can also be investigated by hard axis fallback experiments. The film is saturated by a hard axis uniform field of $\simeq 10\ H_k$ aligned to within 0.25^o. The field is then smoothly reduced to zero (as opposed to A-C demagnetization) and a photograph of the resulting domain pattern is taken with the Kerr magneto-optic camera. Figure 4-6 shows the domains which result after such a hard axis fallback experiment for a typical low dispersion film. Angular dispersion, α_{50}, is only 0.5^o for this film. In large areas extending more than 1mm from the edge of the film the magnetization lies only in one direction yet near the center of the film domain splitting has occurred, and the magnetization has broken up into long slender domains along the easy axis.

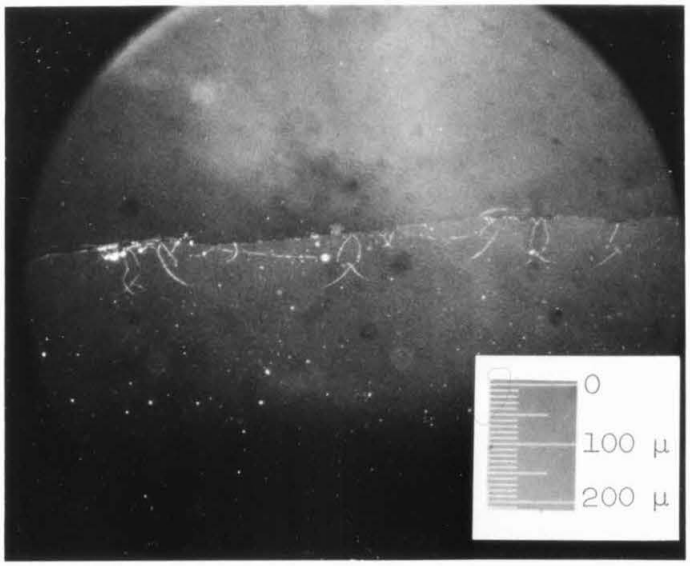

(a)

(b)

Fig. 4-5. (a) A photograph of the Bitter pattern resulting from edge domains at the upper edge of film 81-4-6 shown in Figs. 4-3 and 4-5. (b) A photograph of an edge of film 81-4-6 where no edge domains exist.

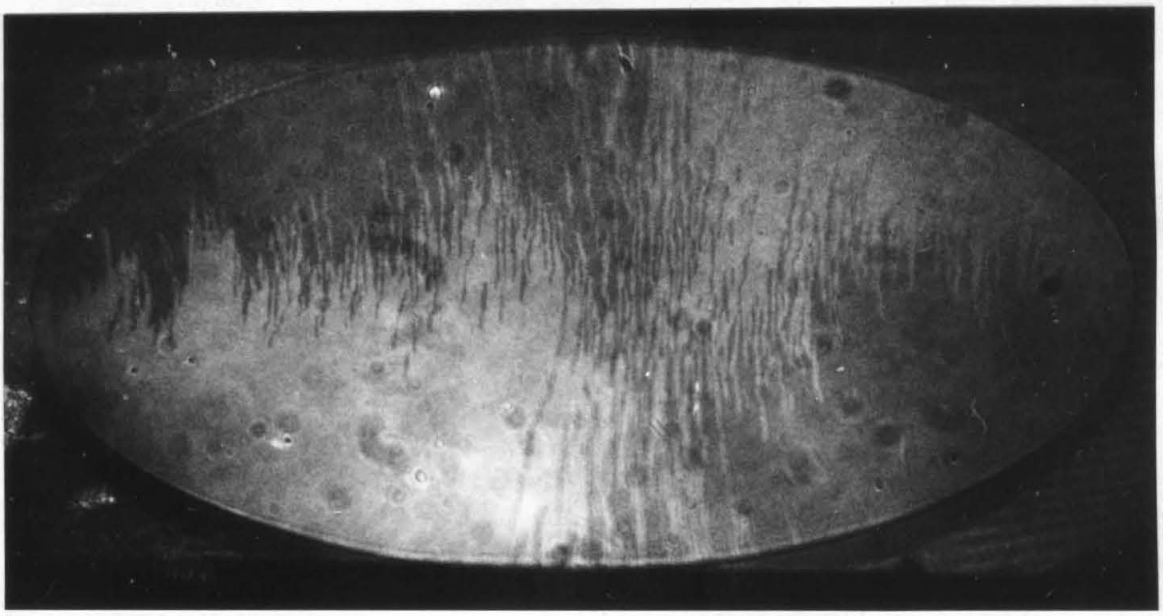

Fig. 4-6. Photograph showing the domain pattern which results when a hard axis saturating field is removed from film 81-4-6.

The demagnetizing field which is caused by the divergence of the magnetization near the edge of the film is, of course, the reason the magnetization tends to fall back into specific directions near the edges of the film rather than breaking up into domains. Consider Fig. 4-7a which is a schematic diagram of a circular thin film saturated in the hard direction with divergences of the magnetization at the edges represented by the + and - signs in the figure. When the hard axis saturating field is removed, the magnetostatic stray fields from the divergence at the edge cause the magnetization near the edges to fall back to the easy axis as shown in Fig. 4-7b. Fallback patterns similar to that shown in Fig. 4-6 were obtained for almost all films of composition near 81% Ni-Fe. For films with α_{50} quite large ($> 1.0^{o}$), dispersion effects in the film tended to dominate the edge effects, although even in these high dispersion films, regions very close to the edges tended to fall back to the easy axis in the directions indicated in Fig. 4-7b.

In films with higher dispersion where the edge effects do not so clearly dominate, transverse walls can nucleate in the center of the film. An example is shown in Fig. 4-8, which shows film 81-10-4 reversing in the presence of a 9.7 oe longitudinal pulse field. By 25 nsec areas of the film are beginning to darken, indicating that the magnetization within these areas is partially rotated. By 75 nsec reversed regions are clearly visible. Some reversed areas are in the central portion of the film while others are at the edges as in Fig. 4-2. By 100 nsec diffuse boundaries are clearly formed, although they are not as symmetrically aligned as in Fig. 4-2. After 100 nsec the

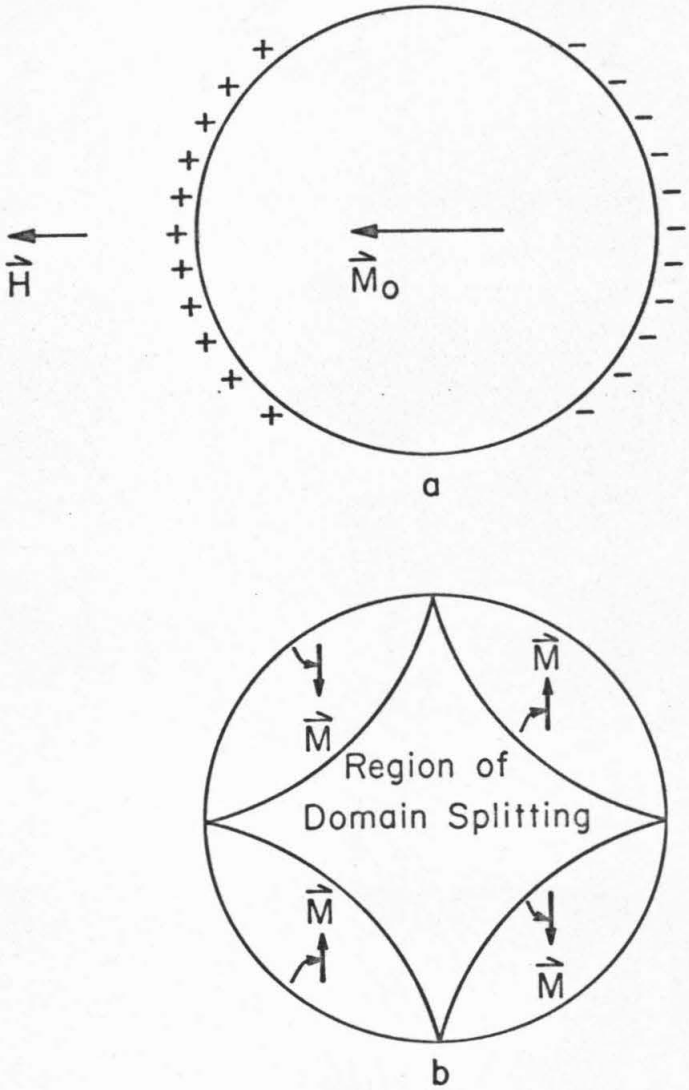

Fig. 4-7 (a) Diagram of a magnetic film saturated in the hard direction, showing the magnetic monopoles resulting at the edges because of the divergence of the magnetization there. (b) Diagram of the film after the hard axis field is removed, showing in which directions the demagnetizing fields cause the magnetization to fall back to the easy axis.

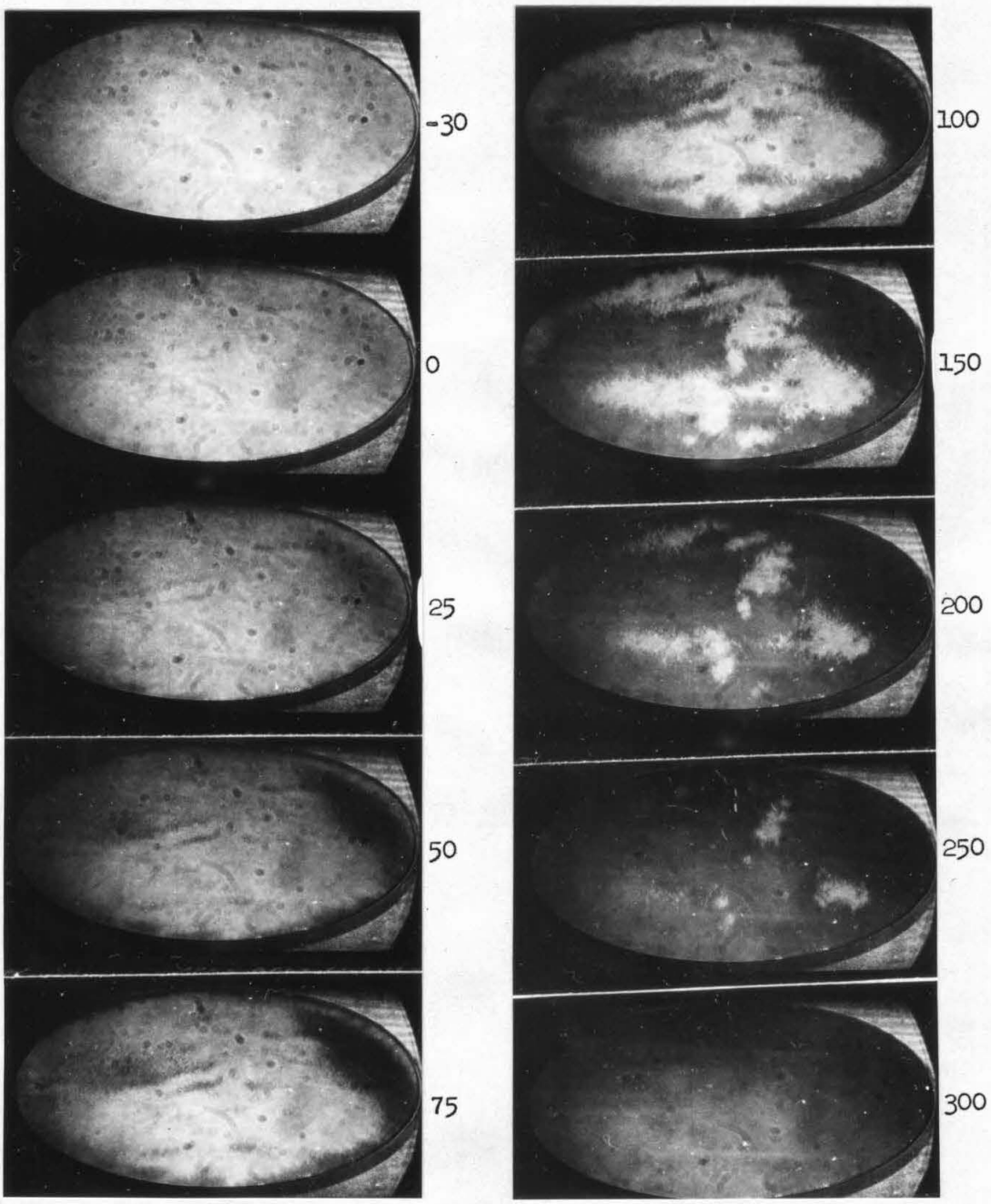

Fig. 4-8. Film 81-10-4 in the process of flux reversal with a 9.7 oe longitudinal pulse field. Time in nanoseconds relative to initial application of pulse field is indicated.

film is switched as the diffuse boundaries propagate and sweep out unswitched portions of the film.

It is clear then, that in very low dispersion films edge effects are important in determining how the diffuse boundaries are formed and that in higher dispersion films macroscopic anisotropy dispersion is important. In the low dispersion films with low fields, the boundaries form by the creation and growth of small domains at the edge; with high fields, by a rotation of the curled magnetization at the edge. In the higher dispersion films, not only do the boundaries form at the edges, but also in the interior of the film around regions which reverse by a rotational process.

4.2.4 One Dimensional and Two Dimensional Boundaries

The initial smooth boundary which forms at the edges of a film has been found to be an unstable configuration, by the fact that it tends to break up into a jagged boundary with two dimensional variations in the magnetization. The reason for this is that the jagged boundary is a lower energy state than is the smooth boundary. Theoretical models of both the smooth and jagged boundaries have been constructed to show that this is true. These models do not include dynamic properties, but rather are based on purely static energy considerations. The dynamic effects can be shown to add small energies in comparison to the large magnetostatic, exchange, applied field, and anisotropy energies already contained within these models.

In a one dimensional transverse boundary existing in static equilibrium between opposing regions of magnetization as in Fig. 4-9, the volume divergences which exist as the magnetization direction

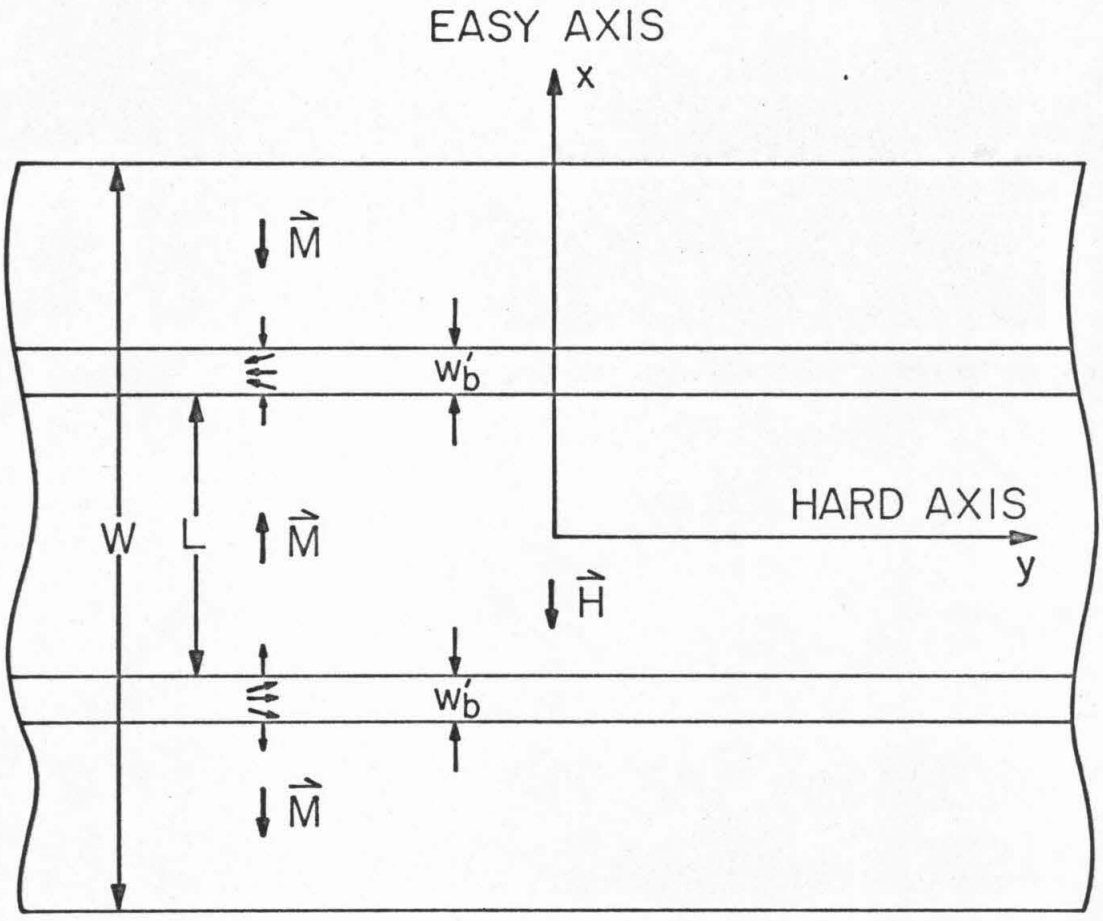

Fig. 4-9. Diagram of the model used to find the energy of a smooth one-dimensional transverse boundary.

varies through the boundary would be equal whether the magnetization stayed in the plane of the film or rotated up out of it. Since the surface divergences would add magnetostatic energy to the boundary, the magnetization would remain in the plane of the film similar to a Neel wall. The familiar case of the Bloch wall in which the magnetization rotates out of the plane of the film producing surface divergences but eliminating volume divergences cannot apply for a transverse wall. The application of a longitudinal field would produce a torque to rotate the magnetization within the boundary slightly out of the plane of the film. Surface divergences created cause the magnetization to rotate in the plane and the boundary to propagate. For the experimentally observed velocities the magnetization need rotate only 2×10^{-3} rad out of the plane of the film, adding negligible energy to the boundary.

To describe the variation of the magnetization direction or the "shape" of the boundary, a third order polynomial is assumed:

$$\theta = \cos^{-1}[1 - (2 + b)u^2 + bu^3] \tag{4.1}$$

with

$$u = \frac{1}{w_b'}\left(\pm x - \frac{L}{2}\right) \quad , \quad L \leq |2x| \leq L + 2b \tag{4.2}$$

where θ is the angle which the magnetization makes with the easy axis, b is the "shape" parameter which will be determined by energy minimization, $L/2$ is the distance the boundary is from the center of the film, and w_b' is the width of the boundary (also to be determined by energy minimization). For the model to have physical significance, b must be within the range

$$-2 \leq b \leq 4 \tag{4.3}$$

Within this range, however, b may vary and hence the shape of the boundary changes. Figure 4-10 shows plots of $\cos\theta$ and of θ as functions of u. The upper and lower bounds, corresponding to the limits of (4.3) are shown. The form of the polynomial was chosen to satisfy the boundary conditions.

$$\text{For } u = 0: \quad M_x = M\cos\theta = M, \frac{\partial M_x}{\partial x} = 0 \tag{4.4a}$$

$$\text{and for } u = 1: \quad M_x = -M \tag{4.4b}$$

The film is assumed to be infinite in the hard axis direction with no specific assumption being made about the film's width in the easy axis direction; however, edge effects are neglected. Furthermore, two parallel boundaries are assumed to exist in the film.

The total energy of the one dimensional transverse boundary is calculated in Appendix B. Exchange energy is negligible because the boundary is so wide. The energy minimum occurs when

$$\text{for } h \geq 3/175: \quad b = 4 \tag{4.5a}$$

$$w_b' = \frac{4M_s d}{H_k}\left(\frac{1}{h+\frac{9}{35}}\right) \tag{4.5b}$$

For $h < 3/175$, the values of b and w_b' corresponding to the energy minimum can in some cases be found, but both are complicated functions of the applied field. Interest here is in the range $0.5 \lesssim h \lesssim 2$, and therefore the results (4.5a,b) are all that is required. The total minimum energy for this model was found to be

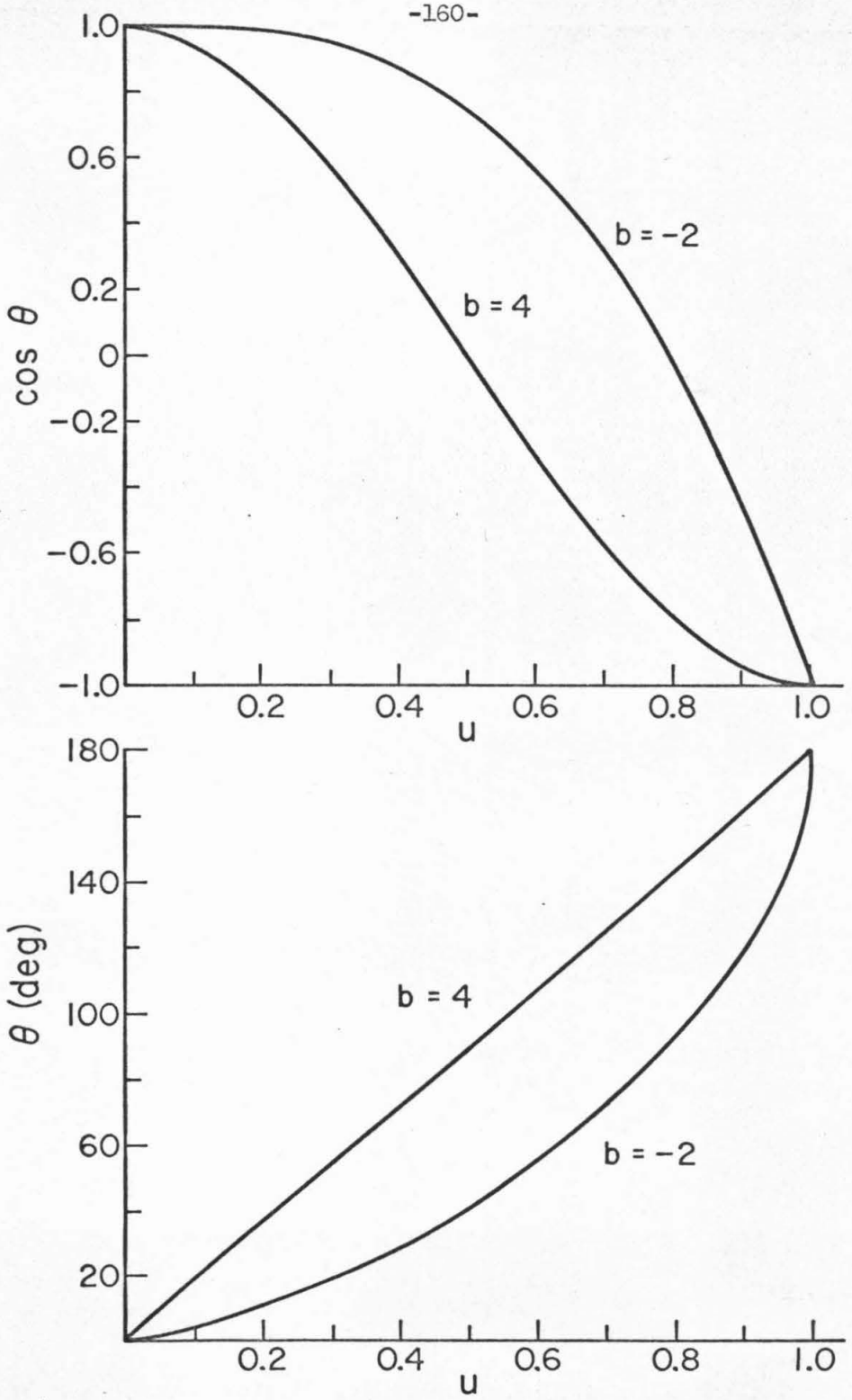

Fig. 4-10. Plots of cos θ and θ versus u for the assumed variation in direction of the magnetization through the smooth, one-dimensional transverse boundary. The limits corresponding to b = -2 and b = 4 are shown.

$$E_b = 22\, M_s^2\, d^2 + 8M_s^2\, d^2\, \ell n \left| \frac{LH_k}{4M_s d} \left(h + \frac{9}{35}\right) \right|$$

$$- M_s d\, HW + 2M_s d\, HL \qquad (4.6)$$

For a typical 1000 Å thick film with M_s = 800 emu, H_k = 3.6 oe, L = 0.5 cm, and h = 1, this yields

$$E_b = 3.6 \times 10^{-3} - M_s dH(W - 2L) \qquad (4.7)$$

In order to compare the total energy of the smooth boundary with one dimensional variations in $\vec{M}$, with that of a jagged boundary with two dimensional variations in $\vec{M}$, it is necessary to estimate the energy of a jagged boundary. A convenient model for the jagged boundary is shown in Fig. 4-11 as consisting of domain walls running in a zig-zag pattern across the film. The pattern has a wavelength of 100μ and peak to peak amplitude of 500μ . As an approximation to the energy contained within the walls, the static wall energy calculated by Middelhoek (1961) will be used. In his calculation Middelhoek assumed a wall parallel to the easy axis in which there was a linear variation of the angle of the magnetization with respect to distance through the wall. He estimated the magnetostatic energy contained in such a wall and calculated the total exchange and anisotropy energies. No applied fields are assumed. After finding the total wall energy as a function of wall width, Middelhoek minimized the energy with respect to the wall width. Unfortunately the model does not lead to simple analytical expressions for the wall width and energy, and therefore only numerical solutions could be obtained. Other researchers such as Dietz and

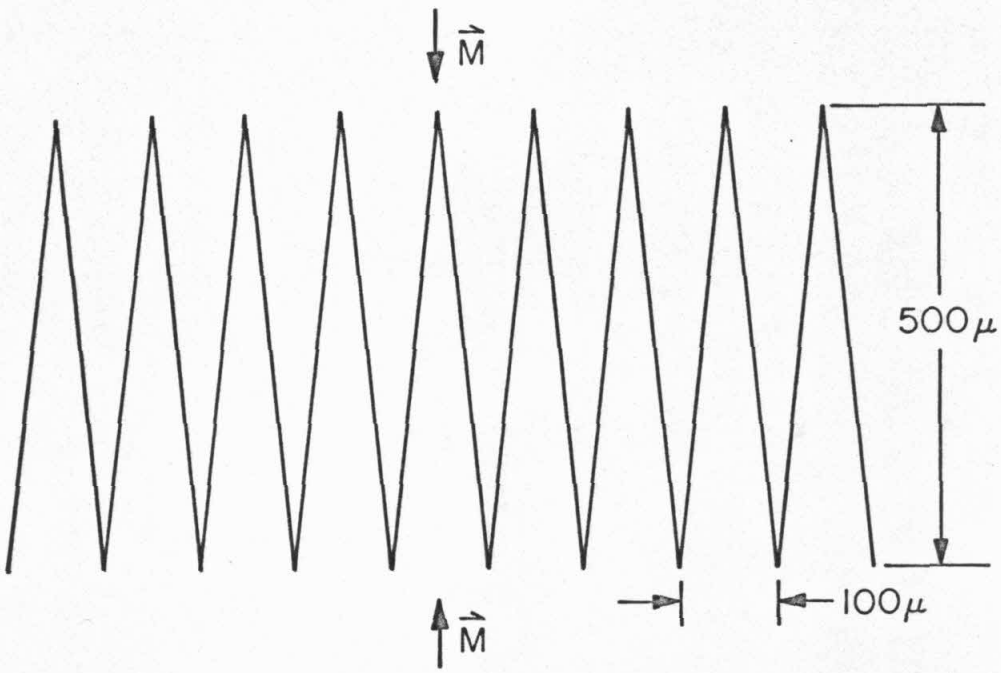

Fig. 4-11. A model of a zig-zag boundary used to approximate the diffuse transverse boundary.

Thomas (1961), Collette (1964), Brown and LaBonte (1965), Aharoni (1967), and Kirchner and Doring (1968) have also made domain wall calculations which agree with Middelhoek's calculation of the wall energy within a factor of two, but in no case is Middelhoek's value lower than the others.

Suzuki (1969) measured domain wall widths as a function of film thickness in various alloys, obtaining reasonable agreement with Middelhoek's predicted widths for films up to 700Å thick. For thicker films his data did not agree with any of the theoretical models, suggesting that there is a wall configuration with a lower energy state than any of the theoretical models thus far suggested. In any case, it appears clear that by using an upper limit of Middelhoek's calculation, the wall energy is not being underestimated. For a 1000Å thick film Middelhoek found the wall energy of a Neel wall to be about 8 ergs/cm^2 and of a Bloch wall to be about 4.6 ergs/cm^2.

Assuming a model like that shown in Fig. 4-9, but with the smooth one dimensional boundaries replaced by jagged two dimensional boundaries like that shown in Fig. 4-11 and conservatively assuming the Neel wall energy, the total energy per unit length of film is

$$E_z = 1.6 \times 10^{-3} - 2M_s\, dH(W - 2L) \qquad (4.8)$$

Comparing (4.8) with (4.7), it is found that when the term $(-2M_s dH(W-2L)$, the field energy in the saturated portions of the magnetic film, is neglected, the energy of the jagged boundary is roughly one-half that of the smooth boundary. In obtaining this result, the fact that the walls are oriented at $\tan^{-1}0.1 \approx 5.7°$ to the easy axis was neglected, and therefore the magnetostatic energy due to the opposing components of

magnetization on either side of the wall was neglected. This energy is proportional to the square of the components of opposing magnetization and, since these components are reduced by about 1/10 from that of the smooth boundary, the energy per unit length of wall could be expected to be reduced by about 1/100. Multiplying by 10 the length of wall per unit zig-zag boundary length, it is found that the additional energy which must be added to (4.8) is approximately 10% of the magnetostatic energy contained in the smooth transverse boundary, which is clearly insufficient to make the energy of the zig-zag boundary equal to that of the smooth boundary.

The additional magnetostatic energy from the opposing components of magnetization would make the wall wider than one parallel to the easy axis and hence the anisotropy energy would increase, but there would be a corresponding decrease in exchange energy. The anisotropy energy accounts for only about 4% of the total energy in the smooth boundary and only 0.5% of the energy in a normal domain wall, so this term is clearly negligible. Therefore, a jagged transverse boundary with two dimensional variations in the mangetization is more favorable than a smooth transverse boundary with one dimensional variations in the magnetization , so that the smooth boundary, which initially is created because of the demagnetizing fields at the film edges should be expected to eventually break up into some sort of jagged boundary.

4.2.5 Boundary Structure, Width, and Velocity

The method of propagation of the boundary can be investigated by studying the boundary structure. Figures 4-12 and 4-13 show film 81-4-12 in the process of flux reversal with zero transverse field and 3.3 oe and 4.7 oe longitudinal pulse fields, repsectively. Note how jagged and diffuse the boundaries are and note in Fig. 4-13 that small

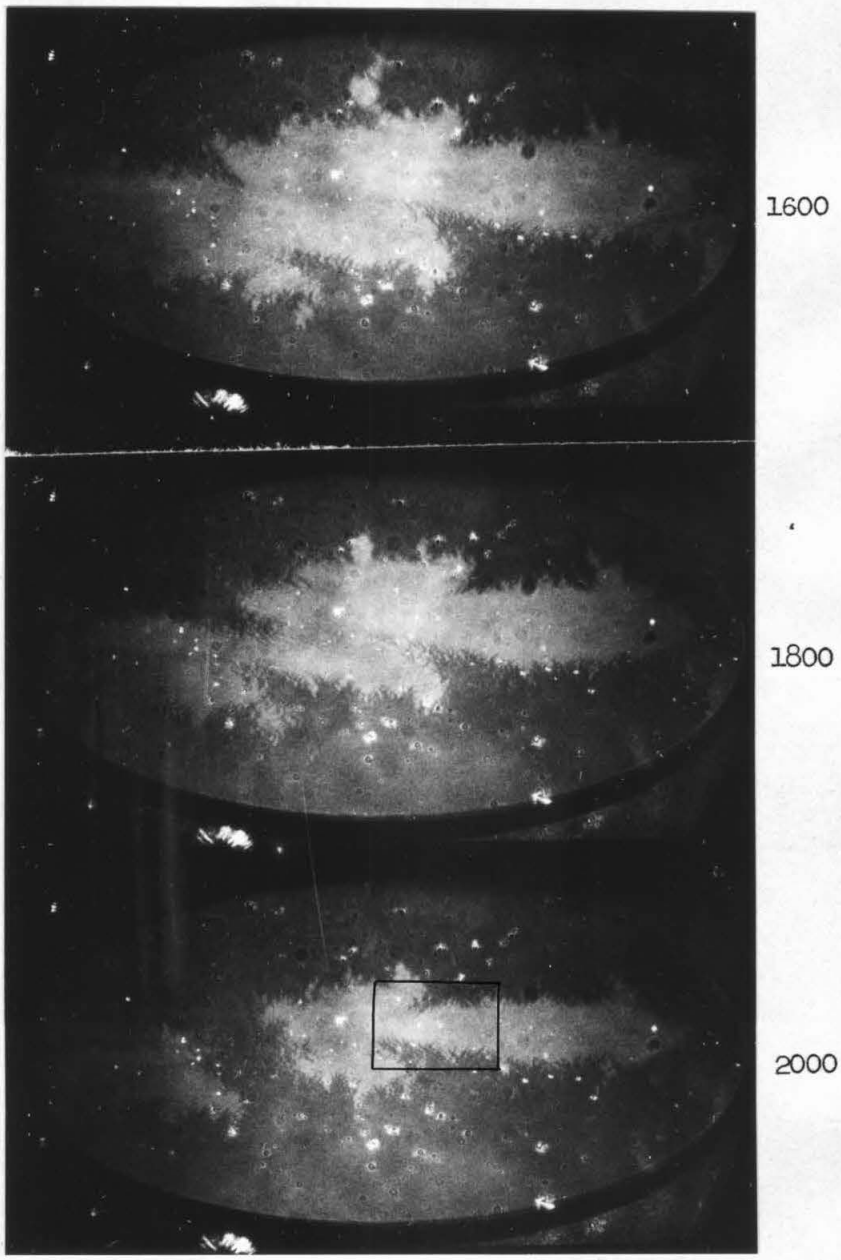

Fig. 4-12. Film 81-4-12 in the process of flux reversal with a 3.3 oe longitudinal pulse field. Time in nanoseconds relative to initial application of pulse field is indicated.

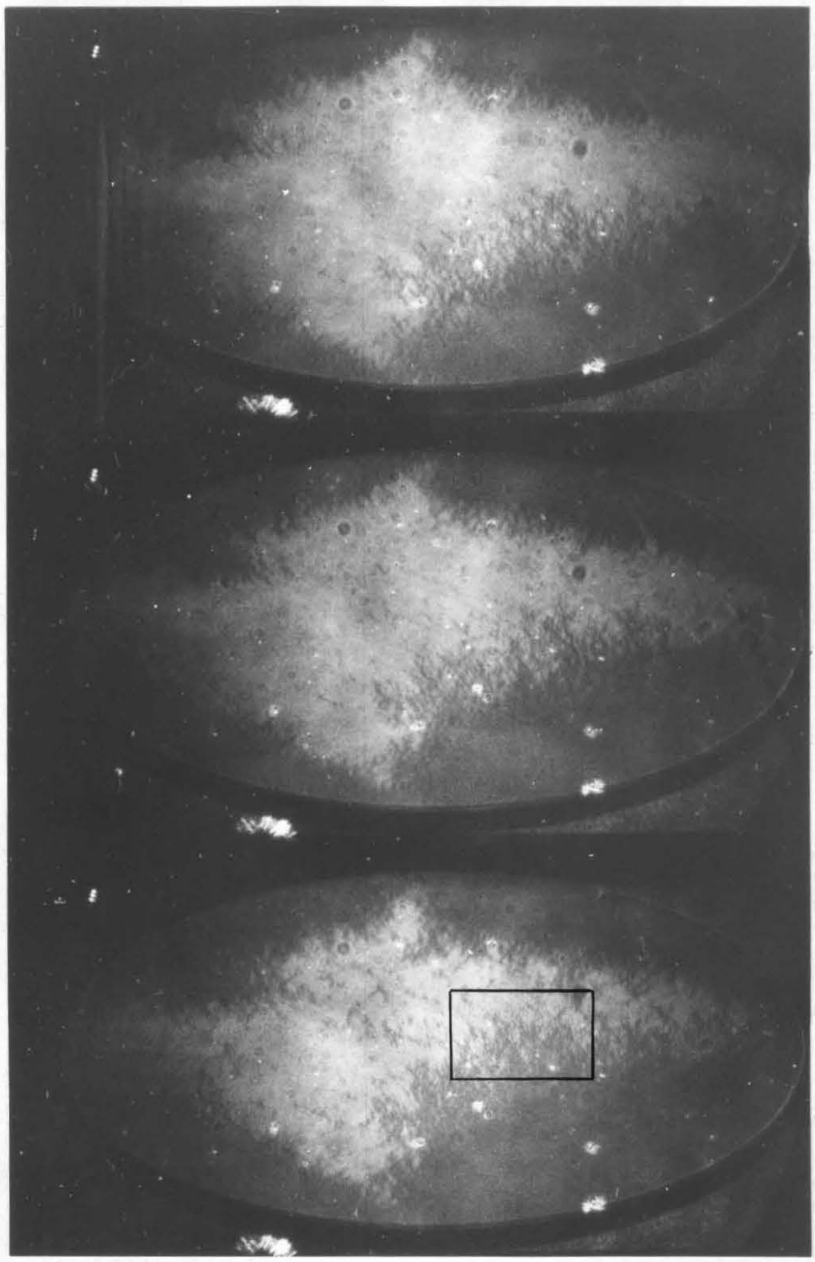

Fig. 4-13. Film 81-4-12 in the process of flux reversal with a 4.7 oe longitudinal pulse field. Time in nanoseconds relative to initial application of pulse field is indicated.

regions are nucleating which are separated from the reversed areas at the edges. Figures 4-14 and 4-15 are highly magnified photographs of the rectangular regions in Figs. 4-12 and 4-13. This magnification is clearly the limit of resolution of the photographs, since approximately 1 mm corresponds to the 10μ minimum width of line which could be resolved with the film used. The boundary is seen to be much more complex than it was represented in the model of Fig. 4-11. With higher fields in Fig. 4-15, small regions of partially rotated magnetization which are not directly connected to the reversed region are observed (indicated by arrows), suggesting that the boundary does not propagate by growth from tips, but rather that it propagates as small regions nucleate ahead of it. At lower fields in Fig. 4-14, many of the tips which do connect to the reversed regions (indicated by arrows) are observed to be lower in contrast and therefore only partially reversed and forming by a rotational process.

Another good example of such propagation by the rotation of magnetization within small regions is shown in Fig. 4-16. Figure 4-16a shows a film with the static domain pattern which results when a 3.0 oe longitudinal pulse field is terminated 1500 nsec after it was applied to a film with H_k = 3.6 oe. Figure 4-16b shows the same film 175 nsec after a second 3.0 oe pulse field was applied. Note that although the boundary is in approximately the same position, in Fig. 4-16b there are slender partially reversed regions extending ahead of the boundary (indicated by arrows). On the other hand, in sections of the boundary it is observed that many tips have not propagated at all. Hence, the boundary does not propagate as walls slowly move over the film, but rather as a large number of small regions directly ahead of the

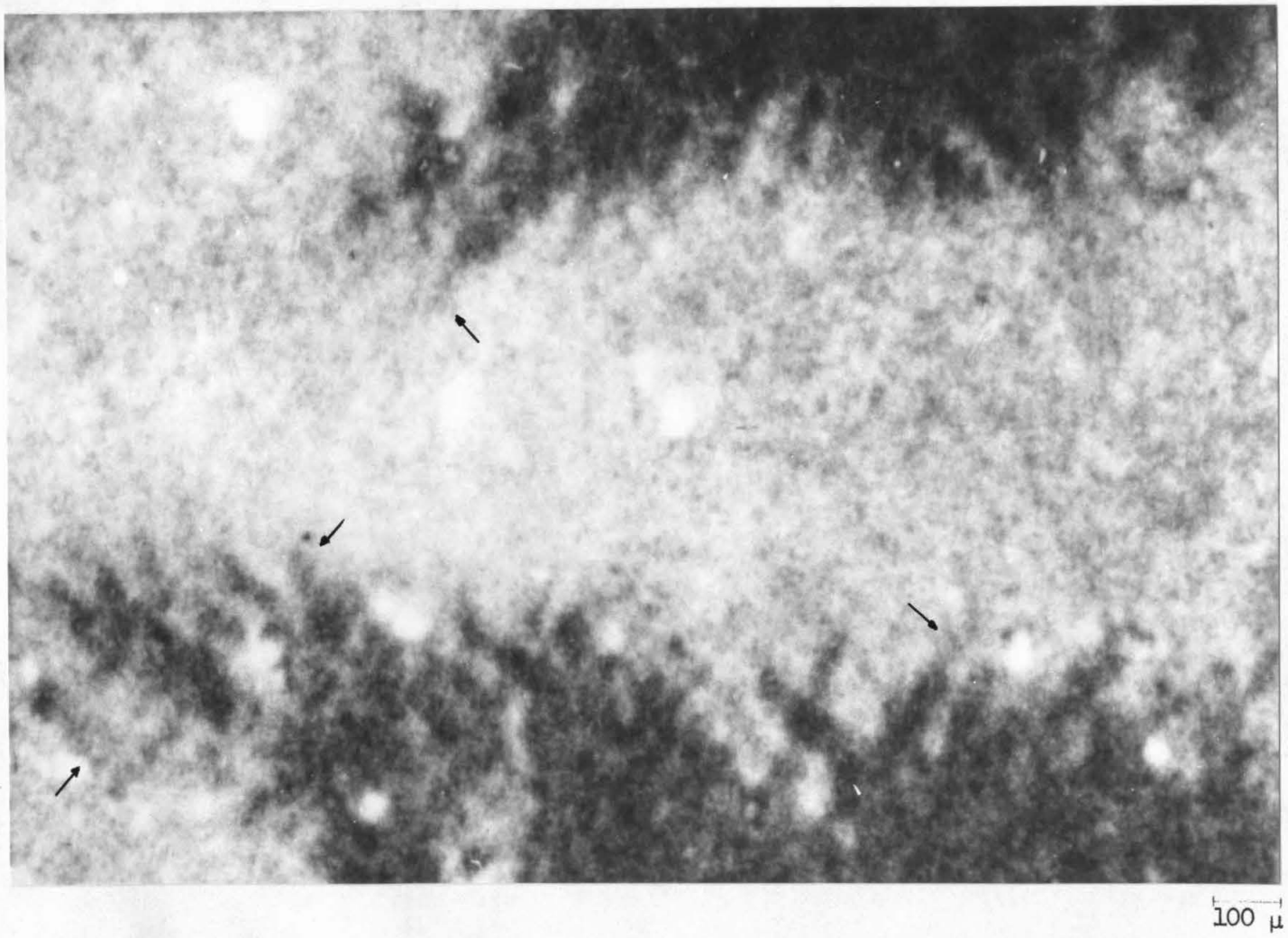

Fig. 4-14. A segment of the boundary within the rectangle in Fig. 4-12 highly magnified.

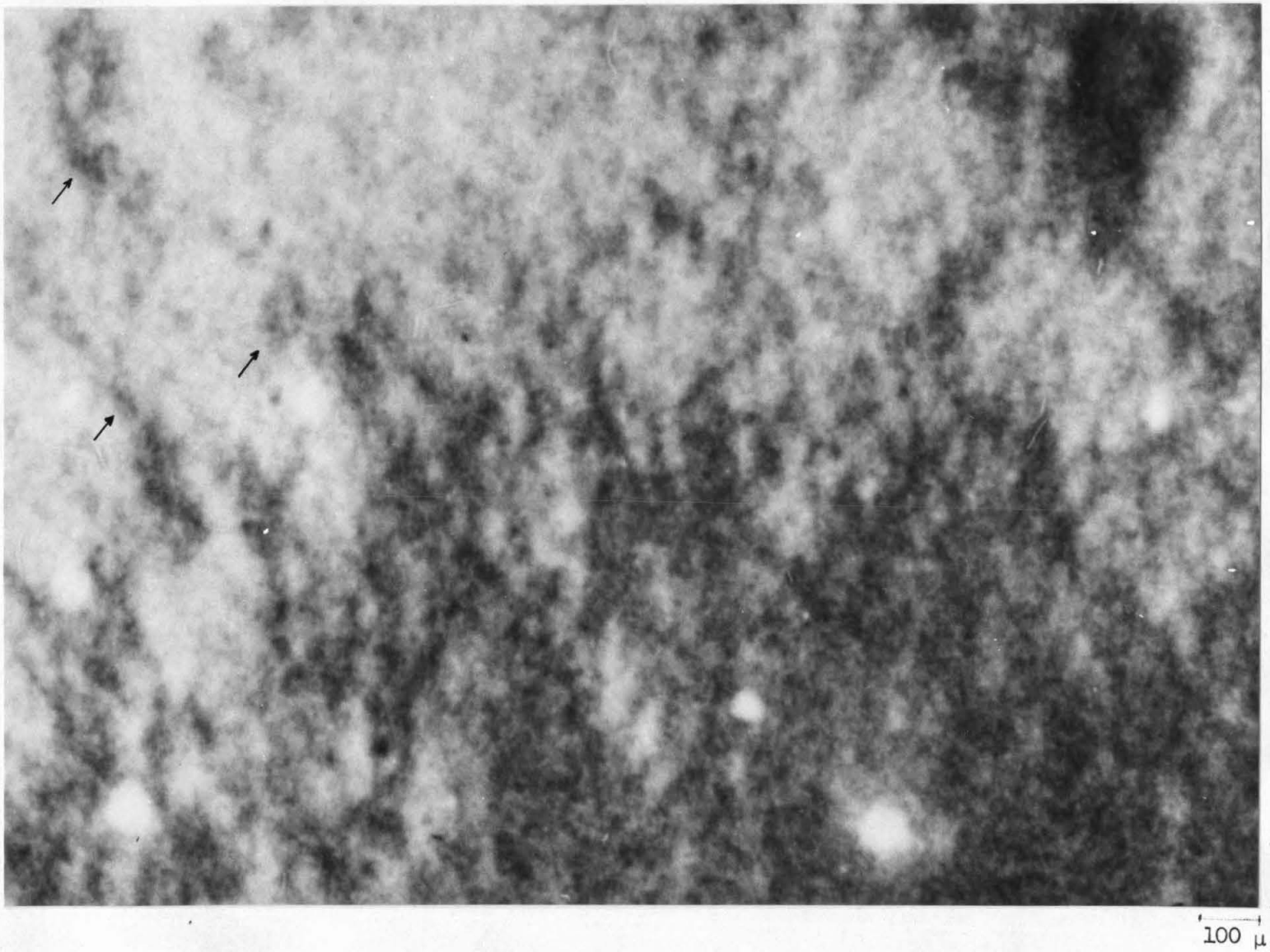

Fig. 4-15. The segment of the boundary within the rectangle in Fig. 4-13 highly magnified.

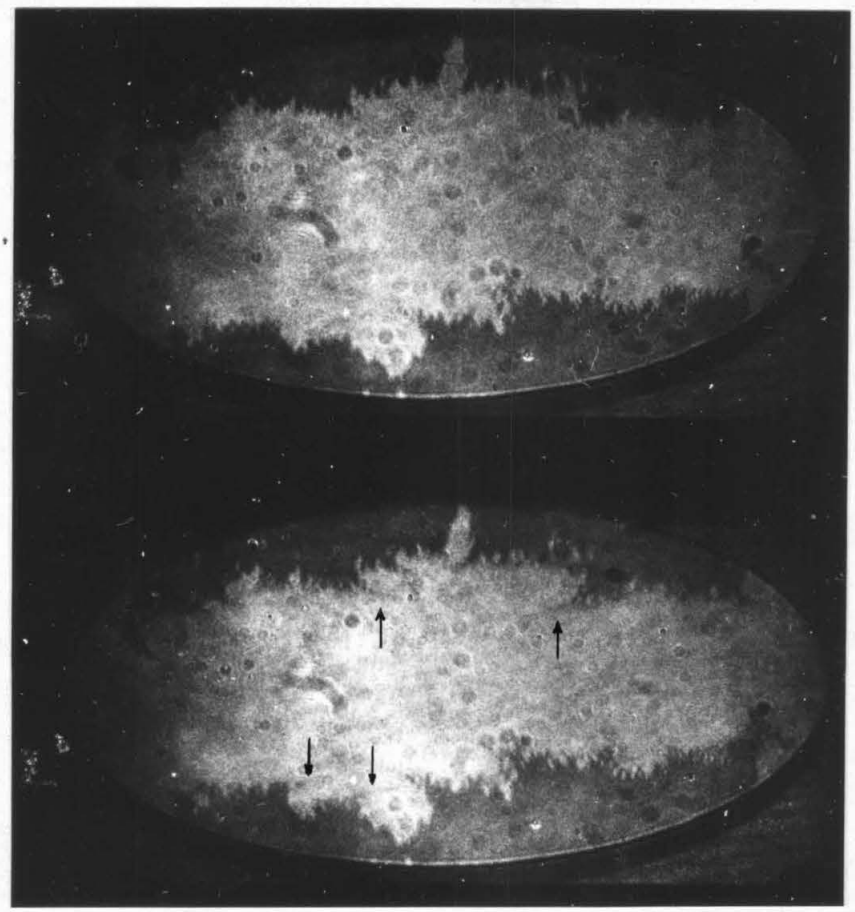

Fig. 4-16 (a) Film 81-4-12 with the static domain pattern which results when a 3.0 oe longitudinal pulse field is terminated 1500 nsec after it was applied. (b) The same film 175 nsec after a second 3.0 oe pulse field was applied.

boundary successively reverse by rotating as the boundary approaches.

The nucleation of small regions ahead of the boundary is believed to be caused by the magnetostatic stray fields produced by the large divergence in the magnetization across the boundary. As the boundary approaches a region of the magnetic film, the magnetostatic fields will increase until the total field is sufficient for rotation to occur in that region. By employing this model, a rough estimate of the expected width of the boundary may be obtained. Approximating the divergence of the magnetization in the boundary by a line charge of $2M_s d$ per unit length, the magnetostatic field produced is $4M_s d/x$ a distance x from the boundary center. It will be shown in Sect. 4.3 that for fields greater than some field H_n, nucleated regions appear over the entire surface of the film. The width of the boundary, then, will be determined by the region within which the applied field plus $4M_s d/x$ exceeds H_n. Therefore,

$$H + \frac{4M_s d}{(w_b''/2)} = H_n \tag{4.9}$$

or

$$w_b'' = \frac{8M_s d}{H_n} \frac{1}{1 - H/H_n} \tag{4.10}$$

where w_b'' is the total width of the boundary. The theoretical curve shown in Fig. 4-17 was plotted for $M_s = 800$ emu, $d = 960\text{Å}$, and $H_n = 5.2$ oe. Also shown in the figure is the measured width of the boundary (defined as the region within which nucleated regions exist

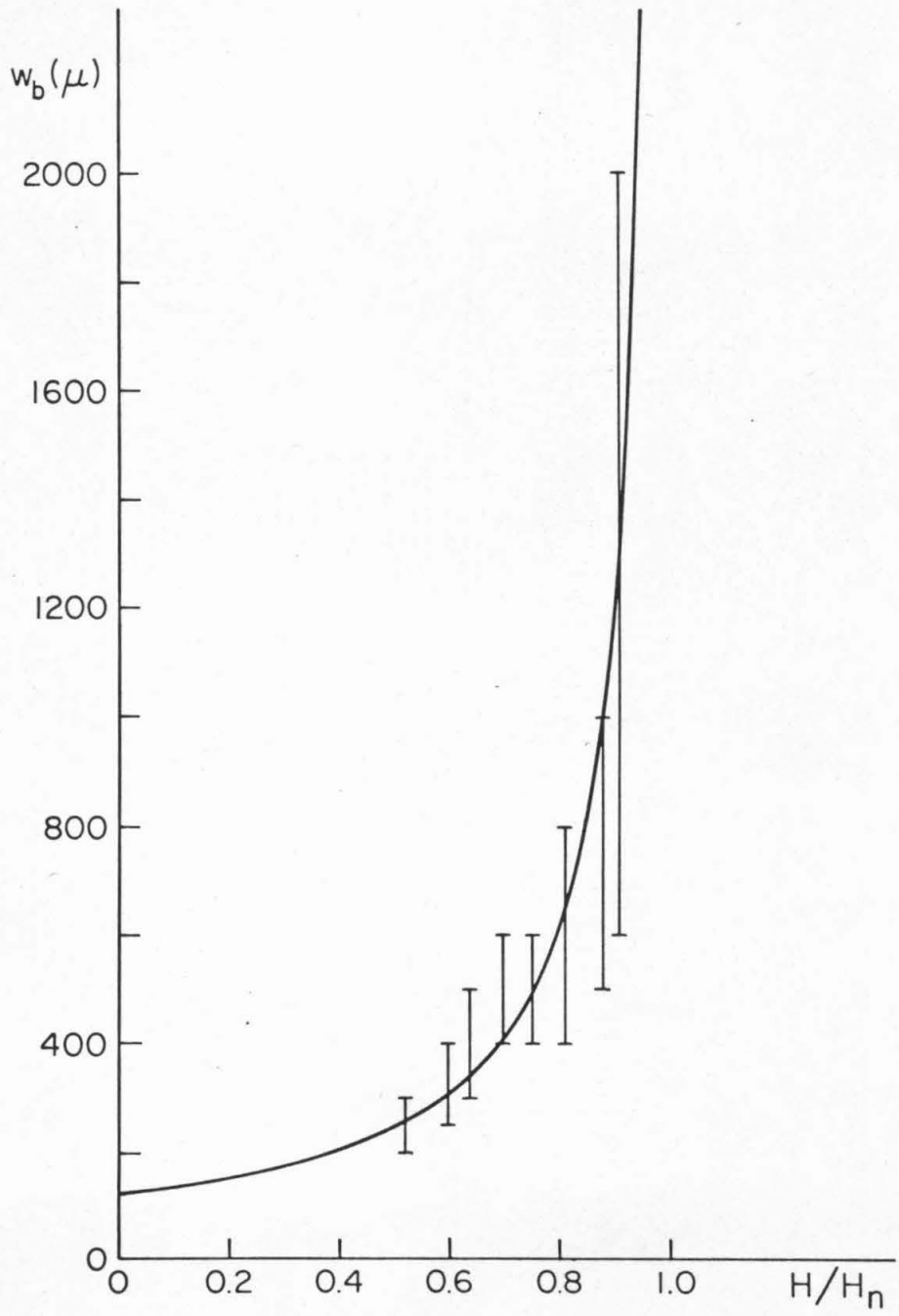

Fig. 4-17. A plot of boundary width versus applied field showing experimental data and theoretical curve for H_n = 5.2 oe.

separating the reversed from the not reversed regions). The error bars show the range of boundary widths observed in different areas of the film. At higher fields this range increases, presumably because the nucleation threshold is a function of position in the film and for fields very close to H_n, a small change in H/H_n should produce a large change in boundary width. The value $H_n = 5.2$ oe was chosen by what appeared to be a best fit to the experimental data. The very crude model predicts surprisingly well the dependence of the width on applied field.

The broad diffuse tips of small reverse domains seen in Figs. 2-7 and 4-1 result from the dynamic nucleation process by which the domains grow. When a pulse field greater than the coercive force is applied to a film, as it was in Figs. 2-7 and 4-1, small reverse domains nucleate by the rotation of magnetization within small areas of the film--mostly near the edge--because the edge demagnetizing fields lower the threshold for rotation in this area. As soon as the small region reverses, however, it itself produces demagnetizing fields in regions near it. If the demagnetizing fields plus the applied field are large enough, then additional reverse domains will nucleate near the first. Spain (1966) investigated the fields around tips of reversed magnetization and found for a 80-17-3, Ni/Fe/Co film that the field fit a relationship of the form $H_i \simeq .023/r$ (r in cm, H_i in oe) and was radially directed. It was seen in Chapter 3 and from the reversal curves of Figs. 2-5 and 2-6 that a transverse component of applied field greatly reduced the reversal times of thin films, producing

rotational processes when easy axis fields sufficient to exceed the Stoner-Wohlfarth threshold were applied. On the other hand, with zero transverse field the easy axis field must exceed the nucleation threshold $H_n > H_k$ for a fast rotational process to occur. Since the demagnetizing field about a tip is radial, it is expected that the observed reverse domains should broaden at the ends, because the transverse component of demagnetizing field greatly lowers the rotational threshold in the transverse directions from the tips.

Perhaps the most striking characteristic of diffuse transverse domain boundaries is that they propagate at unusually high velocities as compared to longitudinal domain walls. Fig. 4-18 shows the observed velocity as a function of applied field for a typical permalloy film. The velocity of the diffuse boundary varies from 0.033 cm/μsec to 1.25 cm/μsec as the applied field varies from 2.1 to 4.7 oe. The differential mobility or slope of the velocity versus field plot varies from 0.057 cm/oe-μsec to 1.4 cm/oe-μsec which is one to three orders of magnitude greater than the mobility of a normal domain wall in a film of similar thickness and composition as measured by Patton (1967). The high velocity of propagation obtained with the diffuse boundary permits reversal of thin films in times the order of 1 μsec which is two orders of magnitude greater than what could be expected with domain wall motion at similar fields. The diffuse boundary propagation, along with the nucleation of partially reversed regions to be discussed in Sect. 4.3, therefore is the reason reversal times as measured by inductive sense loops have

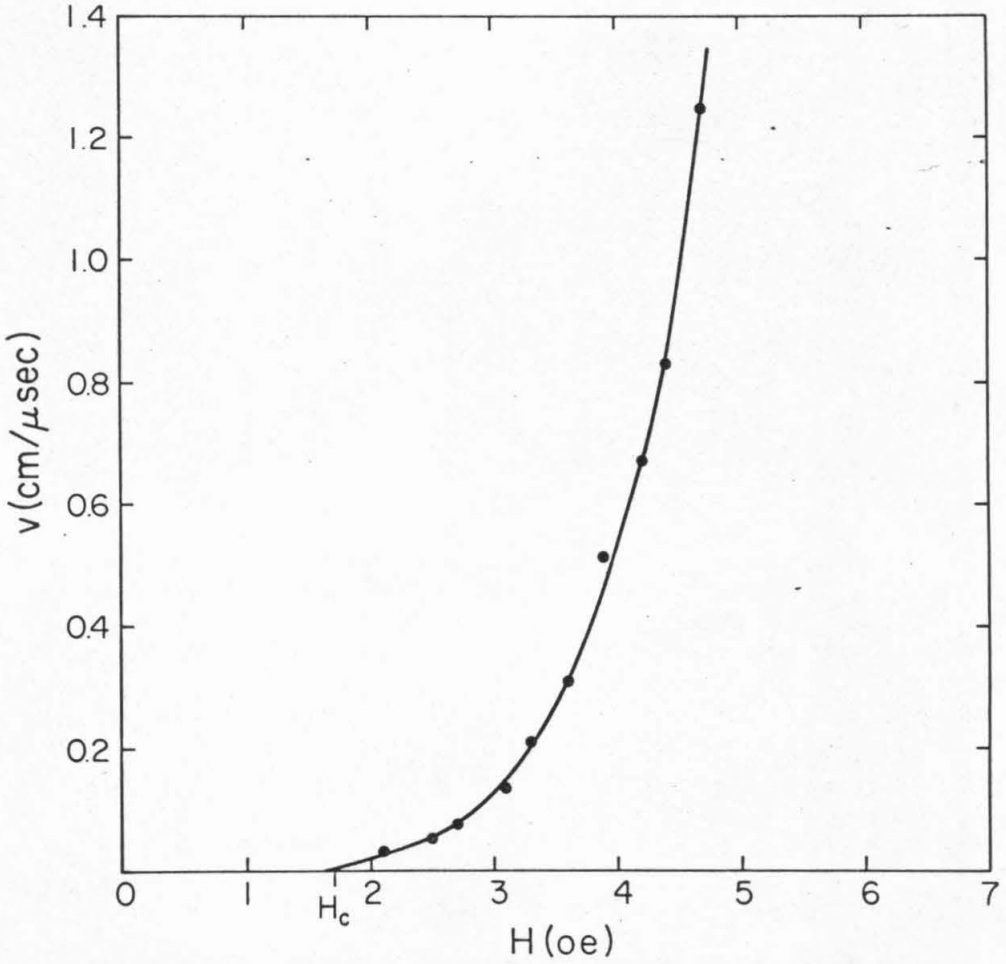

Fig. 4-18. A plot of the experimentally observed velocity versus field dependence of the transverse boundary in film 81-4-12.

been much faster than what can be expected by domain wall motion. The high velocity of the boundary is attributed to its large width. As compared to a domain wall, for a given angular velocity of the magnetization, more of the film is switching per unit time in the diffuse boundary.

The plot of diffuse boundary velocity as a function of field is certainly not linear as in the case of domain wall motion, but varies roughly as the fifth power of the field, going to zero near H_c. In general, if the structure and width of a boundary remain constant, then the viscous flow approximation implies that the velocity should depend linearly on applied field (see Patton and Humphrey (1964)). The nonlinearity of the plot in Fig. 4-18 is attributed to the changes in structure and width that occur as the field is increased. As was seen in Fig. 4-17, the width of the boundary changes considerably as the field is increased; similarly, the photographs of Figs. 4-14 and 4-15 showed that structure changes occur. Qualitatively, it is expected that at higher fields the transverse boundary will propagate with a larger mobility because of the increased width of the boundary; however, until a detailed knowledge of the boundary structure is obtained, it is impossible to understand in detail the velocity dependence of the boundary on the applied field.

4.3 Nucleation of Partially Reversed Regions

Flux reversal by the nucleation of partially reversed regions can be seen in Fig. 4-19. In this case film 81-4-6 is seen reversing with a 5.1 oe longitudinal pulse field and zero transverse bias

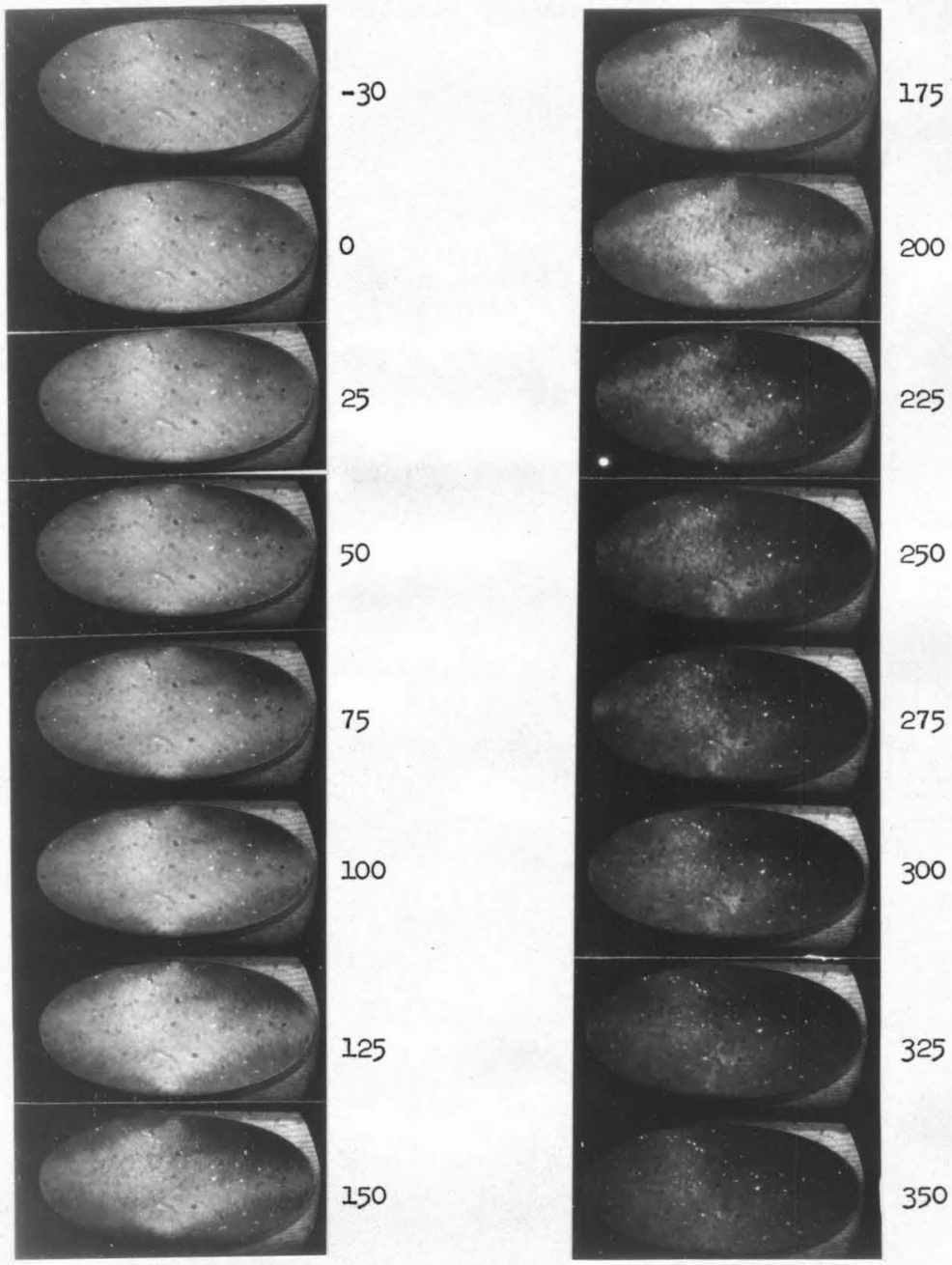

Fig. 4-19. Film 81-4-6 in the process of flux reversal with a 5.1 oe longitudinal pulse field. Time in nanoseconds relative to initial application of pulse field is indicated.

field. Between 0 and 125 nsec a diffuse boundary begins to form much as it did in Fig. 4-2 for lower applied fields. However, from 150 nsec on, nucleated regions begin to appear in the central portion of the film. As time proceeds the film reverses by the nucleation of more and more regions until at 350 nsec it is nearly completely reversed. The nucleation process is more easily seen in Fig. 4-20 which shows the 125, 150, and 175 nsec photographs of Fig. 4-19 with higher magnification. It can be seen that the nucleation is quite complex. The small nucleated regions do not form with well defined shapes nor in a well defined pattern. The tendency for the nucleated regions to extend from the lower left to upper right hand boundary is caused by a slight misalignment ($< 0.1^{o}$ in the clockwise direction) of the pulse field with respect to the easy axis of the film. In cases where the alignment is more precise, the location of the nucleated regions seems to be random.

Figure 4-21 shows film 81-4-12 reversing by the nucleation process with a larger longitudinal pulse field of 7.3 oe. In this case at 25 nsec a reasonably smooth boundary is still evident as it has not had sufficient time to break up and become jagged. At 50 nsec nucleated regions appear throughout the entirety of the central portion of the film. By 75 nsec the nucleated regions have nearly reversed the magnetization in the film and by 100 nsec the reversal is complete. Although much faster, this process is like that in Fig. 4-19.

The nucleation processes seem to be independent of the film edge and hence independent of the shape of the diffuse boundaries. Figure 4-22 shows film 88-14-3 with an applied pulse longitudinal field of 9.4 oe. By 75 nsec small nucleated regions have begun to appear in

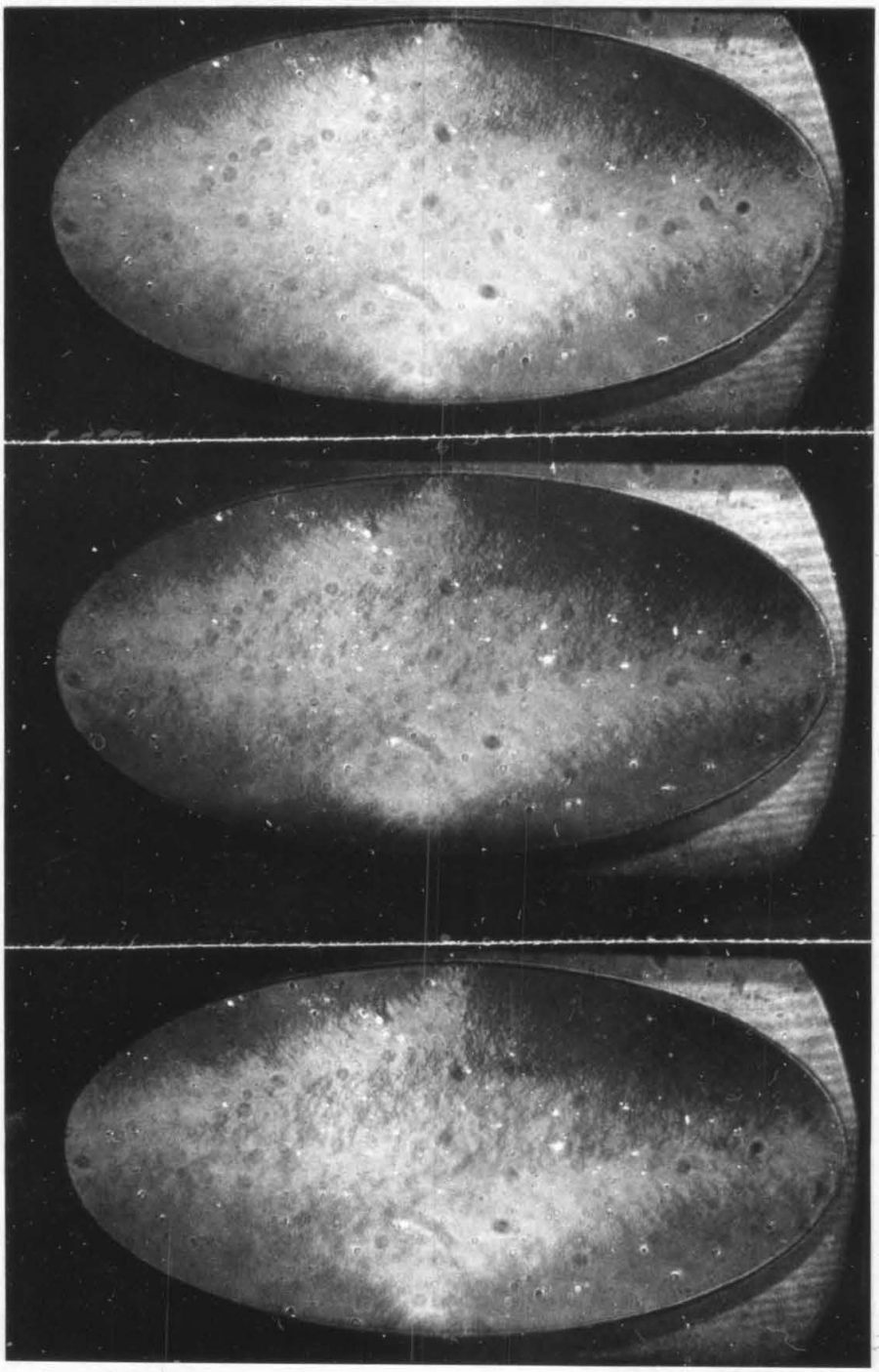

Fig. 4-20. Film 81-4-6 in the process of flux reversal with a 5.1 oe longitudinal pulse field. Time in nanoseconds relative to initial application of pulse field is indicated.

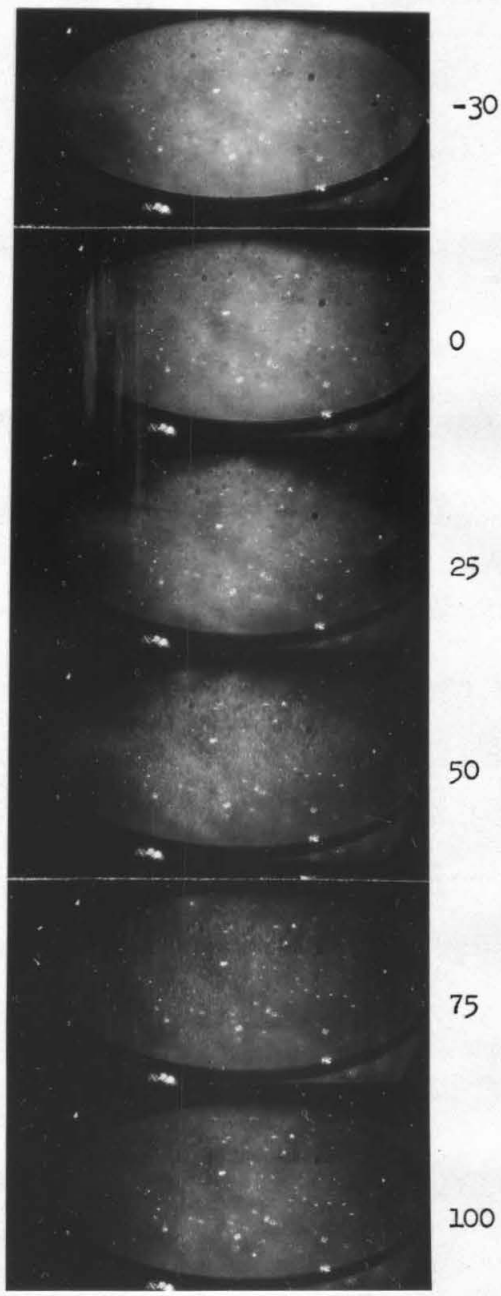

Fig. 4-21. Film 81-4-12 in the process of flux reversal with a 7.3 oe longitudinal pulse field. Time in nanoseconds relative to initial application of pulse field is indicated.

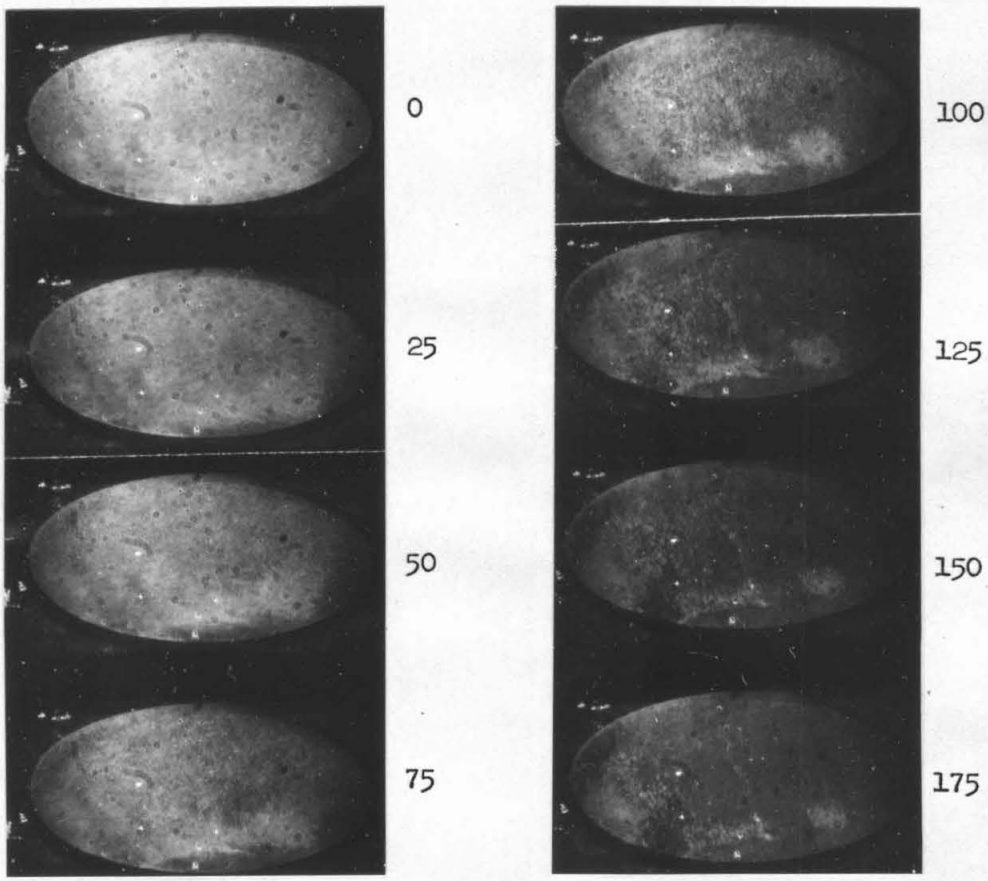

Fig. 4-22. Film 88-14-3 in the process of flux reversal with a longitudinal pulse field of 9.4 oe. Time in nanoseconds relative to initial application of pulse field is indicated.

the film and by 100 nsec they have appeared over most of the film. Diffuse boundaries have not formed at the edges of this film, with the exception of a portion of the lower edge, however. This is because the edges of the film are chamfered, greatly reducing the demagnetizing fields. Thus the boundary is not the cause of the nucleation, but rather as was implied in Sect. 4.2.4, the film seems to have a threshold for nucleation. The presence of magnetostatic fields from a boundary may cause the threshold to be exceeded in regions near the boundary, but the boundary is not necessary for nucleation to occur.

The delay time before nucleated regions begin to appear is significantly long; in Fig. 4-19 they do not appear until 150 nsec; in Fig. 4-21 not until 50 nsec; and in Fig. 4-22 not until 75 nsec. In any one film the delay time is found to decrease with increasing field. The delay is unusual in that no changes in the magnetization configuration are seen to occur in the immediate vicinity of the nucleated regions prior to their appearance. Although Figs. 4-19 and 4-21 seem to indicate the delay is associated with the boundary formation, Fig. 4-22 indicates that the nucleation is independent of the boundaries. The changes which do occur in the magnetization configuration during the delay time must be microscopic in nature, as they cannot be resolved with the Kerr magneto-optic camera. It was observed in Chapter 3 that the nucleation in Figs. 3-1, 3-17 and 3-20 occurred only after the formation of the striped pattern characteristic of the locked ripple configuration. It was suggested then that nucleation only occurred when the reaction torque from the ripple grew large enough to exceed the uniform torque from applied field and uniaxial anisotropy. With zero

transverse field, as was pointed out earlier in Sect. 4.2.2, the uniform torque is very small and the reaction torque from the blocked ripple is believed to prevent the film from reversing. As with a transverse field, it is suggested that the nucleation observed in Figs. 4-19, 4-21 and 4-22 occurs after the blocked ripple builds up in amplitude and rearranges to reduce the magnetostatic fields producing the reaction torque. The long delay time would then be explained by the time required for this rearrangement which, in Fig. 3-17 with a transverse field, took about 100 nsec.

It is probable that the nucleation occurs because of anisotropy dispersion in the magnetic film. Either angular dispersion or amplitude dispersion produces variations in the switching threshold in different regions of the film and it is expected that regions with low thresholds would switch more quickly than those with high thresholds, leading to the observed process. It is also clear, however, that magnetostatic fields must be important, as significant divergences in $\vec{M}$ must occur in the boundaries defining the nucleated regions. Furthermore, the magnetostatic fields from the blocked ripple are believed to prevent the film from reversing when $H_k < H < H_n$, and it is therefore expected that these fields are important in determining the nucleation threshold H_n.

A model of the process leading to the nucleation of partially reversed regions can be made from ripple theory. Remembering that the applied field has a 10 nsec risetime, fast relaxation of the ripple will be assumed as before. As soon as the blocking threshold is

reached, small angle walls form in the ripple and significantly alter its further relaxation. A magnetostatic field results from the blocked ripple which prevents the magnetization from switching, even though the Stoner-Wohlfarth threshold is exceeded. Hence the magnetization remains stable until another threshold is reached at which both the unaxial anisotropy and the magnetostatic stray fields from the blocked ripple are overcome. As $\overline{h_{eff}}(\alpha)$ which is the average effective field from uniaxial anisotropy, external fields and the longitudinal magnetostatic field from the blocked ripple decreases, the local anisotropy fields become important and cause regions of reversed magnetization to nucleate in the film. Using this model, a conservative estimate of the nucleation threshold can be made. Since the largest effective field due to angular and amplitude anisotropy dispersion h_{k2} (given by (2.41a)) is much smaller than the magnetostatic fields h_d (given by (2.41e)), in order for an instability to occur the single domain field $h(\alpha)$ must at least become sufficiently negative to overcome the average magnetostatic fields existing at blocking, h_a (see (2.49)). Using $S = 6.1 \times 10^{-3}$ determined from the data of Fig. 3-14a for film 81-4-6, it is calculated that nucleation cannot be expected at least until $h(\alpha) \simeq -0.2$, or $H = 4.3$ oe. The fact that this estimate is below the observed threshold near 5 oe is expected, since the increase in applied field antiparallel to $\vec{M}_o$ beyond the blocking threshold at $H \simeq 2.9$ oe must certainly increase the blocked ripple amplitude (and therefore increase $\overline{h_d} \propto \varphi^2$) . More must be learned about the blocked ripple state and how the applied

fields affect it before more accurate calculations of H_n can be made, and before the actual nucleation process can be understood.

4.4 Summary.

Switching with zero transverse field has been investigated for fields slightly above H_c, the coercive force, to several times H_k, the anisotropy field. Three mechanisms of reversal have been found to be important: (1) domain wall motion, (2) diffuse boundary propagation, and (3) the nucleation and subsequent reversal of partially reversed regions. In general it has been found that domain wall motion switches most of the film when fields $H \simeq H_c$ are applied and that domain wall motion is gradually replaced by diffuse boundary propagation as the field is increased. Diffuse boundary propagation occurs with fields up to the nucleation threshold $H_n > H_k$. At and above H_n, the nucleation and subsequent reversal of partially reversed regions occurs.

The longitudinal propagation of diffuse transverse domain boundaries is very different from the transverse propagation of longitudinal domain walls. The diffuse boundaries are jagged and have extremely complex structures, while the domain wall is smooth and of a simple structure by comparison. The diffuse boundaries are observed to propagate at velocities which are 1 to 3 orders of magnitude greater than those for domain wall motion. Furthermore, the velocity of the boundary is found to vary nonlinearly with the applied field. Since the structure of the boundary depends upon the applied field, this nonlinear dependence is expected; however, because the detailed structure of the boundary is not understood, no theoretical treatment of

the velocity could be made. The cause of the boundary formation process was shown in some cases to be the edge demagnetizing fields in a film. In other cases macroscopic anisotropy dispersion made it possible for regions to nucleate in the center of a film and hence to form diffuse boundaries there.

Nucleation of partially reversed regions was discussed and estimates of the nucleation threshold were made. The cause of the nucleation process was believed to be local anisotropy variations.

Chapter 5

Relaxation Processes

5.1 Introduction.

Relaxation processes which occur when the pulse magnetic field is terminated during a flux reversal can also be studied with the Kerr magneto-optic camera. These relaxation processes are interesting for at least two major reasons. First, since the relaxation which occurs alters the magnetization configuration, it is misleading to infer the previous dynamic magnetization configuration by observing the static domain pattern after termination of the field. The validity of experiments previously performed using such interrupted pulse techniques is in question. Secondly, the relaxation processes are interesting because they yield additional information about the state of the magnetization during the flux reversal process and give insight into the difference between dynamic and static domain configurations.

The relaxation processes vary according to the flux reversal process which precedes them, so that the relaxation which occurs after a propagational process is different from the relaxation which occurs after a rotational process. In general, it is found that diffuse boundaries become more well defined when the field is terminated and that they remain in approximately the same position. Nucleated regions are frequently observed to revert to the non-reversed state, and the striped configuration characteristic of non-coherent rotation is frequently found to disappear entirely, either as $\vec{M}_o$ continues to reverse or relaxes to the non-reversed state. The one factor common

to all of the relaxation processes is the long time constant for the relaxation to be complete. Static equilibrium is not obtained until at least 200 nsec after the field is terminated which is roughly two orders of magnitude longer than the time constant for decay of oscillations of $\vec{M}_o$ about an equilibrium position.

5.2 Relaxation with Zero Transverse Field.

A typical series of photographs showing relaxation with zero transverse field is shown in Fig. 5-1 where film 81-4-6 is photographed during and after a 70 nsec long 6.0 oe longitudinal pulse field. It can be seen that the reversal begins with the formation of transverse diffuse boundaries at the edges of the film. This boundary formation process is like that described earlier in Sect. 4.2.3. The boundary is seen forming 5 nsec after the field was applied. At 20 nsec the boundaries are still quite broad and relatively smooth and have propagated inwards from the edges of the magnetic film. By 40 nsec the boundaries are beginning to become jagged. At 70 nsec, just prior to the termination of the pulse field, the boundary has become quite jagged and regions of partially reversed magnetization are beginning to appear in the central portion of the magnetic film. Note that even the upper boundaries which are in focus are rather poorly defined. By 100 nsec, 30 nsec after the field began to fall (falltime $\simeq$ 20 nsec), there has been little or no significant change in the magnetization configuration. A comparison of the 120 nsec photograph with the 70 nsec photograph reveals that by 120 nsec the boundary definition is beginning to improve. By 200 nsec the definition has improved still more and by 500 nsec the boundary is sharply defined though still quite jagged. A comparison of the 20,000 nsec photograph with the 70 nsec photograph

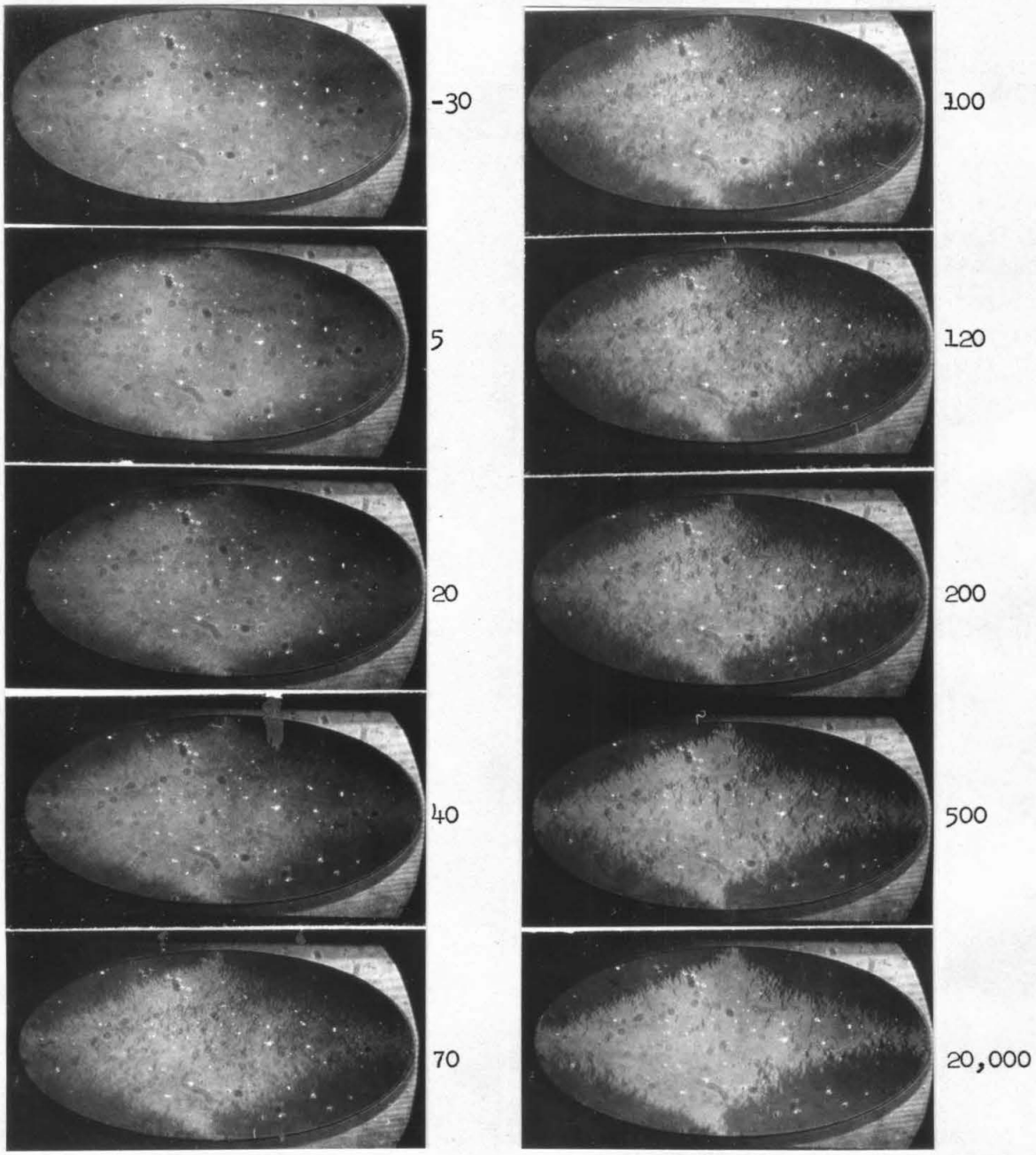

Fig. 5-1. Film 81-4-6 in the process of flux reversal and relaxation to static equilibrium during and after a 70 nsec long 6.0 oe longitudinal pulse field. Time in nanoseconds relative to initial application of pulse field is indicated.

reveals that the boundary which results in the final static state is much more well defined than the dynamic boundary which exists before the field is terminated. Many of the nucleated regions present in the 70 nsec photograph are not present in the 20,000 nsec photograph.

Another example of this type of relaxation is shown in Fig. 5-2 where film 81-4-6 is seen relaxing to static equilibrium after the termination of a 200 nsec long longitudinal pulse field of 5.1 oe. In the 200 nsec photograph, just prior to termination of the drive field, poorly defined diffuse boundaries are visible. Nucleated regions are present in the central portion of the film. By 225 nsec, just 25 nsec after the pulse field began to fall (falltime = 20 nsec) changes have begun to occur in the magnetization configuration. The boundaries have become slightly more well defined and some of the partially reversed regions have begun to relax back to the non-reversed state. It is seen that as time proceeds the boundary becomes ever more sharply defined and most of the nucleated regions revert back to the non-reversed state. Because the relaxation processes are not perfectly reproducible, comparisons between photographs to determine when the relaxation is complete are difficult; however, close inspection of the definition of the boundaries reveals that by roughly 500 nsec the relaxation is complete with the possible exception that some of the nucleated regions have not yet reached static equilibrium.

The relaxation time, or time for the dynamic boundary to become static is seen in Figs. 5-1 and 5-2 to be at least 200 nsec. This is long in comparison to either the experimental or theoretical (see

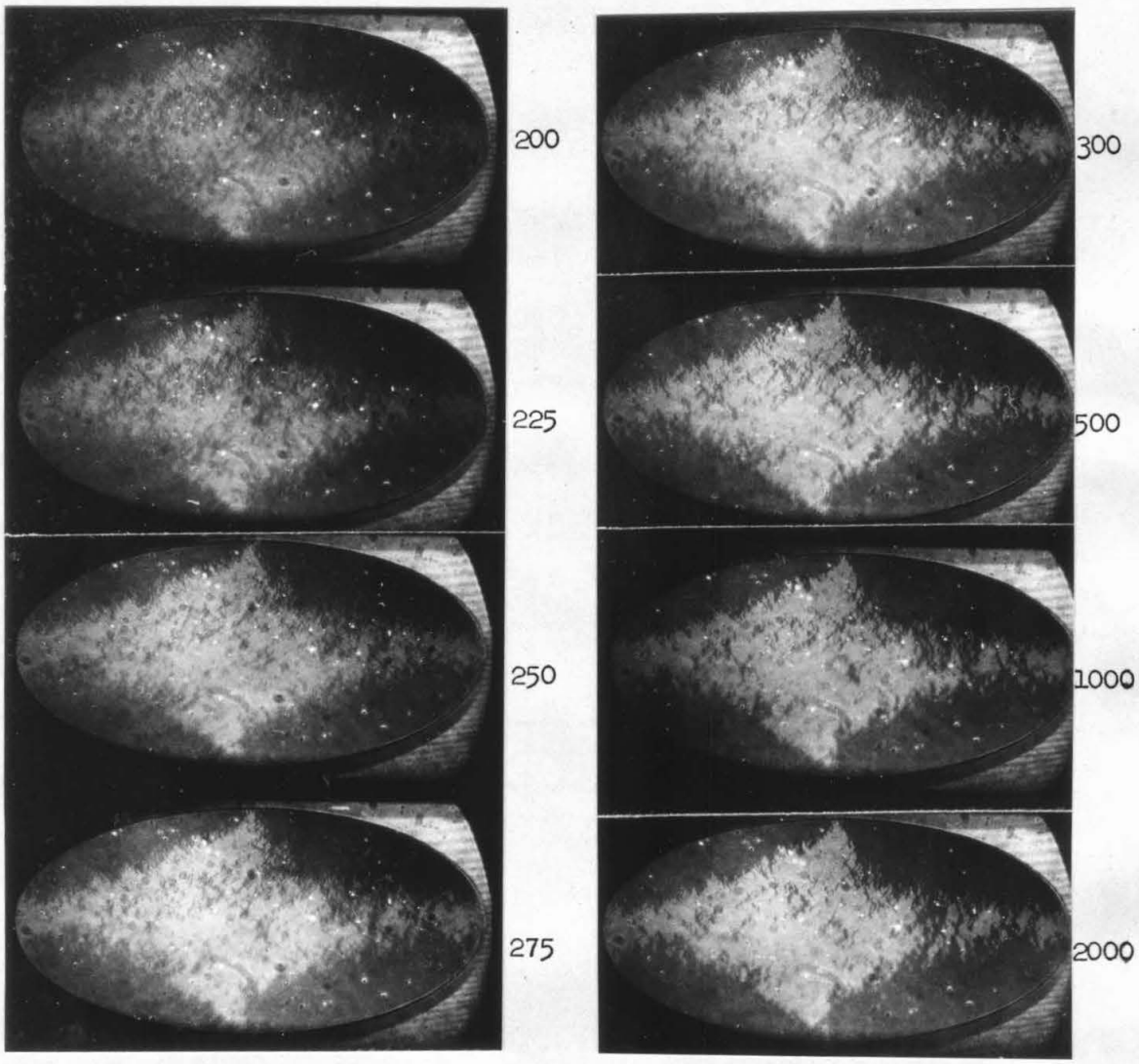

Fig. 5-2. Film 81-4-6 in the process of relaxation to static equilibrium after a 200 nsec long 5.1 oe longitudinal pulse field. Time in nanoseconds relative to initial application of pulse field is indicated.

equation (3.3)) relaxation time for ripple, both of which are of the order of 1 nsec. Similarly it is long compared to the theoretical relaxation time of oscillations of the mean magnetization about an equilibrium position, which can be calculated to be the same as that for ripple relaxation. Jaecklin has done some experimental (1967) and theoretical (1969) work on a problem which, although not directly applicable, provides some insight into why the relaxation time of the diffuse boundary should be so long. A non-uniform transverse pulse field ($> 2H_k$) obtained with a strip line which covered only a small portion of the film (see Fig. 5-3) was applied to a saturated magnetic film with a static, uniform longitudinal field ($< H_c$) applied antiparallel to the mean magnetization. The equilibrium magnetization configuration after application of the fields was calculated to involve a region of "curled" magnetization as indicated in Fig. 5-3. Jaecklin (1967) found that the application of the hard axis pulse field caused a wide propagating wave front to form which traveled as far as 0.63 cm through the material at a velocity of about 10^7 cm/sec. The final equilibrium curled state was not obtained until after 40 nsec (much longer than the risetime of his pulse). Jaecklin (1969) employed the Gilbert (1955) form of the equation of motion with phenomenological damping of $\alpha_d \simeq 0.02$ to obtain reasonable agreement with his experimental values. The reason it took approximately 40 nsec for equilibrium to be established was that the magnetization at the edge of the curled region did not rotate until after sufficient time elapsed for the propagating wavefront to reach it. Thus, the sequential (as opposed to purely rotational) nature of the process was the cause for the long relaxation time.

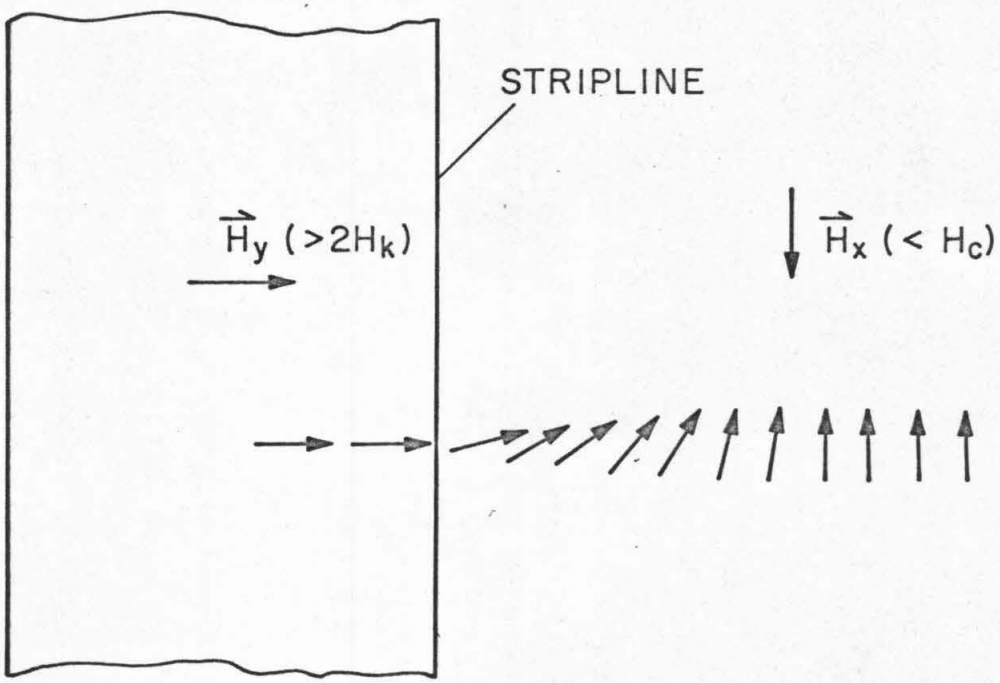

Fig. 5-3. Diagram showing the relative directions of applied fields and the curled magnetization state in the experiments performed by Jaecklin (1967).

The diffuse boundary is, of course, much more complex than the curled magnetization configuration which Jaecklin (1967,1969) considered, but nevertheless his results indicate that relaxation times much greater than the intrinsic relaxation time for oscillations of $\vec{M}_o$ can be expected from sequential processes. In the dynamic diffuse boundary, as was seen in Chapter 4 and in Figs. 5-1 and 5-2, there are regions of partially reversed magnetization. It is reasonable to assume that these partially reversed regions relax by a sequential process much in the same manner as the "curled" region which Jaecklin investigated. Furthermore, the magnetostatic coupling between different partially reversed regions can be expected to cause the different regions to relax successively, thereby further increasing the relaxation time.

An example of the difference between reversals by interrupted pulses and a single pulse is shown in Figs. 5-4a,b. The photographs obtained for a series of 1 μsec interrupted pulses are shown in Fig. 5-4a and at 1 μsec intervals for a continuous pulse in Fig. 5-4b. It is seen that the reversal process remains basically the same whether a continuous pulse or interrupted pulses are used. The boundary is more well defined in the interrupted pulse photographs (Fig. 5-4a) as they show the static boundaries rather than the dynamic boundaries. Reversal with interrupted pulses takes approximately 20% longer than reversal with a continuous pulse, suggesting that either the more sharply defined boundary moves more slowly than the original dynamic boundary, or that 200 nsec is required for the static boundary to again become dynamic.

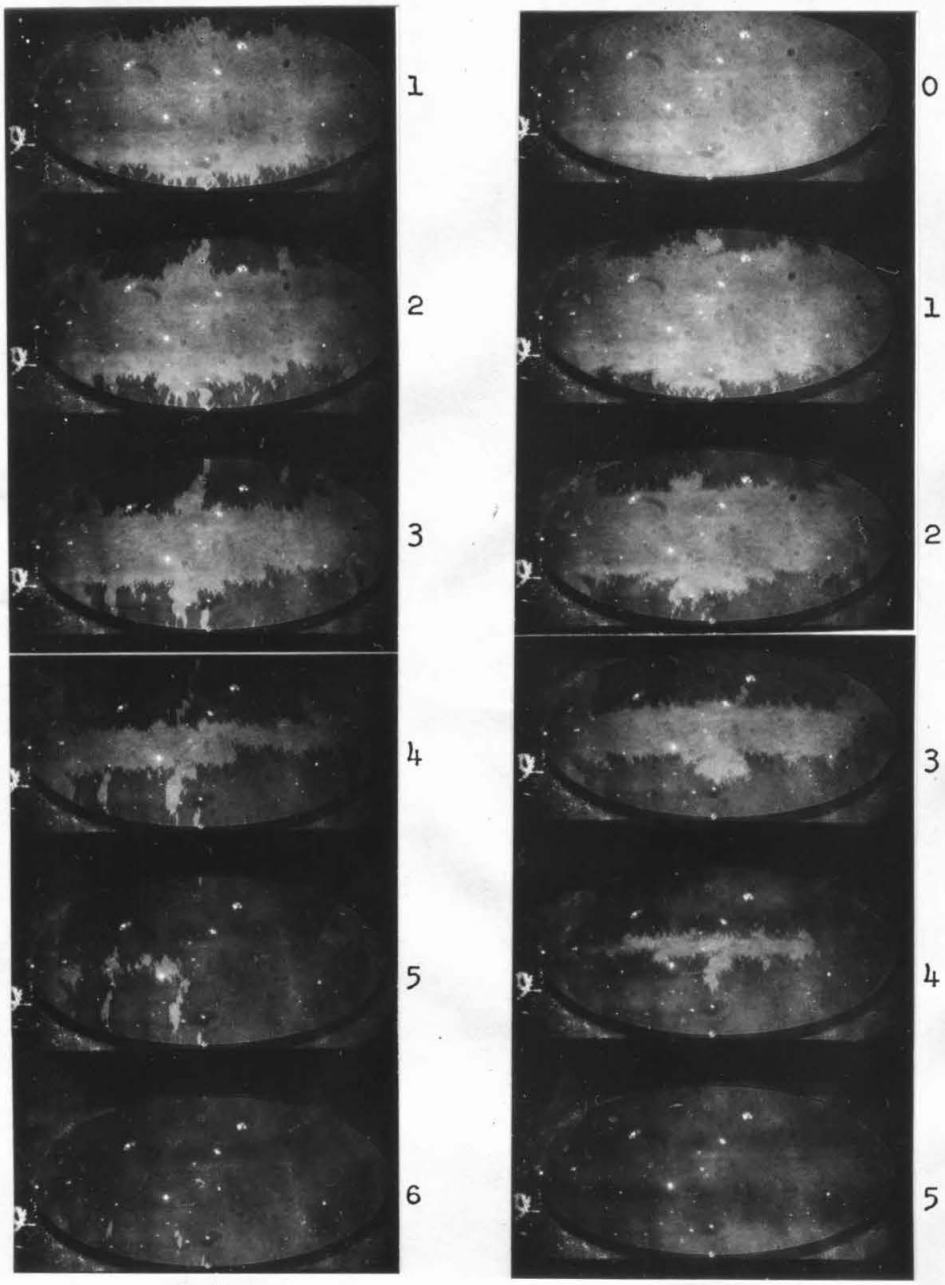

Fig. 5-4 (a) Film 81-4-12 in the static state obtained after multiple 1 μsec long 2.98 oe longitudinal pulses. Number of pulses applied before each photograph is indicated. (b) Film 81-4-12 in the process of flux reversal during a continuous 2.98 oe longitudinal pulse field. Time in microseconds relative to initial application of pulse field is indicated.

In Figs. 5-5a,b is a comparison of flux reversal by a continuous pulse of 2.64 oe and flux reversal by multiple 50 nsec pulses of the same amplitude. The pulse was made 50 nsec wide at the top of the pulse, giving it a 60 nsec width between points of 50% maximum amplitude (risetime = falltime = 10 nsec). It is seen that reversal by multiple 50 nsec pulses is considerably slower than reversal by a continuous pulse with a significant change of mechanism. With the continuous pulse the reversal is accomplished by the propagation of diffuse transverse domain boundaries. With the multiple 50 nsec pulses, reversal is accomplished by a sort of zig-zag boundary. Furthermore, with a continuous pulse the transverse boundaries extend almost completely across the film, while with the multiple pulses they extend only through a portion of the film, leaving the extreme right and left hand edges unswitched.

To further characterize the difference between reversal by continuous and interrupted pulses, photographs were taken during the second pulse. Examples of these photographs are shown in Figs. 5-6a-e. The photographs labeled by "s" show the static boundaries created by a 1.5 μsec long 3.0 oe longitudinal pulse field. The subsequent photograph shows the same boundary at the time shown after the application of a second 3.0 oe pulse field. In Fig. 5-6a it can be seen that very little if any change occurs in the boundary during the first 25 nsec of a second pulse. Fig. 5-6b shows that only very minor changes occur in 50 nsec; for example, within the square a slight change did occur as a slender region of magnetization rotated from the non-reversed state. The contrast clearly indicates that the small region is only partially re-

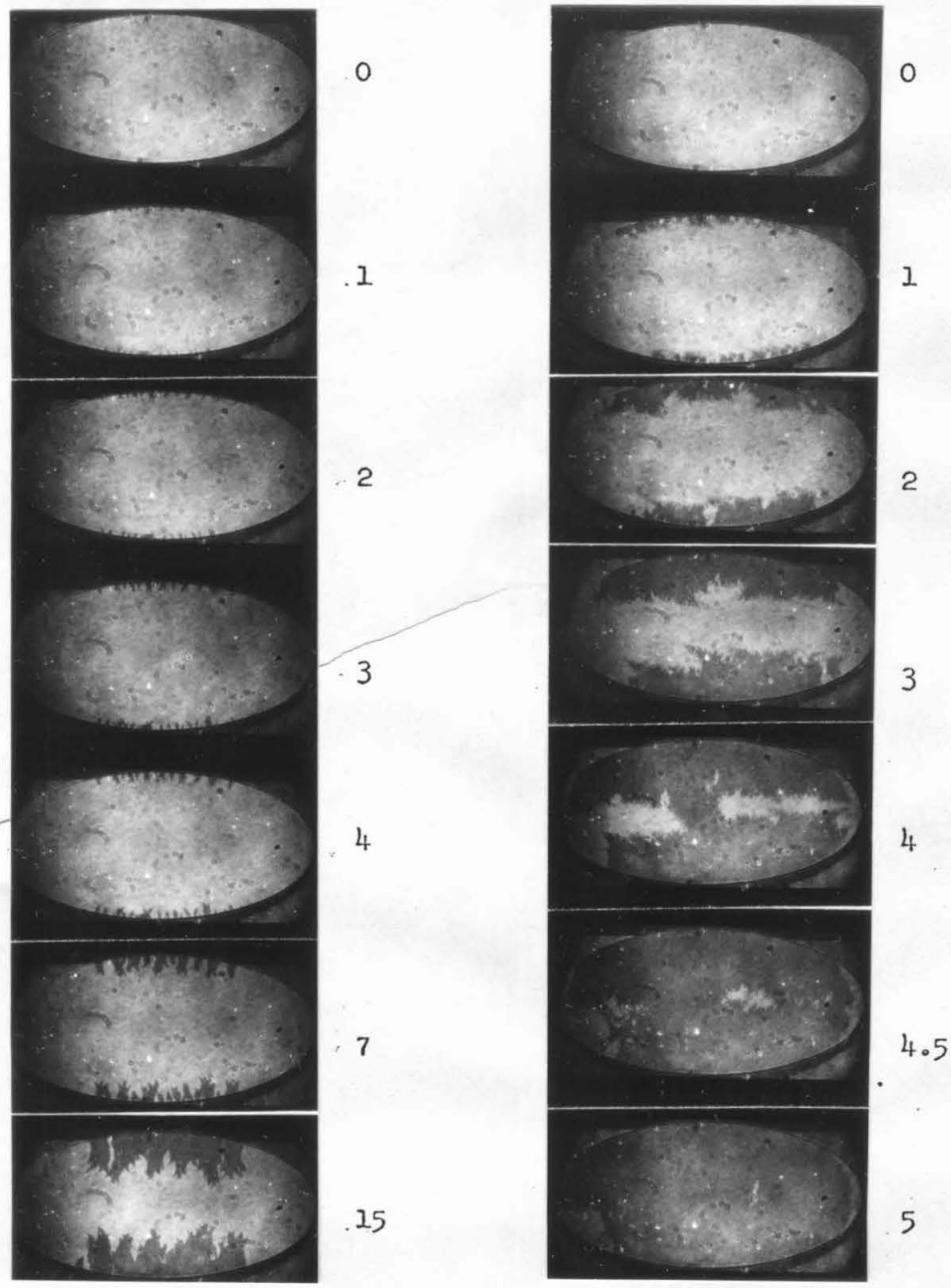

Fig. 5-5 (a) Film 81-4-12 in the static state obtained after multiple 50 nsec long, 2.64 oe longitudinal field pulses. Total duration of pulses in microseconds before each photograph is indicated. (b) Film 81-4-12 in the process of flux reversal during a continuous 2.64 oe longitudinal field pulse. Time in microseconds relative to initial application of pulse field is indicated.

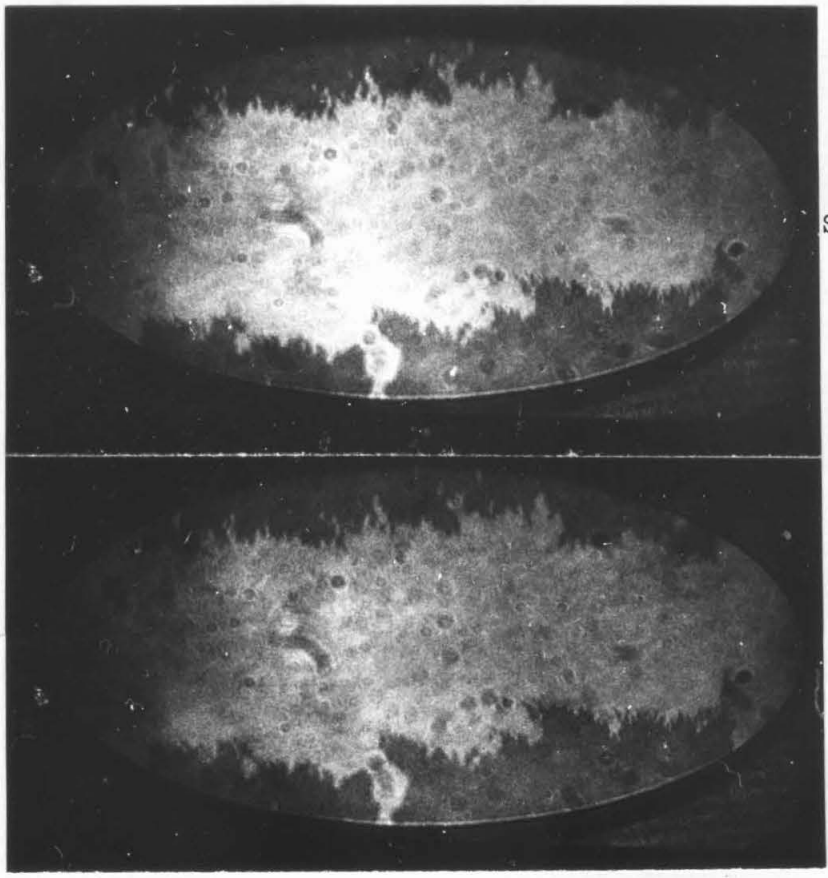

Fig. 5-6 (a) Film 81-4-12 in the static state which results after a 1.5 μsec long, 3.0 oe pulse field (denoted by "S") and in the dynamic state existing 25 nsec after application of a second pulse field of the same amplitude (denoted by 25).

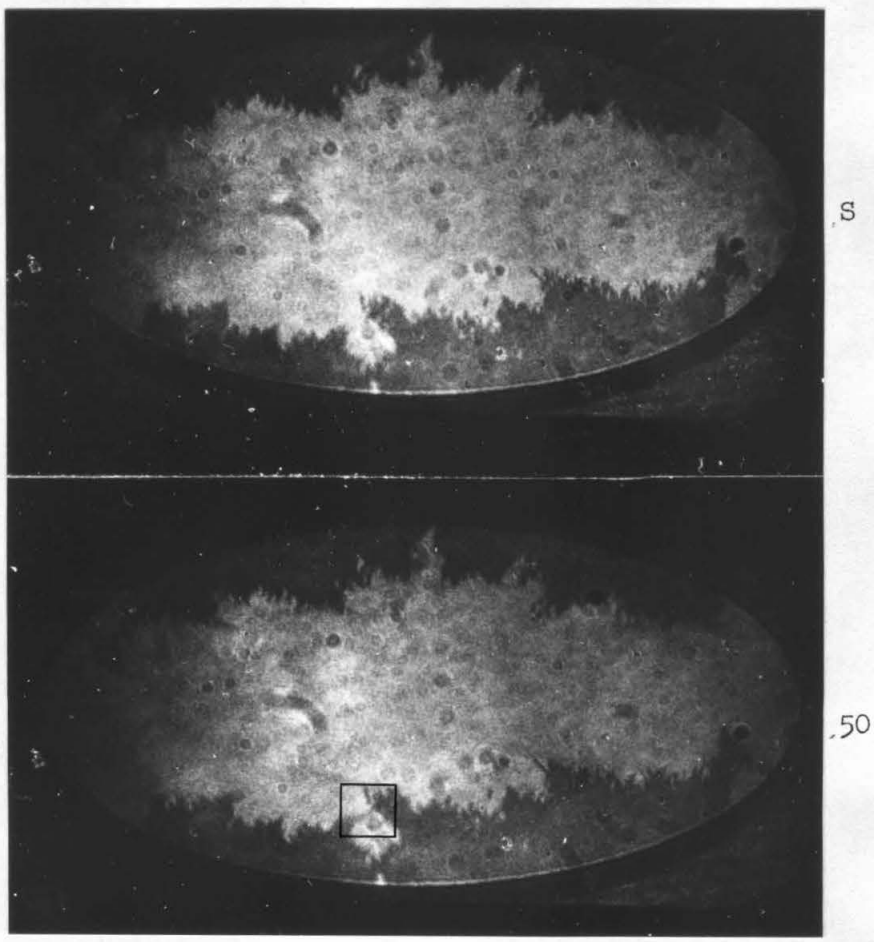

Fig. 5-6 (b) Film 81-4-12 in the static state which results after a 1.5 μsec long, 3.0 oe pulse field (denoted by "S") and in the dynamic state existing 50 nsec after application of a second pulse field of the same amplitude (denoted by 50).

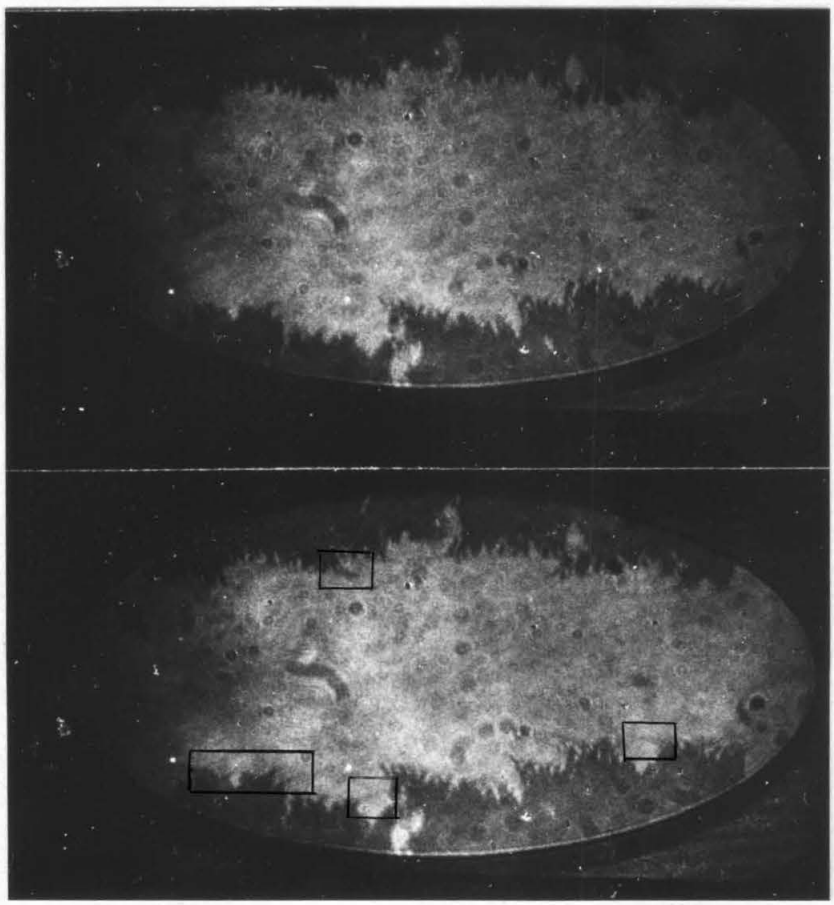

Fig. 5-6 (c) Film 81-4-12 in the static state which results after a 1.5 μsec long 3.0 oe pulse field (denoted by "s") and in the dynamic state existing 100 nsec after application of a second pulse field of the same amplitude (denoted by 100).

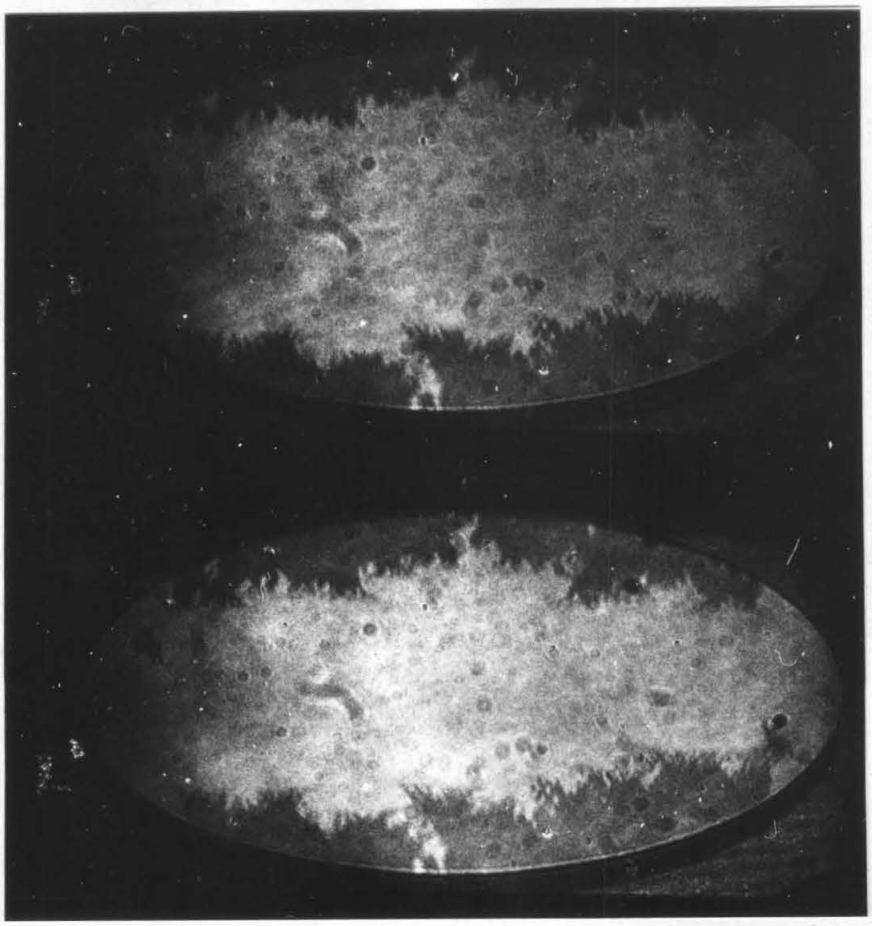

Fig. 5-6 (d) Film 81-4-12 in the static state which results after a 1.5 μsec long 3.0 oe pulse field (denoted by "s") and in the dynamic state existing 150 nsec after application of a second pulse field of the same amplitude (denoted by 150).

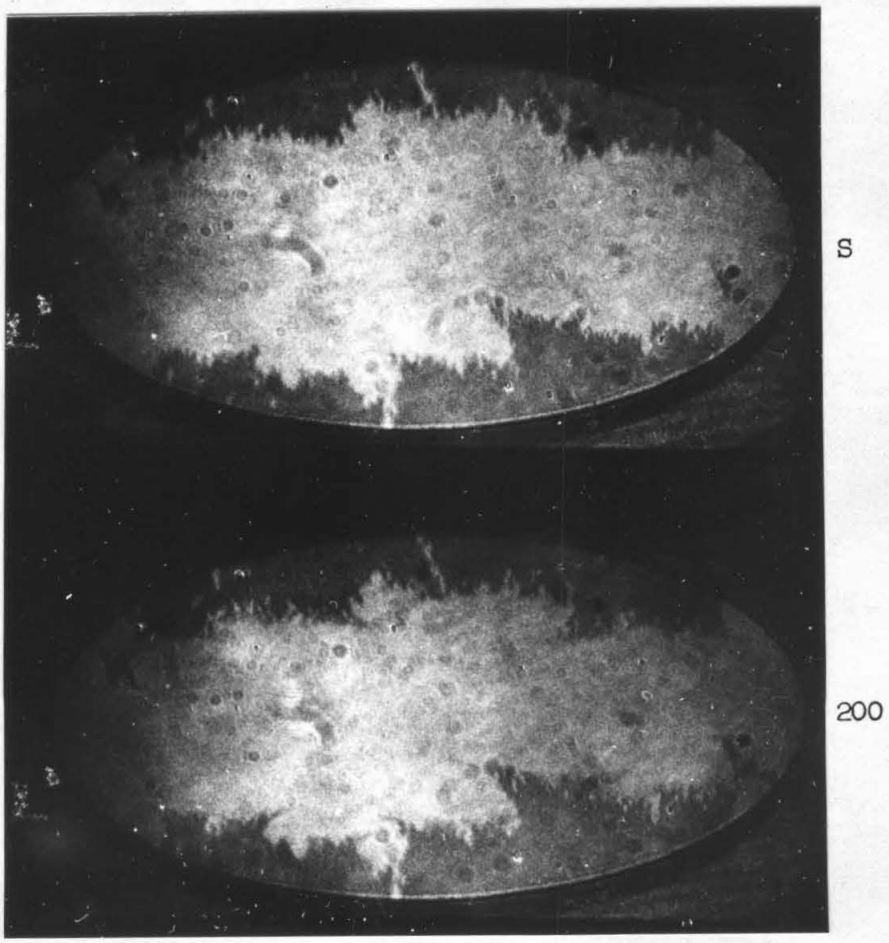

Fig. 5-6 (e) Film 81-4-12 in the static state which results after a 1.5 μsec long 3.0 oe pulse field (denoted by "s") and in the dynamic state existing 200 nsec after application of a second pulse field of the same amplitude (dentoed by 200).

versed. In Fig. 5-6c, 100 nsec after application of a second pulse, much of the boundary has partially rotated regions extending from it. However, there has been very little propagation of the boundary. Again, note the regions in the rectangles where the magnetization has partially rotated. By 150 nsec, in Fig. 5-6d, much of the boundary has become truly dynamic. Large portions of the boundary have propagated and the boundary is becoming much more poorly defined. Fig. 5-6e shows the boundary 200 nsec after the application of a second pulse field. It is seen that essentially all of the boundary has propagated significantly. The dynamic boundary is much more poorly defined than the previous static boundary. This poor definition is caused by the wide areas which are only partially rotated.

The photographs in Figs. 5-1 through 5-6 show that there is a significant difference between the dynamic diffuse boundary and the static boundary which results when the field is terminated. These differences make the use of multiple pulse techniques clearly inappropriate for the study of diffuse boundary propagation. Multiple pulses were used with low applied fields by Bourne et al. (1968) in their study of diffuse boundary propagation leading to errors in the measured velocity. Multiple pulse techniques probably led them to report that, at low fields, flux reversal is accomplished by the propagation of zig-zag boundaries which, as was seen in Fig. 5-5, results when multiple short pulses are applied. In Chapter 4 it was seen that the dynamic boundary is poorly defined and propagates by the rotation of the magnetization in regions ahead of the boundary rather than by the smooth propagation of zig-zag tips of reversed magnetization as Bourne et al. (1968) suggested.

In summary, then, it has been shown that if the longitudinal pulse field is terminated while the magnetic film is in the process of flux reversal, significant changes occur in the magnetization configuration before equilibrium is established. Typically, diffuse boundaries become more sharply defined and nucleated regions tend to relax back to the non-reversed state. Flux reversal by a series of pulses is different and longer than reversal by a single pulse because times of the order of 200 nsec are required for static boundaries to become dynamic when another field pulse is applied. Similarly, the relaxation time of the dynamic boundary was of the order of 200 nsec.

5.3 Relaxation with an Applied Transverse Field.

Relaxation processes occurring after termination of the longitudinal pulse field with a transverse bias field applied, like the zero transverse field case, cause significant changes to occur in the magnetization configuration. Depending on the size of the ripple reaction torque and the direction of the magnetization when the field is terminated, the magnetization in partially reversed regions either continues to reverse after the field is terminated, or reverts to the non-reversed state, further complicating the interpretation of static domain patterns which result when the field pulse ends. Like the case of zero transverse field, the time required for static equilibrium to be obtained after termination of the pulse field is at least 200 nsec.

Relaxation processes which occur after termination of the pulse field cause diffuse boundaries to become sharply defined when the field is terminated, but to remain in roughly the same position. The time

required to obtain static equilibrium is roughly the same whether a transverse field is applied or not. It is reasonable that the relaxation is similar to the zero transverse-field case as the structure of the boundaries is observed to be similar.

With higher drive fields where the flux reversal process is noncoherent rotation, considerable change occurs in the magnetization configuration. Figure 5-7 shows film 81-4-6 in the process of relaxation to static equilibrium after the termination of a 75 nsec long 1.7 oe longitudinal pulse field in the presence of a 1.0 oe transverse bias field. At 75 nsec after the application of the pulse field the film is seen in the dynamic state immediately prior to termination of the longitudinal pulse field. The striped configuration characteristic of the locked state discussed in Chapter 3 is evident. The contrast indicates much of the magnetization in the film is only partially rotated. The field is terminated at 75 nsec with a falltime of approximately 10 nsec. It can be seen that, in the 100 nsec photograph, taken 25 nsec after the start of the falltime, the stripes have begun to break up by a sort of nucleation process. The contrast indicates that the magnetization has begun to rotate to equilibrium, but that many partially rotated regions still exist. By 200 nsec, 125 nsec after the field was terminated, there has been considerable change in the magnetization configuration. The contrast now indicates that most of the magnetization is no longer partially rotated, but is either reversed or not reversed. By 500 nsec additional changes have occurred, as the reversed region has become smaller and the striped pattern is thoroughly broken up by small nucleated regions. After

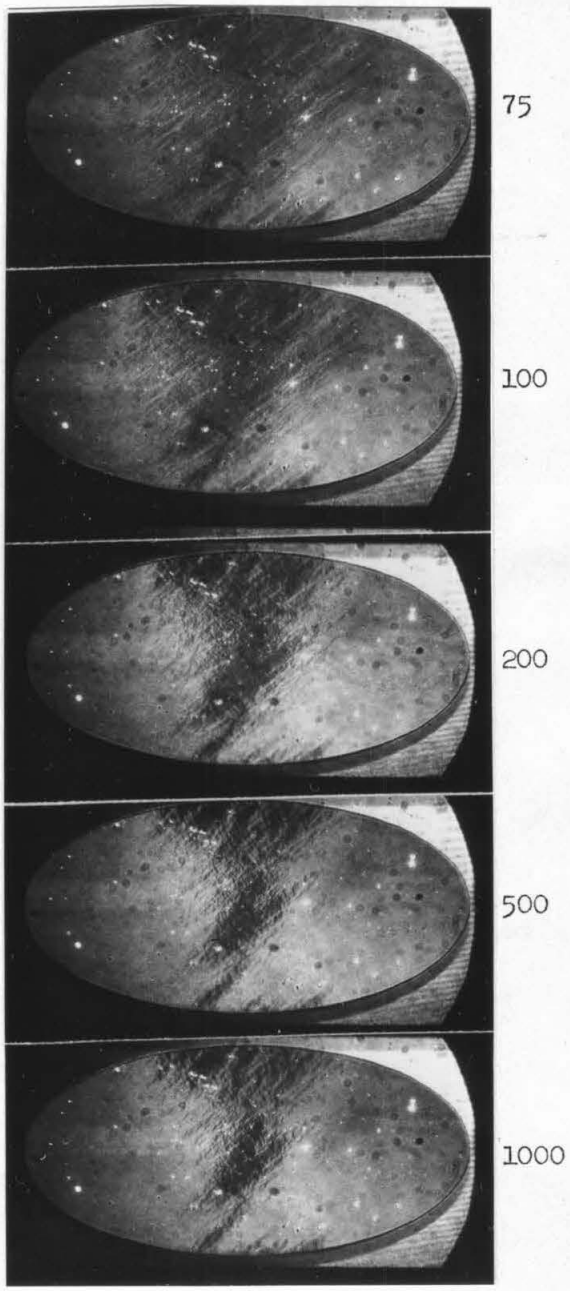

Fig. 5-7. Film 81-4-6 in the process of relaxation to static equilibrium after the termination of a 75 nsec long, 1.7 oe longitudinal pulse field in the presence of a 1.0 oe transverse bias field. Time in nanoseconds relative to initial application of pulse field is indicated.

500 nsec no additional change is seen to occur as the 1000 nsec photograph is essentially identical to the 500 nsec photograph.

From Fig. 5-7 it is seen that relatively large changes occur in the magnetization configuration when the field is terminated. Much of the partially reversed magnetization in the dynamic state reverted to the non-reversed state after the field was terminated. One obvious reason that the magnetization would revert to the non-reversed state in some areas is that where $\varphi_o < 90^o$ the torque from uniaxial anisotropy is negative. In addition to this torque, however, there is the reaction torque from the locked ripple. As long as $\varphi_o - \varphi_\ell < 90^o$ this torque is also negative. Hence, since $\varphi_\ell \simeq 55^o$ in this case, it is possible that in certain areas of the film the magnetization could even be rotated past 90^o and still have a net torque which acts to restore it to the non-reversed state. Unfortunately, the accuracy with which the magnetization direction can be estimated is limited; however, by making visual comparisons of contrast in partially-, totally-, and non-reversed areas of the film, a semi-quantitative determination of Φ can be obtained. On this basis it was determined that the magnetization in the central area of the magnetic film in the 75 nsec photograph was rotated by more than 90^o even though much of the magnetization in this area relaxed to the non-reversed state, demonstrating the reaction torque which is caused by the locked ripple.

Although the final static state in Fig. 5-7 does show some evidence of the stripes which existed prior to termination of the field, their direction is not as well defined as in the dynamic state.

Furthermore, the nucleation has broken up the original stripes. The energy from the magnetostatic stray fields is reduced as a result of this "breaking up" of the long stripes by the elimination of divergences in the form of line-charges along the stripe boundaries and permitting flux closure to be obtained within much smaller areas of the film.

The relaxation which occurs in Fig. 5-7 is an example of the relaxation which occurs after the pulse magnetic field is terminated, but is not what occurs in all cases. Not only are the relaxation processes which occur with different applied fields and pulse lengths very dissimilar, but the relaxation processes are not even reproducible when the fields and pulse lengths are kept the same. Unlike dynamic flux reversal, the relaxation processes change with each subsequent pulse. By taking a large number of photographs at the same delay time setting it is possible to obtain a representative sequence like that in Fig. 5-7.

Figure 5-8 shows film 81-4-6 during and after a 75 nsec long 4.1 oe longitudinal pulse field in the presence of a small 0.1 oe transverse bias field. This sequence shows other typical characteristics of the relaxation. At -30 nsec the film is in the reset condition before the pulse field is applied. There is little or no change in the 0 nsec photograph, but at 25 nsec stripes are barely visible in the region of the film near the upper edge. At 50 nsec stripes are clearly visible and it appears that nucleation like that in Fig. 3-17 is about to occur. At 75 nsec, just prior to termination of the pulse field a large portion of the magnetization in the

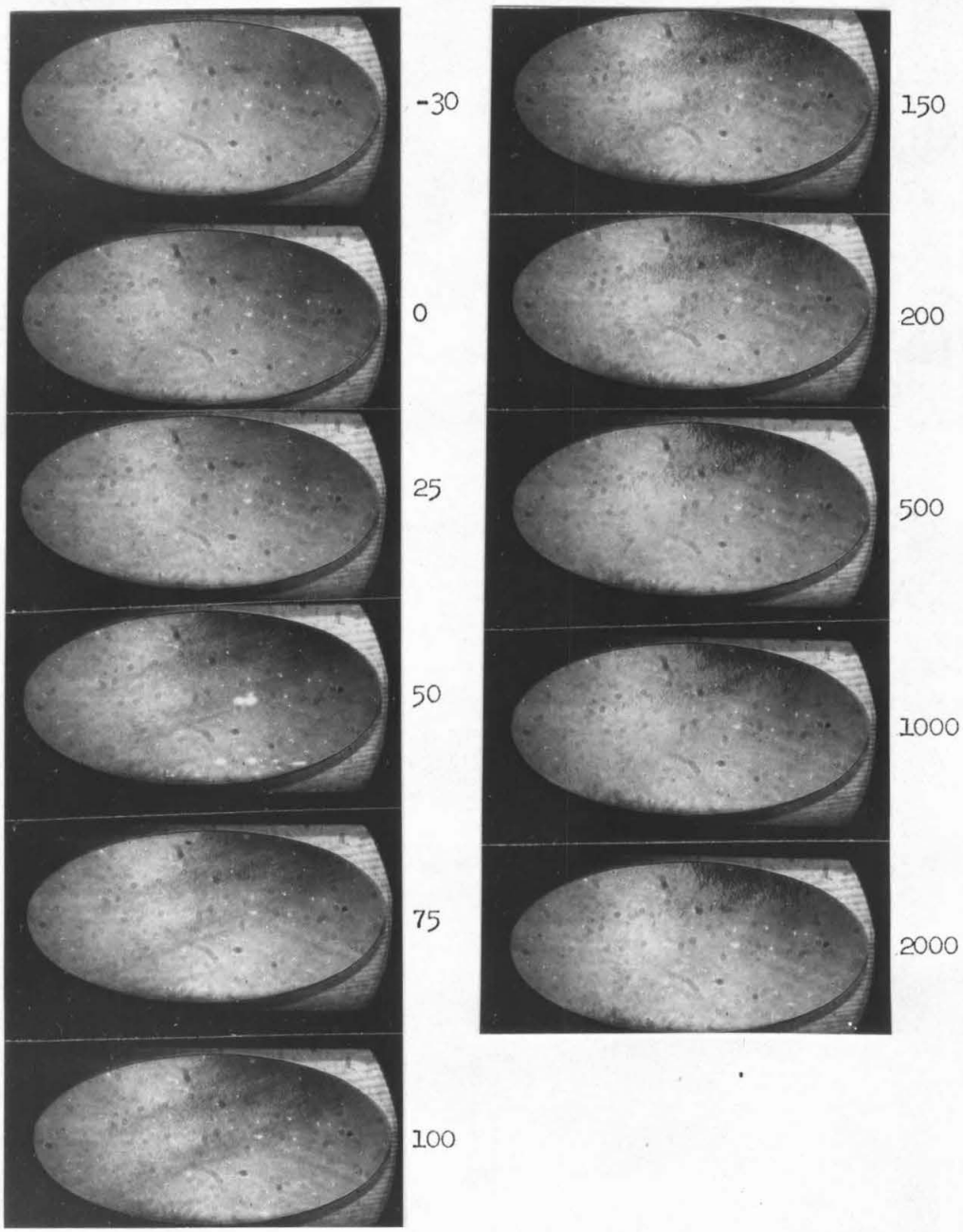

Fig. 5-8. Film 81-4-6 in the process of flux reversal and relaxation to static equilibrium during and after a 75 nsec long, 4.1 oe longitudinal pulse field with 0.1 oe transverse bias field applied. Time in nanoseconds relative to initial application of pulse field is indicated.

film is partially rotated and in a striped pattern with nucleated regions appearing in the more fully reversed areas. The field is terminated at 75 nsec with a falltime of 20 nsec. At 100 nsec (25 nsec after the field began to fall) the magnetization in the partially rotated regions has rotated additionally. However, at 150 nsec the partially rotated magnetization has begun to relax back to its original state. Between 150 and 200 nsec more of the magnetization returns to the non-reversed state and similarly a small amount of relaxation occurs between 200 and 500 nsec. As in Fig. 5-6, there is little or no relaxation after 500 nsec. Comparing the final static state observed at 2000 nsec with the dynamic state which existed at 75 nsec in Fig. 5-6, it is seen that large changes occur during the relaxation process. While at 75 nsec there is a lot of partially rotated magnetization and stripes, at 2000 nsec there is only a small region of reversed magnetization and no stripes at all. There is no evidence in the 2000 nsec photograph that the reversal process was basically rotational in nature; rather it appears that some type of propagation occurred at the upper right hand edge of the film. This series of photographs is therefore a good example of the difficulty encountered in trying to infer the dynamic magnetization configuration from static domain patterns which result after the field is terminated as in an interrupted pulse experiment.

In both Figs. 5-7 and 5-8 the magnetization rotated to a less reversed state after the field was terminated, presumably because of torques from uniaxial anisotropy and the locked ripple, but this need not always occur. Figure 5-9 shows film 81-4-12 during and after a 50 nsec long 2.3 oe longitudinal pulse field with a static 0.5 oe

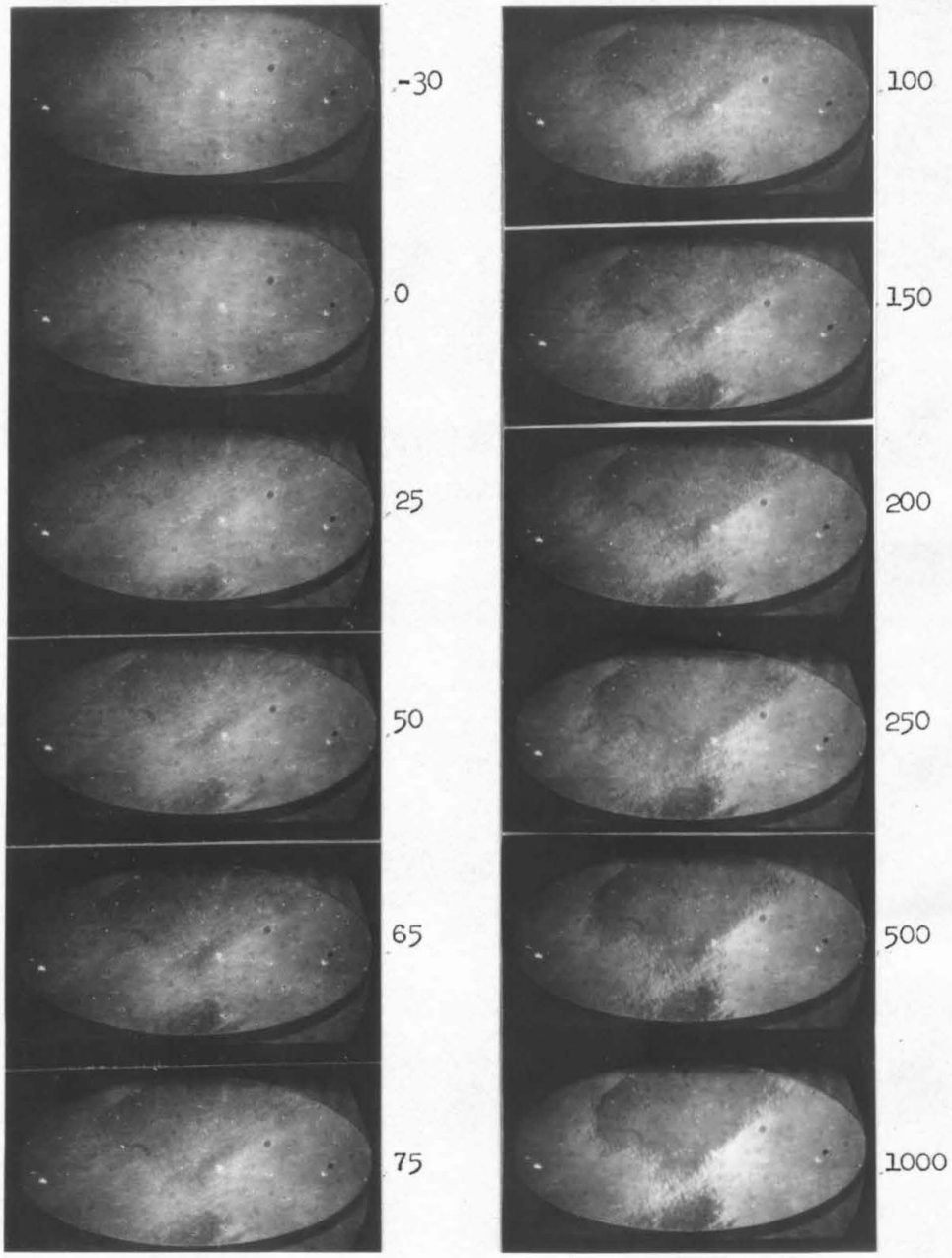

Fig. 5-9. Film 81-4-12 during and after a 50 nsec long, 2.3 oe longitudinal pulse field with a static 0.5 oe transverse bias field applied. Time in nanoseconds relative to initial application of pulse field is indicated.

transverse bias field applied. As usual there is little or no change in the photographs obtained at -30 nsec and 0 nsec. By 25 nsec, however, the magnetization has clearly begun to rotate as the contrast indicates much of the magnetization in the film is partially rotated and in the locked configuration. At 50 nsec just prior to termination of the pulse field the magnetization has rotated still further and stripes are still visible in partially reversed areas of the film. In this case the falltime of the field is 10 nsec. At 65 nsec (15 nsec after the field began to fall) the magnetization has rotated further around than it was at 50 nsec, and the stripes are still visible. By 75 nsec nucleated regions are beginning to break up the striped pattern, and by 100 nsec the magnetization in the partially reversed area has rotated still further and the stripes are beginning to fade away. Between 100 and 150 nsec the partially reversed area becomes slightly darker indicating that rotation is still occurring. At 150 nsec only a few stripes still remain and these fade away as time proceeds until at approximately 500 nsec the magnetization is in static equilibrium.

In the photographs of Fig. 5-9 the partially reversed areas of the film continued to reverse after the field was terminated. The reason for this is believed to be that before the field was completely terminated the magnetization in the partially reversed areas had rotated sufficiently far past 90° that the torque from the uniaxial anisotropy was able to overcome the reaction torque of the locked ripple. Note that although the field began to fall at 50 nsec, it has a falltime of 10 nsec and therefore is not zero until roughly the 65 nsec photograph at which point the partially reversed areas have

become quite dark indicating that the magnetization has rotated significantly past 90°. Also note that the reversal in this case was occuring somewhat faster than in Fig. 5-7 and that therefore the stripes are not as large in amplitude as they are in the case of slower reversal. Because the stripes are of smaller amplitude, it is expected that the reaction torque from the locked ripple is somewhat smaller than in Fig. 5-7. Hence, after the field was terminated the magnetization was able to continue reversing in some portions of the film.

Clearly, it is extremely difficult to infer the dynamic magnetization configuration from the static domain pattern which follows. From Figs. 5-7, 5-8, and 5-9 it can be seen that the final static state gives little or no evidence that the reversal process was rotational. The striped configuration in Figs. 5-8 and 5-9 disappeared, while in Fig. 5-7 the well-defined dynamic stripes broke up into a much less well-defined pattern. In the final photographs of Figs. 5-8 and 5-9 it appears that the reversal was by propagation of diffuse boundaries at the upper and lower edges of the film. Bourne et.al. (1968) did observe such static domains and erroneously infer from them that with a transverse field reversal processes taking place in less than 100 nsec were characterized by a well-defined propagating boundary. As the photographs show, this clearly is not correct. The fact that one cannot even know whether the static state is more or less reversed than the dynamic one preceeding it further complicates the interpretation of the static domain pattern.

As was seen from Figs. 5-7, 5-8, and 5-9, relaxation processes with a transverse field also take 200 nsec or longer to be completed,

which is long compared to the theoretical time for relaxation of uniform magnetization about an equilibrium position ($\sim$1 nsec), but is typical of the times involved in non-coherent rotation and nucleation processes. It is reasonable to assume that the long relaxation time is due to the sequential nature of the nucleation wherein the nucleated regions grow by a wide propagating wavefront as they form and where different regions nucleate at different times as the magnetostatic fields from one region influence others.

5.4 Summary

In this chapter relaxation processes occuring after the termination of the drive field during flux reversal with and without a transverse field have been discussed. With or without a transverse field it was found that the diffuse boundaries, which appear during the diffuse boundary propagation, became more sharply defined when the field was terminated. Fundamental differences exist between the dynamic and static boundaries. The more sharply defined static boundary was found to propagate much more slowly during the first 200 nsec of a second pulse field than did the dynamic boundary, so that flux reversal by numerous short pulses differs greatly from flux reversal by a single continuous pulse. In addition to the changes in the diffuse boundary, with zero transverse field it was seen that, when the field was terminated during the initial nucleation of partially reversed regions, most of the nucleated regions relaxed to the non-reversed state after termination of the field.

With a transverse field applied it was shown that if the drive field was terminated during a non-coherent rotation flux reversal process large changes occured in the magnetization configuration

as static equilibrium was established. Typically the static configuration had little resemblance to the preceding dynamic configuration. Because of this it was concluded that one could learn very little about the the non-coherent rotation process by using interrupted pulse techniques.

The one feature common to all the relaxation processes observed was the long ($\tilde{}$ 200 nsec) time required for equilibrium to be established. It was pointed out that this is two orders of magnitude longer than the time constant for decay of oscillations of the mean magnetization about an equilibrium position. This exceedingly long relaxation time was attributed to the fact that the relaxation processes were sequential in nature.

Chapter 6

Reprinted from THE REVIEW OF SCIENTIFIC INSTRUMENTS, Vol. 40, No. 6, 829-840, June 1969
Printed in U. S. A.

A Nanosecond Kerr Magneto-Optic Camera*

M. H. KRYDER AND F. B. HUMPHREY
California Institute of Technology, Pasadena, California 91109
(Received 30 September 1968; and in final form, 11 February 1969)

A Kerr magneto-optic camera has been constructed which takes 10 nsec exposures of the dynamic magnetization configuration in a magnetic thin film during high speed flux reversal. The photographs obtained have 10 μ resolution and sufficient contrast and brightness to record, in a single exposure, the dynamic state during a 50 nsec or longer flux reversal. The time at which the photograph is taken relative to the application of the switching field is variable from -100 nsec to $+10$ μsec with a relative time stability at any setting of ± 3 nsec. A Q-switched ruby laser is used as a light source. The 10 nsec exposure time is obtained with a Kerr electro-optic shutter. The reversing field has a risetime of 10 nsec, decay time of 20 nsec, variable amplitude (<30 Oe), duration (<10 μsec), and is applied with a stripline. Included in the description of the system are discussions of a blocking oscillator circuit used to drive KU-27 thyratrons with a jitter of less than 1 nsec, an electron multiplier pulse amplifier with a 6 nsec risetime and a 0 to 1.5 kV output into 50 Ω, and a thyratron pulse amplifier with a 10 nsec risetime and a 1.0 to 10 kV output into 50 Ω. The apparatus is particularly suitable for studying high speed flux reversal in that it gives a visual picture of the dynamic state of the magnetization. Examples of sequences of photographs depicting dynamic flux reversal are also included.

INTRODUCTION

THERE are currently two widely used experimental techniques for investigating flux reversal in magnetic thin films. One is to infer the flux changes in the longitudinal and transverse directions by observing the induced voltage in loops around the film.[1] The other is to observe the magnetization configuration with the use of a Kerr magneto-optic effect apparatus.[2] The Kerr effect gives a more detailed picture of the magnetization configuration in a thin film than does the use of pickup loops but has not been used as extensively at higher speeds because the instrumentation required is more complex. In this paper a Kerr apparatus capable of giving a detailed picture of the magnetization configuration at any instant during a flux reversal is discussed. In this way, the dynamic configuration for complete reversals as short as 50 nsec can be observed.

* This research represents one phase of work sponsored by the National Aeronautics and Space Administration under contract NAS 7-100.

[1] F. B. Humphrey, J. Appl. Phys. **38**, 1520 (1967).

[2] C. A. Fowler and E. M. Fryer, Phys. Rev. **100**, 746 (1955).

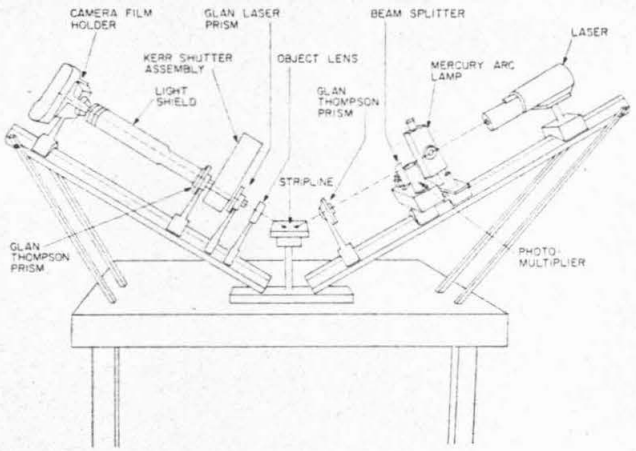

FIG. 1. Sketch showing the relative positions of the various optical components of the Kerr magneto-optic camera.

If a beam of light, plane polarized with its electric vector parallel or perpendicular to the plane of incidence, is incident on the surface of a ferromagnetic material, the reflected wave is slightly elliptically polarized with the major axis of the ellipse rotated through a small angle from the plane of the incident electric vector. This phenomenon is known as the Kerr magneto-optic effect. The magnitude and direction of the rotation is dependent upon the magnitude and direction of the magnetization at the reflecting surface. The three basic types of Kerr effects[3] are (1) the polar Kerr effect which occurs when the magnetization is normal to the reflecting surface, (2) the transverse Kerr effect which occurs when the magnetization is in the plane of the reflecting surface and normal to the plane of incidence of the light wave, and (3) the longitudinal Kerr effect which occurs when the magnetization is in the plane of the reflecting surface and also in the plane of incidence of the light wave. Due to large demagnetizing fields, in the case of thin films, the magnetization lies in the plane of the film. Although either the transverse or longitudinal Kerr effects could be used for observation of the magnetization direction, in the apparatus to be described in this paper the longitudinal Kerr effect is used, with the polarization of the light perpendicular to the plane of incidence. It is used because the transverse effect does not produce a rotation of the plane of polarization, but instead changes the reflection coefficient of the surface for light polarized in the plane of incidence. For light polarized perpendicular to the plane of incidence only the longitudinal effect occurs[3] and therefore is unambiguous.

Williams *et al.*[4] were the first to use the longitudinal Kerr effect for observing domains on finely polished cobalt. Fowler and Fryer[2,5–7] later used it for domain observations on silicon iron and also on thin films. Since then, several investigators have used the Kerr effect to study flux reversal in magnetic thin films. Lee *et al.*[8] first used the Kerr effect to measure domain wall velocities across a a 10 mm^2 region of a thin film; by using a He–Ne laser as a light source, Genovese and Chang[9] have similarly observed nanosecond switching of 25 μ diam spots. Lee[8] and Genovese and Chang[9] used a photomultiplier to detect the Kerr rotation and inferred the changing domain pattern from the changing light intensity. Many investigators have been reluctant to give up observing the entire domain configuration, feeling that it is more informative to compromise by interrupting the drive field during reversal long enough to make the domain observations. Copeland and Humphrey[10] and Patton and Humphrey[11] used this scheme in quasistatic pulse measurements of domain wall velocities. Stein[12] and Bourne *et al.*[13] used a similar technique to investigate high speed flux reversal. Their procedure was to apply a magnetic field pulse to the thin film and then to terminate it before the film was completely switched. A Kerr apparatus was then used to observe the resulting static state and from the static state observations to infer the dynamic state which existed prior to termination of the field. Conger and Moore[14] used a more direct approach when they constructed a Kerr magneto-optical strobing apparatus which was capable of taking 100 nsec exposures of flux reversal. Unfortunately this exposure time did not permit them to observe flux reversal which was faster than 1 μsec. Sarles[15] attempted to build a Kerr apparatus equipped with a Kerr electro-optic shutter to take 10 nsec photographs of flux reversal, but the poor contrast, brightness, and resolution of the photographs also limited its use to relatively slow flux reversal.

In this paper, the optical apparatus and the associated electronics necessary for the operation of a Kerr photoapparatus with a 10 μ resolution and a 10 nsec exposure time are discussed. The complete unit consists of a Kerr magneto-optic apparatus employing the longitudinal Kerr effect as described above. It is equipped with a camera and Kerr electro-optic shutter for photographing the magnetization configuration on the thin film, a stripline for applying a pulse magnetic field, and a laser for a light source.

[3] B. Carey and E. D. Isaac, *Magnetic Domains and Techniques for Their Observation* (Academic Press Inc., New York, 1966), pp. 62 ff.
[4] H. J. Williams, F. G. Foster, and E. S. Wood, Phys. Rev. **82**, 119 (1951).
[5] C. A. Fowler and E. M. Fryer, Phys. Rev. **86**, 426 (1952).
[6] C. A. Fowler and E. M. Fryer, Phys. Rev. **94**, 52 (1954).
[7] C. A. Fowler and E. M. Fryer, Phys. Rev. **104**, 645 (1956).
[8] E. W. Lee, D. R. Callaby, and H. C. Lynch, Proc. Phys. Soc. **72**, 233 (1958).
[9] E. R. Genovese and H. Chang, Rev. Sci. Instrum. **39**, 733 (1968).
[10] J. A. Copeland and F. B. Humphrey, J. Appl. Phys. **34**, 1211 (1963).
[11] C. E. Patton and F. B. Humphrey, J. Appl. Phys. **37**, 4269 (1966).
[12] K. U. Stein, Z. Angew Phys. **20**, 36 (1965).
[13] H. C Bourne, Jr., K. D. Savage, and W. L. Walters, Trans. IEEE Magnetics **MAG-4**, 435 (1968).
[14] R. L. Conger and G. H. Moore, J. Appl. Phys. **34**, 1213 (1963).
[15] F. W. Sarles, "A Magneto-Optic Apparatus for the Dynamic Study for Ferromagnetic Surface Domains" Ph.D. thesis, Massachusetts Institute of Technology, 1961.

The relative time of the application of the magnetic field and the actuation of the Kerr shutter is variable from -100 nsec to 10 μsec and stable to within 3 nsec. Descriptions of the optical alignment procedure, the operational characteristics of the system, and examples of the photographs obtained are given. Included in the description of the electronic apparatus are discussions of a blocking oscillator circuit used to drive KU-27 thyratrons with a jitter of less than 1 nsec, an electron multiplier pulse amplifier with a 6 nsec risetime and a 0 to 1.5 kV output into 50 Ω, and a thyratron pulse amplifier with a 10 nsec risetime and a 1.0 to 10 kV output into 50 Ω.

OPTICAL APPARATUS

Figure 1 is a sketch of the optical apparatus showing the relative position of the various components and Fig. 2 is a photograph of the apparatus as it appears in the laboratory. An optical bench is used that has two sides inclined at 60° to the normal. The thin film is located at the center of the bench, placed horizontally in a stripline used to apply the pulse magnetic field. The light source is a Q-switched ruby laser; however, for alignment and static domain observations a high pressure mercury short arc lamp is also provided. A beam splitter diverts about 1% of the laser light to a photomultiplier used to monitor timing and amplitude. A prism polarizer is used even though the laser light pulse is linearly polarized to correct for any slight optical activity of components between the light source and the thin film and also to facilitate minor adjustment of the incident light polarization. To the left of the thin film are the object lens and a prism analyzer. This analyzer is nearly crossed with respect to the polarizer and the amplitude of light passing through it is proportional to the longitudinal Kerr rotation and hence is directly proportional to the component of magnetization in the plane of incidence. A commercial Kerr electro-optic shutter is used in front of the camera film holder.

The rotation due to the longitudinal Kerr magneto-optic effect is dependent upon the magnetic material from which the light is reflected, the angle of incidence of the light beam, the wavelength of light being used, and also upon the thickness and index of refraction of a dielectric layer with which the magnetic material may be coated.

TABLE I. Extinction ratio of polarizers.

Polarizer	Extinction ratio
Polaroid HN-38	3.75×10^{-4}[a]
Polaroid HN-32	2.7×10^{-5}[a]
Nicol prism	1 to 2×10^{-5}[b]
Glan laser prism	1×10^{-5}[b]
Polaroid HN-22	4.8×10^{-6}[a]
Glan–Thompson prism	2×10^{-6} to 10^{-5}[b]

[a] See Ref. 15.
[b] Private communication with Karl Lambrecht, Crystal Optics.

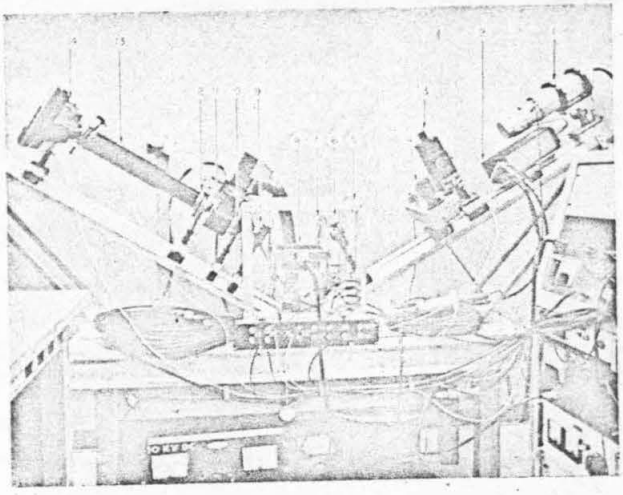

FIG. 2. A photograph of the Kerr magneto-optic camera. The numbers indicate (1) laser, (2) Kerr cell pulse generator, (3) mercury arc lamp, (4) beam splitter and photomultiplier, (5) transverse Helmholtz coils, (6) Glan–Thompson prism polarizer, (7) longitudinal Helmholtz coils, (8) stripline, (9) object lens, (10) Glan laser prism polarizer, (11) Kerr shutter assembly, (12) Glan–Thompson prism polarizer, (13) light shield, and (14) camera film holder including the mechanical shutter and camera lens.

Exact expressions for these dependencies are exceptionally complicated and the reader is referred to work by Sarles,[15] Smith,[16,17] Lissberger,[18] and Yoshino and Tanaka[19] for a theoretical treatment. An experimental investigation of these dependencies was made by Tanaka.[20] His work is especially relevant because it was done on Permalloy which is the material which has been predominantly examined with the apparatus described in this paper. Specifically Tanaka investigated the Kerr rotation as a function of the angle of incidence with wavelength as a parameter. He found that shorter wavelength light experiences a larger Kerr rotation, but unfortunately the wavelength of light used in this apparatus is fixed at 6943 Å due to the choice of a ruby laser as a light source. Furthermore, his results show that with light of 5920 Å wavelength plane polarized perpendicularly to the plane of incidence, the maximum Kerr rotation occurs at an angle of incidence of about 70° and is approximately 4×10^{-4} rad. With the addition of a dielectric layer of appropriate thickness, he found that the maximum Kerr rotation occurs at about 60° and is increased to approximately 7×10^{-4} rad. Although the 6943 Å wavelength used in this apparatus is different from that reported above, since the maximum is quite broad, 60° was chosen as suitable.

To utilize this small Kerr rotation, it is necessary to use extreme care in the selection of the polarizing optics. Several authors have treated this subject in deriving the

[16] D. O. Smith, Opt. Acta 12, 13 (1965).
[17] D. O. Smith, Opt. Acta 12, 193 (1965).
[18] P. H. Lissberger, J. Opt. Soc. Amer. 51, 957 (1961).
[19] T. Yoshino and S. Tanaka, Jap. J. Appl. Phys. 5, 989 (1966).
[20] S. Tanaka, Jap. J. Appl. Phys. 2, 548 (1963).

signal-to-noise ratio obtainable from the Kerr effect.[15,18,21] Table I shows the extinction ratio of several of the present day polarizers. Although the Polaroid HN-22 has an extinction ratio comparable with the Glan–Thompson prism, the principal amplitude transmission coefficient of the HN-22 at 6943 Å is 0.56 while that of the Glan–Thompson prism is 0.96.[15] Because of the large internal absorption of the HN-22, it would be damaged by the high intensity light used in this experiment. For this reason and because it is desirable to avoid optical losses to obtain as short an exposure time as possible, the HN-22 is not used.

Even with prism optics, special precautions must be taken because of the high instantaneous power of the pulse. Because the analyzer is nearly crossed with respect to the polarization of the light, it must be capable of absorbing or diverting the entire output of the laser. For this reason, a modified Glan prism referred to commercially as a Glan laser prism is used. In this prism, an air spaced interface replaces the Canada balsam cement which is used in the Glan–Thompson prism. Also, the extraordinary light ray is provided with a clear path through an open side of the prism mount. Hence the damage which would occur to the normal black side walls of the Glan–Thompson prism is avoided. Although the Glan laser prism has a poorer extinction ratio than the Glan–Thompson prism, the contrast obtained using a Glan laser prism was compared to the contrast when a Glan–Thompson prism was used and no significant degradation could be detected in a visual inspection. Attention is called to the fact that since most of the light goes through the side port, it must be very clean and free of dust to prevent scattered light from obscuring the image of the magnetic domains. To facilitate alignment all the prisms are held in rotatable holders, permitting rotations as small as 0.1° to be made.

To obtain sufficient light to expose the photographic film in a single exposure, with crossed prisms and a 10 nsec exposure time, it is necessary to use a light source with an intensity of a few megawatts. Conger and Moore[14] focused the light from the sun into a narrow beam in order to obtain sufficient intensity to observe switching using strobe techniques and a 100 nsec exposure time. Sarles[15] attempted to use a xenon flash lamp in an apparatus with a 10 nsec exposure time, but found that multiple exposures were necessary to obtain sufficient brightness in his photographs. In the apparatus described in this paper, a Q-switched ruby laser is used for a light source. The laser easily supplies the peak intensity necessary and has the added advantages that its output is plane polarized and well collimated. Hence, its full output can be used for observing the Kerr magneto-optic effect.

In this apparatus the laser light pulse must be synchronized with the actuation of the Kerr shutter to within 3 nsec and it must be possible to predetermine, within 3 nsec, the time between the application of the magnetic field and the photograph. A Kerr electro-optic cell used as a triggerable Q switch has the timing potential and was chosen because of its low capacitance and resultant low operating current, and also because it exhibits low sensitivity to damage by the high field intensity of the laser pulse. More recently, however, Pockels' cells made of KDP crystal have become available and it is quite possible they would do equally well and perhaps better in spite of their higher capacitance and susceptibility to damage, mainly because the nitrobenzene used in Kerr cells often causes large deviations in both pulse shape and spectrum when the light energy flux in the cell becomes of the order of 10 MW/cm^2. These deviations are due to stimulated Raman scattering[22,23] and related parametric effects[24,25] in the nitrobenzene which has one of its strongest Raman active vibrations at a small frequency shift $\Delta/2\pi c \sim 0.5$ cm^{-1}. Therefore, it is difficult to suppress the Raman scattering without also suppressing the desired ruby output.

The laser was constructed to provide the desired illumination of the magnetic thin film. The ruby used in the laser is a 0.635 cm diam by 7.6 cm long cylindrical rod with a totally internally reflecting (TIR) cut on one end and a polished flat surface on the other. It is mounted at one focus of a polished cavity which is shaped as a right elliptical cylinder. A linear flashtube is located at the other focus. A 65% reflective dielectric coated optical flat is placed about 15 cm from the flat end of the ruby and is aligned so that the ruby is normal to its surface. The TIR cut on the end of the ruby reflects predominantly one polarization and, together with the dielectric mirror, forms the laser optical cavity. The nitrobenzene Kerr cell is placed between the ruby and the dielectric mirror, and is aligned so that the ruby is normal to its surface and so that the electric field is applied to the nitrobenzene at 45° to the TIR cut on the ruby. In this way, when 16 kV is applied to the Kerr cell, the polarization of the light reflected from the TIR cut is rotated by 45° on its initial pass through the cell to the mirror and again by 45° as it returns from the mirror. Hence the returning light is polarized at 90° to the favorable polarization of the TIR cut, and the cavity is in a low Q condition until the 16 kV is removed from the Kerr cell. The entire laser is mounted on a stand which fits on the optical bench and permits the laser to be rotated about the axis of the ruby rod, positioned relative to the optical bench, and rotated about an axis perpendicular to the optical bench. This flexibility of the laser mount facilitates alignment. The laser light pulse has a half-width of 10 nsec and a peak pulse power

[21] D. B. Dove, J. Appl. Phys. 35, 1991 (1965).

[22] E. J. Woodbury and W. K. Ng, Proc. IRE 50, 2367 (1962).
[23] R. W. Hellwarth, Appl. Opt. 2, 847 (1963).
[24] A. L. Schawlow, Sci. Amer. 204, 52 (1961).
[25] R. W. Terhune, Solid State Design 4, 38 (1963).

of about 5.5 MW. Unfortunately, however, this light pulse does not, in general, always occur at the same time after the removal of voltage from the Kerr cell. The delay time varies from 50 to 150 nsec and it has been found that when the temperature of the ruby rod is raised, or as damaged areas appear in the ruby, the delay becomes greater. To stabilize the delay time the ruby is allowed to cool in air for 5 min between operations. This reduces the output jitter to 3 nsec and also reduces the rate at which damage occurs to the ruby. An attempt was made to reduce the cooling time by using liquid nitrogen as a coolant, but it was found that the rate of damage of the ruby rod increased and compounded the problem. As damage occurs to the ruby over a period of several thousand pulses, the delay time increases but this is easily compensated. However, when the delay time becomes of the order of 100 nsec, it becomes impossible to obtain less than 3 nsec jitter even with extended cooling times and the ruby must be replaced. Depending upon the original quality of the ruby, this is typically after about 5000 pulses. To reduce this rate of damage it is important that the ruby be kept clean so that particles of foreign matter do not burn on the ruby surface.

Another cause of laser output jitter is variation in the flashtube output. To obtain the same pumping rate during each operation it is necessary that the flash always be of the same intensity and duration. If the capacitor bank supply voltage is well regulated and the flashtube is new, there is seldom a problem. However, it has been found that flashtubes which have been used extensively or which have lain on the shelf for several months frequently produce successive flashes of varying intensity and duration, similarly causing variation in the laser output intensity and delay time.

A stripline section is used to apply the pulse magnetic field and special considerations had to be given to its design in order that the light beam could be passed through it and reflected from the magnetic thin film. Figure 3 is a drawing of the stripline. The magnetic thin film is placed in a square hole in the center of a round 18 cm diameter by 0.08 cm thick Lucite sheet which is placed on the bottom ground plane. The Lucite sheet is held in place by four nylon screws around its circumference in such a way that it can be rotated to orient the easy axis of the thin film at various angles with respect to the pulse field with an accuracy of 0.1°. Two 1 cm diam holes are drilled in the upper ground plane providing access for the incident and reflected light beam. The stripline is mounted on a mechanical stage which allows movement in any of the x, y, or z directions and rotation about the vertical z direction. This control of the stripline position is necessary for the optical alignment.

The lens system was chosen for the desired optical magnification. Using an object lens with a 110 mm focal

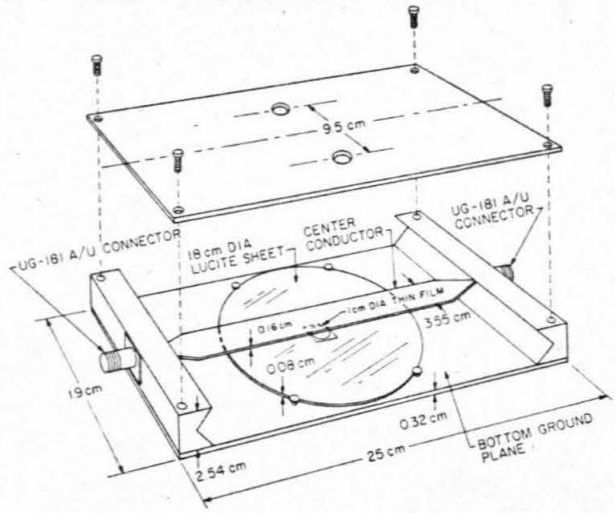

FIG. 3. A drawing of the stripline.

length, and an 88 mm, $f/1.4$ camera lens with a 1:1 object to image ratio, a magnification of 3.7 times is obtained on the Polaroid film used in the camera. The optical resolution is limited by the resolution of the film which is 30 lines/mm. This produces a resolving power on the thin film of about 10 μ. This approximate resolution has been experimentally verified because 20 μ wide domains have been observed with the camera. For observations of thin film flux reversal, 10–20 μ resolution is adequate. Because of space limitations, it was necessary to place the object lens between the thin film and the analyzer. Hence the lens had to be strain-free so that any birefringences would be small compared to 10^{-5} rad, which corresponds to the extinction obtainable with the crossed prisms.

The Kerr electro-optic shutter is used to define the 10 nsec exposure time. It consists of a commercial Kerr electro-optic shutter[26] which has had the Polaroid filters (normally equipped) removed and replaced by prism polarizers because of the higher transmission coefficient of the prisms. The Glan laser prism acts as one of these prism polarizers and a second Glan–Thompson prism as the other.

The film holder used in the apparatus is an adaptation of a commercial oscilloscope camera and consists of the aforementioned 88 mm, $f/1.4$ lens, a Pi Alphax No. 3 mechanical shutter, and a Polaroid camera back. The mechanical shutter is used to prevent stray light from exposing the photographic film between Kerr shutter operations. A light shield is used between the Kerr shutter and the mechanical shutter to prevent the laboratory light from exposing the photographic film when the mechanical shutter is actuated. Polaroid type 413 ir film is used in the camera. For work with holograms and for night time ir photography, faster films and films with

[26] Kappa Scientific Corporation model KS-38-20 Kerr shutter.

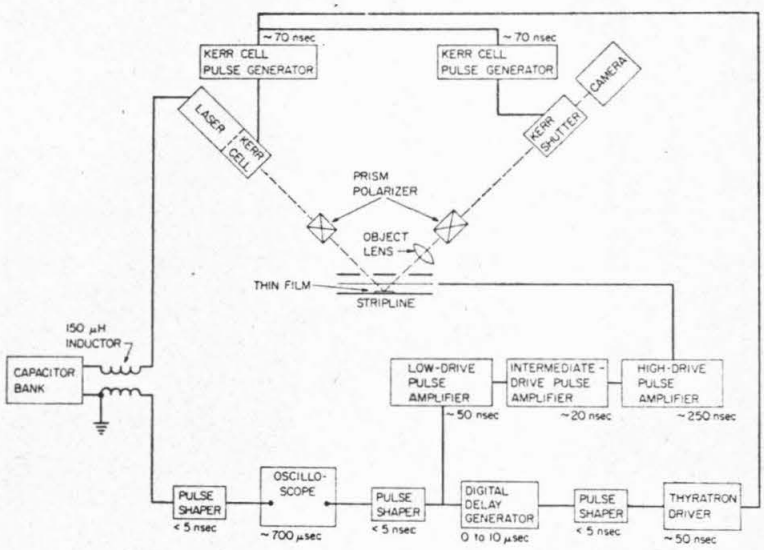

FIG. 4. A block diagram of the electronic apparatus for the Kerr magneto-optic camera, including the time delay of each unit

higher resolution have been developed and are now available in sheet form. With this apparatus, however, it is desirable that film with a fast development time be used, since there is no reliable method of predetermining the desired exposure nor of knowing how quickly the flux reversal is taking place and hence whether the desired process is being photographed. It has been found that changes in the system occur which gradually alter the exposure (for example, changes in the laser output delay time due to ruby damage). These changes can be compensated for, but without rapid development film many photos would be wasted before the error was discovered and the desired correction made. The rapid development film also is necessary because a major portion of the optical alignment and electronic synchronization of the laser and Kerr shutter is best done by experimental optimization of the contrast and brightness of the photographs. If film with better resolution than Polaroid is required, it could be substituted after all alignment procedures were complete and after the desired switching process had been determined to be taking place with the use of Polaroid film. So far, however, the 10 μ resolution already possible with the apparatus has been more than adequate to observe flux reversal processes.

A beam splitter, consisting of a glass microscope slide oriented at 45° to the laser beam, is used to pick off enough light to actuate a 931A photomultiplier tube and produce a pulse voltage waveform proportional to the intensity of the light. The frequency response does not allow an accurate representation in time of the laser pulse; however, the reproducibility of the photomultiplier output does make it possible to obtain a relative measure of the laser output intensity as a function of time. This relative measure may be used as an aid in correcting for changes in power output and timing.

Optical Alignment

A collimated light source consisting of a high pressure mercury short arc lamp[27] and a collimating lens is provided for alignment of the optics on the optical bench as shown in Figs. 1 and 2. The lamp is actually located off the bench so that the beam crosses the bench at right angles, putting the lamp out of the way of the optics for normal operation with the laser. When the lamp is to be used, a mirror is placed in front of it to reflect light in the desired direction. For convenience, both arms of the optical bench are aligned parallel to the light path. Also, all the prism polarizers and the Kerr electro-optic cells are aligned and adjusted so their front surface is normal to the light as evidenced by reflections from these interfaces being directly back along the incident beam. This is necessary if the optimum extinction ratio of the polarizing optics is to be obtained and if the Kerr cells are to rotate the polarization of the light by the correct amount. Using the arc lamp it is possible to look through the camera lens at the sample and observe static domain patterns. A preliminary adjustment of all the optics for proper image size, focus, and contrast is then possible.

The laser components can be aligned in a similar manner. Reflections of the mercury arc light beam can be observed from the dielectric mirror, from the front face of the Kerr cell, from the front face of the ruby rod, and from the TIR end of the ruby rod. Each of these reflections should be made to go directly back along the incident beam. The ruby rod should be rotated so that the apex of the TIR cut is horizontal and the Kerr cell should be rotated so that the parallel electrodes are at 45° to the horizontal. When this has been done, the laser is aligned for operation. Final adjustment of all the optics can then be made using

[27] Consolidated Electronics Corporation type 110 mercury arc lamp.

the laser as a light source. The amount of exposure of the photographs may be controlled by changing the length of time the Kerr shutter is open, or by altering the voltage that is applied to the Kerr cell in the shutter and hence the percentage of the incident light that the shutter passes.

ELECTRONIC APPARATUS

Figure 4 is a block diagram of the electronic apparatus necessary for operating the Kerr shutter, laser, and stripline. Included in the diagram is the time delay of each particular unit. The sequential operation of the apparatus for taking one photograph is as follows. A trigger pulse is applied to the flashtube. Then, simultaneously, the mechanical shutters on both the oscilloscope camera and the optical bench camera are opened for 0.1 sec and the reset magnetic field is removed from the thin film for 10 msec. The current surge from the capacitor bank discharge through the flashtube induces a timing pulse which, when shaped, delayed, and reshaped, triggers both a preset digital nanosecond delay generator and the low-, the intermediate-, and the high-drive pulse amplifier chain. The high-drive pulse amplifier provides the pulse magnetic field at the stripline used to switch the thin film. The preset delay generator output, shaped and amplified, is used to trigger the laser Q-switch and the Kerr shutter. Hence the delay generator controls the time, relative to the application of the magnetic field, at which the picture is taken. With different preset delay settings, a sequence of photographs may be obtained which represents the magnetization configuration during an entire flux reversal. Of course, reproducible domain configurations are necessary, which has been verified by taking photographs on successive reversals with the same delay generator setting.

The FX-42 C-3 flashtube[28] was chosen as adequate to pump the laser ruby with the relatively simple cavity design that is used for the laser. For this tube and cavity design, the total capacitance required is 300 μF and the charging voltage is typically about 1700 V. The flashtube is equipped with a trigger consisting of a short piece of wire wound around the center of the tube. A voltage pulse of about 45 kV, produced when a 2050 thyratron discharges a 0.5 μF capacitor charged to 1000 V through the primary of a photoflash transformer, is used to trigger it. A 150 μH inductor, in addition to acting as a convenient primary for a loosely coupled pulse transformer, serves to limit the rate of rise of current through the flashtube reducing the mechanical shock produced by the high current surge which would destroy the tube. The delay between initial capacitor discharge and laser Q-switching is determined by the oscilloscope[29] and experimentally chosen to be about 700 μsec for optimum laser output.

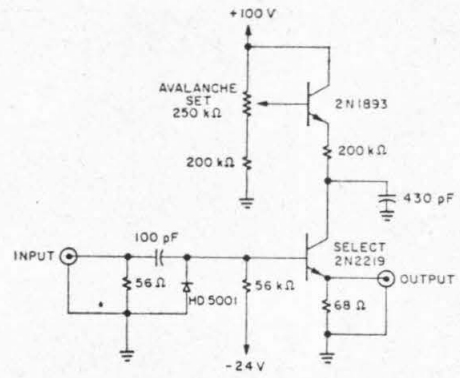

FIG. 5. A schematic diagram of the pulse shapers.

A 50 Ω stripline section (Fig. 3) is used to apply a 10 nsec risetime magnetic field pulse because it produces a magnetic field of good uniformity over the flat thin film. A three septum stripline is used because the relative dimensions of the width of the center conductor and the spacing between ground planes permit easier access for the light beam incident on the magnetic thin film at 60° than in the two septum stripline. The wide ground planes are for convenience since Hayt[30] had shown that, for a 50 Ω stripline, the exact capacitance and the value obtained by assuming infinite width ground planes agree within 0.25% if the width of the ground planes is greater than 2.5 times the spacing between ground planes. Since the holes in the ground planes are 9.5 cm apart, they do not significantly disturb the fields within the stripline. The coax-to-stripline transition is made by placing UG-181 A/U coaxial connectors on the ends of the stripline. The center conductor of the stripline is tapered at the ends and is soldered to the coaxial connectors producing a standing wave ratio of less than 1.1:1. A 150 m section of coaxial cable connects the stripline to the 50 Ω load so that any minor reflections that occur at the load do not interfere with the drive pulse. The magnetic field was calculated to be uniform to 2% over the 1 cm diam thin film and was shown to be adequate for this experiment by moving the thin film by as much as 0.5 cm from the center of the stripline while observing that the flux reversal was the same in all cases.

For the experiments which are to be performed with the apparatus, it is desirable that the stripline calibration be accurate to better than 5%. Because the stripline is not precisely matched to the charge line and because the effects of eddy currents in the stripline are not clearly understood, it is necessary to calibrate experimentally the stripline magnetic field. Using the apparatus, discoveries have been made concerning magnetic thin film switching which have led to the use of a special method for stripline

[28] Manufactured by Edgerton, Germeshausen and Grier, Inc.
[29] Tektronix model 547 oscilloscope with 1A1 plug-in.

[30] W. H. Hayt, Jr., Trans. IRE Microwave Theory Tech. MTT-3, 16 (1955).

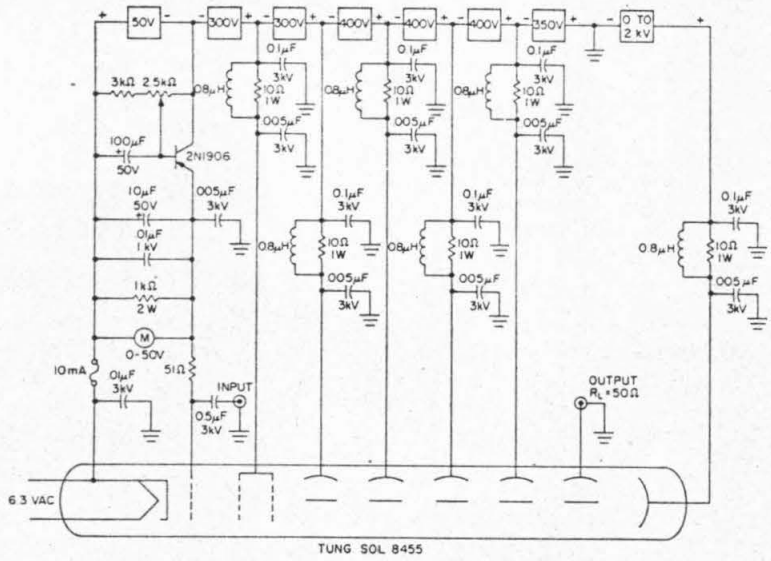

FIG. 6. A schematic diagram of the intermediate-drive pulse amplifier.

calibration. Basically the method is the same as described by Tatsumoto.[31] This method is based on the assumption that the switching process is dependent only upon the applied fields during switching and not on the fields existing prior to application of the pulse switching field. Using this assumption, for a given reversal time, it is observed how much additional pulse amplitude is necessary again to obtain the same switching time for a thin film after a constant known bias field has been applied opposing the pulse field. However, using the Kerr magneto-optic camera it has been observed that when the pulse field is applied opposite to or nearly opposite to the direction of the original magnetization, the switching is influenced by the original state of the magnetization and hence by the longitudinal dc bias fields used for calibration purposes. On the other hand, it has been experimentally verified that during switching processes of roughly 100 nsec duration, so long as the magnetization rotates in only one direction and so long as the ripple relaxation time is short compared to the 10 nsec risetime of the magnetic field (which was verified by Hoper[32] and also with this apparatus), the reversal time is independent of the original state of the magnetization. Therefore in order to insure that rotation in only one direction occurred, the method of Tatsumoto[31] was modified to include the application of a constant hard axis bias field equal to one-half the anisotropy field. Using this method a plot of stripline pulse current vs opposing longitudinal bias field yielded a straight line that was independent of the thin film used.

Two sets of Helmholtz coils are used to cancel the earth's field to less than 0.01 Oe in the longitudinal and transverse directions in the film. The same coils are used to apply bias and reset fields to the magnetic thin film. The longitudinal coils which are mounted on the stripline are 25 cm in diameter and the square transverse coils which are mounted on the aluminum table from which the arms of the optical bench hinge are 35 cm on a side. The coil dimensions were made large so that the stripline and thin film were conveniently accessible.

For jitter-free (<1 nsec) triggering of the oscilloscope, delay generator, and thyratron driver it was desirable that the pulse shapers produce pulses of less than 1 nsec risetime into 50 Ω. Because of their high alpha cutoff frequencies, avalanche transistors permit risetimes of the order of 1 nsec, and used with proper bias they will easily trigger with less than 1 nsec jitter. Hence, selected 2N2219 avalanche transistors are used in the pulse shapers utilized in this apparatus and diagrammed in Fig. 5. The 2N1893 transistor is used to adjust the collector voltage on the 2N2219 transistor to just below the point at which it will free run. This insures that the jitter will be small and also that the input signal level required to trigger the pulse shaper is small. The only requirement on the input signal is then that it have less than a 20 nsec risetime. The output pulse from the pulse shaper has a 0.5 nsec risetime, 40 V maximum amplitude with a 25 nsec exponential tail.

The digital delay generator determines at what time, relative to the application of the magnetic field, the photograph is taken. In order that a sequence of photographs can be taken which depicts flux reversal in times from 50 nsec to 10 μsec, it is necessary that the delay generator be capable of producing delays from 0 to 10 μsec in intervals of at most 5 nsec with jitter of less than 1 nsec. The one used[33] provides up to 100 μsec delays in 1 nsec intervals, with jitter of less than 0.5 nsec.

[31] E. Tatsumoto, M. Nomura, and M. Goto, Jap. J. Appl. Phys. **2**, 254 (1963).
[32] J. H. Hoper, J. Appl. Phys. **39**, 1159 (1968).
[33] Eldorado Electronics model 610 digital delay generator.

The thyratron driver unit was designed to drive the Kerr cell pulse generators[34] with less than 1 nsec jitter. These pulse generators consist mainly of a pulse forming network and a KU-27 thyratron which typically has erratic triggering characteristics when driven from a low voltage, high impedance source. To overcome these poor triggering characteristics, the driver unit must provide a trigger pulse of not less than 500 V amplitude and have an output impedance not higher than 500 Ω. Furthermore, since the firing delay time of the thyratron is critically dependent on the integrated volt-time product of the trigger pulse, it is very important that the driver pulse have repeatable shape and amplitude. Assuming an ideal rectangular pulse shape of 500 V amplitude, the delay time is about 100 nsec. To obtain the desired repeatability of pulse shape and amplitude a blocking oscillator circuit was used for the thyratron driver unit. The driver easily produces a 40 nsec risetime 500 V pulse at the input of the Kerr cell pulse generators which are connected to the thyratron driver by 180 Ω coaxial delay cables cut to the proper length for synchronization of the laser output pulse and the opening of the Kerr shutter. For triggering, the driver requires a 5 V pulse with a 10 nsec risetime and of at least 5 nsec duration from a 50 Ω source. This trigger is easily supplied by the pulse shaper on the output of the digital delay generator.

Pulse Amplifiers

The magnetic field pulse which is applied to the magnetic thin film is variable in amplitude from 0 to 30 Oe, has a risetime of 10 nsec or less, a variable duration up to 1 μsec, and a jitter of less than 2 nsec. To produce the current for such a pulse, two fast risetime pulsers were constructed. The first one, which is referred to in Fig. 5 as the intermediate-drive pulse amplifier, is used to produce fields up to about 5 Oe; while the second, which is referred to as the high-drive pulse amplifier, is used to produce fields from 3 to 30 Oe. The intermediate-drive pulse amplifier is driven by a commercially available[35] pulser (referred to as the low-drive pulse amplifier in Fig. 4). This commercial unit produces a 15 nsec risetime 50 V pulse of variable duration (40 nsec to 10 μsec) into 50 Ω. It also has a variable delay time which may be used to insure that the pulse to the stripline is delayed long enough that the Kerr shutter and laser can be actuated to take a picture before flux reversal begins.

The intermediate-drive pulse amplifier has a variable output of 0 to 30 A into a 50 Ω load. Jitter is less than 1 nsec and the risetime is 6 nsec. Figure 6 is a schematic diagram of this pulse amplifier. Basically it consists of a multistage secondary emission electron multiplier tube (Tung Sol 8455). The anode voltage applied to the tube

[34] Kappa Scientific Corporation model PG-5 pulse generator.
[35] Rutherford Electronics model B7 pulse generator.

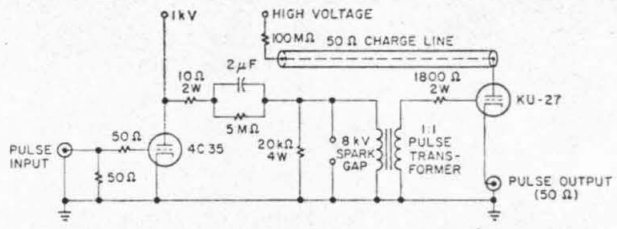

FIG. 7. A schematic diagram of the high-drive pulse amplifier.

determines the pulse amplitude and can be varied from 0 to 2 kV (producing a pulse output of 0 to 1.5 kV into 50 Ω). The pulse width is controlled by the width of the pulse that drives the tube and is continuously variable from 0 to 10 μ sec with less than 5% droop. The low-drive pulser mentioned above is adequate to drive the tube and provides the easily variable pulse width which is convenient for interrupted pulse experiments. Although the manufacturer lists the peak pulse output of the 8455 as 1 kV into a 250 Ω load (4 kW) with a duty cycle of 1%, this pulser has performed satisfactorily with the above mentioned 45 kW output with duty cycles as high as 0.005% without damaging the tube.

The high-drive pulse amplifier produces a 1.0 to 10 kV pulse into 50 Ω with a 10 nsec risetime. Jitter is less than 2 nsec when it is triggered with a 500 V, less than 50 nsec risetime input pulse from a source impedance of 50 Ω that can be obtained from the intermediate-drive pulser. Figure 7 is a schematic diagram of this pulser. Basically it is a coax cable discharged through a KU-27 thyratron which is driven by a 4C35 thyratron driver stage. The driver stage was chosen as being adequate to trigger the KU-27 thyratron with less than the maximum allowable 2 nsec jitter. The use of a high current pulse transformer to isolate the driver stage from the high voltages of the KU-27 necessitated the use of a 4C35 thyratron driver because the intermediate-drive pulser was not capable of producing the 100 A pulse required to trigger reliably the KU-27. On a single shot basis the 4C35 will easily switch this much current. The current pulse to the primary of the transformer is produced when a 2 μF capacitor charged to 1 kV is discharged through the 4C35 and a 10 Ω current limiting resistor. This produces about 1 kV at the open circuit secondary of the pulse transformer and is adequate to reduce jitter in the KU-27 to about 1 nsec. Although the 4C35 typically has jitter of the order of 15 nsec, it can be triggered with jitter of less than 1 nsec if driven with a 500 V, 50 nsec or less risetime pulse from a 50 Ω source like the intermediate-drive pulser.

As was mentioned above, the driver stage is coupled to the grid-cathode circuit of the KU27 thyratron through a current pulse transformer which is used to prevent damage to the driver stage by the high voltage in the grid circuit of the KU-27 when the thyratron is conducting.

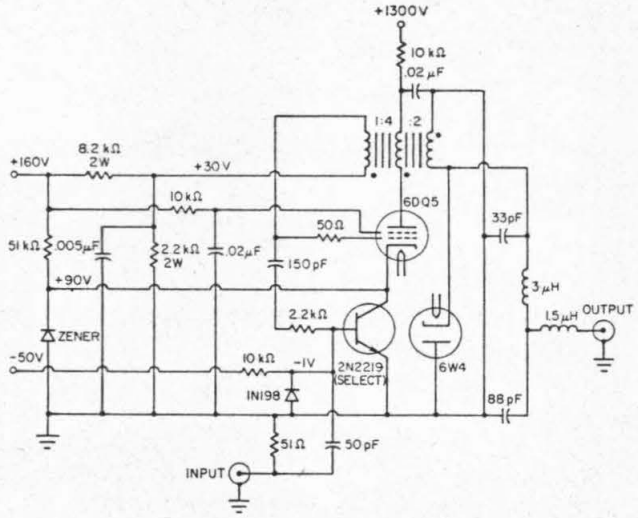

FIG. 8. A schematic diagram of the thyratron driver unit.

This transformer consists of eight turns of RG-8/U wound on a Hypersil iron core. The center conductor of the coaxial cable is used as the primary and the shield as the secondary. The insulation between the center conductor and the shield will withstand 30 kV, and Teflon is used to prevent the shield from shorting to the core. Since the transformer secondary is connected from the grid of the KU-27 thyratron to ground, the current flowing in the grid circuit of the thyratron also flows through the load and adversely alters the pulse shape. An 1800 Ω resistor which connects the grid to the transformer is used to limit this grid current and also to isolate the grid from ground so that a mismatch may be avoided. However, this high grid circuit resistance necessitates the 1 kV grid pulse to reduce the KU-27 jitter to 1 nsec.

The KU-27 thyratron is used as the switching element for the coaxial cable discharge. The requirement of low jitter on a single shot basis precluded the use of a relay with mercury wetted contacts, triggered spark gap, or ignitron. The KU-27 was specifically chosen because of its ability to withstand high voltages, separate reservoir connections, comparatively good firing characteristics, and low internal inductance. The separate reservoir connections make it possible to regulate the reservoir voltage and hence the hydrogen pressure at the optimum value for operation at the desired plate voltage, thus reducing jitter and delay time. High voltage, 50 Ω coaxial cable is used as a charge line for the pulser and the length of the pulse is controlled by the length of cable used. Pulse amplitude is one-half the charge line voltage. Droop with the cable used[36] is less than 3% for a 1 μsec pulse. Since it was desirable to keep the load at ground potential except during the pulse, a special problem was created by the necessity that both the anode and cathode of the thyratron be above ground. Two special filament transformers were made to heat the filament and the reservoir of the KU-27. These transformers have 30 kV insulation and less than 10 pF capacitance to ground. They insured that the thyratron cathode was above ground for frequencies up to about 1 GHz which was adequate in order that a 10 nsec risetime pulse could be obtained into 50 Ω. To keep the risetime at a minimum and to avoid a severe mismatch at the thyratron, the thyratron was placed in a 7.6 cm square by 25.4 cm long metal box. When the thyratron is conducting, the metal box–thyratron combination simulates a section of 50 Ω coaxial line. Coaxial connectors which fasten to the plate and cathode of the thyratron are placed in the ends of the box, and the leads which connect to the anode and the four pins connecting to the cathode are kept as short as possible to minimize both capacitance and inductance.

The low internal inductance of the KU-27 and the above precautions to minimize the external inductance and capacitance facilitate a 10 nsec risetime pulse of 1.0 to 10 kV amplitude into 50 Ω. As was mentioned above the pulse length is determined by the length of coaxial cable and hence short pulses may be produced for interrupted pulse experiments. The fall time of the pulse is dependent upon the length of coaxial cable used and approaches the 10 nsec risetime for short lengths. Jitter in the entire unit is less than 2 nsec when it is triggered by a 500 V, 50 nsec or less risetime pulse supplied by the intermediate-drive pulser. In some cases the high-drive pulser has been used with charge line voltages of 30 kV, and although the manufacturer's peak anode voltage rating is 16 kV, selected KU-27 thyratrons are available[37] that will withstand 35 kV plate to cathode voltage. For this to be possible, a silicone corona shield must be provided around the glass tube. It should also be noted that although the 1 kV grid voltage exceeds the manufacturer's 300 V rating, no damage to the tube has been found in a year's operation.

Thyratron Driver

The thyratron driver is a power pulse amplifier capable of delivering the necessary 500 V pulse with a 40 nsec risetime used to trigger the KU-27 thyratrons in the Kerr cell pulse generators with a jitter of less than 1 nsec. Although it is not necessary in this specific application, the thyratron driver is capable of repetition rates greater than 2000 pulses/sec. Since this driver is somewhat unique and has applications wherever thyratrons are to be driven with low jitter, the description of the circuit and theory of operation will be covered in detail.

Figure 8 is a schematic diagram of the thyratron driver circuit. A blocking oscillator circuit was chosen because the shape and amplitude of the output pulse is dependent upon passive circuit elements and independent of both the

[36] Rowe Electronics type CS-518 coaxial cable.

[37] Such selected KU-27 thyratrons are available from Kappa Scientific Corporation.

input pulse and tube aging. An epitaxial transistor (2N2219 selected) operating in the avalanche mode is well suited to switch about 2 A of pulse current required for the cathode triggering of the blocking oscillator. The input requirements are a 5 V positive pulse with a 10 nsec rise-time and 5 nsec duration. When the circuit is quiescent, the screen grid of the blocking oscillator tube (6DQ5) is held at 160 V while the control grid is held at 30 V and the cathode is at 90 V, placing the tube in cutoff. The base of the avalanche transistor is returned to a bias supply through a 10 kΩ resistor and clamped to ground with a diode. This diode was chosen for its low forward conductance and fast recovery time. The low forward conductance develops 1 V of negative bias at 5 mA of bias current providing cutoff bias for the transistor; the fast recovery insures that the diode will allow the input pulse to drive the base of the avalanche transistor positive when the input current exceeds 5 mA. When the base of the transistor is driven about 2 V positive, the transistor will avalanche, consistently switching 2 A in approximately 6 nsec. The cathode of the oscillator tube drops from 90 V to the transistor's avalanche sustaining voltage which is typically about 35 V, triggering the oscillator into conduction. Once turned on, the blocking oscillator plate voltage falls rapidly while the grid voltage rises by transformer action. This rise in grid voltage is coupled by a resistance–capacitance network back to the base of the transistor; the injected current from this source insures that the transistor will stay on, regardless of the amount of collector current which is now flowing and independent of the presence or absence of the input pulse. The entire process becomes self-sustaining in less than 5 nsec.

The regenerative action of the blocking oscillator continues until the plate voltage reaches a low value and the loop gain drops to one. This condition is stable and continues until the core of the pulse transformer saturates, at which time the grid voltage drops and the regenerative action turns the tube off. The cathode circuit rapidly returns to 90 V, while the grid returns from a low value to 30 V in about 50 μsec due to the long time constant in the grid bias circuit. The damping diode (6W4) in the output circuit conducts during the turnoff or backswing transient to absorb energy stored in the transformer leakage inductance and to prevent the circuit from turning itself on again.

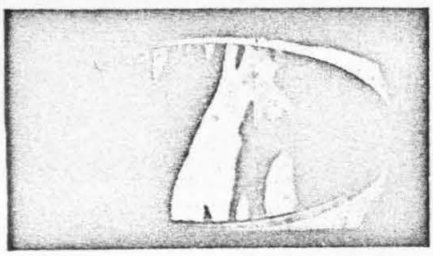

FIG. 9. A photograph of film A with static domains on it.

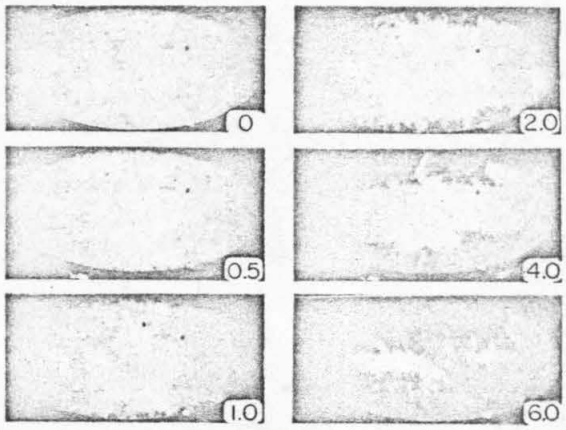

FIG. 10. A series of photographs showing film B during flux reversal by the longitudinal propagation of a diffuse domain boundary when no transverse field is applied. The numbers indicate the time in microseconds at which the photograph was taken relative to the initial application of the 2.7 Oe longitudinal pulse field.

A two-section LC filter is incorporated into the output circuit to prevent the ignition transient at the hydrogen thyratron from destroying the pulse transformer. This filter increases the risetime of the pulse to 40 nsec and increases the delay to 46 nsec. Ignition is accomplished in about 60 to 80 nsec, depending on hydrogen reservoir pressure and anode voltage. The total ignition delay is approximately 100–120 nsec from the trigger pulse.

EXPERIMENTAL

Thin Film Preparation

As reported by Lissberger,[38] Tanaka,[20] Ahn,[39] and others, the Kerr effect signal-to-noise ratio may be enhanced by coating the magnetic thin film with a thin dielectric layer. Here, a SiO dielectric layer has been used exclusively with an experimentally determined 330 Å thickness in agreement with Ahn's data.[39] To show the contrast obtained between regions of oppositely directed magnetization separated by a pure 180° domain wall, a 10 nsec photograph of a suitably coated thin film with static domains on it was taken. A reproduction of it is shown in Fig. 9. The contrast and clarity makes identification of the domain walls quite simple. The light pulse, with such high instantaneous power, will sometimes cause local damage to the SiO which will in turn scatter the incident light and appear as bright spots on the photographs. Such bright spots appear in the photographs in Fig. 10. It has been found that by overcoating the magnetic thin film with SiO before removing the thin film from the vacuum that these damaged regions appear less frequently.

An apparent inconvenience is caused by the 60° angle at which the picture is taken with respect to the normal

[38] P. H. Lissberger, J. Opt. Soc. Amer. **51**, 948 (1961).
[39] K. Y. Ahn, Trans. IEEE MAG-2, 678 (1966).

of the film plane; the photographs depict the circular 1 cm diam thin film as an ellipse. This may be corrected by taking a second photograph of the original, again at an angle of 60° to the normal and with the major axis of the ellipse in a line which passes beneath the camera. Generally this added photography was not done since the corrections which must be applied to measurements made on the photographs are extremely simple because of the 2 to 1 ratio of the major to minor axes of the ellipse.

The Ni–Fe alloy films shown in the photographs in this paper were vacuum evaporated from a melt of 83% Ni and 17% Fe onto glass substrates at 200°C in a vacuum of 10^{-6} Torr in the presence of a uniform magnetic field in the plane of the substrate. The anisotropy field, coercive force, and film thickness were measured using a 20 Hz hysteresis loop tracer and found to be 3.45 Oe, 1.7 Oe, and 1000 Å, respectively, for film A, and 3.7 Oe, 1.7 Oe, and 1000 Å, respectively, for film B. In the photographs shown in this paper, the easy axis of the thin film corresponds to the minor axis of the ellipse.

Flux Reversal

As mentioned earlier, there have been many previous attempts to understand high speed magnetic thin film switching. The magnetic processes involved have been too complicated to rely only on the use of inductive sense loops around the thin film. Use of a Kerr magneto-optic apparatus allows one to observe domains on the thin film, but most previous attempts could observe only quasistatic domains and hence relied upon the very tenuous assumption that the static domain pattern was identical or at least similar to the dynamic magnetization configuration. The interrupted pulse experiments of Hagedorn[40] show that reversal by a series of pulses is different from reversal by a single pulse of the same amplitude. Likewise, the results of interrupted pulse experiments with this apparatus[41–43] have shown that large relaxation effects occur when the field is terminated so that the resulting static domain pattern can be quite different from the preceding dynamic magnetization configuration.

Conger and Moore's[14] apparatus did not rely on the quasistatic approach, but did require several thousand 100 nsec exposures to obtain adequate light for the photographic film. Sarles'[15] apparatus did allow him to obtain a 10 nsec exposure time with only a few exposures and was a significant improvement over previous attempts. However, his lack of an adequate light source necessitated the use of extremely grainy film which reduced resolution and contrast. In the apparatus described in this paper, the problem of a light source was overcome with the use of a Q-switched ruby laser.

An example of a series of pictures depicting flux reversal in film B is shown in Fig. 10. In this case there is no transverse field and the applied longitudinal pulse field is 2.7 Oe. The easy axis of the film is vertical. The flux reversal is nearly complete in 7 μsec and the mechanism is the longitudinal propagation of a diffuse transverse domain boundary. The clarity of the domain boundary makes measurement of the boundary velocity quite simple. Although the magnetization direction in the light and dark regions differs by 180° in this case, in higher speed switching, variations in the direction of the magnetization are not so large and variations as small as 20° are easily seen on the photographs. Sequences of pictures depicting the higher speed flux reversal have been published elsewhere.[41–43]

Sequences of photographs such as those shown in Fig. 10 have shown the importance of aligning the easy axis of the thin film with respect to the applied pulse magnetic field. With misalignment of 0.1°, the reversal pattern observed in Fig. 10 changed considerably. By rotating the thin film counterclockwise by roughly 0.1° the diffuse boundary which forms near the upper right and lower left hand edges of the film moves diagonally and more rapidly than the corresponding boundaries in the upper left and lower right hand edges. This is discussed in more detail elsewhere.[43] For low dispersion films, the quadrantal symmetry of the reversal pattern with zero transverse field is therefore a sensitive indicator of alignment. A less accurate but suitable method of alignment of higher dispersion films with which the quadrantal symmetry cannot be obtained is to observe flux reversals with a fixed longitudinal pulse field and with equal but oppositely directed transverse bias fields of the order of $0.1H_k$. If the film is aligned, flux reversal takes place at the same speed regardless of the polarity of the transverse field, but if misaligned, flux reversal with one polarity field will be faster than with the other. It is found that easy axis alignment with an accuracy of $\pm 0.25°$ is possible with use of this criterion.

ACKNOWLEDGMENTS

The authors would like to thank John E. Guisinger for his invaluable technical assistance in the design and construction of much of the electronic apparatus for this project. Also we thank him for his technical description of the thyratron driver unit which has been largely reproduced in this paper.

[40] F. B. Hagedorn, J. Appl. Phys. **30S**, 245S (1959).
[41] M. H. Kryder and F. B. Humphrey, Jet Propulsion Laboratory SPS 37-50 Vol. III (1968), p. 115.
[42] M. H. Kryder and F. B. Humphrey, International Colloquium on the Phys of Magnetic Films, Irkutsk, USSR (1968).
[43] M. H. Kryder and F. B. Humphrey, J. Appl. Phys. **40**, 1225 (1969).

APPENDIX A

In this appendix the reaction torque from mean ripple components with $\eta = \varphi_o - \bar{\Phi}_{\vec{k}} \ll 1$ is calculated. Since ripple relaxation is incompletely understood, it is necessary to assume a ripple configuration. Since the calculation is intended to be accurate only for small η, it is reasonable to approximate the magnitude of various ripple components by using the result (2.34) but with $\varphi_o - \eta$ substituted for φ_o:

$$\varphi_{\vec{k}} = \frac{-K_s}{2 K_u \bar{h}_{eff}} \frac{f_{1\vec{k}}}{1+r_e^2 k^2 + \frac{2r_m}{t} \tilde{\chi}_{\vec{k}} \sin^2(\varphi_o - \eta - \Phi_{\vec{k}})} \tag{A.1}$$

Now Harte (1964) showed that the effect of the ripple components was to produce a reaction torque given by

$$\vec{T}_r = \vec{i}_Z 2\pi M_s^2 \sum_{\vec{k}\neq 0} \tilde{\chi}_{\vec{k}} \sin 2(\varphi_o - \Phi_{\vec{k}}) \overline{|\varphi_{\vec{k}}|^2} \tag{A.2}$$

Furthermore, Harte (1968) showed that $\overline{|f_{1\vec{k}}|^2}$ is given by

$$\overline{|f_{1\vec{k}}|^2} = \frac{\pi}{0} D^2 (1+k^2 D^2)^{\frac{3}{2}} \tag{A.3}$$

where 0 = surface area of film. Therefore,

$$\overline{|\varphi_{\vec{k}}|^2} = \frac{\pi}{0} \frac{K_s^2 D^2}{4K_u^2 \overline{h_{eff}^2}} (1+r_e^2 k^2 + \frac{2r_m}{d} \tilde{\chi}_{\vec{k}} \sin^2(\varphi_o - \eta - \Phi_{\vec{k}}))^{-2} (1+k^2 D^2)^{-\frac{3}{2}} \tag{A.4}$$

Substituting (A.4) into (A.2), and substituting an integral for the summation over $\vec{k}$, one obtains:

$$\vec{T}_r = \vec{i}_z \frac{M_s^2 (DK_s)^2}{4K_u^2 \bar{h}_{eff}^2} \sin 2\eta$$

$$\times \int_0^{\infty} \int_{\varphi_o - \frac{\pi}{2}}^{\varphi_o + \frac{\pi}{2}} \frac{\tilde{\chi}_{\vec{k}} \cos 2(\varphi_o - \Phi_{\vec{k}}) k \, dk \, d\Phi_{\vec{k}}}{\left[1 + r_e^2 k^2 + \frac{2r_m}{d} \tilde{\chi}_k \sin^2(\varphi_o - \Phi_{\vec{k}})\right]^2 (1 + D^2 k^2)^{\frac{3}{2}}} \tag{A.5}$$

The integration over $d\Phi_{\vec{k}}$ may be done after substituting $\gamma = \varphi_o - \Phi_{\vec{k}}$ and $\cos 2\gamma = \cos^2\gamma - \sin^2\gamma$ into (A.5). The result is

$$\vec{T}_r = \vec{i}_z \left[M_s^2 \frac{(DK_s)^2}{4K_u^2 \bar{h}_{eff}^2} \sin 2\eta \right] \left[\frac{B(\frac{1}{2}, \frac{3}{2})}{2} I_1 - \frac{B(\frac{3}{2}, \frac{1}{2})}{2} I_2 \right] \tag{A.6}$$

where

$$I_1 = \int_0^{\infty} \frac{\tilde{\chi}_k \, k dk}{\left(1 + \frac{\frac{2r_m}{d} \tilde{\chi}_k}{1 + r_e^2 k^2}\right)^{\frac{1}{2}} \left(1 + D^2 k^2\right)^{\frac{3}{2}} \left(1 + r_e^2 k^2\right)^2} \tag{A.7a}$$

$$I_2 = \int_0^{\infty} \frac{\tilde{\chi}_k k dk}{\left(1 + \frac{\frac{2r_m}{d} \tilde{\chi}_k}{1 + r_e^2 k^2}\right)^{\frac{3}{2}} \left(1 + D^2 k^2\right)^{\frac{3}{2}} \left(1 + r_e^2 k^2\right)^2} \tag{A.7b}$$

and $B(x,y)$ is the Beta Function. Both I_1 and I_2 can be evaluated approximately, but $I_2 \ll I_1$, and therefore I_2 is neglected. I_1 is most easily evaluated if it is noted that the major contribution to the integral comes from k-values such that $(2r_m/d)\tilde{\chi}_k >> r_e^2 k^2 >> 1$. Using this fact, I_1 may be evaluated approximately:

$$I_1 \approx \frac{d}{4 r_m^{\frac{1}{2}} r_e^{\frac{5}{2}}} B\left(\frac{5}{4}, \frac{1}{4}\right) . \qquad (A.8)$$

Substituting (A.8) into (A.6) and neglecting $I_2 \approx 0$, the total result is

$$\vec{T}_r = \vec{i}_z M_s H_k \bar{h}_d \frac{\sin 2\eta}{2} . \qquad (A.9)$$

where, as in Chapter 2, it is necessary to adjust the numerical factor in $\bar{h}_d$ to generalize to the case $\sigma_1 \neq \frac{1}{\sqrt{2}}$, $n \neq 1$.

APPENDIX B

First, the magnetostatic energy, E_m, of the model shall be evaluated. The volume divergence of the magnetization is

$$-(\nabla \cdot \vec{M}) = - M_s \frac{\partial}{\partial X_1} (\cos \theta)$$

$$= \mp \frac{M_s}{w_b'} [-2(2+b)u + 3\, b\, u^2] \qquad (B.1)$$

where the + sign is for $-\frac{L}{2} - w_b' < x < -\frac{L}{2}$ and the - sign for $\frac{L}{2} < x < \frac{L}{2} + w_b'$. This divergence produces effective filamentary line charges

$$\sigma = \mp \frac{M_s}{w_b'} \, d\, [-2(2+b)u + 3\, b\, u^2] \, dx_1 \qquad (B.2)$$

at the positions $\pm x_1$. A pair of these line charges at positions $\pm x_1$ produce a potential at a position x_o in the film equal to

$$d\psi = \frac{2M_s d}{w_b'} [\ln|x_o - x_1| - \ln|x_o + x_1|][3bu^2 - 2(2 + b)u]dx_1 \qquad (B.3)$$

where $u = u(x_1)$. The approximation of the divergence by filamentary line charges of zero width is reasonable if $|x_o - x_1|, |x_o + x_1| \gg d$. Since it will be found that $w_b' \gg d$, this approximation should be reasonable and (B.3) should be valid except for a very small portion of the boundary at which $x_1 \approx x_o$. To calculate $d\psi$ at $x_1 = x_o$ it is necessary to calculate the potential from a pair of lines with magnetic poles evenly distributed throughout the thickness, d:

$$\lim_{x_1 \to x_o} d\psi = \frac{2M_s}{w_b'} \lim_{x_1 \to x_o} \left\{[3bu^2 - 2(2+b)u][\int_o^d \ln\sqrt{(x_o - x_1)^2 + (z - z_o)^2}\, dz \right.$$

$$\left. - d \ln 2x_o] \, dx_1 \right\} \qquad (B.4)$$

where the potential is being calculated at the point (x_o, y, z_o).

Taking the limit and doing the integration yields:

$$\lim_{x_1 \to x_o} d\psi = \frac{2M_s}{w_b'} [3bu^2 - 2(2+b)u]$$

$$x[d \ln (\frac{d-z_o}{2\, x_o}) + z_o \ln \frac{z_o}{d-z_o} - d]\, dx_o \qquad (B.5)$$

where $0 < z_o < d$. It is then possible to average the potential over the thickness of the film obtaining

$$\lim_{x_1 \to x_o} d\psi = \frac{2M_s d}{w_b'} [3bu^2 - 2(2+b)u][\ln \frac{W}{2x_o} - \frac{3}{2}]dx_o \, . \qquad (B.6)$$

After integration of (B.3) and the addition of (B.6):

$$\psi = 2M_s d \left\{-2 \ln \frac{1-u}{1+u+\frac{L}{w_b'}} + [(2+b)u^2 - bu^3]\ln(\frac{1-u}{u})\right.$$

$$\left. + 1 + \frac{b}{6} + (2+\frac{b}{2})u - bu^2\right\} \qquad (B.7)$$

where $u = \frac{1}{w_b'} (x_o - \frac{L}{2})$, $\frac{L}{2} < x_o < \frac{L}{2} + w_b'$ and where the approximations made were

$$W >> w_b' >> d \qquad (B.8)$$

Using (B.1) and (B.7), the magnetostatic energy may be calculated from

$$E_m = -\frac{1}{2} \int_V (\nabla \cdot \vec{M})\, \psi \, dV \qquad (B.9)$$

where V = volume. Doing the integration yields

$$E_m = 2M_s^2 d^2 [b^2/12 - b/3 + 7 + 4 \ln (L/w_b')] \qquad (B.10)$$

The anisotropy and field energies are found to be

$$E_a = \int_V K_u \sin^2 \theta \, dV = 2 \, d \, w_b' \, K_u \, [8/15 + b/30 - b^2/105] \qquad (B.11)$$

$$E_f = -\int_V \vec{M} \cdot \vec{H} \, dV = M_s H d \, [8/3 \, w_b' - b \, w_b'/6 - W + 2L] \, . \qquad (B.12)$$

In this calculation, exchange energy is negligible as the width w_b' of the boundary is large. Then

$$E_{tot} = E_m + E_u + E_f \qquad (B.13)$$

and to find the minimum energy it is necessary to solve simultaneously the equations:

$$\frac{\partial E_{tot}}{\partial b} = 0 \qquad (B.14a)$$

$$\frac{\partial E_{tot}}{\partial w_b'} = 0 \qquad (B.14b)$$

The energy minimum is found to occur when

$$\text{for } h \geq \frac{3}{175} : \quad b = 4 \qquad (B.15a)$$

$$w_b' = 4 \frac{M_s d}{H_k} \left(\frac{1}{h + \frac{9}{35}}\right) \, . \qquad (B.15b)$$

For $h < \frac{3}{175}$, the values of b and w_b' corresponding to the energy minimum can in some cases be found, but are both complicated functions of the applied field. Since interest here is in solutions for $0.5 \leq h \leq 2$, the results (B.15a,b) are all that is required.

The value of b determines the boundary condition at u = 1: for b = 4,

$$\nabla \cdot \vec{M}\big|_{u=1} = 0 \ . \tag{B.16}$$

This is physically reasonable since it along with (4.4 a) and (4.4b) implies that the divergence of the magnetization varies continuously throughout the boundary and has no discontinuities at the edge of the boundary.

The result (B.15b) shows that w_b', the width of the boundary, decreases for larger applied fields. If h becomes too large then the approximation that $w_b' >> d$ will no longer hold and the analysis is incorrect. However, for $h \approx 1$, which is the region of interest, $w_b' \approx 1000\ d$ and the analysis should be good. By substituting (B.15a,b) back into (B.13), the total energy of the model may be found:

$$E_{tot} = 22M_s^2\, d^2 + 8M_s^2\, d^2 \ln\left[\frac{LH_k}{4M_s d}\left(h + \frac{9}{35}\right)\right] - M_s dH(W-2L). \tag{B.17}$$

Bibliography

1. A. Aharoni, J. Appl. Phys. 38, 3196 (1967).

2. A. Baltz, Proc. Intl. Conf. Magnetism (Nottingham) 845 (1964).

3. F. Bitter, Phys. Rev. 38, 1903 (1931).

4. M. S. Blois, Jr., J. Appl. Phys. 26, 975 (1955).

5. H. C. Bourne, Jr., K. D. Savage and W. L. Walters, Trans. IEEE Magnet. MAG-4, 435 (1968).

6. R. M Bozorth, Ferromagnetism (D. Van Nostrand Company, Inc., Princeton, New Jersey, 1951).

7. W. F. Brown, Jr. and A. E. LaBonte, J. Appl. Phys. 36, 1380 (1965).

8. W. F. Brown, Jr., J. Appl. Phys. 40, 1214 (1969).

9. R. Collette, J. Appl. Phys. 35, 3294 (1964).

10. J. A. Copeland and F. B. Humphrey, J. Appl. Phys. 34, 1211 (1963).

11. T. Crowther, M.I.T. Lincoln Laboratory Group Report 51-2, (1959).

12. H. D. Dietz and H. Thomas, Z. Physik 163, 523 (1961).

13. N. C. Ford, Jr., J. Appl. Phys. 31, 300S (1960).

14. E. Fuchs, Z. Angew. Phys. 13, 157 (1961).

15. H. W. Fuller and M. E. Hale, J. Appl. Phys. 31, 238 (1960).

16. J. K. Galt, Phys. Rev. 85, 664 (1952).

17. T. L. Gilbert, Armour Research Foundation, Report No. 11 (25 January 1955).

18. K. J. Harte, M.I.T. Lincoln Laboratory Technical Report 364, (1964).

19. K. J. Harte, J. Appl. Phys. 38, 1341 (1967).

20. K. J. Harte, J. Appl. Phys. 39, 1503 (1968).

21. H. Hoffmann, Phys. Stat. Sol. 5, 187 (1964).

22. H. Hoffmann, IEEE Trans. Magnet. MAG-2, 566 (1966).

23. H. Hoffmann, IEEE Magnet. MAG-4, 32 (1968).

24. H. Hoffmann, "An Experimental Verification of the 'Blocking Curve' in Thin Permalloy Films," to be published (1969).

25. J. H. Hoper, J. Appl. Phys. 39, 1159 (1968).

26. F. B. Humphrey, J. Appl. Phys. 29, 284 (1958).

27. F. B. Humphrey, J. Appl. Phys. 38, 1520 (1967).

28. F. B. Humphrey and E. M. Gyorgy, J. Appl. Phys. 30, 935 (1959).

29. F. B. Humphrey and A. R. Johnston, Rev. Sci. Instr. 34, 348 (1963).

30. E. N. Il'icheva and I. S. Kolotov, Bull. Acad. Sci. USSR 29, 559 (1965).

31. J. D. Jackson, Classical Electrodynamics(John Wiley and Sons, Inc. New York, 1965).

32. A. A. Jaecklin, IEEE Trans. Magnet. MAG-3, 616 (1967).

33. A. A. Jaecklin and S. Strässler, "Theory of Switching Dynamics under Inhomogeneously Applied Fields," Intl. Conf. Magnet., Amsterdam, Holland (1969).

34. K. Kempter and H. Hoffmann, Phys. Stat. Sol. 34, 237 (1969).

35. R. Kirchner and W. Döring, J. Appl. Phys. 39, 855 (1968).

36. L. Landau and E. Lifshitz, Physik Z. Sowjetunion 8, 153 (1935).

37. N. Menyuk, J. Appl. Phys. 26, 692 (1955).

38. S. Middelhoek, "Ferromagnetic Domains in Thin Ni-Fe Films," Academisch Proefshrift, Amsterdam, Holland (1961).

39. S. Middelhoek, IBM J. Res. Develop. 10, 4 (1966).

40. C. D. Olson and A. V. Pohm, J. Appl. Phys. 24, 284 (1958).

41. C. E. Patton and F. B. Humphrey, J. Appl. Phys. 35, 921 (1964).

42. C. E. Patton and F. B. Humphrey, J. Appl. Phys. 37 1270 (1966).

43. C. E. Patton, T. C. McGill and C. H. Wilts, J. Appl.Phys. 37, 3594 (1966).

44. C. E. Patton, "Dynamic Processes in Magnetic Thin Films - Domain Wall Motion and Ferromagnetic Resonance" (Ph. D. Dissertation, California Institute of Technology, Pasadena, California, 1967).

45. Y. Sakurai, T. Kusuda, S. Konishi, and S. Sugatani, IEEE Trans. Magnet. MAG-2, 570 (1966).

46. D. O. Smith and K. J. Harte, J. Appl. Phys. 33, 1399 (1962).

47. R. J. Spain, J. Appl. Phys. 37, 7 (1966).

48. K. U. Stein, Z. Angew. Phys. 18, 528 (1965a).

49. K. U. Stein, Z. Angew. Phys. 20, 36 (1965b).

50. K. U. Stein, A. Angew. Phys. 20, 323 (1966).

51. E. C. Stoner and E. P. Wohlfarth, Phil. Trans. Roy. Soc. A240, 599 (1948).

52. T. Suzuki, C. H. Wilts and C. E. Patton, J. Appl. Phys. 39, 1983 (1968).

53. T. Suzuki and C. H. Wilts, J. Appl. Phys. 39, 1151 (1968).

54. T. Suzuki, "(1) Anisotropy and Crystal Structure of Ferromagnetic Thin Films. (2) Investigations into Magnetic Microstructure by Lorentz Microscopy (Ph. D. Dissertation, California Institute of Technology, Pasadena, California, 1969).

55. S. Tolansky, Multiple Beam Interferometry of Surface Films (Oxford University Press, London, 1948).

56. H. J. Williams, W. Shockley and C. Kittel, Phys. Rev. 80, 1090 (1950).